STRUCTURAL AND BIOCHEMICAL CHARACTERISATION OF BACTERIAL METALLO-β-LACTAMASES

Anne Makena

Somerville College, 2016



A thesis submitted to the board of the Faculty of Physical Sciences of the University of Oxford in partial fulfilment of the requirements for the degree of Doctor of Philosophy.

ABSTRACT

Anne Makena, Somerville College
DPhil Thesis, Hilary 2016

Structural and Biochemical Characterisation of Bacterial Metallo- β-Lactamases

One of the most prominent ways by which bacteria develop resistance to the widely used β-lactam antibiotics is by production of β-lactamases. Metallo-β-lactamases (MBLs) in particular pose an increasing public health risk due to the wide dissemination and broad substrate profile. The successful development of novel MBL inhibitors for clinical use is also dependent on sufficient understanding of the structural and functional properties of the target MBLs. From a medicinal chemistry point of view, the combination of biological diversity and structural similarity of MBLs presents a rather challenging task for the development of selective small molecules for inhibitors for bacterial MBLs. The progress made in this quest thus far is discussed at length in the introduction (Chapter 1).

Robust and affordable high throughput screening platforms are indispensable in drug development. Chapter 2 of the thesis describes the identification of a novel cephalosporin-based substrates, **CLS405**, for MBL activity and inhibition assays. The **CLS405**-based assay is used in an exemplary screening of potential MBL inhibitors, resulting in the identification of *N*-hydroxythiazoles as novel MBL inhibitor scaffolds. An umbelliferone-derived cephalosporin substrate (**FC-5**) is also investigated for application in screening of MBL activity *in vivo*.

Clinically useful MBL inhibitors must have a sufficient breadth of selectivity against multiple variants MBLs; this is particularly challenging due to the rapid MBL evolution. In Chapters 3 and 4, comparative studies of the activity, stability and structural properties of some of the clinically reported variants of the New Delhi metallo-β-lactamases (NDMs) are described. Nominal differences are noted in the kinetic parameters of the recombinant proteins, except for the apparent substrate inhibition observed with nitrocefin for variants containing the M154L substitution. Further investigations reveal significant differences in thermal stability of the NDM variants with the double mutants (NDM-5, NDM-7, NDM-8 and NDM-12) being the most stable variants, suggesting that protein stability may be a driver of MBL evolution.

The Verona imipenemase metallo-β-lactamases (VIM) enzymes are among the most widely distributed MBLs with >40 variants reported (Chapter 5). Comparative studies on the biochemical and biophysical properties were carried out for five VIM variants: VIM-1, VIM-2, VIM-4, VIM-5 and VIM-38. Clear differences in the thermal stabilities of the variants are observed, despite their similar β-lactamase activities, as previously shown for NDM variants. Interestingly, the variants show marked differences in the inhibition profile, with isoquionolone-based inhibitors selectively inhibiting VIM-5 and VIM-38 compared to VIM-1 and VIM-2.

Overall, the work supports the proposal that protein stability may be an important factor in MBL evolution. Crucially, the study highlights the importance of screening MBL variants during inhibitor development programs.

ACKNOWLEDGEMENT

I'd like to thank my supervisor Prof. Chris Schofield for being an ever present source of guidance and support. Thank you for the great ideas and for believing in my potential.

I am very grateful to the Rhodes Trust, The British Federation for Women Graduate and Pamela and Andrew Banks family for financial support throughout my studies.

To Dr. Geoffrey Maiyoh, thank you for patiently inspiring in me the love of Biochemistry.

To Jürgen and Sander, thank you for all the training and guidance and for being my scientific superheroes. I hope someday I'll make you proud!

To Sarah and Leah, for your support and friendship both in and out of the lab that has seen me through some of my most daunting experiences.

To my amazing 'thesis whisperer' Sam, and to Rich, Hannah, Ilaria and Gareth, thank you for very thoroughly going through my entire thesis!

To the best tea/lunch buddies in the world, David, Leah, Cyrille, Chris and Joanna, you make my days exceptionally joyful.

To the entire CJS group and especially Adam, Wendy, Manso, Jenny, Val and the 'Jurglings', I'm truly grateful for creating such a supportive environment for me throughout my studies.

To the residents of the Palace of Wisdom, thank you for providing such a loving and peaceful home, you make me long to come home every day.

To the Rhodes Christian ladies, the Rhodes scholars community, the Blackfriars family, the Winton ladies, the Oxford-Kenyans team and all my friends, thank you for helping me find joy, whatever the circumstances.

To my parents Florence and David, my brothers, Allan and Denis, and my families in Kenya and Ghana, thank you for never giving up on me.

To Bina, Grace, Qhelile and Shmona, you are the strongest anchors a girl would ever need!

To my husband Fafa, thank you for being ever so loving and for choosing me, every day.

AUTHOR CONTRIBUTIONS

At the start of each chapter, a description of contributions from collaborators is summarised in italics and in addition their names are included in parentheses in the main text anywhere their experiments are described.

All other experiments described in this thesis were carried out by myself, unless otherwise stated.

TABLE OF CONTENTS

Abstract i
Acknowledgement ii
Author contributions iii
Table of contents iv
Abbreviations ix
Chapter 1: Introduction 1
1.1 Antibiotics: The silver bullet 3
1.2 β-Lactam antibiotics 4
1.2.1 A brief history 5
1.2.2 Mechanism of action of β-lactam antibiotics 7
1.3 β-Lactam antibiotics resistance mechanisms 8
1.3.1 β-Lactamases 9
1.4 Metallo-β-lactamases 11
1.4.1 Class B β-lactamases (MBLs) 12
1.4.2 Classification of MBLs 13
1.4.3 Structural features of MBLs 14
1.4.4 MBL-mediated β-lactam hydrolysis 18
1.5 Evolution of B1 mbls 21
1.5.1 Influencing ligand binding 23
1.5.2 Improving biophysical properties 25
1.6 β-Lactamase inhibitor development 26
1.6.1 Serine β-lactamase inhibitors 26
1.6.2 MBL Inhibitor development 28
1.7 Summary 34
1.8 Research Objectives 35
1.9 References 36
Chapter 2: Development of a Novel Chromogenic Substrate (CLS405) for MBL assays 63
2.1 Introduction 65

2.1.1 β-lactamase assays 65
2.1.2 Spectrophotometric techniques 66
2.1.3 Chapter Objectives 68
2.2 Production and purification of MBLs 69
2.2.1 Cloning 69
2.2.2 Recombinant protein production 70
2.2.3 Mass Analyses 71
2.3 **CLS405** substrate synthesis 72
2.4 Substrate characterisation 73
2.4.1 Spectroscopic analyses 73
2.4.2 Stability of **CLS405** 74
2.5 Evaluation of Kinetic Parameters 76
2.5.1 Steady-State Kinetic Analyses 76
2.6 Assay validation 80
2.6.1 Residual activity determination 80
2.6.2 Determination of IC_{50} values 84
2.7 Fluorogenic substrate for cell-based assays 87
2.8 Summary 89
2.9 References 90
Chapter 3: Biochemical Characterisation of New Delhi Metallo-β-lactamase (NDM) Variants 97
3.1 Introduction 99
3.1.1 Evolution of NDM variants 99
3.1.2 Biochemical Studies of NDMs 101
3.1.3 Chapter Objectives 101
3.2 β-Lactam susceptibility analyses 102
3.2.1 Determination of MIC values 102
3.3 Production and purification of recombinant NDMs 104
3.3.1 Cloning and site directed mutagenesis 104
3.3.2 Protein production and purification 105
3.4 Comparison of hydrolytic activities of NDM variants 106

3.4.1 Steady-state kinetic analyses 106
3.4.2 Investigation of inhibition by nitrocefin 112
3.5 Biophysical characterisation of NDM variants 114
3.5.1 Secondary structure analyses by Circular Dichroism (CD) 114
3.5.2 Investigation of thermal stability of NDM variants 116
3.6 Summary 119
3.7 References 120
Chapter 4: Role of M154L Substitution in the Activity and Stability of NDM Variants 127
4.1 Introduction 129
4.1.1 NDM substitutions 130
4.1.2 Chapter Objectives 131
4.2 Protein production 132
4.2.1 Cloning and Mutagenesis 132
4.2.2 Purification of Recombinant NDM Variants 133
4.2.3 Size Exclusion Chromatography-Multi-Angle Light Scattering (SEC-MALS) Analyses 134
4.3 Hydrolysis of Cephalosporins by NDM variants 135
4.3.1 Steady-State Kinetic Analyses 135
4.4 Crystallographic analyses of NDM variants 139
4.4.1 Overall Structural Properties of NDM Variants 139
4.5 M154L substitution influence on stability of NDM Variants 144
4.5.1 Circular Dichroism Analyses (CD) 144
4.5.2 Dynamic Scanning Calorimetric Analyses 146
4.5.3 Cellular Thermal Shift Assays (CETSA) 148
4.6 Summary 151
4.7 References 152
Chapter 5: Comparison of stability and inhibition profiles of Verona Integron-Borne Metallo-β-lactamase (VIM) Variants 160

5.1 Introduction 162
5.1.1 Evolution and Biochemistry of VIM variants 162
5.1.2 Chapter Objectives 165
5.2 Production and purification of Recombinant VIM variants 166
5.2.1 Cloning and Mutagenesis 166
5.2.2 Protein production and purification 167
5.2.3 Mass spectrometric analyses 167
5.3 Functional Analyses of VIM variants 169
5.3.1 Steady-state kinetic analyses 169
5.4 Inhibition profiles of VIM variants 174
5.4.1 Determination of residual activities 174
5.4.2 Differential inhibition of VIM variants 176
5.5 Biophysical characterisation 178
5.5.1 Structural properties of VIM-5 178
5.5.2 Investigation of thermal stability 179
5.5.3 Crystallographic Analyses of VIM-5 181
5.6 Summary 186
5.7 References 187
Chapter 6: Conclusions and future work 194
6.1 **CLS405**: An efficient substrate for screening MBL activity and inhibition 196
6.2 **FC-5**: A potential substrate for cell-based assays 197
6.3 MBL variants display similar hydrolytic efficiencies 198
6.4 Protein Stability: a potential driver the evolution of MBLs 198
6.5 Evolution of MBLs affects inhibitor development 200
6.6 Structural analyses reveal subtle but crucial interactions 201
6.7 General conclusions 202
6.8 References 203
Chapter 7: Appendices 204
7.1 Reagents and general practice 206
7.2 Molecular biology 206

7.2.1 Site-directed mutagenesis 206
7.2.2 Transformation 207
7.2.3 Preparation of competent cells 208
7.3 Protein production 208
7.3.1 Bacterial growth media 208
7.3.2 Protein expression trials 210
7.3.3 Large scale protein production 210
7.4 Protein Purification 212
7.4.1 Protein purification buffers 213
7.4.2 Cell lysis 213
7.4.3 Purification protocol 213
7.4.4 Determination of protein concentrations 214
7.4.5 SDS PAGE analyses 214
7.4.6 Western blot analysis 215
7.5 Mass Spectrometric analyses 216
7.5.1 Non-denaturing mass spectrometry 216
7.5.2 Denaturing mass spectrometry 217
7.6 Enzyme assays 217
7.6.1 Steady-state kinetic assays 218
7.6.2 Enzyme Inhibition assay 218

ABBREVIATIONS

2TY	2 × Tryptone/yeast extract
APS	Ammonium persulfate
AU	Absorbance Units
Bc-II	*Bacillus cereus* metallo-β-lactamase II
BSA	Bovine Serum Albumin
CD	Circular dichroism
CETSA	Cellular thermal shift assay
C-terminus	carboxy terminus
DMSO	Dimethyl sulfoxide
DNA	Deoxyribosenucleic acid
DSC	Differential scanning calorimetry
DSF	Dynamic scanning fluorimetry
E. coli	*Escherichia coli*
EDTA	Ethylenediaminetetraacetic acid
ESI-MS	Electrospray ionisation Mass spectrometry
FPLC	Fast protein liquid chromatography
His_6	Hexa-histidine tag
IC_{50}	Inhibitor concentration at half maximal enzyme activity
IMP	Imipenamase
IPTG	Isopropyl β-D-thiogalactopyranoside
k_{cat}	Number of substrate molecules turned to product per enzyme per unit time (Turnover number)
K_D	Binding constant
kDa	Kilo Daltons
K_i	Inhibition constant
K_M	Michaelis contant
LC-MS	Liquid chromatography mass spectrometry
LIC	Ligation independent cloning
m/z	Mass to charge ratio
MBL	Metallo-β-lactamase

MES	2-(*N*-morpholino)ethanesulfonic acid
MS	Mass Spectrometry
ND	Not determined
NDM	New Delhi metallo-β-lactamase
NMR	Nuclear Magnetic Resonance
N-terminus	amino terminus
OD	Optical Density
OPPF	Oxford Protein Production Facility
PBS	Phosphate-buffered saline
PCR	Polymerase chain reaction
PDB	RCSB protein data bank
Pfu-Turbo	Pyrococcus furiosus polymerase
Q-TOF	Quadruple Time-of-flight
RMSD	Root mean square deviation
SBL	Serine-β-lactamases
SDS-PAGE	Sodium dodecylsulfate polyacrylamide gel electrophoresis
SPM	Sao Paulo metallo-β-lactamase
TB	Terrific Broth
TEMED	*N,N,N',N'*-Tetramethylethylenediamine
TEV	Tobacco etch mosaic virus
Tris	Tris-(hydroxylmethyl)aminomethane
v/v	Volume for volume
VIM	Verona integron-encoded metallo-β-lactamase
V_{max}	Maximum velocity
w/v	Weight for volume
wt	Wild type
RNA	Ribonucleic acid
7-ACA	7-aminocephalosporanic acid
KPC	*Klebsiella pneumoniae* carbapenemase
ESBL	Extended spectrum beta-lactamases
FDA	Food and Drug Administration
HTS	High Throughput screening

TABLE OF CONTENTS

Abstract i
Acknowledgement ii
Author contributions iii
Table of contents iv
Abbreviations x
Chapter 1: Introduction 1
1.1 Antibiotics: The silver bullet 3
1.2 β-Lactam antibiotics 4
1.2.1 A brief walk down memory lane 5
1.2.2 Mechanism of action of β-lactam antibiotics 7
1.3 β-Lactam antibiotics resistance mechanisms 8
1.3.1 β-Lactamases 9
1.4 Metallo-β-lactamases 11
1.4.1 Class B β-lactamases (MBLs) 12
1.4.2 Classification of MBLs 13
1.4.3 Structural features of MBLs 14
1.4.4 MBL-mediated β-lactam hydrolysis 18
1.5 Evolution of B1 mbls 21
1.5.1 Influencing ligand binding 23
1.5.2 Improving biophysical properties 25
1.6 β-Lactamase inhibitor development 26
1.6.1 Serine β-lactamase inhibitors 26
1.6.2 MBL Inhibitor development 28
1.7 Summary 34
1.8 Research Objectives 35
1.9 References 36

Chapter 2: Development of a Novel Chromogenic Substrate (CLS405) for MBL assays 63
2.1 Introduction 65
2.1.1 β-lactamase assays 65
2.1.2 Spectrophotometric techniques 66
2.1.3 Chapter Objectives 68
2.2 Production and purification of MBLs 69
2.2.1 Cloning 69
2.2.2 Recombinant protein production 70
2.2.3 Mass Analyses 71
2.3 **CLS405** substrate synthesis 72
2.4 Substrate characterisation 73
2.4.1 Spectroscopic analyses 73
2.4.2 Stability of **CLS405** 74
2.5 Evaluation of Kinetic Parameters 76
2.5.1 Steady-State Kinetic Analyses 76
2.6 Assay validation 80
2.6.1 Residual activity determination 80
2.6.2 Determination of IC_{50} values 84
2.7 Fluorogenic substrate for cell-based assays 87
2.8 Summary 89
2.9 References 90
Chapter 3: Biochemical Characterisation of New Delhi Metallo-β-lactamase (NDM) Variants 97
3.1 Introduction 99
3.1.1 Evolution of NDM variants 99
3.1.2 Biochemical Studies of NDMs 101

3.1.3 Chapter Objectives 101
3.2 β-Lactam susceptibility analyses 102
3.2.1 Determination of MIC values 102
3.3 Production and purification of recombinant NDMs 104
3.3.1 Cloning and site directed mutagenesis 104
3.3.2 Protein production and purification 105
3.4 Comparison of hydrolytic activities of NDM variants 106
3.4.1 Steady-state kinetic analyses 106
3.4.2 Investigation of inhibition by nitrocefin 112
3.5 Biophysical characterisation of NDM variants 114
3.5.1 Secondary structure analyses by Circular Dichroism (CD) 114
3.5.2 Investigation of thermal stability of NDM variants 116
3.6 Summary 119
3.7 References 120
Chapter 4: Role of M154L Substitution in the Activity and Stability of NDM Variants 127
4.1 Introduction 129
4.1.1 NDM substitutions 130
4.1.2 Chapter Objectives 131
4.2 Protein production 132
4.2.1 Cloning and Mutagenesis 132
4.2.2 Purification of Recombinant NDM Variants 133
4.2.3 Size Exclusion Chromatography-Multi-Angle Light Scattering (SEC-MALS) Analyses 134
4.3 Hydrolysis of Cephalosporins by NDM variants 135
4.3.1 Steady-State Kinetic Analyses 135
4.4 Crystallographic analyses of NDM variants 139

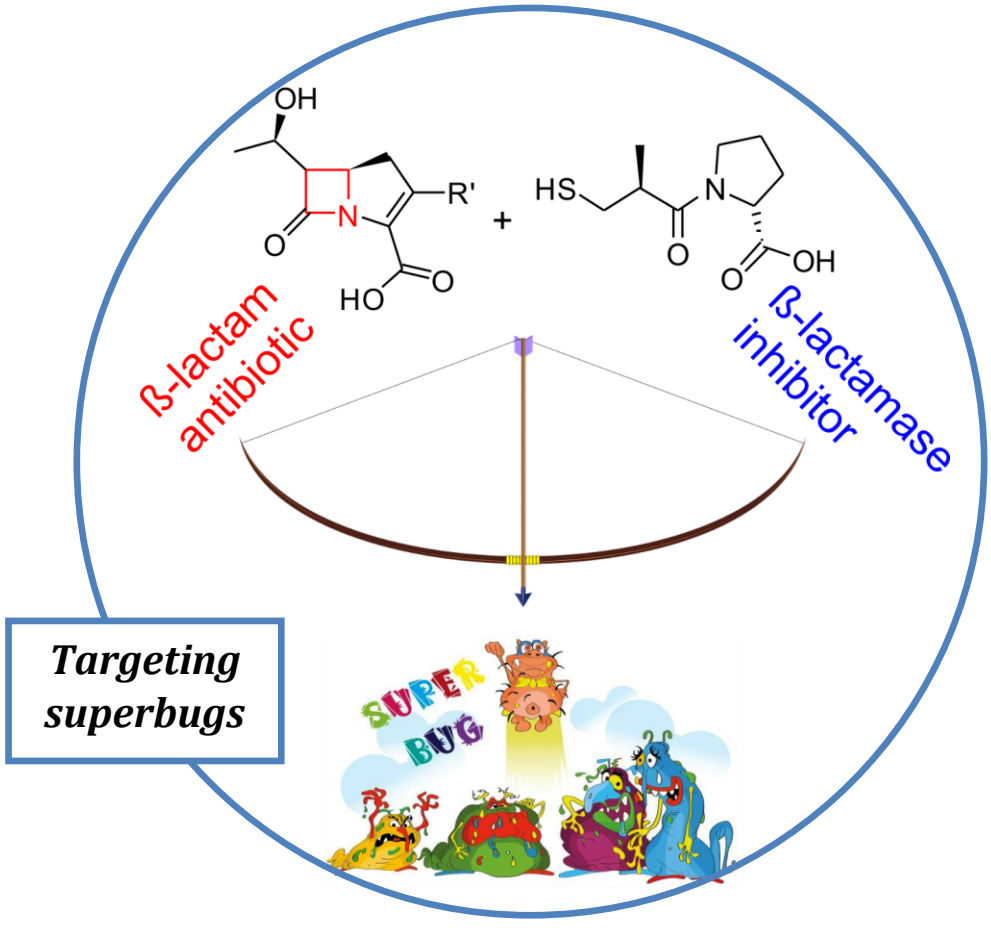
4.4.1 Overall Structural Properties of NDM Variants 139
4.5 M154L substitution influence on stability of NDM Variants 144
4.5.1 Circular Dichroism Analyses (CD) 144
4.5.2 Dynamic Scanning Calorimetric Analyses 146
4.5.3 Cellular Thermal Shift Assays (CETSA) 148
4.6 Summary 151
4.7 References 152
Chapter 5: Comparison of stability and inhibition profiles of Verona Integron-Borne Metallo-β-lactamase (VIM) Variants 160
5.1 Introduction 162
5.1.1 Evolution and Biochemistry of VIM variants 162
5.1.2 Chapter Objectives 165
5.2 Production and purification of Recombinant VIM variants 166
5.2.1 Cloning and Mutagenesis 166
5.2.2 Protein production and purification 167
5.2.3 Mass spectrometric analyses 167
5.3 Functional Analyses of VIM variants 169
5.3.1 Steady-state kinetic analyses 169
5.4 Inhibition profiles of VIM variants 174
5.4.1 Determination of residual activities 174
5.4.2 Differential inhibition of VIM variants 176
5.5 Biophysical characterisation 178
5.5.1 Structural properties of VIM-5 178
5.5.2 Investigation of thermal stability 179
5.5.3 Crystallographic Analyses of VIM-5 181
5.6 Summary 186
5.7 References 187

Chapter 6: Conclusions and future work 194
6.1 **CLS405**: An efficient substrate for screening MBL activity and inhibition.....196
6.2 **FC-5**: A potential substrate for cell-based assays 197
6.3 MBL variants display similar hydrolytic efficiencies 198
6.4 Protein Stability: a potential driver the evolution of MBLs.....198
6.5 Evolution of MBLs affects inhibitor development 200
6.6 Structural analyses reveal subtle but crucial interactions 201
6.7 General conclusions 202
6.8 References 203
Chapter 7: Appendices..... 204
7.1 Reagents and general practice.....206
7.2 Molecular biology 206
7.2.1 Site-directed mutagenesis..... 206
7.2.2 Transformation 207
7.2.3 Preparation of competent cells 208
7.3 Protein production.....208
7.3.1 Bacterial growth media..... 208
7.3.2 Protein expression trials..... 210
7.3.3 Large scale protein production 210
7.4 Protein Purification.....212
7.4.1 Protein purification buffers 213
7.4.2 Cell lysis..... 213
7.4.3 Purification protocol 213
7.4.4 Determination of protein concentrations 214
7.4.5 SDS PAGE analyses..... 214
7.4.6 Western blot analysis..... 215
7.5 Mass Spectrometric analyses 216

7.5.1 Non-denaturing mass spectrometry 216
7.5.2 Denaturing mass spectrometry 217
7.6 Enzyme assays 217
7.6.1 Steady-state kinetic assays 218
7.6.2 Enzyme Inhibition assay 218

CHAPTER 1: INTRODUCTION

Since their introduction over 75 years ago, β-lactam antibacterials have been of paramount clinical importance. Today they remain some of the most frequently prescribed antibiotics for the treatment of bacterial infections. The emergence and proliferation of resistance mechanisms including the production of β-lactamases, however, threatens to render this important class of antibiotics much less effective, especially against multi-drug-resistant Gram-negative bacteria. This introductory chapter provides a brief history of the development of β-lactam antibacterials as therapeutic agents and gives a contemporary overview of the structural and functional properties of the different classes of β-lactamases. Selected β-lactamase inhibitors are discussed with a focus on considerations for future inhibitor development programs. This chapter also outlines the motivations and objectives of the work described in this thesis.



CONTENTS

CHAPTER 1: INTRODUCTION 1

1.1 ANTIBIOTICS: THE SILVER BULLET 3

1.2 β-LACTAM ANTIBACTERIALS 5

1.2.1 Penicillins: A brief History 6

1.2.2 Mechanism of action of β–lactam antibacterials 10

1.3 β-LACTAM ANTIBACTERIAL RESISTANCE MECHANISMS 11

1.3.1 β-Lactamases 13

1.4 METALLO-β-LACTAMASES 15

1.4.1 Class B metallo-β-lactamases (MBLs) 16

1.4.2 Classification of MBLs 17

1.4.3 Structural features of MBLs 18

1.4.4 MBL-mediated β-lactam hydrolysis 22

1.5 EVOLUTION OF B1 MBLs 29

1.5.1 Influencing ligand binding 31

1.5.2 Improving biophysical properties 32

1.6 β-LACTAMASE INHIBITOR DEVELOPMENT 34

1.6.1 Serine β-lactamase inhibitors 34

1.6.2 MBL inhibitor development 36

1.7 SUMMARY 42

1.8 RESEARCH OBJECTIVES 43

1.9 REFERENCES 44

1.1 ANTIBIOTICS: THE SILVER BULLET

Throughout history, the emergence of infectious diseases has raised significant public health concerns including as associated with historically famous plagues. Infectious diseases remain an important global health concern, and increasingly so, given the rise of severe drug resistant nosocomial infections[1,2]. Following the pioneering work of Paul Ehrlich with arsenic containing compounds[3], scientists and physicians have employed various strategies to combat infections with small molecule drugs. One of the most successful infection control strategies involves the use of antibiotics. Antibiotic, a term coined by Selman Waksman in the 1940s, describes small molecules that antagonise the growth of microbes[4,5].

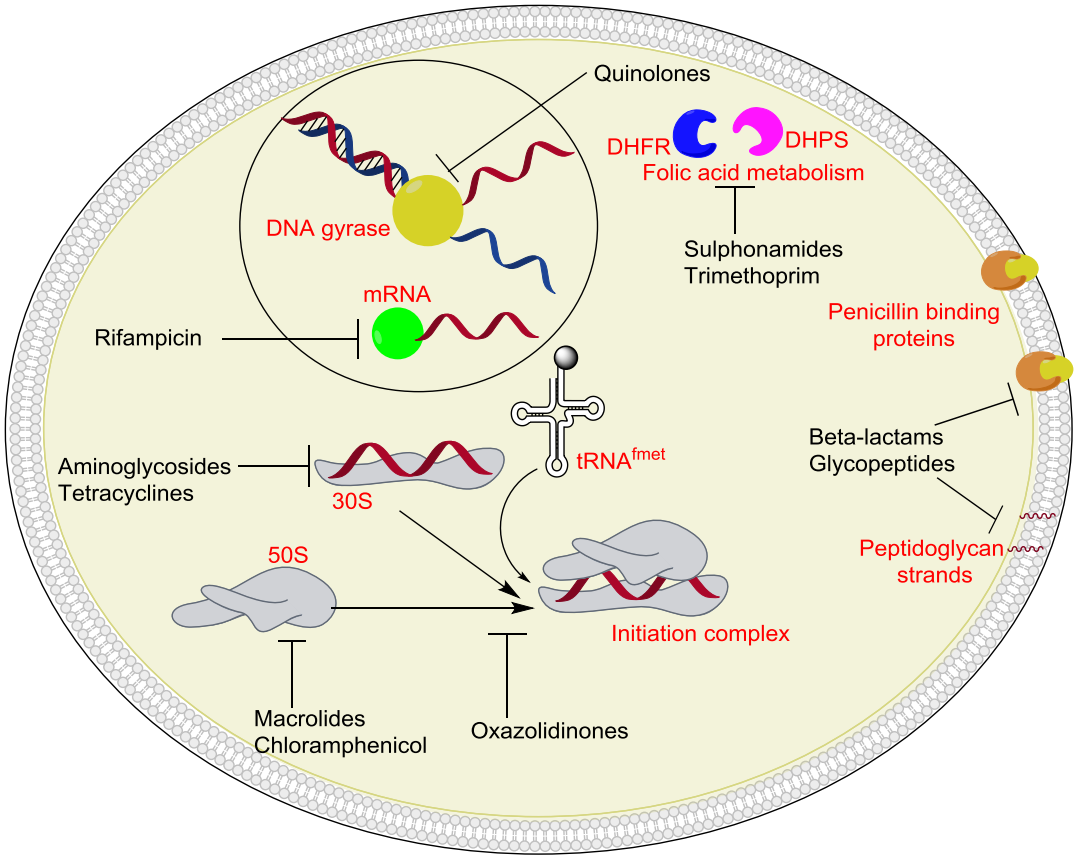


***Figure 1-1*: An illustration of established antibacterial agents (black) and their respective bacterial targets (red); DNA replication machinery (quinolones), DNA-directed RNA synthesis (rifampicin), protein synthesis (aminoglycosides, macrolides, oxazolidinones), metabolic enzymes (sulphonamides) and cell wall synthesis (β-lactams and glycopeptides).**

Antibacterials are antibiotics with activity specifically against bacteria. Established antibacterials exert their effects by interacting with specific bacterial protein targets including those involved in DNA and RNA replication, protein synthesis, cell wall synthesis and metabolic processes such as folic acid metabolism (*Figure 1-1*). The discovery and development of antibacterials revolutionised medical practice and ushered in a new age of often successful treatment, prevention, and control of infections, to the extent that some clinical experts proposed to 'close the book on infectious diseases'[2,6]. In some regard, it had seemed that the success of the contemporary antibacterials actually led to disinvestment in antibiotic discovery. As a consequence, the antibiotic pipeline appeared to dry up from early 1970s. Until the introduction of linezolid in 2000, the vast majority of developed antibiotics were analogues of existing drugs, with one exception being the Gram-positive topical antibiotic mupirocin introduced in 1985[7-9]. Only five new classes of antibiotics have been introduced for clinical use since 1970. In comparison 14 classes were introduced between 1935 and 1968 (*Figure 1-2*). This 'barren' period has been marked with increased global reports of the emergence and spread of antibiotic-resistant bacteria, gradually rendering current antibiotics ineffective.

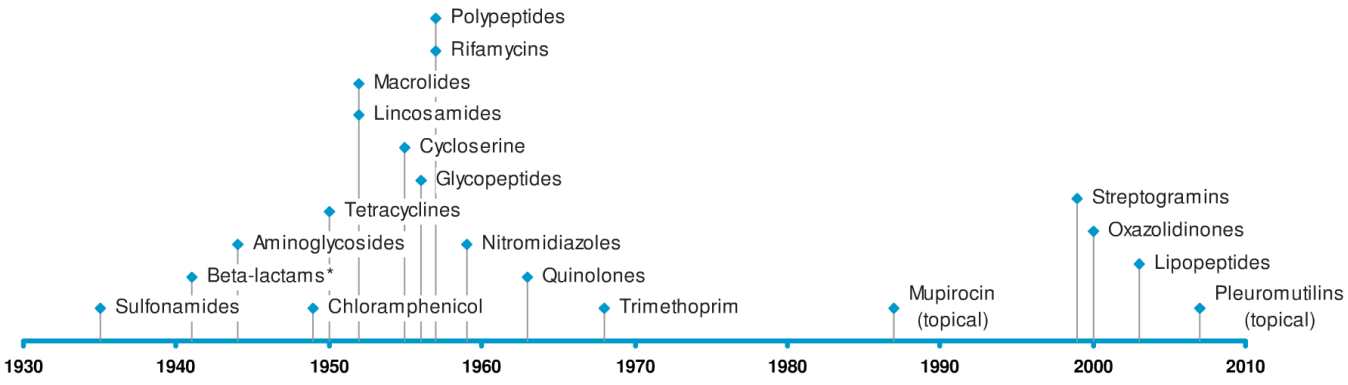


***Figure 1-2*: A timeline of antibacterials discovery showing the 'golden' era, the barren period and the renewed interest in the development of new antibacterials. Figure reproduced with permission from CDDEP policy brief (http://www.cddep.org/)**

Attempts are now being made to develop novel antibacterial agents, identify new bacterial targets and develop strategies to circumvent the emergence and spread of antibiotic resistance[10,11].

1.2 β-LACTAM ANTIBACTERIALS

Since their isolation and structural characterisation about 70 years ago, the β-lactams have remained a preferred class of antibacterials due to their high efficacy, affordability, and low toxicity[12,13]. The β-lactam antibacterials remain of immense clinical utility, being among the most frequently prescribed antibiotics for the treatment of bacterial infections[13]. The β-lactam antibacterial class is comprised of structurally different subtypes including the penams, cephems, carbapenems, and monobactams (*Figure 1-3*). The penams include both naturally occurring (i.e. fermented) penicillins e.g. benzylpenicillin and semi-synthetic derivatives (i.e. derived by synthetic modifications of fermented materials) such as ampicillin. The penems contain a β-lactam fused dihydrothiazole ring such as faropenem, with the sulfur atom being replaced by a carbon at C-1 in the carbapenems. The cephems include the classical cephalosporins derived from 7-aminocephalosporanic acid (7-ACA) and cephamycins, which are 7-α-methoxy-substituted cephalosporins, Monocyclic β-lactams such as aztreonam and nocarcidin, lack the β-lactam fused ring present in the penicillins, cephalosporins, and carbapenems (*Figure 1-3*).

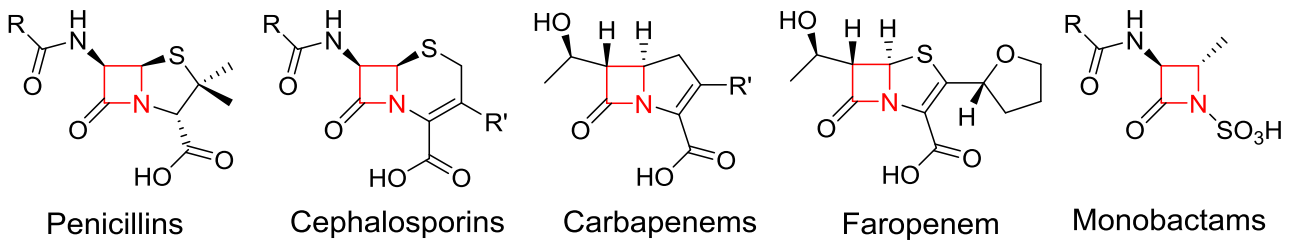


***Figure 1-3*: Structures of selected classes of β-lactam antibacterials.**

1.2.1 PENICILLINS: A BRIEF HISTORY

Way before Fleming's time, moulds formed an important part of antibacterial therapy with Chinese scribes apparently using mouldy soya beans in 3000 BC and Egyptian physicians prescribing "spoiled barley bread" for treating infected wounds[14]. More modern scientific approaches, as undertaken in the late 19th century, pioneered the study of the antibacterial properties of *Penicillium* species[15]. The scientific phase of penicillin research began with the English physician and bacteriologist John Sanderson, who, in 1871, showed that the presence of *Penicillium* prevented the growth of bacteria both in media and on the muscle tissue of a guinea pig[15]. Although Sanderson did not attribute the effect to the action of the fungus, his work inspired further studies by Joseph Lister, Williamson Roberts and John Tyndall amongst other researchers[16]. In France, the inhibitory effect of moulds on *Bacillus anthracis* was reported by Louis Pasteur and Jules Joubert, while in Belgium, Andre Gratia and Sara Dath verified that a *Penicillium* strain exhibited high bacteriolytic activity against *Bacillus anthracis*[17,18]. In many of these earlier studies, the antibacterial effect could not be solely attributed to penicillin or any other active metabolite produced by the fungi. It was not until the celebrated report by Alexander Fleming in 1929[19], that the inhibitory effect of *P. chrysogenum* on *Staphylococci*, was attributed to crude "penicillin" activity.

Needless to say, this and the earlier research laid the foundation for the subsequent isolation and widespread use of the natural and later synthetic penicillins. The realm of the modern development of penicillins as therapeutic agents began with the initial characterisation of the systemic activity and toxicity of penicillin by Howard Florey's team leading to the first systematic clinical trials in the 1940s [20,21].

Concerted multinational efforts led to the isolation and purification of the initial natural penicillins from *P. chrysogenuma*. In efforts to improve the yield and potency of natural penicillin, it was discovered that fermentation methods using corn-steep liquor yielded penicillin G (benzylpenicillin), due to the presence of phenylacetate (*Figure 1-4*)[22]. Another marked event in the penicillins story is the solution of the β-lactam-containing ring structure of penicillin 1945 by Dorothy Hodgkin[23]. These and other pivotal events initiated research into the chemical modifications of penicillins by altering fungal strains and media compositions as well as introducing synthetic chemistry steps[24,25], spurring the discovery of penicillin derivatives.

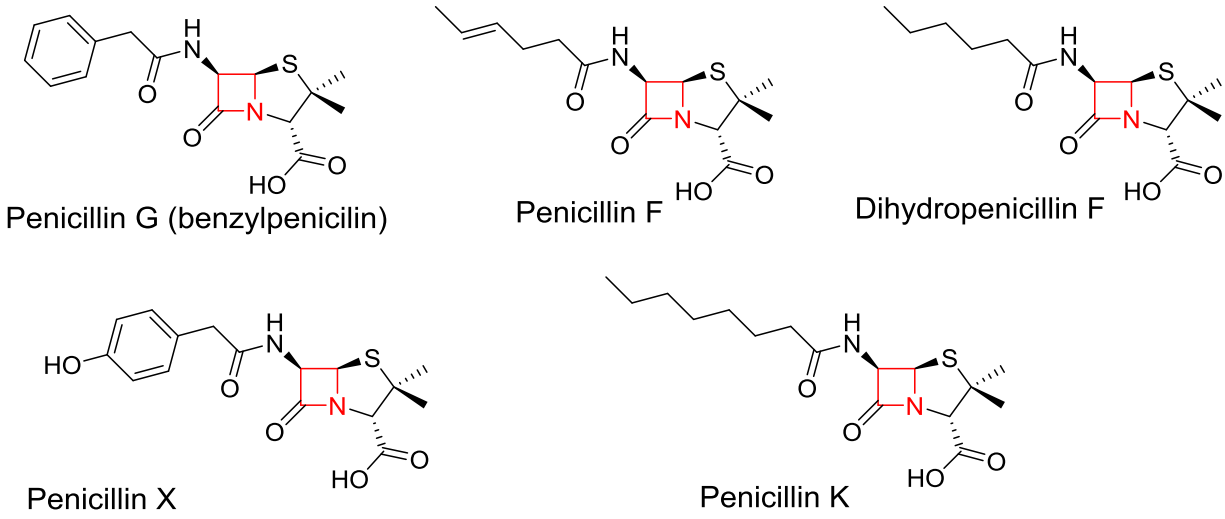


Figure 1-4: **Structures of the first isolated and purified natural penicillins, with the β-lactam ring highlighted in red.**

The β-lactam nucleus, 6-aminopenicillanic acid (6-APA) proved to be key in penicillin synthesis and modification. The initial work by Sheehan and Logan lead to the production of penicillin V via the acylation of chemically synthesized 6-APA and helped to pioneer the mass production of novel semi-synthetic β-lactam antibiotics (e.g. methicillin and ampicillin) by adding 'unnatural' side chains to the 6-APA core[26,27].

Even with the increased focus on semi-synthetic penicillins, the exploration of natural β-lactam compounds was still of interest. A new class β-lactam antibiotics was identified with the isolation of cephalosporin C from a strain of *Cephalosporium acremonium*, by Abraham and Newton in 1961[28]. Cephalosporin C showed low, but relatively broad activity, and more importantly, was, at least partially, resistant to hydrolysis by penicillinases. The cephalosporin nucleus, 7-aminocephalosporinic acid (7-ACA) has since been used as a precursor for extensive chemical modification for the production of different generations of cephalosporins, with potent broad-spectrum activity[12]. The semi-synthetic cephalosporins are commonly grouped into four generations, based on their ring substitutions and antibacterial activity[14,29].

Towards the end of the 1960s, industrial screens for β-lactamase inhibitors yielded a series of carbapenems identified in fermentation broths of *Streptomyces* species. These included thienamycin, and subsequently thienamycin derivatives such as imipenem[30,31]. Due to the susceptibility of the naturally derived carbapenems to hydrolysis by the renal dehydropeptidase (DHP-I), imipenem was co-administered with a DHP-1 inhibitor cilastatin. This problem was later circumvented with the synthesis of analogues with a 1 β-methyl substituent (meropenem, ertapenem, doripenem) which retained potent antibacterial activity and were stable towards DHP-1[32].

Monocyclic β-lactams were also identified in industrial β-lactamase inhibitor screens, with norcacidin, formadicin and sulfazecin being isolated from *Nocardia uniformis tsuyamanensis*, *Flexibacter alginoliquefaciens*, and *Pseudomonas acidophila*, respectively[14]. Later, synthetic approaches starting from the azetidinone ring led to the discovery of the first marketed monobactam, aztreonam as well as carumonam and tigemonam[33-35]. Although they are readily hydrolysed by class A extended spectrum

β-lactamases (ESBLs), monobactams are inhibitors of most class C β-lactamases and importantly they are not hydrolysed by metallo-β-lactamases (MBLs) (discussed in subsequent sections).

β-Lactam antibacterials have thus continued to provide much needed antibacterial chemotherapy options, with the derivatisation of naturally occurring or synthetic compounds, further expanding the antibacterial spectrum of β-lactam agents (*Figure 1-5*).

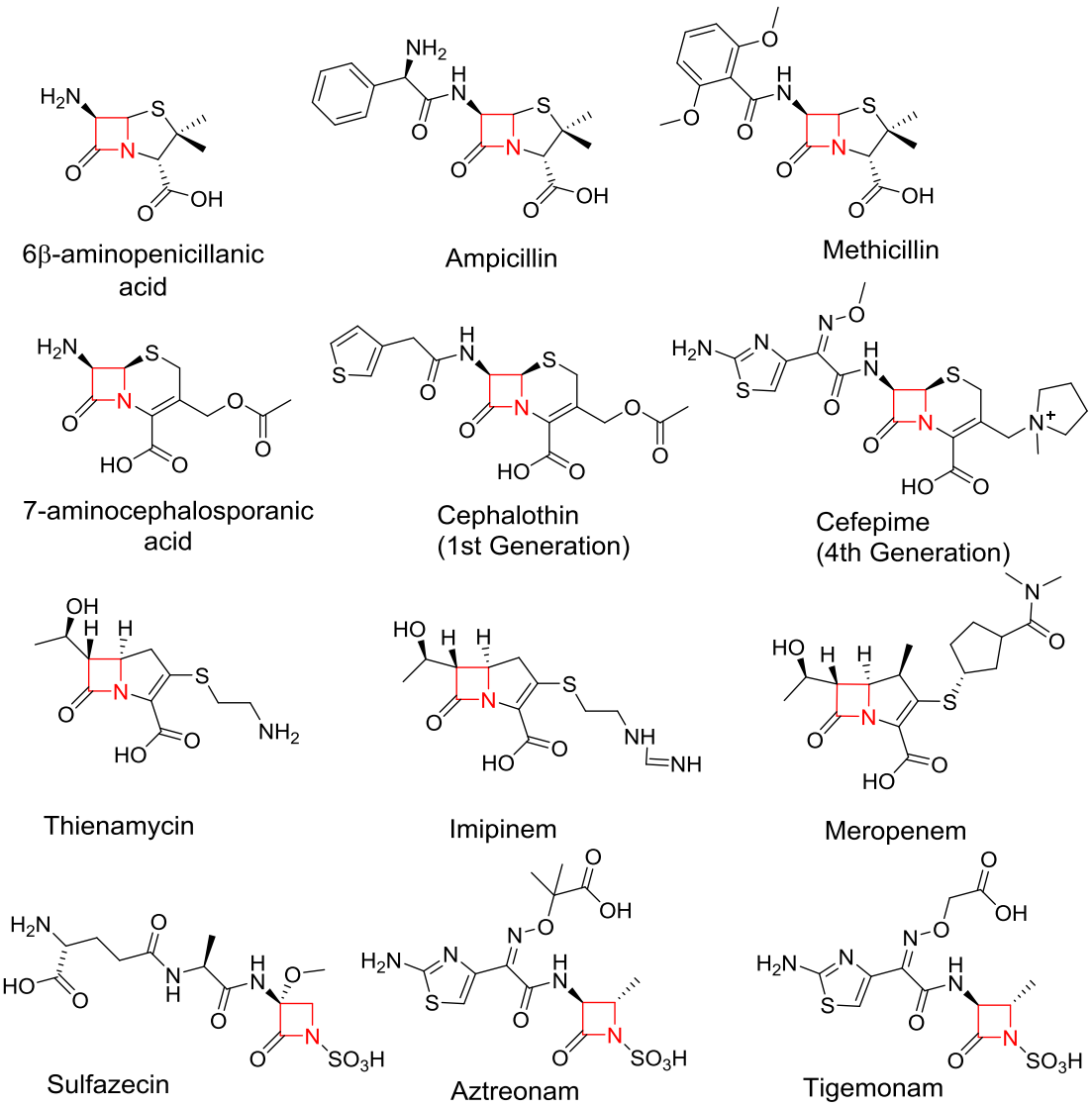


Figure 1-5: **Structures of representative β-lactam antibacterials from the penicillin, cephalosporin, carbapenems and monobactam classes. The β-lactam ring is indicated in red.**

1.2.2 MECHANISM OF ACTION OF β–LACTAM ANTIBACTERIALS

In the mid 1960's, Tipper and Strominger proposed that penicillins act as structural analogues of the acyl-D-alanyl-D-alanine terminus of peptidoglycan strands, and as such can effectively bind and inhibit peptidoglycan transpeptidases (penicillin binding proteins/PBPs)[36]. Several studies then validated that penicillins exert their bactericidal effect by inhibiting a late step in cell wall synthesis i.e. the crosslinking of the peptide chains of the peptidoglycan strands[37-40]. Mechanistic studies have revealed that β-lactam antibiotics bind covalently to PBPs via an active site serine residue to form stable acyl-enzyme complexes, and thus compete with the D-alanyl-D-alanine substrate for binding to the active site (*Figure 1-6*). It has also been noted that β-lactams might mimic the transition state for active-site serine acylation of PBPs[41-43].

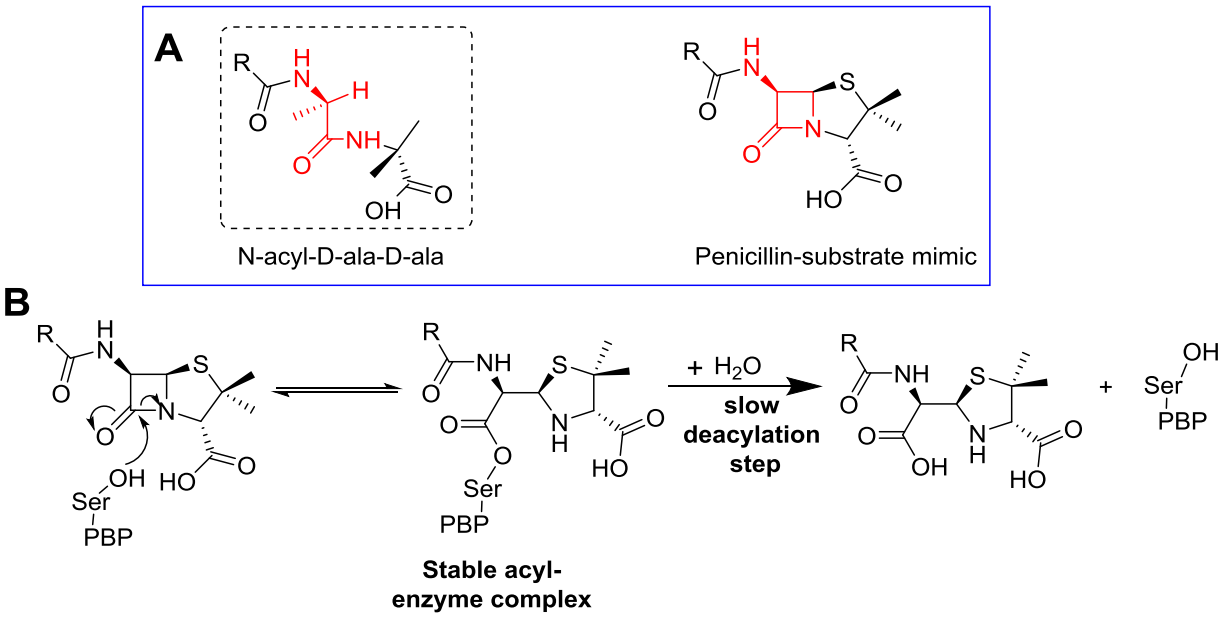


***Figure 1-6*: A) Structural similarities of penicillin β-lactam core to the PBP's D-ala-D-ala substrate; B) Scheme of inhibition of PBPs by β-lactam antibiotics involving the formation of a stable acyl enzyme complex.**

Although the specific molecular details of the bactericidal effects of β-lactam antibiotics are still being unravelled, the inhibition of PBPs by β-lactam antibiotics has been shown to halt cell wall synthesis, inhibit cell growth by compromising the

integrity of the cell-wall and eventually lead to cell lysis due to osmotic pressure[44-46]. By having very specific and essential bacterial targets with no human protein analogues (PBPs), β-lactam antibiotics have been able to maintain a reliable clinical efficacy and reduced toxicity.

1.3 β-LACTAM ANTIBACTERIAL RESISTANCE MECHANISMS

In what was possibly the first report of bacteria resistance to penicillins, John Tyndall observed a persistence of some healthy bacteria in the presence of the *Penicillium* mould and reported that in that case, the bacteria had an 'upper-hand in the fight for existence'[47]. Wide-ranging studies have since identified innate and acquired mechanisms by which bacteria develop resistance in response to attack by β-lactam antimicrobials (*Figure 1-7*)[48]. One response to the rise of antimicrobial resistance to β-lactam antibacterials has been to modify existing drug scaffolds to increase their spectrum of activity and overcome resistance mechanisms. The development of the cephems and carbapenems following the discovery of penicillins is a good example of this approach. However, as the antibacterial arsenal undergoes 'evolution' by stepwise tailoring of core scaffolds, many bacteria, in turn, have adapted to counteract these drugs. Mechanisms by which bacteria develop resistance to β-lactam antimicrobials include the following *(Figure 1-7)*:-

Target modification: By acquiring mutations in PBP genes resulting in the modification of the PBP active site, bacteria are able to maintain the functions of the PBPs while significantly lowering the affinity of the enzymes to β-lactam antibacterials. This phenomenon is exemplified by the acquisition of *mecA* gene, which encodes for the β-lactam resistant PBP2a, by resistant strains of *Staphylococcus* species[49].

Reduced permeability: Reduced outer membrane permeability by porin loss or changes in porin structure can confer resistance by limiting the entry of β-lactam antibacterials. Resistance to meropenem and imipenem has been shown to be mediated by loss of the outer membrane proteins OprD and CarO in *Pseudomonas aeruginosa* and multi-drug resistant *Acinetobacter baumanni* respectively, both of which are bacteria responsible for severe hospital acquired infections[50,51].

Extrusion by efflux pumps: Multi-drug resistant Gram-negative pathogens, particularly the *Pseudomonas* and *Acinetobacter* species, overexpress efflux pumps to actively extrude the antibiotics from the periplasm to the environment, in a bid to reduce the effective concentrations of β-lactam antibacterials in the cell[52].

Production of β-lactamases: The production of β-lactamases, enzymes catalysing the hydrolysis of the β-lactam ring, is arguably the most common and important mechanism of resistance to β-lactam antibacterial exposure. This mechanism is main focus of this thesis.

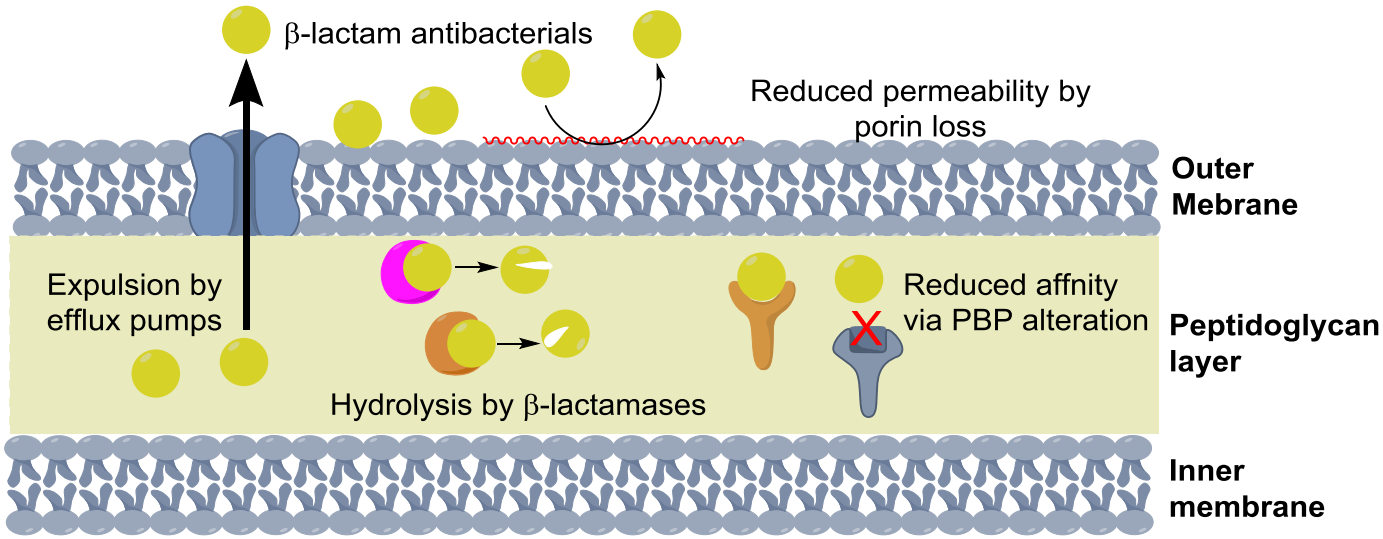


Figure 1-7: **The four main mechanisms of resistance to β-lactam antibacterials.**

1.3.1 β-LACTAMASES

An early detailed description of the resistance of Gram-negative bacteria to penicillin was provided by Fleming in 1929[53], but the first penicillinase/β-lactamase enzyme was identified much later by Abraham and Chain in *Bacillus coli* (now named *Escherichia coli*), about a decade later[54].

β-Lactamases were not considered to be of significant clinical relevance until the isolation of 'penicillin inactivators' from the clinical pathogen *Staphylococcus aureus* became a major clinical problem by the late 1950s[55]. Selection pressure from antibiotics coupled with rapid bacteria replication and the associated high mutation frequency has since resulted in the escalation of the numbers of reported β-lactamases to >1,300 as of 2013[56].

1.3.1.1 SERINE β-LACTAMASES

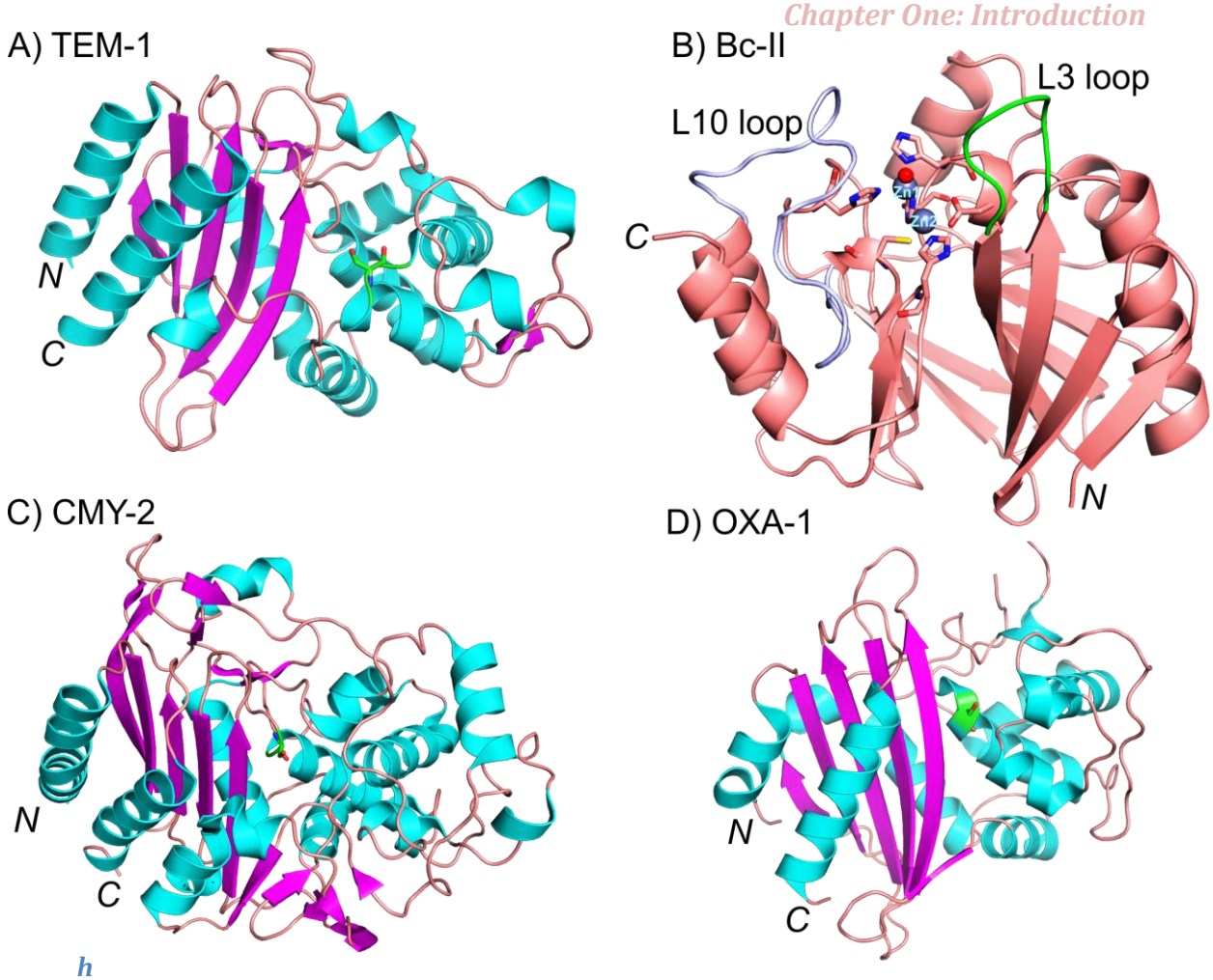
Based on the amino acid sequence similarities and catalytic mechanisms, β-lactamases are broadly classified into two mechanistically distinct groups; serine β-lactamases (SBLs) which employ a hydrolysis mechanism involving a nucleophilic serine residue and metallo-β-lactamases (MBLs), which require metal ions for catalysis[57-59] .

SBLs can be further categorised into class A (penicillinases), class C (cephalosporinases) and class D (oxacillinases) based on their amino acid sequence similarity and substrate profiles[57] (*Figure 1-8*). Class A SBLs are the most widely studied β-lactamases and comprise of over 90 enzymes including TEM and SHV enzymes as well as the extended-spectrum β-lactamases (ESBLs), CTX-M, and the carbapenem hydrolysing enzymes IMI, SME, and KPC[60].

Although many of class A SBLS are sensitive to commercially available SBL inhibitors, inhibitor resistant TEM and SHV enzymes continue to be reported worldwide[56].

Class C SBLs including CMY-2, P99, ACT-1, and DHA-1, are generally chromosomally encoded although plasmid-borne enzymes are becoming more prevalent[61]. Bacteria producing class C SBLs are mostly susceptible to carbapenems, although carbapenems resistance does arise in organisms with overproduction of efflux pumps or porin loss[61]. In many *Enterobacteriaceae*, the expression of class C SBLs is inducible, and resistance is amplified by overexpression of the β-lactamases.

Initially categorised as oxacillinases, class D SBLs (OXAs) are also capable of conferring resistance to penicillins, cephalosporins, and carbapenems[57]. OXAs, both plasmid-mediated and chromosomally-encoded, have been identified mostly in *Acinetobacter baumannii* and *Pseudomonas aeruginosa*. With a few exceptions, class D SBLs are generally resistant to inhibition by class A SBL inhibitors, i.e. clavulanic acid, sulbactam and tazobactam (see below), but their activities have been reported to be inhibited *in vitro* by sodium chloride[62,63].



h

***Figure 1.8*: 'Family portrait' of β-lactamases showing views from crystal structures of representative enzymes from Class A (TEM-1, PDB code: 1ZG4[64]), Class B (Bc-II; PDB code: 1BVT[65]), Class C (CMY-2, PDB code: 1ZC2) and Class D (OXA-1, PDB code: 1M6K[66]). The SBLs active site serine residues are shown as green sticks and the zinc (II) ions (grey spheres), the hydrolytic water (red sphere) and coordinating residues (in sticks) are shown for Bc-II.**

1.4 METALLO-β-LACTAMASES

The metallo-β-lactamase (MBL) fold enzymes belong to family of metallohydrolases, sharing a common αββα sandwich scaffold and a similar metal-binding motif[67]. The MBL superfamily is presently estimated to include > 34,000 members, widely distributed in nature and catalysing a myriad of reactions[68]. The MBL fold enzymes are generally classified into 16 groups based on their biological functions[67], including class B β-lactamase, glyoxalases, flavoproteins, arylsulfatases, DNA and RNA

processing enzymes and methyl parathion hydrolases among others[69]. The β-lactam-hydrolysing bacterial enzymes constitute the class B β-lactamases group (referred to as MBLs henceforth).

1.4.1 CLASS B METALLO-β-LACTAMASES (MBLs)

MBLs have emerged in the last two decades to become a significant mechanism of resistance to carbapenems, which are sometimes "last resort" β-lactam antibiotics used for the treatment of infections caused by multi-drug resistant pathogens[70]. Sabbath and Abraham reported the first MBL in 1966, a chromosomally encoded cephalosporinase from *Bacillus cereus*, whose activity was inhibited by EDTA[71]. For a long while after, MBLs were considered a scientific curiosity and not of great clinical relevance since they were commonly isolated in non-pathogenic or opportunistic organisms[68,72,73]. The situation drastically changed with the emergence and spread of acquired plasmid-mediated MBLs in nosocomial strains including *Pseudomonas aeruginosa*, *Bacteroides Fragilis* and *Chryseobacterium* (*Flavobacterium*) *meningosepticum* [74-76].

The efficient transfer of MBLs across unrelated bacterial species via horizontal gene transfer mechanisms largely accounts for the increased epidemiological reports of MBLs in multiple major Gram-negative pathogens, including members of the *Enterobacteriaceae, Pseudomonas* and *Acinetobacter* species[77-81]. MBLs have also been identified in environmental strains which might act as reservoirs for MBL genes[82-84]. From a clinical perspective, MBLs pose an increasing public health risk, in particular due to their ability to confer bacteria with resistance to virtually all β-lactam antibiotics, including the 'last resort' antibiotics such as carbapenems[85-87]. As previously mentioned, MBLs are not susceptible to the current therapeutically used

class A SBL inhibitors, resulting in a limited range of treatment options for infections caused by MBL producing bacteria. While MBLs do not hydrolyse monobactams such as aztreonam[85,88], MBL- producing organisms have been shown to co-produce SBLs which can efficiently hydrolyse aztreonam[89-91]. Additionally, mobile genetic elements encoding for MBLs tend to co-harbour genes conferring resistance to other antibiotics including quinolones and aminoglycosides giving rise to multi-drug resistant strains, thus limiting therapeutic options to the more toxic and sometimes less efficient antibiotics[92,93].

1.4.2 CLASSIFICATION OF MBLs

Due to variations in their sequences (in some cases < 20% similarity), substrate profiles and structures [94,95], MBLs are generally classified into three subclasses, B1, B2 and B3[96,97]. The B1 MBL subclass is the presently the largest group and contains several well-studied enzymes including Bc-II[71], IMP[98], VIM[99] and NDM[92] variants. The B1 subclass currently comprises 22 different enzyme groups, sharing more than 23% identity[60,68]. These enzymes are mostly encoded by mobile genetic elements including plasmids and transposons, and hence can be readily transferred among unrelated pathogenic bacteria. The B1 MBLs are dizinc enzymes, and exhibit a broad substrate profile with the ability to hydrolyse penicillins, carbapenems and cephalosporins, and are thus considered the most clinically relevant MBLs. They manifest a wide range of hydrolytic efficiencies *in vitro* and an equally broad range of in cell β-lactam antibacterial susceptibility profiles[95].

The B2 MBLs are a much smaller group, and include monozinc enzymes such as CphA and ImiS both from *Aeromonas* species and Sfh-I from an environmental isolate of *Serratia fonticola*[84,100,101]. The B2 MBLs have been proposed to be more phylogenetically similar to B1 class than B3 MBLs[102]. However, unlike the B1

MBLs, the B2 MBLs appear to be preferentially carbapenemases; and in some cases have been shown to be inhibited by the binding of a second zinc (II) ion[103,104].

Subclass B3 MBLs are a highly divergent group of MBLs (sharing as few as 9 conserved residues with the rest of MBLs) and have been identified mostly in environmental isolates such as *Stenotrophomonas maltophilia* (L1)[73], *Janthinobacterium lividum* (THIN-B)[82], *Chryseobacterium meningosepticum* (GOB-1)[105], and *Legionella gormanii* (FEZ-1)[106]. The recently reported SMB-1 and AIM-1 enzymes were identified in *Serratia marcescens*[107] and *Pseudomonas aeruginosa*[108] clinical isolates, respectively. With the exception of the monozinc GOB-1, B3 enzymes contain a dinuclear metal center, closely resembling that of B1 enzymes although the zinc coordinating residues differ (discussed in the next section).

1.4.3 STRUCTURAL FEATURES OF MBLs

Crystallographic analyses of MBLs have enabled the identification of functionally crucial residues and continue to provide essential information for development of MBL inhibitors with more precisely defined targets. Pioneering X-ray crystallographic investigation of cadmium (II) bound Bc-II (3.5 Å)[109] provided insights into the Bc-II metal binding residues. A higher resolution structure of monozinc Bc-II (2.5 Å), was reported 8 years later [110] describing for the first time a compact αββα sandwich fold. The zinc (II) ion in this structure was coordinated by three histidine residues and a water molecule, and extended loop regions were observed connecting some of the secondary structure elements[110]. This work was followed by a series of reports of dizinc crystal structures for CcrA (1.85 Å)[111], Bc-II (1.9 Å)[112] and L1 (1.7 Å)[113]. So far, > 140 structures of B1 MBLs have been reported[60,114,115]. Collectively, these structures enable a structural and mechanistic comparison of the B1, B2 and B3 MBLs.

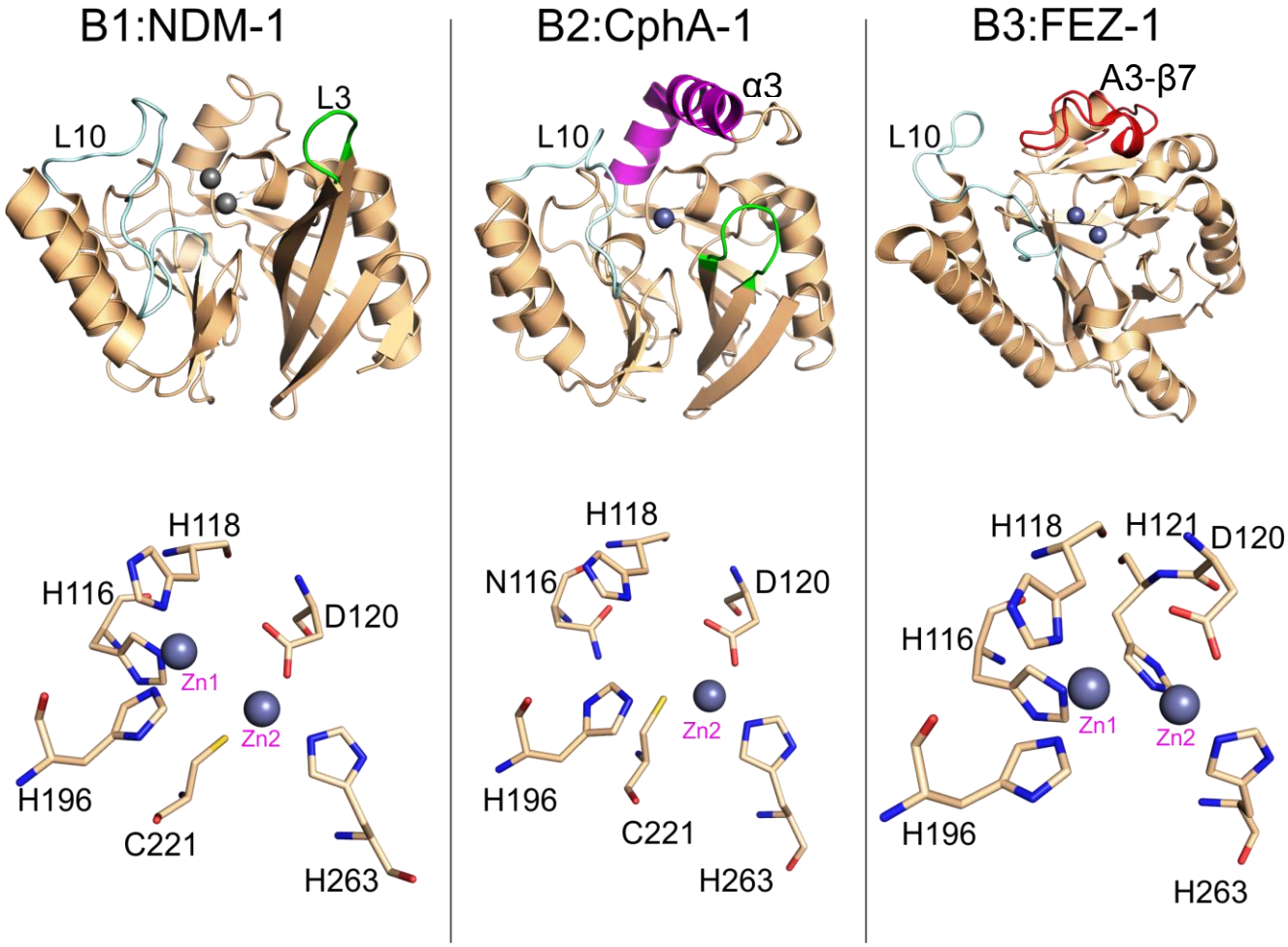


***Figure 1.9*: Ribbon representations showing the overall folds and view of the active site zinc coordination geometry of MBL subclasses. For the B1 enzyme NDM-1 (PDB code: 3SPU)[116], the active site loops L10 and L3 loops are marked in cyan and green respectively. For B2 enzyme CphA-1 (PDB code: 1X8G)[117], the *α3* loop is indicated in magenta and for the B3 enzyme FEZ-1 (PDB code: 1K07)[118], the *α3*-β7 loop is coloured red. Zinc (II) ions are shown as grey spheres in all structure.**

1.4.3.1 ACTIVE SITE GEOMETRY OF THE MBLs

Despite their often low amino acid sequence similarity, MBLs have common structural features including their characteristic αββα sandwich fold, comprising of two β-sheets at the core of the enzyme, flanked by five solvent-exposed α-helices (*Figure 1-9*). The zinc-binding active site is positioned at the bottom of a shallow groove in between the two β-sheets.

For the B1 enzymes, the first zinc ion (designated as Zn1 or 3H site) is coordinated in a tetrahedral geometry by three histidine residues (H116, H118, H196; according to the BBL numbering scheme[97]) and a bridging water/hydroxide ion (Wat1).

The second zinc site (Zn2/DCH site) assumes a trigonal bipyramidal coordination, with the D120, C221, and H263 metal binding ligands, the bridging water/hydroxide ion (Wat1) and an additional apical water molecule (Wat2)[119,120]. The two zinc (II) ions are in close proximity though the distances between them varies in different structures e.g. the distance between zinc ions in NDM-1 structures ranges on average from 3.4 Å to 4.6 Å. The zinc binding ligands are conserved in the B1 subclass but differ in the B2 and B3 enzymes (*Table 1-1*). Mutational analyses have validated the importance of these metal-binding residues, by showing that substitutions of these ligands greatly compromise the activities of the enzymes and are thus rarely tolerated[121,122].

***Table 1.1*: The zinc binding ligands in B1, B2 and B3 MBLs.**

Subclass	Zn1 ligands	Zn2 ligands
B1	H116, H118, H196	D120, C221, H263
B2	N116, H118, H196	D120, C221, H263
B3	Q/H116, H118, H196	D120, H121, H263

1.4.3.2 ACTIVE SITE LOOPS

Another important structural feature of MBLs is the presence of flexible L3 and L10 loops (*Figure 1-9*) flanking the active site that have been suggested to influence the substrate profiles of the MBLs[68,110]. Structural studies on B1 MBLs highlight the presence of a short mobile loop between the β3 and β4 sheets, commonly referred to as the L3 loop (residues 60-66), with most crystal structures showing very poor or missing electron density for this loop region[123].

The flexibility of this loop allows it to 'close' upon ligand binding forming hydrophobic interactions with substrates and inhibitors via aromatic residues on the loop (*Figure 1-10*)[119,123,124]. NMR-based structural and dynamic studies of inhibitor binding in Bc-II, CcrA and NDM-1 have validated the observed flexibility of the L3 loop and indeed its importance in substrate recognition[125-127]. Interestingly, the L3 loop is replaced by a tight turn in structures of SPM-1 and in B2 enzymes. SPM-1 instead possesses a central insertion of 24 amino acids in the region between α3-α4 helices; the deletion of this insertion seems to have marginal effects on the enzyme's activity[128]. Crystal structures of CphA reveal an elongated hydrophobic α3 helix (R140-L161), which serves to define the narrow active site of the enzyme and contribute to the binding of carbapenems substrates (*Figure 1-9*).

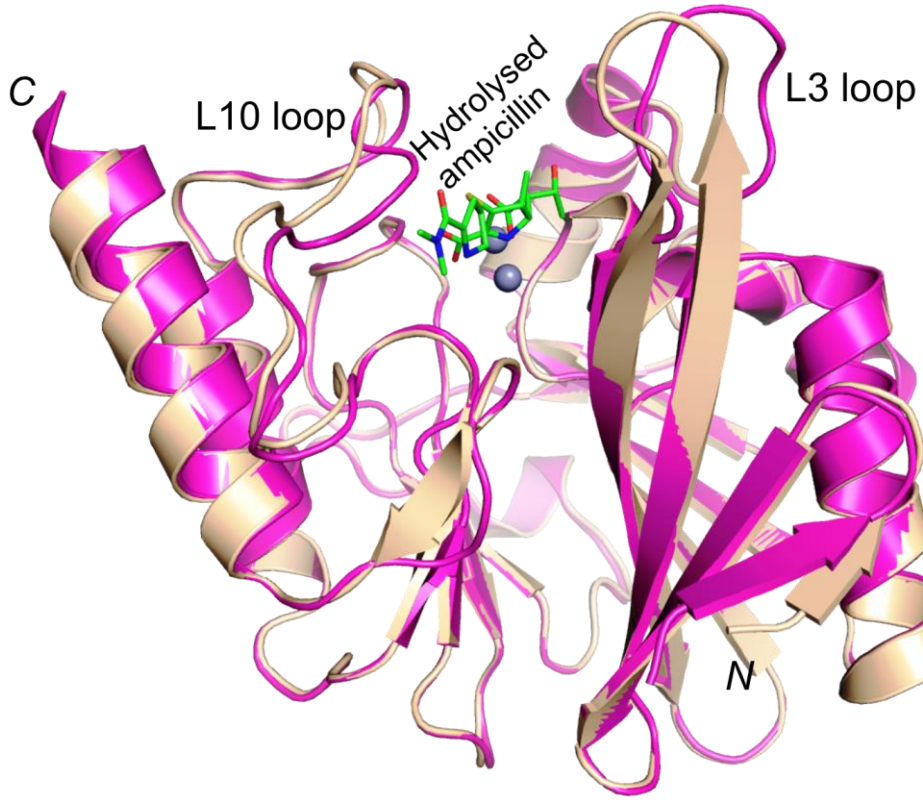
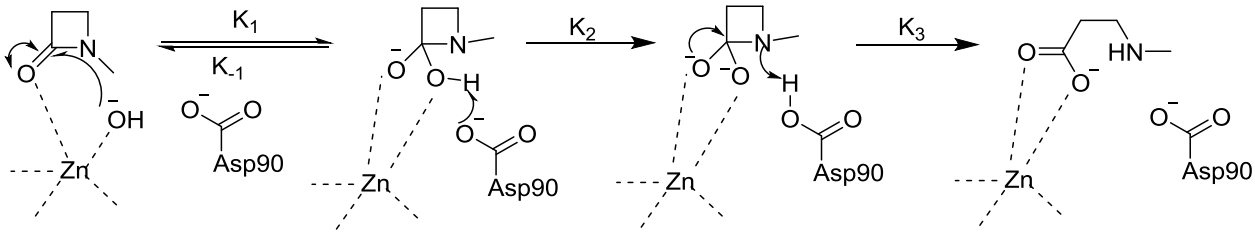


***Figure 1-10*: A superimposition of crystal structures of apo-NDM-1 in brown (PDB code: 3SPU) [116] and NDM-1 complexed with hydrolysed ampicillin in magenta (PDB code: 3Q6X)[129] revealing the shifting of the L3 and L10 loop upon ligand binding.**

Another equally important loop is the L10 loop, found between β11–α4 (residues 223–241). Structural analyses have shown that binding of β-lactam substrates is dependent on key interactions with conserved residues on the L10 loop including K224 (R228 in VIM-2) and N233. In IMP-1, the position 233 is more tolerant to substitutions, while variations at positon 224 tend to have detrimental effects on the enzymes' activity[95,114]. The Zn2 ligand C221 (C208 in NDM-1) is also on the L10 loop, and the conformation of the loop is said to be stabilised by hydrophobic interactions with Y229 in NDM-1, to facilitate ligand binding[129].

1.4.4 MBL-MEDIATED β-LACTAM HYDROLYSIS

Although the mechanism of action of MBLs is still being explored, the consensus is that β-lactam hydrolysis by MBLs involves the nucleophilic attack on the carbon of the carbonyl group of the antibiotics' β-lactam ring, followed by the C-N bond cleavage and the protonation of the amide nitrogen before the release of the hydrolysed product[130]. Shortly after the initial identification of Bc-II, a systematic analysis of metal requirements of the enzymes revealed that at least two metal ions (preferentially zinc (II)) could bind, with the second metal binding at a lower affinity[131]. Initial mechanistic studies on monozinc Bc-II (with the zinc (II) ion bound at the Zn1/Histidine site) proposed that the metal ion acts as a Lewis acid to provide the nucleophilic hydroxide ion by lowering the pK_a of zinc (II)-bound water[132]. It was suggested that reaction occurred via the formation of tetrahedral intermediates after the nucleophilic attack, with the dianionic form of the intermediate stabilised by the zinc (II) ion. The carboxylate anion of D90 (D120 using BBL numbering[97]) was proposed to act as a general base forming the dianion intermediate and also as the proton-donor to the β-lactam nitrogen, thus facilitating the β-lactam ring opening (Scheme 1-1)[68,132].



Scheme 1-1: The initially proposed mechanism for mono-zinc Bc-II, in which two intermediates (stabilised by Zn (II)) are formed and Asp90 acts as the proton donor[132].

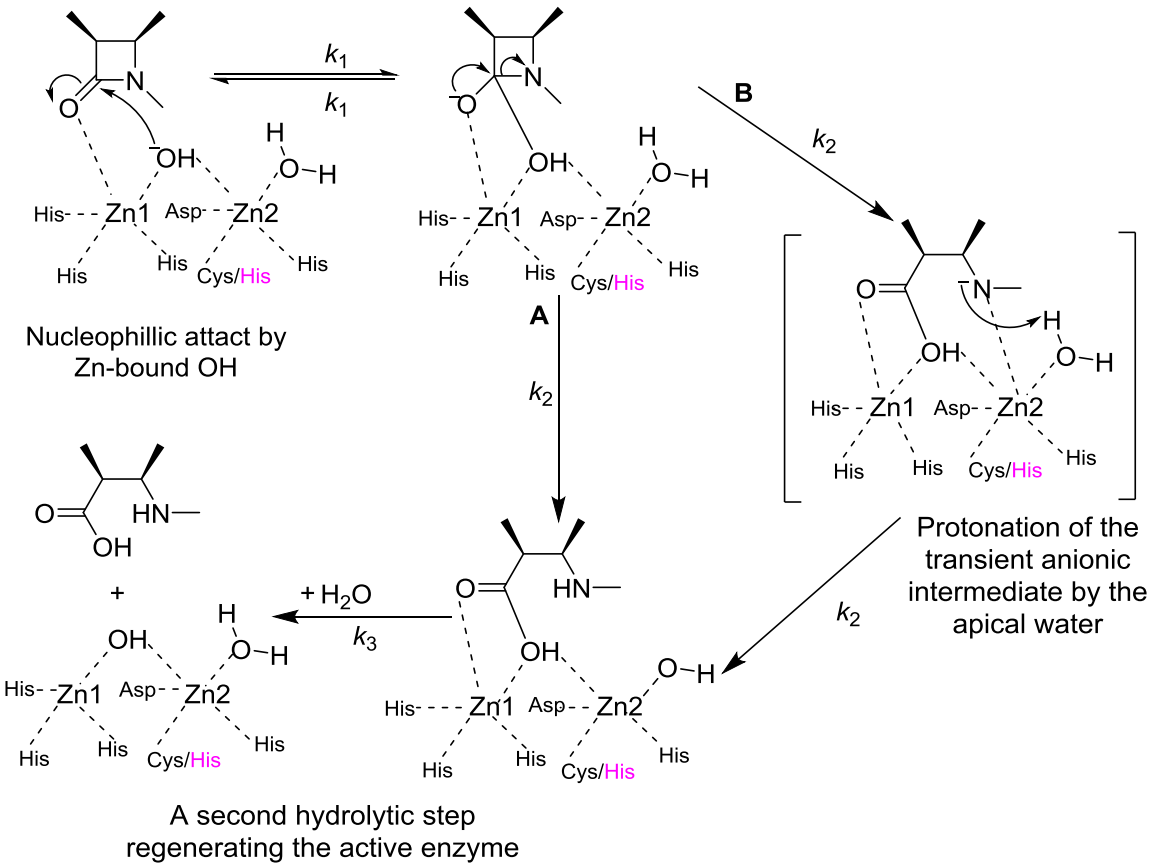
Various facets of this proposed mechanism have since been scrutinised by mutations of active site residues, steady-state and pre-steady-state kinetics, as well as crystallography and NMR analyses. The most contested issues include the precise roles of the zinc ions in catalysis, the identities and sources of the nucleophilic water and the proton and the sequence of the reaction steps, particularly with respect to the accumulation of reaction intermediates (for reviews see [14,115,132]).

1.4.4.1 HYDROLYSIS MECHANISM OF B1 AND B3 MBLs

As in many metallo-hydrolyses, there are several potential mechanistic roles for the zinc ions which may vary depending on the enzyme, substrate, and experimental conditions e.g. pH[133]. Although the metal-ion requirement in MBL-mediated hydrolysis of β-lactam antibiotics still remains a matter of debate[134], the catalytic mechanisms of the dizinc B1 MBLs including for Bc-II, CcrA, IMP-1 and NDM-1, and B3 MBLs (L1), have been studied in some detail[115,130].

Steady-state and pre-steady-state mechanistic analyses as well as crystallographic studies with product or intermediate bound enzyme complexes have provided information on the catalytic mechanisms of MBLs. Although the hydrolysis of the reporter substrates such as nitrocefin has been argued to be atypical[115], chromogenic reporter substrates including nitrocefin, chromacef and CENTA continue to be

employed as important mechanistic probes for spectroscopic analysis[135]. Substitution of the spectroscopically silent zinc (II) by divalent metal ions such as cobalt (II) has also facilitated the use of spectroscopic techniques for monitoring of the enzymatic changes during catalysis. The reduced activity of the cobalt (II)-substituted, compared to the zinc (II)-bound MBLs, enables efficient monitoring of both accumulation and loss of intermediate species[136].



***Scheme 1-2*: The presently proposed pathways for the hydrolysis of β-lactams by B1 and B3 MBLs, indicating possible reaction intermediates. C221 in B1 is replaced with H121 in B3 MBLs (in magenta). Figure adapted with permission from Moali *et al*[123].**

For the dizinc B1 and B3 MBLs, β-lactam hydrolysis is proposed to begin with the binding of the β-lactam substrate at the active site metal centre, with the carbonyl oxygen interacting with Zn1 and with Zn2 coordinating the carboxyl group on the 5- or 6-membered fused β-lactam substrate ring. It is presently accepted by most

researchers that the zinc ions coordinate the nucleophilic hydroxide and by lowering the pK_a of the bound water molecule[137]. The first zinc ion (Zn1) has been proposed to act as a Lewis acid co-ordinating the carbonyl oxygen, polarising the carbonyl bond to facilitate the nucleophilic attack by the metal bound hydroxide ion[130].

Pre-steady kinetic analyses on cobalt (II) substituted Bc-II indicated a branched kinetic mechanism with two enzyme intermediate species, ES1 (di-cobalt active enzyme intermediate) and ES2 (mononuclear and inactive enzyme intermediate), suggesting that the two metal ions are required for the hydrolytic activity of native class B1 MBLs[137-139]. In contrast, crystallographic analyses of mono and dizinc C221D mutants of Bc-II have been interpreted as suggesting that the Zn1 is sufficient for nucleophile activation while Zn2 is more essential for substrate binding, C-N bond cleavage and intermediate stabilization. This hypothesis is based on the lower nucleophilic potency of a bridging hydroxide in comparison to a terminal hydroxide[115,140].

The nucleophilic attack of the hydroxide ion on the carbonyl carbon leads to formation of a tetrahedral intermediate whose breakdown has been another issue of contention (*Scheme 1-2*). Two suggested possible fates of the tetrahedral intermediate involve the rate-limiting cleavage of the C-N bond concomitant with the protonation of the amide nitrogen, or alternatively, the C-N bond cleavage being followed by the accumulation of anionic nitrogen intermediate, whose protonation is rate-limiting[114].

Pre-steady-state kinetic analyses of nitrocefin hydrolysis by the B1 enzyme CcrA[141] and later with the B3 enzyme L1[142,143] provided evidence for a kinetic mechanism involving the accumulation of an enzyme-bound anionic nitrogen intermediate with an intense absorbance at 665 nm.

The protonation of the intermediate was initially proposed to be the rate-limiting step, although it was later argued that the atypical dinitrostyryl substituent on nitrocefin may be serve to selectively stabilise the observed intermediate. Later studies on L1-catalysed hydrolysis of cefaclor and meropenem, proposed that the rate-determining step was cleavage of the β-lactam amide bond, which occurs concomitantly to the protonation of the nitrogen of the β-lactam ring[144]. In contrast, subsequent stopped flow kinetic studies on IMP-type MBLs have shown that an anionic intermediate accumulate during the hydrolysis of meropenem and chromacef by IMP-25 and IMP-1[145]. Similarly, pre-steady-state kinetic studies for the NDM-1-mediated hydrolysis of nitrocefin and chromacef indicate that the NDM-1 kinetic mechanism involves a reactive nitrogen anion intermediate stabilised by Zn2, whose protonation is rate-limiting[146].

There is also evidence that hydrolysis of the carbapenem substrate meropenem by zinc (II) and cobalt (II) substituted SPM-1 proceeds via an anionic intermediate, (with a strong absorption at 408 nm), as previously proposed for Bc-II[136,147] (*Figure 1-11*).

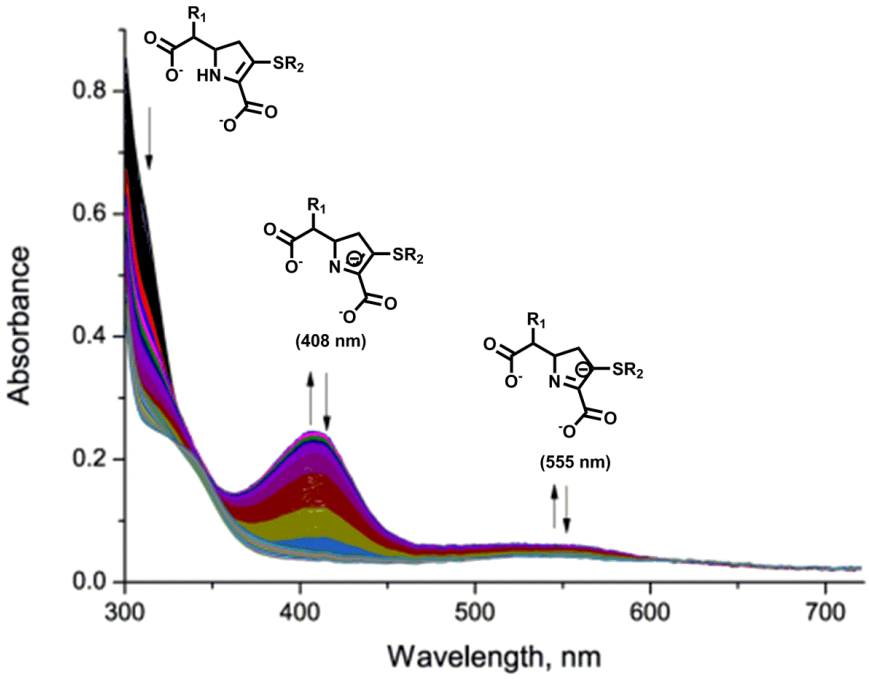


***Figure 1-11*: A proposed mechanism for the hydrolysis of imipenem by cobalt (II) substituted SPM-1 showing the accumulation of an anionic nitrogen intermediate (408 nm). Figure adapted from Brem *et al*[147].**

The protonation of the anionic nitrogen precedes the release of the hydrolysed product and the regeneration of the active enzyme. Mutational analyses of D120 argued against the earlier hypothesis that D120 was the (essential) proton donor[148], and indeed suggested that D120 did not have an essential role in nucleophilic activation[149]. It has been proposed that the carboxylic acid formed on β-lactam hydrolysis serves to protonate the nitrogen based on the structural analyses of NDM-1 with the hydrolyzed ampicillin product[129]. However, the general consensus is the proposal that a second (apical) water molecule coordinated by Zn2 is more likely to donate a proton to the leaving amine nitrogen[130,150,151].

The monozinc B2 enzymes display a narrow substrate profile, with carbapenems being the primary substrates. Crystallographic analyses of CphA and Sfh-1 MBLs reveal the binding of the zinc (II) on the second site (Zn2) and a hydrolytic water molecule coordinated by H118 and D120.

Based on the Sfhi-1 structure, it has been proposed that the hydrolytic water molecule is activated by His118 rather than by Asp120 and/or zinc (II)[152]. Structural analyses of biapenem-bound CphA revealed that the β-lactam carbonyl group is polarized by interaction with H196 (present in the Zn1 site) with the kinetic mechanism proposed to proceed via the accumulation of anionic nitrogen intermediate stabilized by Zn2 (*Figure 1-12*). The protonation of the nitrogen has been proposed to occur via a water molecule bound by H118 and D120 or via water bound to Zn2[117]. This proposed mechanism has however been challenged by QM/MM computational analyses demonstrating that the enzyme-intermediate complex observed in the crystal structure represents a stable intermediate or product in a minor pathway in CphA catalysis[153].

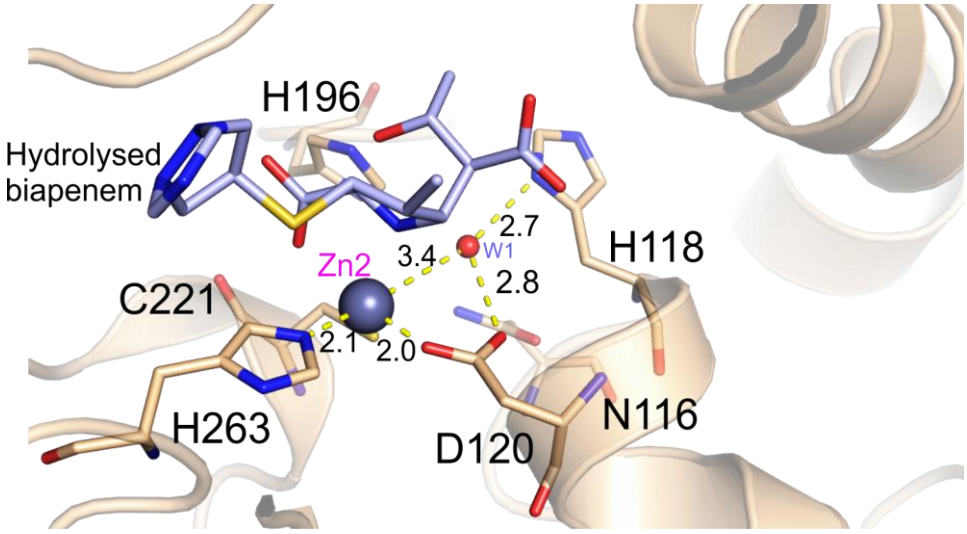


***Figure 1-12*: View from a structure of CphA-1 complexed with hydrolysed biapenem (PDB Code: 1X8I), showing the active site co-ordination of the hydrolytic water (red sphere) and zinc (II) ion (grey sphere). Yellow lines depict distances in Å[118].**

The heterogeneity of MBLs continues to raise interesting questions on their mechanistic features including the rate limiting steps (which may vary with the substrate) and the chemical nature of reaction intermediates. A comprehensive investigation of the mechanism of MBL catalysis will go a long way in facilitating rational design of potent MBL inhibitors.

1.5 EVOLUTION OF B1 MBLs

Despite having similar active site architecture, MBLs generally exhibit important structural and functional heterogeneity resulting in significant differences in substrate profiles[154]. Amongst the B1 enzymes, the IMP, VIM and NDM groups are presently the most clinically relevant, with their global spread and rapid evolution raising concerns for antimicrobial chemotherapy[70,95].

The IMP-1 enzyme, the first transferable MBL to be identified, was initially isolated from a *Pseudomonas aeruginosa* clinical isolate in Japan[75]. About two decades later, IMP-type enzymes have been reported worldwide in various pathogenic bacteria including *Enterobacteriacea* and *Acinetobacter* species. More than 50 IMP variants have been reported or assigned, thus far with amino acid sequence similarity between 80-99.6% with respect to IMP-1[155].

VIM enzymes are the second largest subgroup of the B1 MBLs, with 46 variants reported since the identification of VIM-1 in 1999[99]. Of the clinical variants of VIM types, VIM-2 is the most prevalent and widely distributed while VIM-7 is the most divergent of the VIM variants[156]. The more recently identified NDM-1 has 16 reported variants, with NDM-10 being the most divergent[157]. Analyses of mutation profiles of the three B1 MBL groups (IMP, VIM and NDM) demonstrated that the IMP variants are more evenly distributed over the sequence space while the VIM variants exhibit more directional evolution with formation of two major clusters; VIM-1 and VIM-2 (*Figure 1-13*)[94]. Since NDM-1 was identified more recently[92], NDM variants are still relatively fewer and as such are less diversified.

Since the variants of the different MBLs manifest similar overall folds, it has been proposed that substitutions on the flexible loops flanking the active site or on the second shell residues interacting with the zinc binding residues are the primary sites for fine-tuning the substrate profiles[158]. Changes with respect to the size, solubility, flexibility and conformation of these residues could influence the activity and folding stability of the resultant proteins[159].

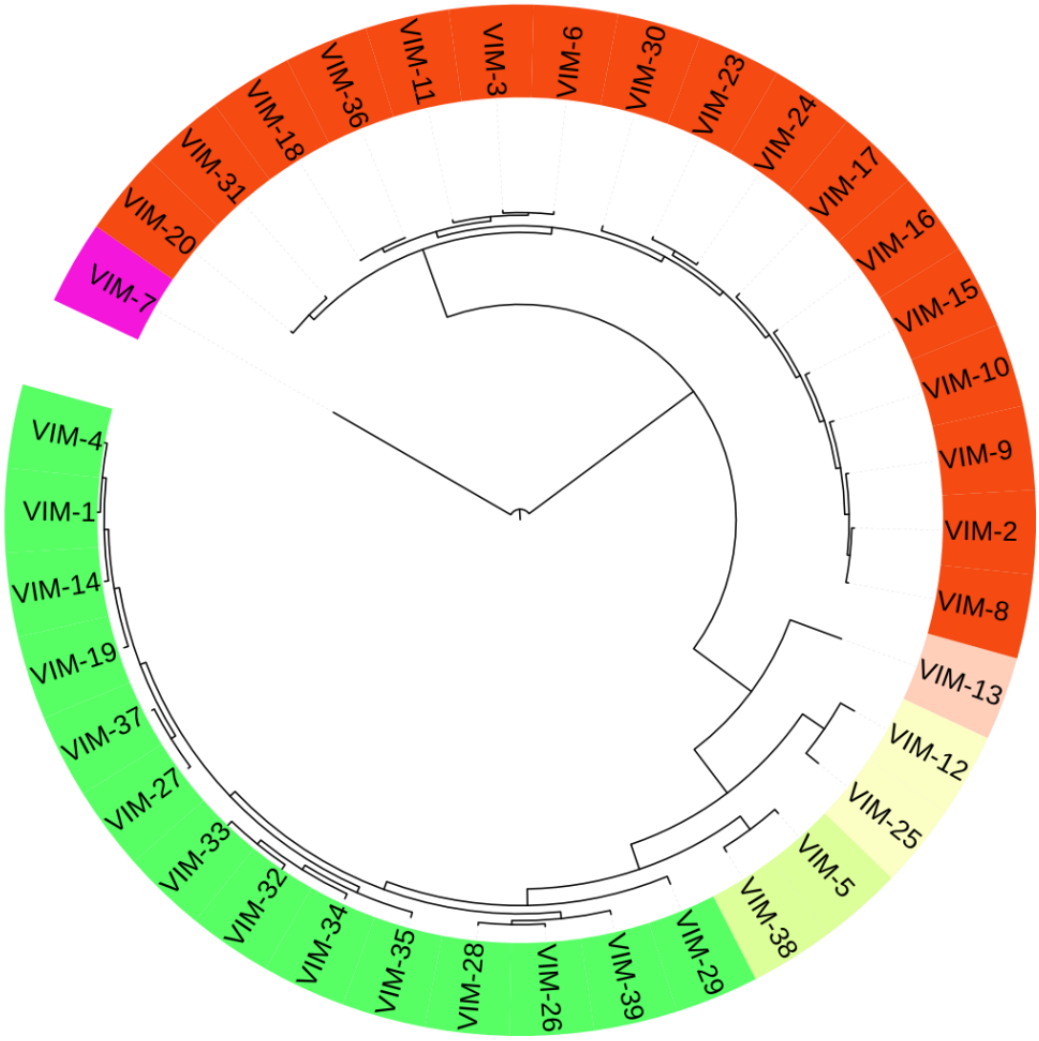


***Figure 1-13*: Phylogenetic analysis of VIM variants showing the main clusters, VIM-1 (green) and VIM-2 (red) as well as VIM-1/2 intermediate variants. The more divergent VIM-7 (purple) is also shown. The phylogenetic tree was generated using the Interactive Tree of Life (iTOL) program (http://itol.embl.de/).**

1.5.1 INFLUENCING LIGAND BINDING

The evolutionary pathways leading to improved catalytic efficiency toward β-lactam antibiotics among B1 enzymes are not completely clear[95]. However, the comparison of the substrate profiles of existing MBL variants provides valuable insights on the activity-driven evolution. For IMP variants, substitution at residue 262, located near the active site, proximal to the zinc (II) ligand H263, has been shown to influence their substrate profiles (*Figure 1-14*). Comparison of IMP variants containing S262 (IMP-1-like variants) with variants containing G262 (IMP-3, IMP-6 and IMP-25) revealed that the S262G substitution conferred improved activity towards newer carbapenems, particularly meropenem, an effect that came at the expense of penicillinase activity[160,161]. It has been proposed that serine or alanine residues at 262 support the zinc binding H263 thus facilitating the stabilisation of the enzyme-substrate complex, while V262 allows for a greater flexibility of H263[162,163]. The comparison of the importance of several residues for IMP-1 activity, demonstrated that the residue requirements were substrate specific, with S262 being important for hydrolysis of ampicillin, imipenem or cephaloridine and G262 essential for cefotaxime hydrolysis[164].

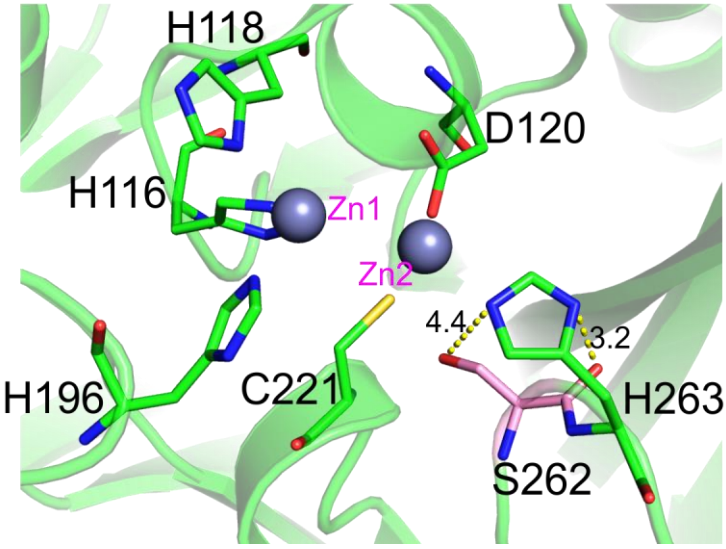


***Figure 1-14*: View from the structure of IMP-1 (PDB code: 1DDK) showing the proximity of the S262 t the zinc binding residue H263.**

For clinically observed VIM variants, the residues associated with changes in substrate profile are mostly located on the active site L3 and L10 loops. Despite being tolerant to substitutions, hydrophobic residues at positions 61 and 67 on the L3 loop have been shown to influence activity profiles by favouring interactions with hydrophobic side chains of β-lactam antibcterials and inhibitors[165,166]. The presence of H224 in VIM-7, VIM-1, and related variants has also been proposed to disrupt hydrogen-bonding networks close to the active site in comparison to VIM-2-like variants with Y224[167]. Variants containing R228 (mostly VIM-2 like enzymes), display lower efficiency against cephalosporins containing bulky positively charged C3 substituent in comparison VIM-1 like enzymes with S228, possibly due to the narrowing of the active site cavity by R228[154,168]. Further biochemical characterization of MBL variants particularly with respect to correlation of catalytic activity and *in vivo* antibiotic susceptibility is still required for reliable assessment of the roles of the clinically observed residue substitutions.

1.5.2 IMPROVING BIOPHYSICAL PROPERTIES

Studies on protein evolution have led to the proposal that loss of protein stability is a cost of improved catalytic efficiency/function[170]. Extensive studies on TEM SBLs support this 'stability-function' hypothesis with mutant enzymes increasing cephalosporinase activity with a concomitant loss in thermodynamic stability[169,170]. The biophysical drivers of evolution have not been sufficiently explored with respect to MBLs, although there is increasing evidence for changes in biophysical properties of emergent MBL variants (including the work reported in this thesis). Studies on IMP-1 demonstrated the importance of the solvent-exposed residue W87 on the stability of the enzymes[166]. Substitutions of the W87 with alanine or phenylalanine did not have significant effects on the activity but significantly decreased the stability

of the enzymes[166]. Remote substitutions in SPM-1 (G121S and S84G) have also been shown to exhibit higher metal-induced stabilisation, thus optimising the activity of the enzymes in lower zinc (II) concentrations[171]. Recently, computational analyses have identified residues on IMP and VIM variants whose substitution may have an effect on functional flexibility and structural stability of the enzymes, although a correlation of these predicted effects with experimental data is not apparent.

An in-depth understanding of the sequence and structural determinants of MBL function and substrate selectively enables the development of targeted MBL inhibitors and equally provide vital insights into the chemistry underlying protein evolution and design. Additionally, comparative analyses of MBL variants could provide insights into the evolutionary drivers of new variant MBLs and guide the development of strategies to circumvent the selection pressure. However, despite the growing numbers of MBL variants, there are as yet no consensus on protocols for the evaluation of the catalytic activity or β-lactam susceptibility of MBL producing strains.

A reliable comparison of the activity and biophysical profiles of MBL variants is therefore hampered by the differences in assay conditions, enzyme constructs, bacterial strains, and conflicting data interpretation. Comprehensive studies linking the structural and biophysical features of MBLs with overall organismal fitness of resistant bacterial strains would also be desirable.

1.6 β-LACTAMASE INHIBITOR DEVELOPMENT

1.6.1 SERINE β-LACTAMASE INHIBITORS

Historically, the rise of resistance has been combatted by developing β-lactamase stable antibiotics such extended-spectrum cephalosporins, carbapenems, and monobactams, and by identifying β-lactamase inhibitors to revive the efficacy of β-lactam antibiotics.

As mentioned earlier, class A SBLs inhibitors, including clavulanic acid, sulbactam and tazobactam are presently in clinical use in combination with various β-lactam antibiotics. Clavulanic acid, isolated from *Streptomyces clavuligerus* in the 1970s, was the first β-lactamase inhibitor to be used in clinical practice[63]. Clavulanic acid in combination with amoxicillin (augmentin) was shown to be effective against SBL producing *S. aureus, K. pneumoniae, Proteus mirabilis,* and *E. coli*[172]. Penicillinate sulphone tazobactam (used in combination with piperacillin) and sulbactam (combined ampicillin or cefoperazone), were synthesised in the early 1980's and are used for treatment of infections caused by β-lactamase-producing *S. aureus, E. coli* and species of *Klebsiella*[135].

The three clinically used class A inhibitors are structurally related to the penicillins (*Figure 1-14*) and have been shown to follow similar inactivation mechanisms with SBLs as penicillins with PBPs (though they are not efficient PBP inhibitors)[63]. Kinetic, mass spectrometric and crystallographic analyses have shown that the 'suicide' inhibition mechanism of class A SBL inhibitors begins with the formation of the acyl-enzyme complex which then undergoes complex reaction schemes with multiple branch points, including formation of a transient intermediate and subsequent irreversible inactivation as a covalent acyl-enzyme species or deacylation to regenerate the active enzyme.

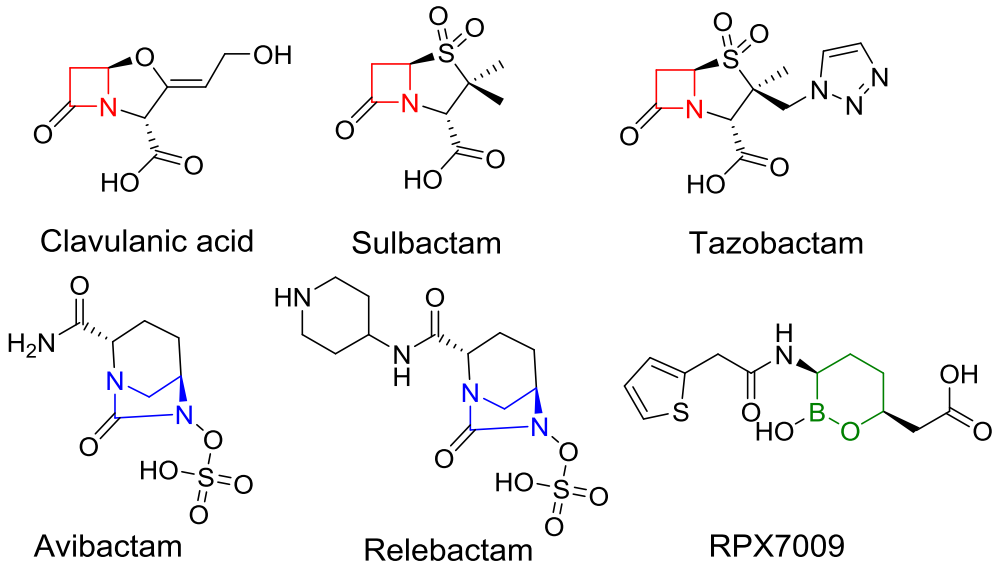


Figure 1-14: **Structures of currently used (Clavulanic acid, sulbactam and tazobactam) and newer (avibactam, relebactam and RPX7009) SBL inhibitors.**

The efficacy of the clinically used class A mechanism-based inhibitors varies greatly both within and between the classes of β-lactamases; hence there is still a need for new compounds for the emergent inhibitor resistant SBLs. Besides, the three class A SBLs inhibitors are generally less effective against class C and class D β-lactamases.

The recently FDA approved avibactam-ceftazidime combination (class C inhibitor) is set to boost the β-lactam arsenal particularly in treatment of hospital acquired infections caused by cephalosporin-resistant Gram-negative isolates[173]. New class A and class C inhibitors, a piperadine-substituted avibactam (relebactam) and a cyclic boronic acid (RPX7009) in combination with imipenem and meropenem respectively are also in the pipeline (*Figure 1-14)*[174].

The discovery of SBL inhibitors has to a great extent increased the lifetimes of β-lactam antibacterials by restoring their efficiency towards previously resistant bacteria strains. Due to mechanistic differences, MBLs are not susceptible to inactivation by the presently used β-lactamase inhibitors and, as yet, there is no clinically available MBL inhibitor.

1.6.2 MBL INHIBITOR DEVELOPMENT

As previously alluded to, the development of MBL inhibitors presents unique challenges due to the structural diversity and mechanistic complexities of the enzymes. The focus in MBL inhibitor design has primarily been the chelation of active site zinc (II) ions and establishment of favourable interactions with conserved active site residues such as R228/K224, N233 and hydrophobic residues on the L3 loop[63,175-177]. It is estimated that at least one-third of human proteins are metalloproteins[178], therefore indiscriminately inhibiting MBLs by simply chelating metal ions could have significant untoward biological effects. Another bottle-neck in the development of MBL inhibitors is the paucity of facile and efficient assay platforms for high throughput inhibitor screening (HTS) or that provide sufficient mechanistic information important for inhibitor design.

Although the rational design of mechanism-based MBL inhibitors is impeded by differences in mechanistic features between the B1, B2 and B3 subclasses, recent studies have identified commonalities in the mechanisms of MBLs that can exploited as possible targets for inhibition[115]. The utility of MBL inhibitors have been reviewed[63,135,179]; selected MBL inhibitors are briefly highlighted below with a focus on possible future strategies.

1.6.2.1 THIOL DERIVATIVES

The affinity of sulfur for zinc has been exploited in the development of thiol-based MBL inhibitors including simple thiols, mercaptotriazoles, mercaptophosphonates and cysteine derivatives among others[63,179]. The inhibitors are designed such that the thiolate anion can bind between the active-site zinc ions, displacing the bridging hydroxide ion or interact covalently with zinc binding residues. For instance,

mercaptoacetic acid thiol ester derivatives have been reported to inhibit Bc-II by a mechanism-based delivery of mercaptoacetic acid, which forms a disulfide linkage with the active site cysteine residue[180]. In VIM-2, the synergistic effect of residues at positions 223, 224 and 228 on the L10 loop have been exemplified in a VIM-2 structure in complex with a mercaptocarboxylate inhibitor, where R228 adjusts its position to accommodate the inhibitor phenyl group and is stabilized in its new conformation by interaction with the Y224 hydroxyl groups, via the A231 carbonyl oxygen (*Figure 1-15*)[165].

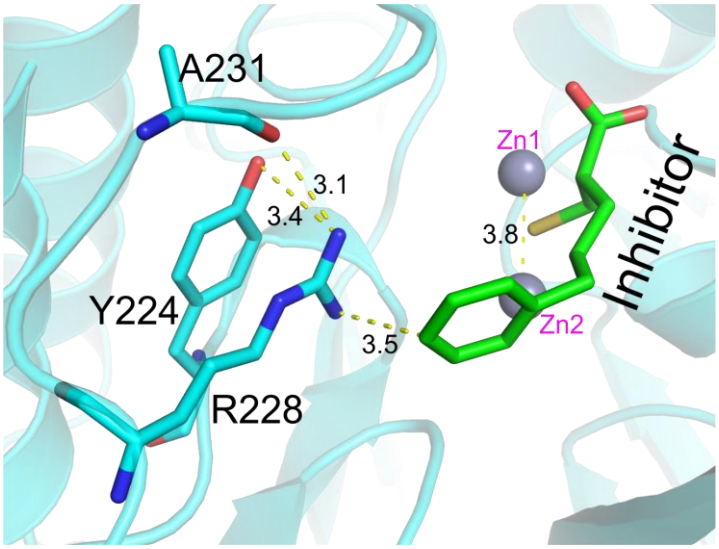


Figure 1-15: **View from a crystal structure of VIM-2 (PDB code: 2YZ3) complexed with mercaptocarboxylate inhibitor showing the interactions with residues on the L10 loop. The dashed yellow lines indicate the distances between the atoms in Å.**

Another notable inhibitor in the class of thiol based MBL inhibitors is L-captopril, an angiotensin-converting enzyme (ACE) inhibitor. L-captopril, used clinically in treatment of hypertension, inhibits several MBLs from all three subclasses via the chelation of the active site zinc (ions) by the thiol group. The enantiomer D-captopril has been reported to be more active than L-captopril against some MBLs including

NDM-1, Bc-II, CcrA as well as the monozinc CphA[127,181,182]. Recent structural studies on the inhibition of B1 MBLs (IMP-1, BcII, and VIM-2) by four captopril stereoisomers indicated that in the D-configuration, the inhibitor's carboxylate is positioned to form electrostatic and hydrogen-bonding interaction with the conserved K224/R228 residue, resulting in the increased inhibition potency (*Figure 1-16*) [183]. These compounds thus provide a basis for future development of inhibitors of the three MBL subclasses.

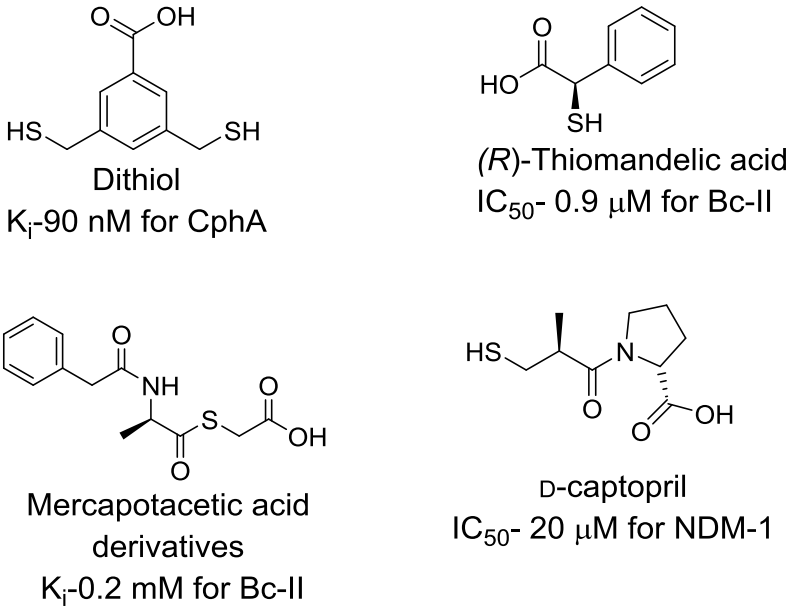


***Figure 1-16*: Structures of selected thiol-containing MBL inhibitors.**

1.6.2.2 SUBSTRATE ANALOGUES

Designing MBL inhibitors based on the β-lactam core allows for the specificity afforded by mimicking natural MBL substrates or hydrolytic intermediates derived from them. This strategy is also promising in the quest for identifying inhibitors against both MBLs and SBLs. The inhibitor design is greatly aided by the wealth of structural, biochemical and computational information available on the interaction of MBLs with different β-lactam substrates. In this regard, penicillin, cephalosporin and carbapenem-derived inhibitors have been screened for potential MBL inhibition.

A series of 6-(mercaptomethyl)penicillinate derivatives have been shown to be efficient inhibitors of both SBLs and MBLs including TEM-1, P99, L1, Bc-II, with selected compounds displaying synergism with piperacillin against β-lactamase producing bacteria strains[184]. Thioxo-cephalosporins have also been shown to act as weak competitive inhibitors for Bc-II, with their hydrolysis products exhibiting higher inhibition potency[185]. The inhibition of CphA by the oxacephem moxolactam, suggests that substituted cephalosporins may serve as inhibitors of both PBPs and MBLs simultaneously. Additionaly, 1β-methylcarbapenem analogues with fused bicyclic C-2 substituents (thiophene, pyrazole, and imidazole) have been shown to be potent inhibitors (sub-micromolar K_is) of B1 MBLs IMP-1, CcrA and L1 as well as some SBLs. Among the tested derivatives, the compound having a benzothienylthio moiety at the C-2 position was the most potent inhibitor of MBLs with K_i values ranging between 1μM- 4 nM for the three MBLs[186] (*Figure 1-17*).

Another interesting class of β-lactam analogues is the cyclobutanones, which have been reported as dual inhibitors of SBLs and PBPs. The utility of cyclobutanone derivatives in MBL inhibition is attributed to substitution of the amide nitrogen with a carbon thus escaping MBL-mediated hydrolysis. However, tested cyclobutanones exhibit modest inhibition of IMP-1 with the reported IC_{50} values being >100 μM[187].

Despite the progress made with these inhibitors, the challenge of inherent β-lactam resistance mechanisms including rapid drug efflux and difficulty accessing the periplasmic space in Gram-negative bacteria could limit their clinical utility.

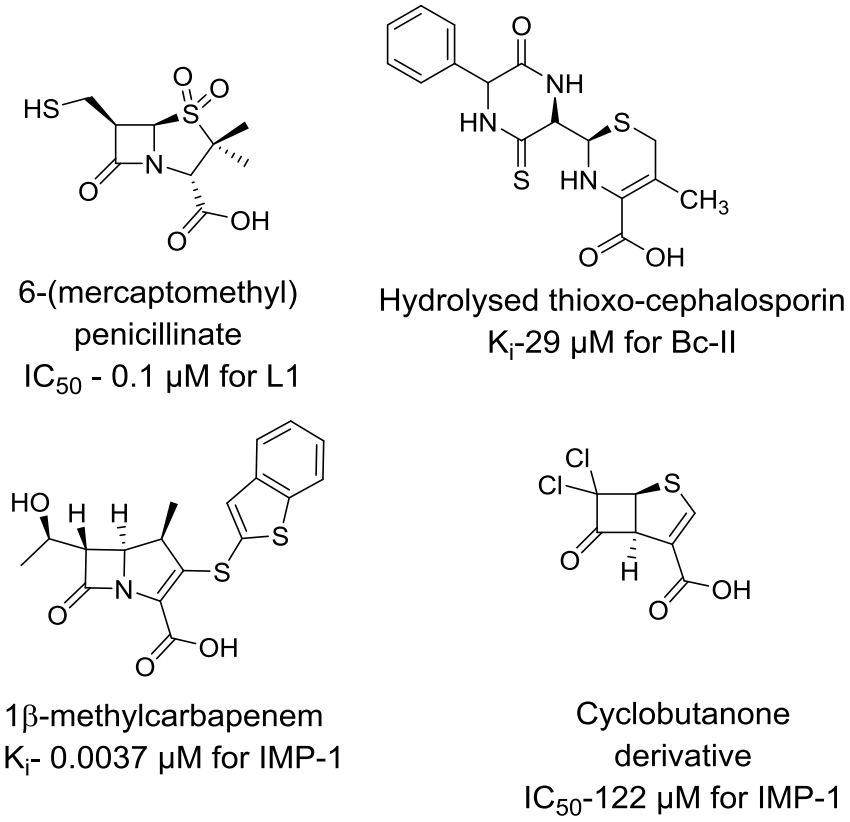


***Figure 1-17*: Structures of selected β-lactam analogues tested for MBL inhibition and the respective inhibition potency.**

1.6.2.3 ZINC CHELATORS

Walter *et al* reported trifluoromethyl ketones as synthetic inhibitors of MBLs which bind to the active site zinc (II) ions[188,189]. The design of the inhibitors was based on the binding of the active site zinc-ion to the trifluoromethyl ketone and interaction of the attached phenyl side-chain with the active site pocket residues, mimicking the interactions with the side-chains of β-lactam antibiotics. Some of the different *N*-phenoxyacetyl-substituted trifluoromethyl ketones and alcohols were shown to effectively inhibit MBLs from *B. cereus*, *P. aeruginosa*, *S. maltophilia*, and *A. hydrophila in vitro* (*Figure 1-18*)[188,189].

Soon after the identification of trifluoromethyl ketones, biphenyl tetrazoles were identified as potent competitive inhibitors of the *B. fragilis* MBL[190].

Crystallographic analyses have revealed that the tetrazole moiety of these inhibitors interacts directly with the zinc (II) ions, and further substitution at the 4′-position of the compounds with phenyl groups increases the inhibitory activity of the compounds against IMP-1[190]. Succinic acid and phthalic acid derivatives have also been reported as promising inhibitors for IMP-1, with some of inhibitors acting synergistically with biapenem against IMP-1-producing *P. aeruginosa*[191]. Crystallographic analysis with IMP-1 revealed that the carboxylate groups of succinic acid interact with the dizinc centre in a similar conformation as carboxylate groups of hydrolysed β-lactam substrates[191]. The inherent ability of heteroatoms to co-ordinate zins ions has been exploited in the development MBL inhibitors with of heterocyclic moieties including pyrroles, pyridines and triazoles[179].

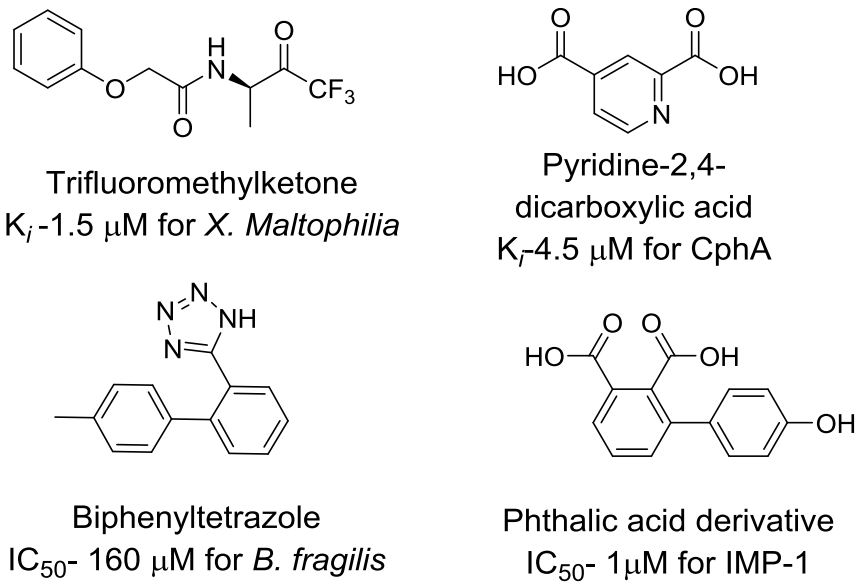


***Figure 1-18*: Structures of zinc chelators and respective inhibition potency against various MBLs.**

Most zinc chelators are non-specific and the enzymes' activities are usually restored when zinc levels are increased. Despite this obstacle, the concept of chelator fragments with improved specificity may still be viable, as exemplified by a recent inhibitor development strategy for metallo-enzyme HIV integrase[192].

1.7 SUMMARY

With the increased reports of multi-drug resistant infectious diseases, it is my view that β-lactam antibiotics provide an 'old but gold' therapeutic option for bacterial infections – well established, but one in which there is still plenty of new opportunities. The emergence and spread of drug resistance in pathogenic bacteria, especially as mediated by β-lactamases, continue to cause a global health problem, with some experts predicting the advent of a 'post-antibiotic era'[193]. With this in mind, researchers have embarked on extensive chemical modifications on the β -lactam ring to improve efficiency and escape hydrolysis by β-lactamases. While this strategy has been successful in some cases, the heterogeneity of β-lactamases continues to render even the most recent generations of β-lactam antibiotics like carbapenems ineffective.

MBLs and in particular, the NDM, VIM, and IMP groups present a prevalent and immediate clinical problem due to their rapid dissemination and evolution[87,194]. A proven strategy to circumvent the β-lactamase-mediated resistance is the development of β-lactamase inhibitors which are co-administered with β-lactams to restore the activity of the antibiotics against previously resistant strains. In this regard, class A SBL inhibitors including clavulanic acid, sulbactam and tazobactam have been in clinical use and novel class C SBLs inhibitor, avibactam, has recently been approved, in combination with ceftazidime. While several studies have reported MBL inhibitory activity of various compounds, the search for an MBL inhibitor with clinically utility is still underway. Despite the increased clinical identification of various MBLs, an important knowledge gap exists with respect to the relationship between the sequence, structure and functional properties of MBLs and their emergent variants.

1.8 RESEARCH OBJECTIVES

The seemingly subtle but significant differences in the amino acid sequences, structural features and catalytic mechanisms of MBLs, present a formidable challenge to useful MBL inhibitor development. The timely success of MBL inhibitor development programs may hinge on a comprehensive understanding of the targets' functional and biophysical characteristics. The work described in this thesis thus seeks to expound on the structural and activity profiles of different types of B1 MBLs and their variants. This information is relevant both for understanding the drivers of MBL evolution and for providing mechanistic insights that will ultimately support the design and development of novel MBL inhibitors. The specific aims of the work described in this thesis were to;

- Identify and develop an expedient assay platform for screening the activity and effective inhibition of MBLs,
- Establish a standardised protocol for MBL enzymatic studies to ensure reproducible and comparable results,
- Investigate potential differences in the structure and function of the clinically reported NDM variants,
- Compare structural and biophysical properties of VIM variants from different clusters and investigate the implications of MBL evolution for inhibitor development.

1.9 REFERENCES

1. Coates A, Hu Y, Bax R, Page C. The future challenges facing the development of new antimicrobial drugs. *Nat Rev Drug Discov*. 2002;1(11):895-910.

2. Cohen ML. Changing patterns of infectious disease. *Nature*. 2000;406(6797):762-767.

3. Kaufmann SH. Paul Ehrlich: Founder of chemotherapy. *Nat Rev Drug Discov*. 2008;7(5):373.

4. Clardy J, Fischbach MA, Currie CR. The natural history of antibiotics. *Curr Biol*. 2009;19(11):R437-41.

5. Waksman SA. Antibiotic substances-contribution of the microbiologist. *Ann N Y Acad Sci*. 2010;1213:107-111.

6. Lorber B. Changing patterns of infectious diseases. *Am J Med*. 1988;84(3 Pt 2):569-578.

7. Ford CW, Zurenko GE, Barbachyn MR. The discovery of linezolid, the first oxazolidinone antibacterial agent. *Curr Drug Targets Infect Disord*. 2001;1(2):181-199.

8. Lewis K. Platforms for antibiotic discovery. *Nat Rev Drug Discov*. 2013;12(5):371-387.

9. Butler MS, Blaskovich MA, Cooper MA. Antibiotics in the clinical pipeline in 2013. *J Antibiot (Tokyo)*. 2013;66(10):571-591.

10. Garber K. A β-lactamase inhibitor revival provides new hope for old antibiotics. *Nat Rev Drug Discov*. 2015;14(7):445-447.

11. Payne DJ, Gwynn MN, Holmes DJ, Pompliano DL. Drugs for bad bugs: Confronting the challenges of antibacterial discovery. *Nat Rev Drug Discov*. 2007;6(1):29-40.

12. Demain AL, Elander RP. The β-lactam antibiotics: Past, present, and future. *Antonie Van Leeuwenhoek*. 1999;75(1-2):5-19.

13. Elander RP. Industrial production of β-lactam antibiotics**.** *Applied Microbiology and Biotechnology*. 2003;61(5-6):385-392.

14. Page M. β-lactam antibiotics. In: Dougherty TJ, Pucci M, eds. *Antibiotic discovery and development*; 2012:79-117.

15. Selwyn S. Pioneer work on the 'penicillin phenomenon', 1870-1876. *J Antimicrob Chemother*. 1979;5(3):249-255.

16. Abraham EP. The β-lactam antibiotics. *Sci Am*. 1981;244(6):76-86.

17. Wainwright M. Andre gratia (1893-1950): Forgotten pioneer of research into antimicrobial agents. *J Med Biogr*. 2000;8(1):39-42.

18. Pasteur L, Chamberland, Roux. Summary report of the experiments conducted at pouilly-le-fort, near melun, on the anthrax vaccination, 1881. *Yale J Biol Med*. 2002;75(1):59-62.

19. Fleming A. On the antibacterial action of cultures of a penicillium, with special reference to their use in the isolation of *B. influenzae*. 1929. *Bull World Health Organ*. 2001;79(8):780-790.

20. Florey HW, Chain EB, Heatley NG, Jennings MA, *et al*. *Antibiotics.* Vol 2. London: Oxford University Press; 1949.

21. Chain E, Florey HW, Adelaide MB, *et al*. Penicillin as a chemotherapeutic agent. 1940. *Clin Orthop Relat Res*. 1993;(295)(295):3-7.

22. Moyer AJ, Coghill RD. Penicillin X: The effect of phenylacetic acid on penicillin production. *J Bacteriol*. 1947;53(3):329-341.

23. Hodgkin DC. The X-ray analysis of the structure of pencillin. *Adv Sci*. 1949;6:85-89.

24. Elander RP AH. Beta-lactam-producing microorganisms: Their biology and fermentation behavior. In: Morin RB GM, ed. *The chemistry and biology of β-lactam antibiotics.* Vol 3. New York: Academic Press; 1982:85-153.

25. Elander RP. Strain improvement and preservation of β-lactam-producing microorganisms. In: Demain AL SN, ed. *Antibiotics containing the β-lactam structure*. Vol 1. Berlin Heidelberg: Springer; 1983:97-146.

26. Sheehan JC, Henery Logan KR. A general synthesis of the penicillins. *J Am Chem Soc*. 1959;81(21):5838-5839.

27. Acred P, Brown DM, Knudsen ET, Rolinson GN, Sutherland R. New semi-synthetic penicillin active against *Pseudomonas pyocyanea*. *Nature*. 1967;215(5096):25-30.

28. Abraham EP, Newton GG. The structure of cephalosporin C. *Biochem J*. 1961;79(2):377-393.

29 Williams JD. Classification of cephalosporins. *Drugs*. 1987;34(Supp 2):15-22.

30. Nagarajan R, Boeck LD, Gorman M, *et al*. Beta-lactam antibiotics from *Streptomyces*. *J Am Chem Soc*. 1971;93(9):2308-2310.

31. Kahan JS, Kahan FM, Goegelman R, Currie SA, *et al*. Thienamycin, a new beta-lactam antibiotic. I. discovery, taxonomy, isolation and physical properties. *J Antibiot (Tokyo)*. 1979;32(1):1-12.

32. Andrus A, Baker F, Bouffard FA, *et al*. Structure activity relationships among some totally synthetic carbapenems. In: Brown AG RS, ed. *Recent advances in the chemistry of beta-lactam antibiotics.*Special Publication No. 52. London: Royal Society of Chemistry; 1985:86-99.

33. Imada A, Kondo M, Okonogi K, Yukishige K, Kuno M. *In vitro* and *in vivo* antibacterial activities of carumonam (AMA-1080), a new *N*-sulfonated monocyclic beta-lactam antibiotic. *Antimicrob Agents Chemother*. 1985;27(5):821-827.

34. Sykes RB, Bonner DP, Bush K, Georgopapadakou NH. Azthreonam (SQ 26,776), a synthetic monobactam specifically active against aerobic Gram-negative bacteria. *Antimicrob Agents Chemother*. 1982;21(1):85-92.

35. Tanaka SK, Summerill RA, Minassian BF,*et al*. *In vitro* evaluation of tigemonam, a novel oral monobactam. *Antimicrob Agents Chemother*. 1987;31(2):219-225.

36. Tipper DJ, Strominger JL. Mechanism of action of penicillins: A proposal based on their structural similarity to acyl-D-alanyl-D-alanine. *Proc Natl Acad Sci U S A*. 1965;54(4):1133-1141.

37. Wise EM,Jr, Park JT. Penicillin: Its basic site of action as an inhibitor of a peptide cross-linking reaction in cell wall mucopeptide synthesis. *Proc Natl Acad Sci U S A*. 1965;54(1):75-81.

38. Strominger JL, Blumberg PM, Suginaka H,*et al*. How penicillin kills bacteria: Progress and problems. *Proc R Soc Lond B Biol Sci*. 1971;179(1057):369-383.

39. Yocum RR, Waxman DJ, Rasmussen JR, Strominger JL. Mechanism of penicillin action: Penicillin and substrate bind covalently to the same active site serine in two bacterial D-alanine carboxypeptidases. *Proc Natl Acad Sci U S A*. 1979;76(6):2730-2734.

40. Yocum RR, Rasmussen JR, Strominger JL. The mechanism of action of penicillin. penicillin acylates the active site of *Bacillus stearothermophilus* D-alanine carboxypeptidase. *J Biol Chem*. 1980;255(9):3977-3986.

41. Lee B. Conformation of penicillin as a transition-state analog of the substrate of peptidoglycan transpeptidase. *J Mol Biol*. 1971;61(2):463-469.

42. Boyd DB. Transition state structures of a dipeptide related to the mode of action of β-lactam antibiotics. *Proc Natl Acad Sci U S A*. 1977;74(12):5239-5243.

43. Silvaggi NR, Josephine HR, Kuzin AP, *et al*. Crystal structures of complexes between the R61 DD-peptidase and peptidoglycan-mimetic β-lactams: A non-covalent complex with a "perfect penicillin". *J Mol Biol*. 2005;345(3):521-533.

44. de Pedro MA, Holtje JV, Schwarz H. Fast lysis of escherichia coli filament cells requires differentiation of potential division sites. *Microbiology*. 2002;148(Pt 1):79-86.

45. Chung HS, Yao Z, Goehring NW, Kishony R, Rapid β-lactam-induced lysis requires successful assembly of the cell division machinery. *Proc Natl Acad Sci U S A*. 2009;106(51):21872-21877.

46. Yao Z, Kahne D, Kishony R. Distinct single-cell morphological dynamics under β-lactam antibiotics. *Mol Cell*. 2012;48(5):705-712.

47. Tyndall J. Observations on the optical deportment of the atmosphere in reference to the phenomena of putrefaction and infection. *Br Med J*. 1876;1(787):121-124.

48. Poole K. Resistance to β-lactam antibiotics. *Cell Mol Life Sci*. 2004;61(17):2200-2223.

49. Chambers HF. Penicillin-binding protein-mediated resistance in *Pneumococci* and *Staphylococci*. *J Infect Dis*. 1999;179(Supp. 2):S353-359.

50. Farra A, Islam S, Stralfors A, *et al*. Role of outer membrane protein OprD and penicillin-binding proteins in resistance of *Pseudomonas aeruginosa* to imipenem and meropenem. *Int J Antimicrob Agents*. 2008;31(5):427-433.

51. Siroy A, Molle V, Lemaitre-Guillier C, *et al.* Channel formation by CarO, the carbapenem resistance-associated outer membrane protein of *Acinetobacter baumannii*. *Antimicrob Agents Chemother*. 2005;49(12):4876-4883.

52. Livermore DM. Multiple mechanisms of antimicrobial resistance in *Pseudomonas aeruginosa*: Our worst nightmare? *Clin Infect Dis*. 2002;34(5):634-640.

53. Fleming A. Classics in infectious diseases: On the antibacterial action of cultures of a *Penicillium*, with special reference to their use in the isolation of *B. influenzae* by Alexander Fleming, reprinted from the British Journal of Experimental Pathology 10:226-236, 1929. *Rev Infect Dis*. 1980;2(1):129-139.

54. Abraham EP, Chain E. An enzyme from bacteria able to destroy penicillin. 1940. *Rev Infect Dis*. 1988;10(4):677-678.

55. Kirby WM. Extraction of a highly potent penicillin inactivator from penicillin resistant *Staphylococci*. *Science*. 1944;99(2579):452-453.

56. Bush K. Proliferation and significance of clinically relevant β-lactamases. *Ann N Y Acad Sci*. 2013;1277:84-90.

57. Ambler RP. The structure of β-lactamases. *Philos. Trans. R. Soc. London B.* 1980;289:321-331.

58. Bush K. The evolution of β-lactamases. *Ciba Found Symp*. 1997;207:152-63; discussion 163-6.

59. Matagne A, Dubus A, Galleni M, Frère JM. The β-lactamase cycle: A tale of selective pressure and bacterial ingenuity. *Nat Prod Rep*. 1999;16(1):1-19.

60. Naas T, Iorga IB. Beta-lactamase Database- Structure and Function Web site. http://bldb.eu/. Updated January 13, 2016. Accessed March 24, 2016.

61. Jacoby GA. AmpC β-lactamases. *Clin Microbiol Rev*. 2009;22(1):161-182.

62. Naas T, Nordmann P. OXA-type β-lactamases. *Curr Pharm Des*. 1999;5(11):865-879.

63. Drawz SM, Bonomo RA. Three decades of β-lactamase inhibitors. *Clin Microbiol Rev*. 2010;23:160-201.

64. Stec B, Holtz KM, Wojciechowski CL, Kantrowitz ER. Structure of the wild-type TEM-1 β-lactamase at 1.55 Å and the mutant enzyme Ser70Ala at 2.1 Å suggest the mode of noncovalent catalysis for the mutant enzyme. *Acta Crystallogr D Biol Crystallogr*. 2005;61(Pt 8):1072-1079.

65. Carfi A, Duee E, Galleni M, *et al*. 1.85 Å resolution structure of the zinc (II) β-lactamase from *Bacillus cereus*. *Acta Crystallogr D Biol Crystallogr*. 1998;54(Pt 3):313-323.

66. Sun T, Nukaga M, Mayama K,*et al*. Comparison of β-lactamases of classes A and D: 1.5-Å crystallographic structure of the class D OXA-1 oxacillinase. *Protein Sci*. 2003;12(1):82-91.

67. Daiyasu H, Osaka K, Ishino Y, Toh H. Expansion of the zinc metallo-hydrolase family of the β-lactamase fold. *FEBS Lett*. 2001;503(1):1-6.

68. Bebrone C. Metallo-β-lactamases (classification, activity, genetic organization, structure, zinc coordination) and their superfamily. *Biochem Pharmacol*. 2007;74:1686-1701.

69. Pettinati I, Brem J, Lee SY,*et al*. The chemical biology of human metallo-β-lactamase fold proteins. *Trends Biochem Sci*. 2016; article in press.

70. Cornaglia G, Giamarellou H, Rossolini GM. Metallo-β-lactamases: A last frontier for β-lactams? *Lancet Infect Dis*. 2011;11(5):381-393.

71. Sabath LD, Abraham EP. Zinc as a cofactor for cephalosporinase from *Bacillus cereus* 569. *Biochem J*. 1966;98(1):11C-3C.

72. Shaw RW, Clark SD, Hilliard NP, Harman JG. Hyperexpression in *Escherichia coli*, purification, and characterization of the metallo-β-lactamase of *Bacillus cereus* 5/B/6. *Protein Expr Purif*. 1991;2(2-3):151-157.

73. Walsh TR, Hall L, Assinder SJ, *et al*. Sequence analysis of the L1 metallo-β-lactamase from *Xanthomonas maltophilia*. *Biochim Biophys Acta*. 1994;1218(2):199-201.

74. Bandoh K, Watanabe K, Muto Y, *et al*. Conjugal transfer of imipenem resistance in *Bacteroides fragilis*. *J Antibiot (Tokyo)*. 1992;45(4):542-547.

75. Watanabe M, Iyobe S, Inoue M, Mitsuhashi S. Transferable imipenem resistance in *Pseudomonas aeruginosa*. *Antimicrob Agents Chemother*. 1991;35(1):147-151.

76. Rossolini GM, Franceschini N, Riccio ML, *et al*. Characterization and sequence of the *Chryseobacterium* (*Flavobacterium*) *meningosepticum* carbapenemase: A new molecular class B β-lactamase showing a broad substrate profile. *Biochem J*. 1998;332 (Pt 1):145-152.

77. Nordmann P, Poirel L. Emerging carbapenemases in Gram-negative aerobes. *Clin Microbiol Infect*. 2002;8(6):321-331.

78. Miriagou V, Cornaglia G, Edelstein M, *et al*. Acquired carbapenemases in Gram-negative bacterial pathogens: Detection and surveillance issues. *Clin Microbiol Infect*. 2010;16(2):112-122.

79. Grundmann H, Livermore DM, Giske CG, *et al*. Carbapenem-non-susceptible *Enterobacteriaceae* in Europe: Conclusions from a meeting of national experts. *Euro Surveill*. 2010;15(46):19711.

80. Diene SM, Rolain JM. Carbapenemase genes and genetic platforms in Gram-negative *Bacilli*: *Enterobacteriaceae, Pseudomonas* and *Acinetobacter species*. *Clin Microbiol Infect*. 2014;20(9):831-838.

81. Johnson AP, Woodford N. Global spread of antibiotic resistance: The example of New Delhi metallo-β-lactamase (NDM)-mediated carbapenem resistance. *J Med Microbiol*. 2013;62:499-513.

82. Rossolini GM, Condemi MA, Pantanella F, *et al*. Metallo-β-lactamase producers in environmental microbiota: New molecular class B enzyme in *Janthinobacterium lividum*. *Antimicrob Agents Chemother*. 2001;45(3):837-844.

83. Stoczko M, Frère JM, Rossolini GM, Docquier JD. Postgenomic scan of metallo-β-lactamase homologues in *Rhizobacteria*: Identification and characterization of BJP-1, a subclass B3 ortholog from *Bradyrhizobium japonicum*. *Antimicrob Agents Chemother*. 2006;50(6):1973-1981.

84. Saavedra MJ, Peixe L, Sousa JC, Henriques I, Alves A, Correia A. Sfh-I, a subclass B2 metallo-β-lactamase from a *Serratia fonticola* environmental isolate. *Antimicrob Agents Chemother*. 2003;47(7):2330-2333.

85. Walsh TR, Toleman MA, Poirel L, Nordmann P. Metallo-β-lactamases: The quiet before the storm? *Clin Microbiol Rev*. 2005;18(2):306-325.

86. Nordmann P, Poirel L, Toleman MA, Walsh TR. Does broad-spectrum β-lactam resistance due to NDM-1 herald the end of the antibiotic era for treatment of infections caused by Gram-negative bacteria? *J Antimicrob Chemother*. 2011;66(4):689-692.

87. Walsh TR. Emerging carbapenemases: A global perspective. *Int J Antimicrob Agents*. 2010;36 Suppl 3:S8-14.

88. Spencer J, Walsh TR. A new approach to the inhibition of metallo-β-lactamases. *Angew Chem Int Ed Engl*. 2006;45:1022-1026.

89. Hayes MV, Thomson CJ, Amyes SG. The 'hidden' carbapenemase of *Aeromonas hydrophila*. *J Antimicrob Chemother*. 1996;37(1):33-44.

90. Matagne A, Dubus A, Galleni M, Frère JM. The β-lactamase cycle: A tale of selective pressure and bacterial ingenuity. *Nat Prod Rep*. 1999;16(1):1-19.

91. Fisher JF, Meroueh SO, Mobashery S. Bacterial resistance to β-lactam antibiotics: Compelling opportunism, compelling opportunity. *Chem Rev*. 2005;105(2):395-424.

92. Yong D, Toleman MA, Giske CG, *et al*. Characterization of a new metallo-β-lactamase gene, *bla*$_{\text{NDM-1}}$, and a novel erythromycin esterase gene carried on a unique genetic structure in *Klebsiella pneumoniae* sequence type 14 from India. *Antimicrob Agents Chemother*. 2009;53(12):5046-5054.

93. Bebrone C, Lassaux P, Vercheval L, *et al*. Current challenges in antimicrobial chemotherapy: Focus on β-lactamase inhibition. *Drugs*. 2010;70:651-679.

94. Widmann M, Pleiss J, Oelschlaeger P. Systematic analysis of metallo-β-lactamases using an automated database. *Antimicrob Agents Chemother*. 2012;56(7):3481-3491.

95. Meini MR, Llarrull LI, Vila AJ. Evolution of metallo-β-lactamases: Trends revealed by natural diversity and evolution. *Antibiotics (Basel)*. 2014;3(3):285-316.

96. Galleni M, Lamotte-Brasseur J, Rossolini GM, *et al*. Standard numbering scheme for class B β-lactamases. *Antimicrob Agents Chemother*. 2001;45(3):660-663.

97. Garau G, Garcia-Saez I, Bebrone C, *et al*. Update of the standard numbering scheme for class B β-lactamases. *Antimicrob Agents Chemother*. 2004;48(7):2347-2349.

98. Watanabe M, Iyobe S, Inoue M, Mitsuhashi S. Transferable imipenem resistance in *Pseudomonas aeruginosa*. *Antimicrob Agents Chemother*. 1991;35(1):147-151.

99. Lauretti L, Riccio ML, Mazzariol A, *et al*. Cloning and characterization of *bla*$_{\text{VIM}}$, a new integron-borne metallo-β-lactamase gene from a *Pseudomonas aeruginosa* clinical isolate. *Antimicrob Agents Chemother*. 1999;43(7):1584-1590.

100. Massidda O, Rossolini GM, Satta G. The *Aeromonas hydrophila* CphA gene: Molecular heterogeneity among class B metallo-β-lactamases. *J Bacteriol*. 1991;173(15):4611-4617.

101. Rossolini GM, Zanchi A, Chiesurin A, *et al*. Distribution of CphA or related carbapenemase-encoding genes and production of carbapenemase activity in members of the genus *Aeromonas*. *Antimicrob Agents Chemother*. 1995;39(2):346-349.

102. Hall BG, Salipante SJ, Barlow M. The metallo-β-lactamases fall into two distinct phylogenetic groups. *J Mol Evol*. 2003;57(3):249-254.

103. Simona F, Magistrato A, Vera DM, *et al*. Protonation state and substrate binding to B2 metallo-β-lactamase CphA from *Aeromonas hydrofila*. *Proteins*. 2007;69:595-605.

104. Bebrone C, Delbrück H, Kupper MB, *et al*.The structure of the dizinc subclass B2 metallo-β-lactamase CphA reveals that the second inhibitory zinc ion binds in the histidine site. *Antimicrob Agents Chemother*. 2009;53:4464-4471.

105. Bellais S, Aubert D, Naas T, Nordmann P. Molecular and biochemical heterogeneity of class B carbapenem-hydrolyzing β-lactamases in *Chryseobacterium meningosepticum*. *Antimicrob Agents Chemother*. 2000;44(7):1878-1886.

106. Boschi L, Mercuri PS, Riccio ML, *et al*. The *Legionella* (*Fluoribacter*) *gormanii* metallo-β-lactamase: A new member of the highly divergent lineage of molecular-subclass B3 β-lactamases. *Antimicrob Agents Chemother*. 2000;44(6):1538-1543.

107. Wachino J, Yoshida H, Yamane K, *et al*. SMB-1, a novel subclass B3 metallo-β-lactamase, associated with ISCR1 and a class 1 integron, from a carbapenem-resistant *Serratia marcescens* clinical isolate. *Antimicrob Agents Chemother*. 2011;55(11):5143-5149.

108. Yong D, Toleman MA, Bell J, *et al*. Genetic and biochemical characterization of an acquired subgroup B3 metallo-β-lactamase gene, $bla_{\text{AIM-1}}$, and its unique genetic context in *Pseudomonas aeruginosa* from Australia. *Antimicrob Agents Chemother*. 2012;56(12):6154-6159.

119. Sutton BJ, Artymiuk PJ, Cordero-Borboa AE, *et al*.An X-ray-crystallographic study of β-lactamase II from *Bacillus cereus* at 0.35 nm resolution. *Biochem J*. 1987;248(1):181-188.

110. Carfi A, Pares S, Duee E, *et al*. The 3-D structure of a zinc metallo-β-lactamase from *Bacillus cereus* reveals a new type of protein fold. *EMBO J*. 1995;14(20):4914-4921.

111. Concha NO, Rasmussen BA, Bush K, Herzberg O. Crystal structure of the wide-spectrum binuclear zinc β-lactamase from *Bacteroides fragilis*. *Structure*. 1996;4(7):823-836.

112. Fabiane SM, Sohi MK, Wan T, *et al*. Crystal structure of the zinc-dependent β-lactamase from *Bacillus cereus* at 1.9 Å resolution: Binuclear active site with features of a mononuclear enzyme. *Biochemistry*. 1998;37(36):12404-12411.

113. Ullah JH, Walsh TR, Taylor IA, *et al*. The crystal structure of the L1 metallo-β-lactamase from *Stenotrophomonas maltophilia* at 1.7 Å resolution. *J Mol Biol*. 1998;284(1):125-136.

114. Palzkill T. Metallo-β-lactamase structure and function. *Ann N Y Acad Sci*. 2013;1277:91-104.

115. Meini MR, Llarrull LI, Vila AJ. Overcoming differences: The catalytic mechanism of metallo-β-lactamases. *FEBS Lett*. 2015;589(22):3419-3432.

116. King D, Strynadka N. Crystal structure of New Delhi metallo-β-lactamase reveals molecular basis for antibiotic resistance. *Protein Sci*. 2011;20:1484-1491.

117. Garau G, Bebrone C, Anne C, *et al*. A metallo-β-lactamase enzyme in action: Crystal structures of the monozinc carbapenemase CphA and its complex with biapenem. *J Mol Biol*. 2005;345(4):785-795.

118. Garcia-Saez I, Mercuri PS, Papamicael C, *et al*. Three-dimensional structure of FEZ-1, a monomeric subclass B3 metallo-β-lactamase from *Fluoribacter gormanii*, in native form and in complex with D-captopril. *J Mol Biol*. 2003;325(4):651-660.

119. Concha NO, Janson CA, Rowling P, *et al*. Crystal structure of the IMP-1 metallo β-lactamase from *Pseudomonas aeruginosa* and its complex with a mercaptocarboxylate inhibitor: Binding determinants of a potent, broad-spectrum inhibitor. *Biochemistry*. 2000;39(15):4288-4298.

120. Garcia-Saez I, Docquier JD, Rossolini GM, Dideberg O. The three-dimensional structure of VIM-2, a zn-β-lactamase from *Pseudomonas aeruginosa* in its reduced and oxidised form. *J Mol Biol*. 2008;375(3):604-611.

121. Materon IC, Palzkill T. Identification of residues critical for metallo-β-lactamase function by codon randomization and selection. *Protein Sci*. 2001;10(12):2556-2565.

122. de Seny D, Prosperi-Meys C, Bebrone C, *et al*. Mutational analysis of the two zinc-binding sites of the *Bacillus cereus* 569/H/9 metallo-β-lactamase. *Biochem J*. 2002;363(Pt 3):687-696.

123. Moali C, Anne C, Lamotte-Brasseur J, *et al*. Analysis of the importance of the metallo-β-lactamase active site loop in substrate binding and catalysis. *Chem Biol*. 2003;10(4):319-329.

124. Kim Y, Cunningham MA, Mire J, *et al*. NDM-1, the ultimate promiscuous enzyme: Substrate recognition and catalytic mechanism. *FASEB J*. 2013; 27(5):1917-1927

125. Scrofani SD, Chung J, Huntley JJ, *et al*. NMR characterization of the metallo-β-lactamase from *Bacteroides fragilis* and its interaction with a tight-binding inhibitor: Role of an active-site loop. *Biochemistry*. 1999;38(44):14507-14514.

126. Karsisiotis AI, Damblon CF, Roberts GC. Solution structures of the *Bacillus cereus* metallo-β-lactamase BcII and its complex with the broad spectrum inhibitor R-thiomandelic acid. *Biochem J*. 2013;456(3):397-407.

127. Rydzik AM, Brem J, van Berkel SS, *et al*. Monitoring conformational changes in the NDM-1 metallo-β-lactamase by ^{19}F NMR spectroscopy. *Angew Chem Int Ed Engl*. 2014;53(12):3129-3133.

128. Murphy TA, Catto LE, Halford SE, *et al*. Crystal structure of *Pseudomonas aeruginosa* SPM-1 provides insights into variable zinc affinity of metallo-β-lactamases. *J Mol Biol*. 2006;357(3):890-903.

129. Zhang H, Hao Q. Crystal structure of NDM-1 reveals a common β-lactam hydrolysis mechanism. *FASEB J*. 2011;25:2574-2582.

130. Page MI, Badarau A. The mechanisms of catalysis by metallo β-lactamases. *Bioinorg Chem Appl*. 2008:576297

131. Davies RB, Abraham EP. Metal cofactor requirements of β-lactamase II. *Biochem J*. 1974;143(1):129-135.

132. Bounaga S, Laws AP, Galleni M, Page MI. The mechanism of catalysis and the inhibition of the *Bacillus cereus* zinc-dependent β-lactamase. *Biochem J*. 1998;331(Pt 3):703-711.

133. Weston J. Mode of action of bi- and trinuclear zinc hydrolases and their synthetic analogues. *Chem Rev*. 2005;105(6):2151-2174.

134. Hu Z, Periyannan G, Bennett B, Crowder MW. Role of the Zn1 and Zn2 sites in metallo-β-lactamase L1. *J Am Chem Soc*. 2008;130(43):14207-14216.

135. Fast W, Sutton LD. Metallo-β-lactamase: Inhibitors and reporter substrates. *Biochim Biophys Acta*. 2013;1834(8):1648-1659.

136. Tioni MF, Llarrull LI, Poeylaut-Palena A, *et al*. Trapping and characterization of a reaction intermediate in carbapenem hydrolysis by *B. cereus* metallo-β-lactamase. *J Am Chem Soc*. 2008;130:15852-15863.

137. Badarau A, Page MI. Enzyme deactivation due to metal-ion dissociation during turnover of the cobalt-β-lactamase catalyzed hydrolysis of β-lactams. *Biochemistry*. 2006;45(36):11012-11020.

138. Badarau A, Damblon C, Page MI. The activity of the dinuclear cobalt-β-lactamase from *Bacillus cereus* in catalysing the hydrolysis of β-lactams. *Biochem J*. 2007;401(1):197-203.

139. Badarau A, Page MI. Loss of enzyme activity during turnover of the *Bacillus cereus* β-lactamase catalysed hydrolysis of β-lactams due to loss of zinc ion. *J Biol Inorg Chem*. 2008;13(6):919-928.

140. Gonzalez JM, Meini MR, Tomatis PE, *et al*. Metallo-β-lactamases withstand low zn (II) conditions by tuning metal-ligand interactions. *Nat Chem Biol*. 2012;8(8):698-700.

141. Wang Z, Fast W, Benkovic SJ. On the mechanism of the metallo-β-lactamase from *Bacteroides fragilis*. *Biochemistry*. 1999;38(31):10013-10023.

142. McManus-Munoz S, Crowder MW. Kinetic mechanism of metallo-β-lactamase L1 from *Stenotrophomonas maltophilia*. *Biochemistry*. 1999;38(5):1547-1553.

143. Garrity JD, Bennett B, Crowder MW. Direct evidence that the reaction intermediate of metallo-β-lactamase L1 is metal bound. *Biochemistry*. 2005;44(3):1078-1087.

144. Spencer J, Clarke AR, Walsh TR. Novel mechanism of hydrolysis of therapeutic β-lactams by *Stenotrophomonas maltophilia* L1 metallo-β-lactamase. *J Biol Chem*. 2001;276(36):33638-33644.

145. Oelschlaeger P, Aitha M, Yang H, *et al*. Meropenem and chromacef intermediates observed in IMP-25 metallo-β-lactamase-catalyzed hydrolysis. *Antimicrob Agents Chemother*. 2015;59(7):4326-4330.

146. Yang H, Aitha M, Hetrick AM, *et al*. Mechanistic and spectroscopic studies of metallo-β-lactamase NDM-1. *Biochemistry (N Y)*. 2012;51:3839-3847.

147. Brem J, Struwe WB, Rydzik AM, *et al*. Studying the active-site loop movement of the Saõ Paulo metallo-β-lactamase-1. *Chem Sci*. 2015;6(2):956-963.

148. Garrity JD, Carenbauer AL, Herron LR, Crowder MW. Metal binding Asp-120 in metallo-β-lactamase L1 from *Stenotrophomonas maltophilia* plays a crucial role in catalysis. *J Biol Chem*. 2004;279(2):920-927.

149. Llarrull LI, Fabiane SM, Kowalski JM, *et al*. Asp-120 locates Zn2 for optimal metallo-β-lactamase activity. *J Biol Chem*. 2007;282(25):18276-18285.

150. Concha NO, Rasmussen BA, Bush K, Herzberg O. Crystal structure of the wide-spectrum binuclear zinc β-lactamase from *Bacteroides fragilis*. *Structure*. 1996;4(7):823-836.

151. Dal Peraro M, Vila AJ, Carloni P, Klein ML. Role of zinc content on the catalytic efficiency of B1 metallo β-lactamases. *J Am Chem Soc*. 2007;129(10):2808-2816.

152. Fonseca F, Bromley EH, Saavedra MJ, *et al*. Crystal structure of S*erratia fonticola* Sfh-I: Activation of the nucleophile in mono-zinc metallo-β-lactamases. *J Mol Biol*. 2011;411(5):951-959.

153. Wu S, Xu D,Guo H. QM/MM studies of monozinc β-lactamase CphA suggest that the crystal structure of an Enzyme−Intermediate complex represents a minor pathway. *J Am Chem Soc*. 2010;132(51):17986-17988.

154. Docquier JD, Lamotte-Brasseur J, Galleni M, *et al*. On functional and structural heterogeneity of VIM-type metallo-β-lactamases. *J Antimicrob Chemother*. 2003;51(2):257-266.

155. Zhao WH, Hu ZQ. IMP-type metallo-β-lactamases in Gram-negative *Bacilli*: Distribution, phylogeny, and association with integrons. *Crit Rev Microbiol*. 2011;37(3):214-226.

156. Pal A, Tripathi A. An *in silico* approach for understanding the molecular evolution of clinically important metallo-β-lactamases. *Infect Genet Evol*. 2013;20:39-47.

157. Makena A, Brem J, Pfeffer I, *et al*. Biochemical characterization of New Delhi metallo-β-lactamase variants reveals differences in protein stability. *J Antimicrob Chemother*. 2015;70(2):463-469.

158. Murphy TA, Catto LE, Halford SE, *et al*. Crystal structure of *Pseudomonas aeruginosa* SPM-1 provides insights into variable zinc affinity of metallo-β-lactamases. *J Mol Biol*. 2006;357(3):890-903.

159. Worth CL, Gong S, Blundell TL. Structural and functional constraints in the evolution of protein families. *Nat Rev Mol Cell Biol*. 2009;10(10):709-720.

160. Yano H, Kuga A, Okamoto R, *et al*. Plasmid-encoded metallo-β-lactamase (IMP-6) conferring resistance to carbapenems, especially meropenem. *Antimicrob Agents Chemother*. 2001;45(5):1343-1348.

161. Liu EM, Pegg KM, Oelschlaeger P. The sequence-activity relationship between metallo-β-lactamases IMP-1, IMP-6, and IMP-25 suggests an evolutionary adaptation to meropenem exposure. *Antimicrob Agents Chemother*. 2012;56(12):6403-6406.

162. Pegg KM, Liu EM, George AC, *et al*. Understanding the determinants of substrate specificity in IMP family metallo-β-lactamases: The importance of residue 262. *Protein Sci*. 2014;23(10):1451-1460.

163. Oelschlaeger P, Mayo SL, Pleiss J. Impact of remote mutations on metallo-β-lactamase substrate specificity: Implications for the evolution of antibiotic resistance. *Protein Sci*. 2005;14(3):765-774.

164. Materon IC, Beharry Z, Huang W, *et al*. Analysis of the context dependent sequence requirements of active site residues in the metallo-β-lactamase IMP-1. *J Mol Biol*. 2004;344(3):653-663.

165. Yamaguchi Y, Jin W, Matsunaga K, *et al*. Crystallographic investigation of the inhibition mode of a VIM-2 metallo-β-lactamase from *Pseudomonas aeruginosa* by a mercaptocarboxylate inhibitor. *J Med Chem*. 2007;50(26):6647-6653.

166. Borgianni L, Vandenameele J, Matagne A, *et al*. Mutational analysis of VIM-2 reveals an essential determinant for metallo-β-lactamase stability and folding. *Antimicrob Agents Chemother*. 2010;54(8):3197-3204.

167. Borra PS, Leiros HK, Ahmad R, *et al*. Structural and computational investigations of VIM-7: Insights into the substrate specificity of VIM metallo-β-lactamases. *J Mol Biol*. 2011;411(1):174-189.

168. Lassaux P, Traore DA, Loisel E, *et al*. Biochemical and structural characterization of the subclass B1 metallo-β-lactamase VIM-4. *Antimicrob Agents Chemother*. 2011;55(3):1248-1255.

169. Shoichet BK, Baase WA, Kuroki R, Matthews BW. A relationship between protein stability and protein function. *Proc Natl Acad Sci U S A*. 1995;92(2):452-456.

170. Thomas VL, McReynolds AC, Shoichet BK. Structural bases for stability-function tradeoffs in antibiotic resistance. *J Mol Biol*. 2010;396(1):47-59.

171. Gonzalez LJ, Moreno DM, Bonomo RA, Vila AJ. Host-specific enzyme-substrate interactions in SPM-1 metallo-β-lactamase are modulated by second sphere residues. *PLoS Pathog*. 2014;10(1):e1003817.

172. Brown AG. Clavulanic acid, a novel β-lactamase inhibitor--a case study in drug discovery and development. *Drug Des Deliv*. 1986;1(1):1-21.

173. Zhanel GG, Lawson CD, Adam H, *et al*. Ceftazidime-avibactam: A novel cephalosporin/β-lactamase inhibitor combination. *Drugs*. 2013;73(2):159-177.

174. Bush K, Macielag MJ. New β-lactam antibiotics and β-lactamase inhibitors. *Expert Opin Ther Pat*. 2010;20(10):1277-1293.

175. Minond D, Saldanha SA, Subramaniam P, *et al*. Inhibitors of VIM-2 by screening pharmacologically active and click-chemistry compound libraries. *Bioorg Med Chem*. 2009;17(14):5027-5037.

176. Brem J, van Berkel SS, Aik W, *et al*. Rhodanine hydrolysis leads to potent thioenolate mediated metallo-β-lactamase inhibition. *Nat Chem*. 2014;6(12):1084-1090.

177. Liénard BM, Garau G, Horsfall L, *et al*. Structural basis for the broad-spectrum inhibition of metallo-β-lactamases by thiols. *Org Biomol Chem*. 2008;6(13):2282-2294.

178. Franz KJ. Clawing back: Broadening the notion of metal chelators in medicine. *Curr Opin Chem Biol*. 2013;17(2):143-149.

179. Faridoon, Ul Islam N. An update on the status of potent inhibitors of metallo-β-lactamases. *Sci Pharm*. 2013;81(2):309-327.

180. Payne DJ, Bateson JH, Gasson BC, *et al*. Inhibition of metallo-β-lactamases by a series of mercaptoacetic acid thiol ester derivatives. *Antimicrob Agents Chemother*. 1997;41:135-140.

181. Antony J, Gresh N, Olsen L, *et al*. Binding of D- and L-captopril inhibitors to metallo-β-lactamase studied by polarizable molecular mechanics and quantum mechanics. *J Comput Chem*. 2002;23(13):1281-1296.

182. Heinz U, Bauer R, Wommer S, *et al*. Coordination geometries of metal ions in D- or L-captopril-inhibited metallo-β-lactamases. *J Biol Chem*. 2003;278(23):20659-20666.

183. Brem J, van Berkel SS, Zollman D, *et al*. Structural basis of metallo-β-lactamase inhibition by captopril stereoisomers. *Antimicrob Agents Chemother*. 2015;60(1):142-150.

184. Buynak JD, Chen H, Vogeti L, *et al*. Penicillin-derived inhibitors that simultaneously target both metallo- and serine-β-lactamases. *Bioorg Med Chem Lett*. 2004;14(5):1299-1304.

185. Tsang WY, Dhanda A, Schofield CJ, *et al*. The inhibition of metallo-β-lactamase by thioxo-cephalosporin derivatives. *Bioorg Med Chem Lett*. 2004;14(7):1737-1739.

186. Nagano R, Adachi Y, Imamura H, *et al*. Carbapenem derivatives as potential inhibitors of various β-lactamases, including class B metallo-β-lactamases. *Antimicrob Agents Chemother*. 1999;43(10):2497-2503.

187. Johnson JW, Gretes M, Goodfellow VJ, *et al*. Cyclobutanone analogues of β-lactams revisited: Insights into conformational requirements for inhibition of serine- and metallo-β-lactamases. *J Am Chem Soc*. 2010;132(8):2558-2560.

188. Walter MW, Felici A, Galleni M, *et al*. Trifluoromethyl alcohol and ketone inhibitors of metallo-β-lactamases . *Bioorg Med Chem Lett*. 1996;6:2455-2458.

189. Walter MW, Adlington RM, Baldwin JE, Schofield CJ. Synthesis of metallo-β-lactamase inhibitors. *Tetrahedron*. 1997;53:7275-7290.

190. Toney JH, Fitzgerald PM, Grover-Sharma N, *et al*. Antibiotic sensitization using biphenyl tetrazoles as potent inhibitors of *Bacteroides fragilis* metallo-β-lactamase. *Chem Biol*. 1998;5(4):185-196.

191. Toney JH, Hammond GG, Fitzgerald PM, *et al*. Succinic acids as potent inhibitors of plasmid-borne IMP-1 metallo-β-lactamase. *J Biol Chem*. 2001;276(34):31913-31918.

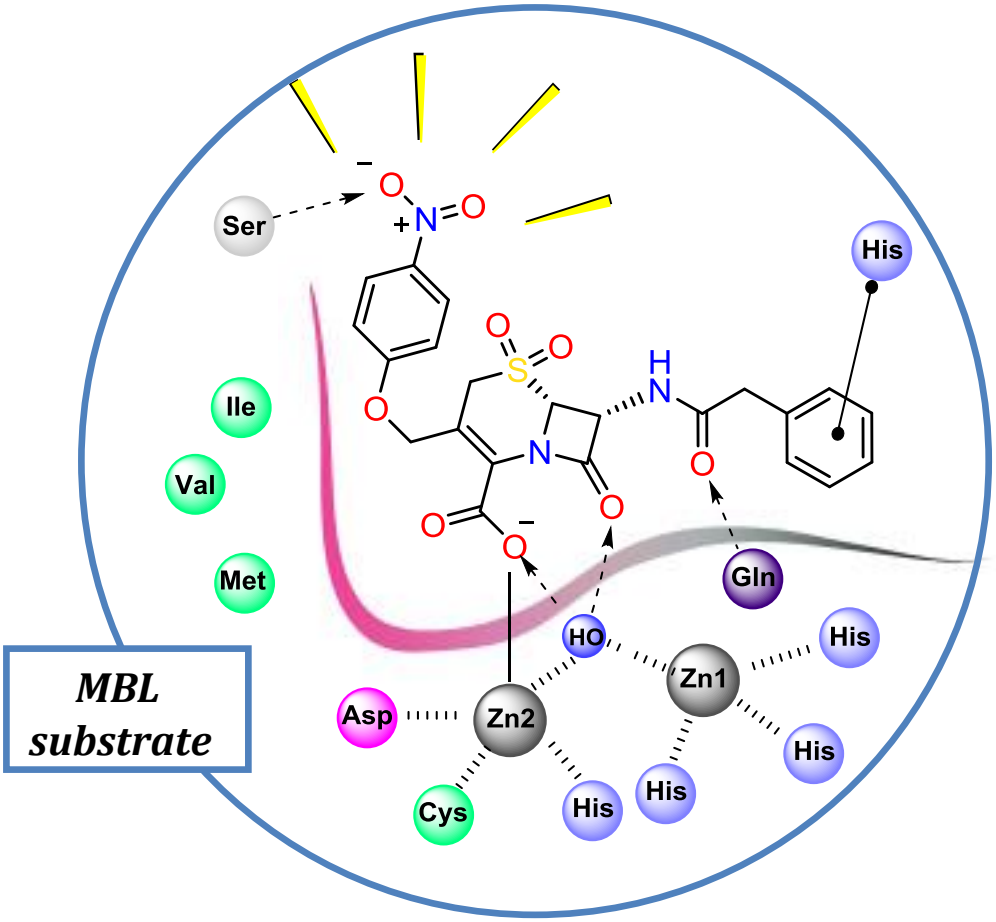
192. Agrawal A, DeSoto J, Fullagar JL, *et al*. Probing chelation motifs in HIV integrase inhibitors. *Proc Natl Acad Sci U S A*. 2012;109(7):2251-2256.

193. World Health Organisation (WHO). Antimicrobial resistance: Global report on surveillance 2014. Updated 2014. Accessed March, 2016.

194. Bonnin RA, Poirel L, Naas T, *et al*. Dissemination of New Delhi metallo-β-lactamase-1-producing *Acinetobacter baumannii* in Europe. *Clin Microbiol Infect*. 2012;18:E362-5.

CHAPTER 2: DEVELOPMENT OF A NOVEL CHROMOGENIC SUBSTRATE (**CLS405**) FOR MBL ASSAYS

The efficient development of MBL inhibitors hinges on the availability of suitable screening platforms for the rapid determination of β-lactamase activity and inhibition. At the onset of my work, the presently available screening platforms had limited applicability for high throughput screening. This chapter describes work on the development of an inexpensive and reliable chromogenic substrate for screening the activity and efficient inhibition of MBLs. Preliminary attempts to develop a fluorescent cell-based assay are also described.



CONTENTS

CHAPTER 2: DEVELOPMENT OF A NOVEL CHROMOGENIC SUBSTRATE (**CLS405**) FOR MBL ASSAYS 63

2.1 INTRODUCTION 65

2.1.1 β-lactamase assays 65

2.1.2 Spectrophotometric techniques 66

2.1.3 Chapter Objectives 68

2.2 PRODUCTION AND PURIFICATION OF MBLS 69

2.2.1 Cloning 69

2.2.2 Recombinant protein production 70

2.2.3 Mass Analyses 71

2.3 **CLS405** SUBSTRATE SYNTHESIS 72

2.4 SUBSTRATE CHARACTERISATION 73

2.4.1 Spectroscopic analyses 73

2.4.2 Stability of **CLS405** 74

2.5 EVALUATION OF KINETIC PARAMETERS 76

2.5.1 Steady-State Kinetic Analyses 76

2.6 ASSAY VALIDATION 80

2.6.1 Residual activity determination 80

2.6.2 Determination of IC_{50} values 84

2.7 FLUOROGENIC SUBSTRATE FOR CELL-BASED ASSAYS 87

2.8 SUMMARY 89

2.9 REFERENCES 90

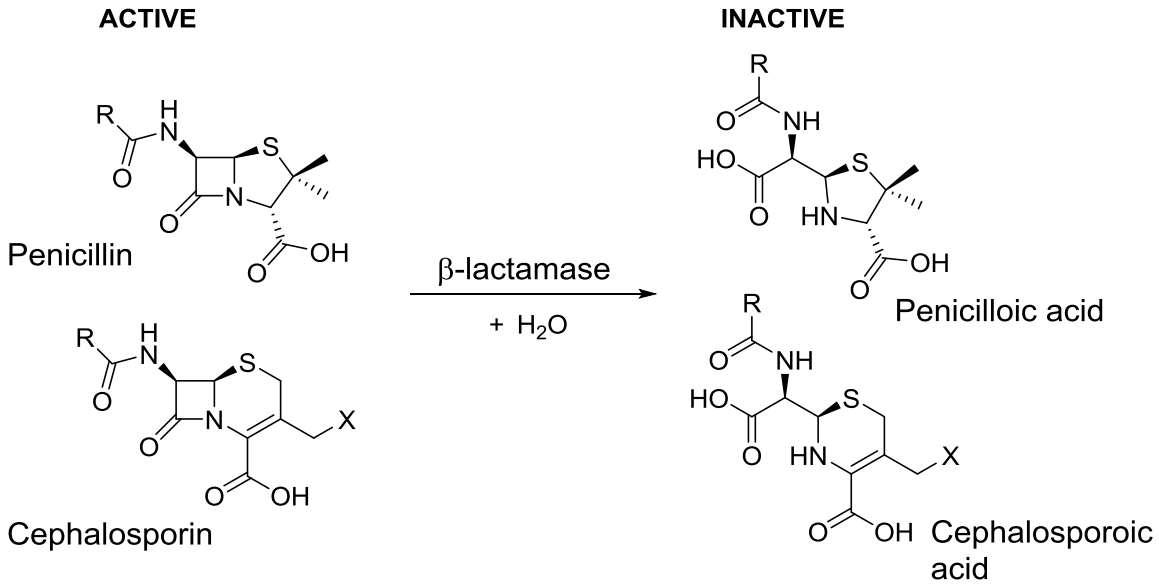
2.1 INTRODUCTION

The binding of small ligands to macro-molecules is crucial to most aspects of biological function. Understanding the structural, kinetic and thermodynamic aspects of ligand binding interactions can therefore provide relevant mechanistic information for rational drug design and development. Consequently, the development of expedient assay platforms, in this case for the evaluation of β-lactamase activity, is vital for the discovery of potent, broad-spectrum inhibitors of metallo-β-lactamases (MBLs). Although various studies have and continue to identify different potential MBL inhibitors[1-3], a potent MBL inhibitor with a sufficient breath of selectively for clinical use has yet to be identified. The therapeutic use of the classical serine β-lactamase inhibitors (avibactam, clavulanic acid, tazobactam and sulbactam) in combination with β-lactams is currently one of the most successful strategies to combat serine β-lactamase-mediated resistance. It is therefore anticipated that an MBL inhibitor should restore the effectiveness of β-lactam antibiotics against MBL producing bacteria. Ideally, an MBL assay would be affordable, sensitive and efficient for the rapid detection of MBL activity and application in high-throughput screening (HTS) of compounds for their potential inhibitory activity.

2.1.1 β-LACTAMASE ASSAYS

β-Lactamase assays are primarily based on the ability of the enzymes to catalyse the hydrolysis of the β-lactam ring, resulting in reaction products with physicochemical properties different from those of the substrate (*Scheme 2-1*). β-Lactamase assays based on the loss of antibiotic activity of the hydrolysed product (biological assays) and its ability to behave as an acid or as a reducing agent have been reported. The assays relying on the changed chemical properties include iodometric assays based on the reduction of iodine by the hydrolysed product resulting in decolourisation of the starch–iodine complex[4], pH-stat titrations[5], acidometric assays employing colorimetric pH indicators such as phenol red[6] and

manometric assays involving the measurement of CO_2 released by the interaction of sodium bicarbonate with the hydrolysed product[7].



***Scheme 2-1*: Hydrolysis of β-lactam antibiotics and the resultant inactive products.**

The iodometric assays were time consuming and temperature dependent and most of the pH-based assays lacked sensitivity and yielded inconsistent results due to the differences in the hydrolysed products of various β-lactam substrates[8]. In addition, reaction intermediates and products of cephalosporin and carbapenem hydrolysis are often not well characterised[9]. These pioneering assays have largely been superseded by more robust spectrophotometric methods based on distinct change in UV/Vis absorbance between the substrate and the resultant hydrolysed product[10].

2.1.2 SPECTROPHOTOMETRIC TECHNIQUES

Spectrophotometric methods are normally designed to measure either the concentration of the residual intact substrate or that of the hydrolysed products at their respective maximum absorption wavelengths (λ_{max}). Earlier direct β-lactamase assays included an assay which relied on the reaction of hydroxylamine with β-lactams to produce hydroxamic acid, which would then react with ferric ions to give a chromogenic product[11].

These hydroxylamine assays were rather unreliable and are no longer in use[12]. The initial spectrophotometric cephalosporinase assays were described by O'Callaghan *et al*, in which the absorption of cephaloridine was monitored at 255 nm[13,14]. This work led to the identification of nitrocefin as a chromogenic cephalosporin-based reporter substrate for β-lactamase activity[15]. The assay was later adapted for monitoring penicillinase activity[16], and exemplified by the synthesis of a chromogenic penicillin substrate, *N*-(2-furyl)acryloyl penicillin[17]. Spectrophotometric methods have since become the preferred β-lactamase assay platforms with other chromogens being developed as reporter substrates including PADAC[18], CENTA[19], chromacef[20] and the recently reported nitrocefin derivatives[21] (*Figure 2-1*). Cephalosporin-based substrates typically rely on the attachment of either a chromogenic leaving group (as in CENTA) or a highly conjugated group (as in chromacef and nitrocefin) at the C3 position of the cephem ring, inducing a bathochromic shift in λ_{max} upon the hydrolysis of the β-lactam ring.

Previously used β-lactam reporter antibiotics such as imipenem suffer from poor analytical sensitivity due to lower molar extinction coefficients and interference from other assay components in the shorter wavelengths, limiting the use of such substrates at high concentrations. Chromogenic substrates circumvent this problem and enable the use of spectrophotometric assays in the visible light spectral range with little interference from most common assay components. However, the use of currently used cephalosporin-based chromogenic substrates in high throughput screening is often limited by the substrates' low stability, light sensitivity, and high cost (in particular for nitrocefin). Although more sensitive fluorogenic substrates have been developed for MBL assays[22-24], the simplicity of chromogenic assays coupled with the low cost of a spectrophotometer remains a notable advantage.

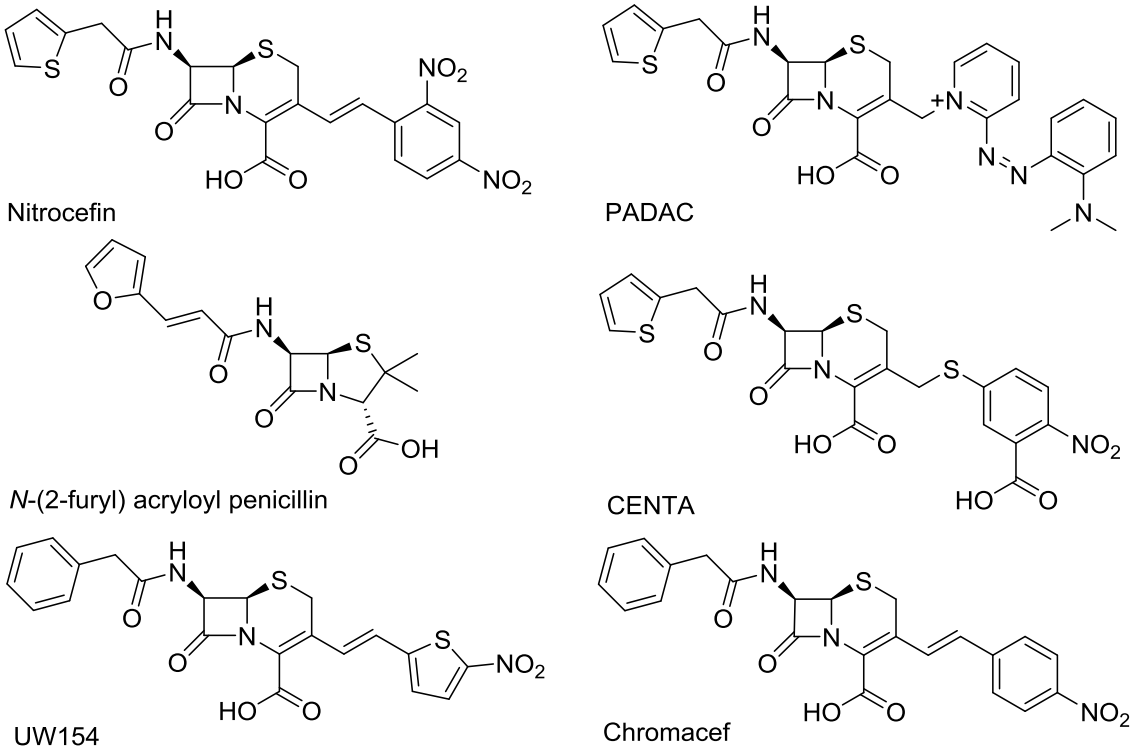


***Figure 2-1*: Structures of commonly used β-lactam substrates.**

2.1.3 CHAPTER OBJECTIVES

Owing to the limitations of the presently available MBL assay platforms, the main goal of the work described in this chapter was to identify a broadly applicable and cost-efficient chromogenic substrate that is suitable for MBLs activity and inhibitor screening. This work aims to describe the identification of a novel cephalosporin-based chromogenic substrate **CLS405** and subsequent spectroscopic and stability analysis of the substrate. The chapter elucidates the biological evaluation of this substrate using a representative set of clinically relevant MBLs and the assessment of the suitability of the **CLS405**-based assay in MBL inhibition assays. Additionally, possible improvements on the assay platform are discussed, with preliminary results on a sequel fluorescence cell-based assay presented. Most the work described in this chapter has been reported in academic literature[25].

This work was performed in collaboration with Dr. Sander van Berkel who synthesised the substrates and Dr. Jurgen Brem, who obtained the MBL-encoding plasmids and facilitated the protein production.

2.2 PRODUCTION AND PURIFICATION OF MBLS

Five of the most clinically relevant MBLs were selected for this study, including Imipenemase-1 (IMP-1), Verona Integron-Borne metallo-β-lactamases (VIM-1, VIM-2), Sao Paulo metallo-β-lactamases (SPM-1) and New Delhi metallo-β-lactamases (NDM-1). BcII, a model MBL from the innocuous *Bacillus cereus*, was also included. Protein production and purification protocols were first optimised to obtain high yields of the purified proteins for subsequent analyses.

2.2.1 CLONING

Recombinant BcII and IMP-1 were produced using the previously reported pET-9a-BcII[26] pET-26b-IMP-1[27] vectors. The pOPIN-F plasmids (based on the pTriEx vectors)[28] were used for the production of recombinant NDM-1, VIM-1, VIM-2 and SPM-1. Codon-optimised genes encoding full-length and truncated constructs of the proteins (*Table 2-1*) were inserted into the *E. coli* vectors. Using the standard heat shock technique, *E. coli* BL21 (DE3) pLysS cells were then transformed with the MBL-encoding plasmids for the overproduction of the recombinant MBLs via the T7 expression system.

***Table 2-1*: Constructs used for production of recombinant MBLs.**

Name	Construct	Vector	Tag	Cleavage site	References
NDM-1	G42–R273	pOPIN-F	*N*-terminal His_6	3C protease	[29]
IMP-1	A19–N245	pET-26b	No tag	N/A	[27]
VIM-1	L2–E266	pOPIN-F	*C*-terminal His_6	none	[25]
VIM-2	V27–E266	pOPIN-F	*N*-terminal His_6	3C protease	[23]
SPM-1	K29–L276	pOPIN-F	*N*-terminal His_6	3C protease	[23]
BcII	S31–K257	pET-9a	No tag	N/A	[26]

2.2.2 RECOMBINANT PROTEIN PRODUCTION

Expression trials were initially carried out to determine conditions most favourable for protein production. Cells expressing the different MBLs were cultured in 2TY media and the recombinant MBLs were produced efficiently in the optimised conditions as outlined in Chapter 7. Standard chromatographic techniques including nickel affinity, size exclusion and ion exchange chromatography were utilized for purification of recombinant MBLs[23,25]. Elution fractions containing the target proteins were concentrated by centrifugal ultrafiltration and the purity of all the produced recombinant MBLs was ascertained to be > 90% by SDS-PAGE analysis (*Figure 2-2*). The optimized protein production and purification protocols yielded recombinant MBLs purified to near homogeneity (as judged by SDS PAGE analyses) and in sufficient quantities for the subsequent analyses.

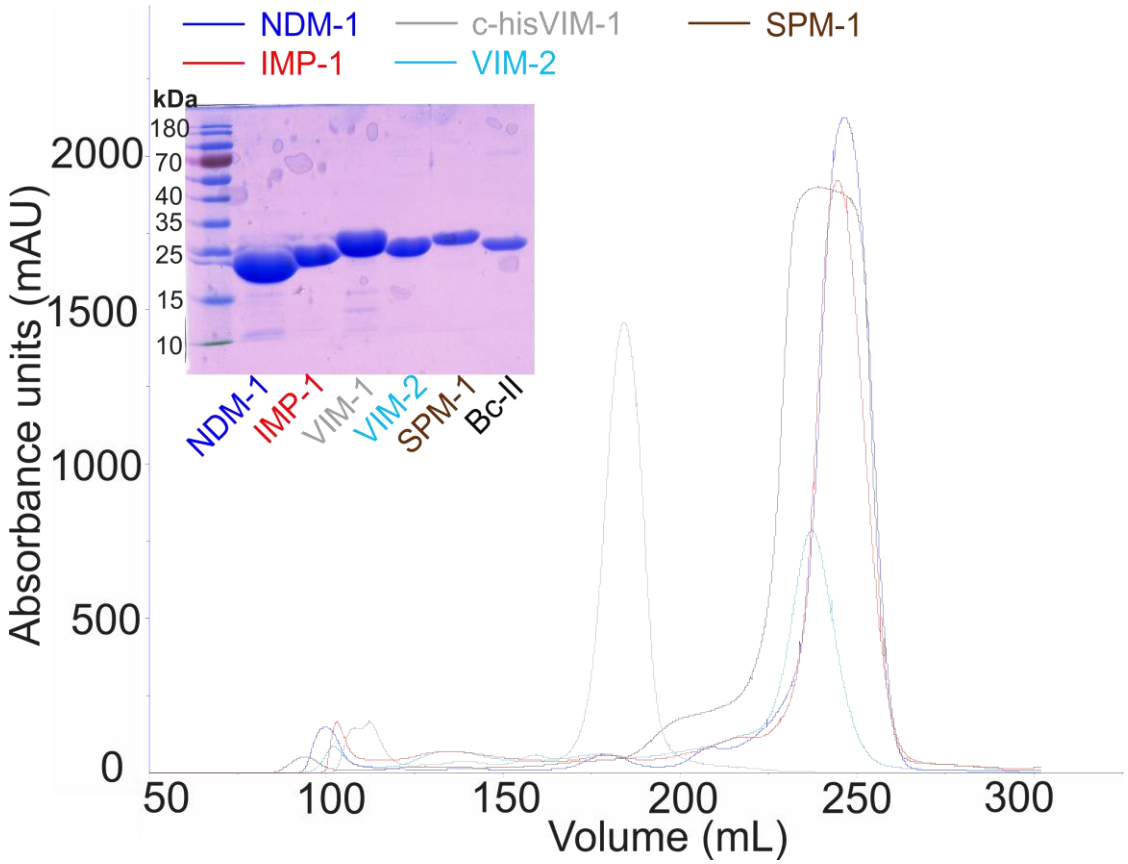
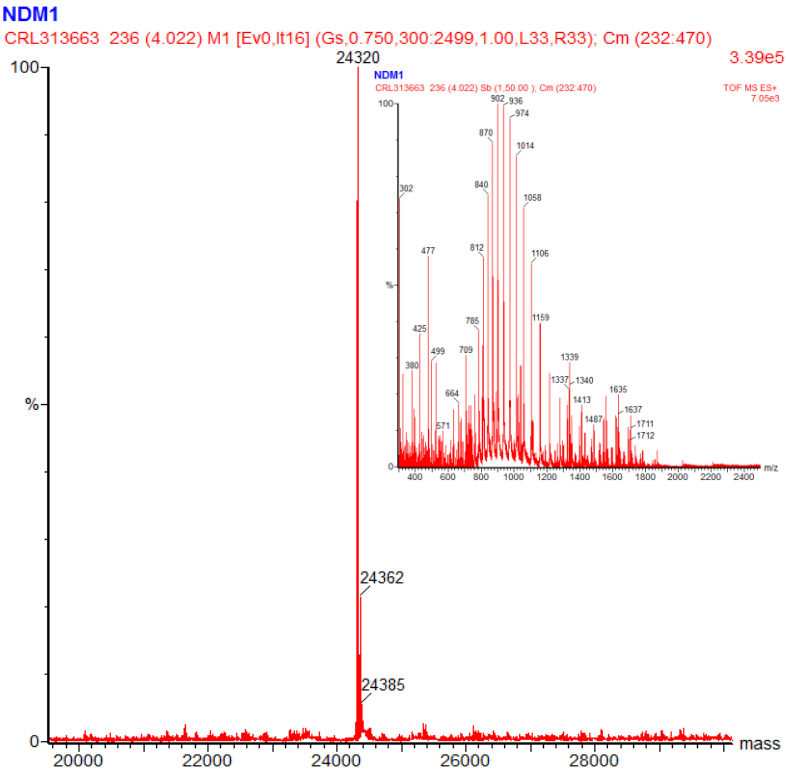


***Figure 2-2*: Overlaid chromatograms of NDM-1, VIM-1, VIM-2, SPM-1 and IMP-1 after size exclusion chromatography. Inset: SDS PAGE analyses showing the purity of the produced recombinant proteins.**

2.2.3 MASS ANALYSES

To verify the masses of the recombinant enzymes, electrospray ionisation mass spectra (ESI-MS) were acquired in the positive ion mode under denaturing conditions using a micromass LCT Premier time-of-flight mass spectrometer coupled to an Agilent 1100 Series HPLC. The resulting combined positive ion series was deconvoluted using a maximum entropy algorithm (*Figure 2-3*) and analysed using the MassLynx v4.0 software (Chapter 7.5).

The observed masses were found to be in close agreement with the predicted masses obtained using the ExPasy ProtParam tool (http://web.expasy.org/protparam/). Mass spectrometic analyses therefore confirmed the masses and further verified the purity of the produced MBLs.



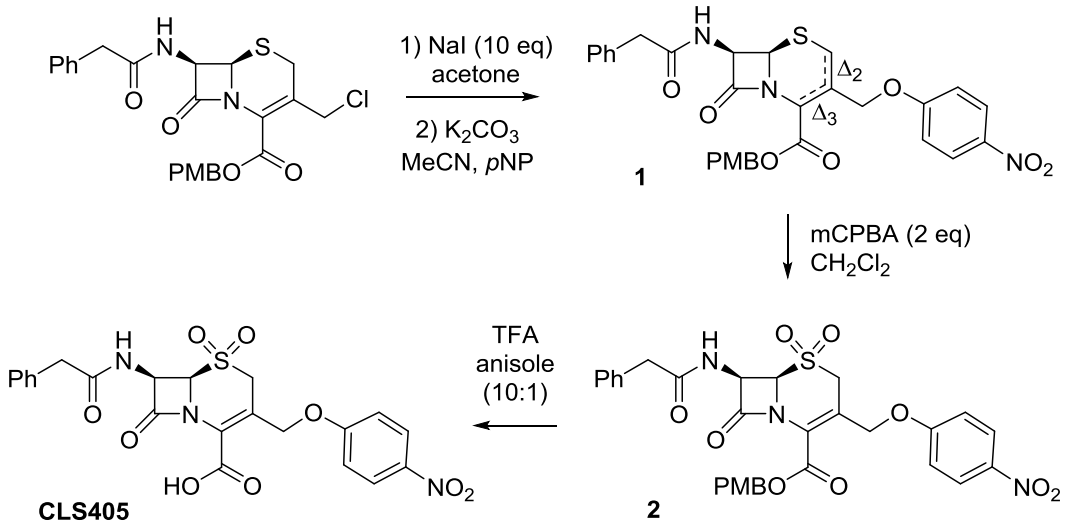
	Predicted	Obtained	shift
NDM-1	24318	24320	2
IMP-1	25112	25110	2
VIM-1	26273	26275	2
VIM-2	25669	25670	1
SPM-1	27884	27888	4
BcII	24960	24952	8

***Figure 2-3*: Combined ion series and deconvoluted mass spectra for NDM-1 after applying the maximum entropy algorithm to the shown ion series. Inset: Comparison of the predicted and obtained masses (in Daltons) for the tested MBLs.**

2.3 **CLS405** SUBSTRATE SYNTHESIS

For efficient hydrolysis by target MBLs, a cephalosporin substrate with a UV active 'leaving group' was desirable. Various chromophore-based cephalosporins were evaluated and nitrophenol-linked cephalosporins were selected based on the frequent use of the chromogenic *p*-nitrophenol (pNP) leaving group in protease, esterase and in early β-lactamase assays[30-32]. This led to the identification of the 'chromophore linked substrate', aptly named **CLS405**, as a candidate substrate. The hydrolysis of the β-lactam ring in **CLS405** results in the release of the *p*-nitrophenol (pNP) leading to a distinct change in UV/Vis absorbance.

The substrate was thus synthesised (by Dr. S. van Berkel) using a three-step protocol starting from commercially available PMB-protected chloro-cephalosporin (*Scheme 2-2*) to efficiently produce the desired chromogenic substrate **CLS405** (52% yield).



***Scheme 2-2*: Three-step protocol for the synthesis of chromogenic substrate CLS405.**

2.4 SUBSTRATE CHARACTERISATION

The chromogenic substrates (CENTA, nitrocefin and **CLS405**) were prepared as stock solutions in DMSO, which were diluted in the MBL assay buffer (50 mM HEPES buffer, pH 7.2, supplemented with 1 µg/mL BSA, 1 µM $ZnSO_4$ and 0.01% Triton X-100). To determine the maximum absorption wavelengths of the substrates, the absorption spectra of the substrates (30-600 µM) were determined using a Varian Cary 4000 UV-Vis spectrophotometer. The substrates were then incubated with 1 mM NDM-1 and the absorbance spectra of their corresponding hydrolysis products collected (*Figure 2-4*).

2.4.1 SPECTROSCOPIC ANALYSES

The maximum absorbance wavelength of **CLS405** (λ_{max} = 305 nm) differed significantly from that of its hydrolysis product, pNP, whose maximum absorbance is 405 nm (*Figure 2-4*). This was comparable to nitrocefin, which recorded a $\Delta\lambda_{max}$ of 107 nm. The hydrolysis of CENTA to its 3′ leaving group (5-mercapto-2-nitrobenzoic acid) yields a $\Delta\lambda_{max}$ of 59 nm in comparison. Due to the larger $\Delta\lambda_{max}$ of **CLS405**, there is a significantly less overlap between the substrate and the product peaks, thus enabling the monitoring of either substrate degradation or product formation with higher analytical accuracy.

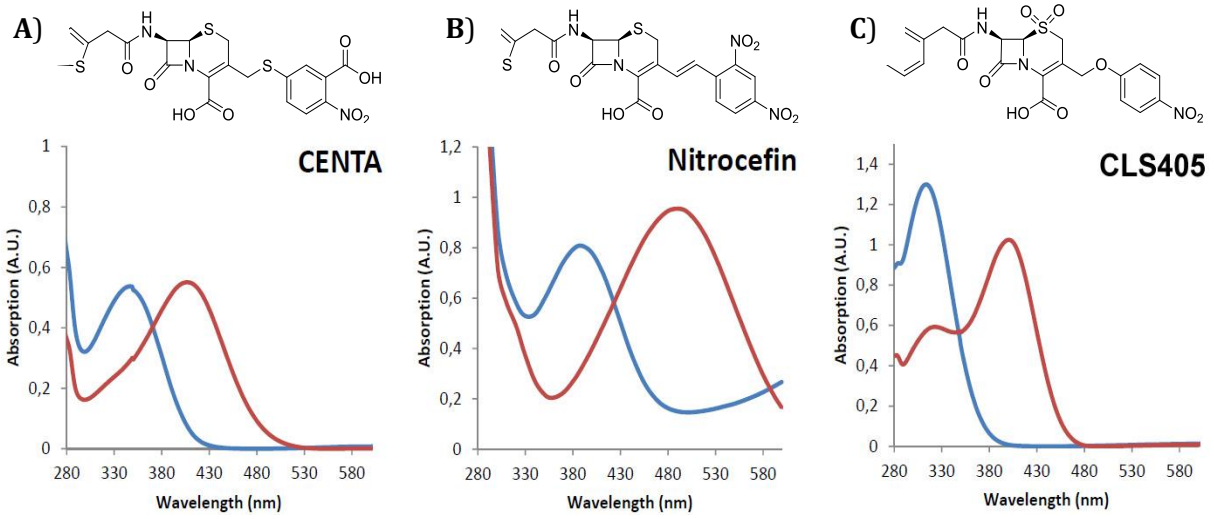


Figure 2-4: **Substrate and product absorption spectra for CENTA (λ_{max}S=347 nm, λ_{max}P=406 nm), nitrocefin (λ_{max}S=389 nm, λ_{max}P=496 nm) and CLS405 (λ_{max}S=305 nm, λ_{max}P=405 nm). Blue and red lines represent the substrate (S) and product (P) spectra respectively.**

2.4.2 STABILITY OF **CLS405**

To assess the stability of **CLS405**, a solution of the substrate (100 µM) was incubated at 25 °C in buffers at varying pH values and the absorbance of the substrate and the hydrolysis product monitored at 305 and 405 nm respectively every 30 minutes for 12 hours. Phosphate-citrate buffer was used to obtain a pH range of 3 to 7, and Tris-HCl buffer was used for a pH range of 8 to 10. The stabilities of **CLS405**, CENTA and nitrocefin in the MBL assay buffer (at pH 7.2) were also investigated by monitoring the changes in the absorbance of the substrates and products at their respective wavelengths.

2.4.2.1 pH STABILITY

CLS405 appears to be more stable in higher pH ranges. In the pH range of 3-6, about 50% of the substrate signal is diminished after 12 hours as judged by changes in absorbance values at 305 nm (*Figure 2-5 A*). However, in the alkaline pH ranges (7-10), the absorbance values are reduced by < 20% over the 12 hour incubation. The absorbance of the hydrolysis product at 405 nm shows similar results where the absorbance of the product is highest from pH 8. These results are in agreement with the established behaviour of p-nitrophenol in aqueous solutions[33].

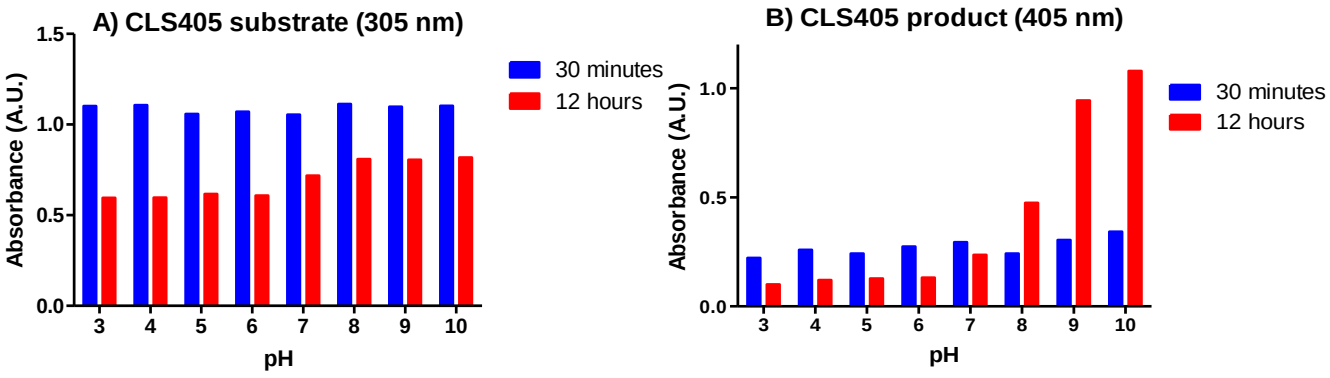


Figure 2-5: **Stability of CLS405 at varying pH monitored at A) 305 nm for the substrate absorbance; B) 405 nm for product absorbance. The blue and red bars represent absorbance values taken after 30 min and 12 hours respectively.**

2.4.2.2 STABILITY IN ASSAY BUFFER

Further investigations were then carried out to compare the stability of the chromogenic substrates in the MBL assay buffer typically used in kinetic experiments.

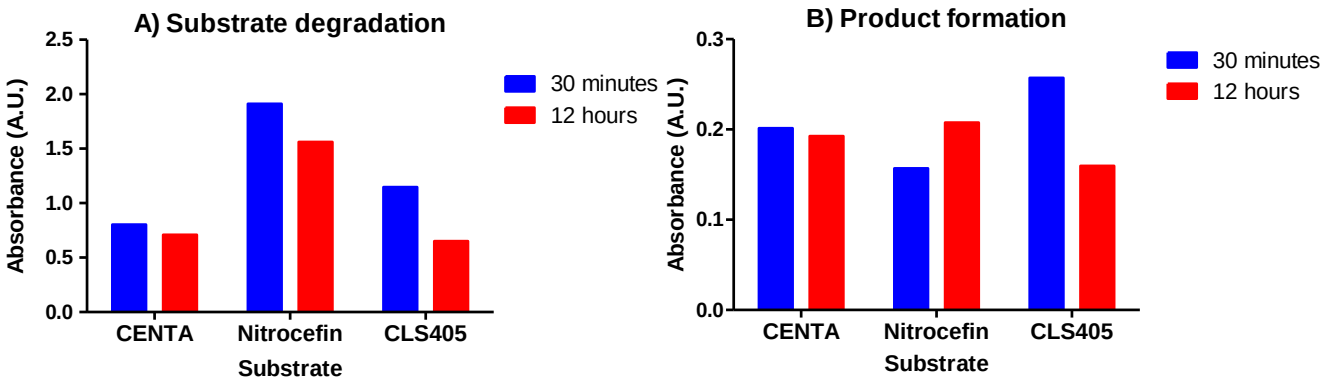


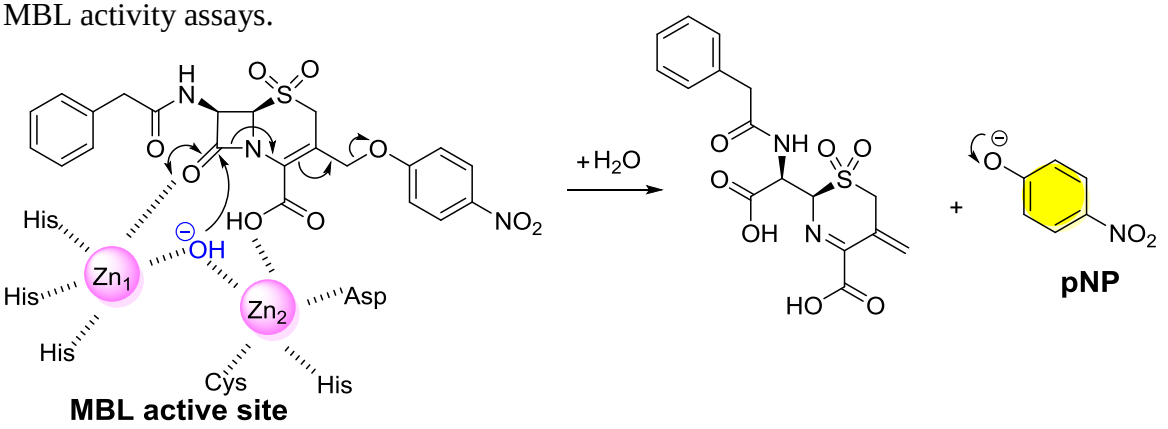
Figure 2-6: **Stability of the tested substrates MBL assay buffer monitored at their respective substrate (A) and product (B) wavelengths. Absorbance values measured after 30 min and 12 hours are shown in blue and red bars respectively.**

CENTA was the most stable substrate in the MBL assay buffer with <10 % reduction in the absorbance of the substrate within the 12 hour period (*Figure 2-6 A*). Although **CLS405** was shown to be less stable than the other substrates in the MBL assay buffer at room temperature, it was established that **CLS405** solutions in the buffer could be used for 1–2 days when stored on ice while the DMSO stock solutions (100 mM) could be stored at −20 °C for up to four months after preparation without any detectable decomposition. The substrate could also be stored for months as a solid at 4 °C allowing the use of this compound over a prolonged period of time.

The described favourable spectral and stability properties observed made **CLS405** a suitable substrate for subsequent application in MBL activity and inhibition assays.

2.5 EVALUATION OF KINETIC PARAMETERS

The hydrolytic activity of a representative panel of clinically relevant MBLs was compared using the CENTA, nitrocefin and **CLS405** substrates, to investigate the suitability of **CLS405** in MBL activity assays.



Scheme 2-3: **Proposed mechanism of MBL-mediated CLS405 hydrolysis with the release of UV-active *p*-nitrophenolate anion.**

2.5.1 STEADY-STATE KINETIC ANALYSES

Steady-state kinetic assays were carried out by monitoring enzyme-mediated changes in absorbance at 495 nm for nitrocefin and 405 nm for CENTA and **CLS405** (i.e. product formation). The experiments were carried out at 25 °C in triplicate ($n \geq 3$) and the absorbance values were read using a Pherastar FS plate reader (BMG Labtech), with the enzyme and substrate stocks diluted in MBL assay buffer (Chapter 7.6). To determine the effective molar absorption coefficients, the varying concentrations of the substrates were incubated with 1 nM NDM-1 and a calibration curve was generated by plotting the absorbance units against increasing concentrations of the hydrolysis products (*Figure 2-7*).

Kinetic constants (K_M and k_{cat}) were obtained by determining the initial rate of hydrolysis (as defined by product formation) at different substrate concentrations (0.4-500 µM) using the determined optimum enzyme concentrations (*Table 2-2*). The concentration-dependence of the initial rate was fitted and analysed using GraphPad Prism® 5.01 software to generate Michaelis-Menten curves (*Figure 2-8*).

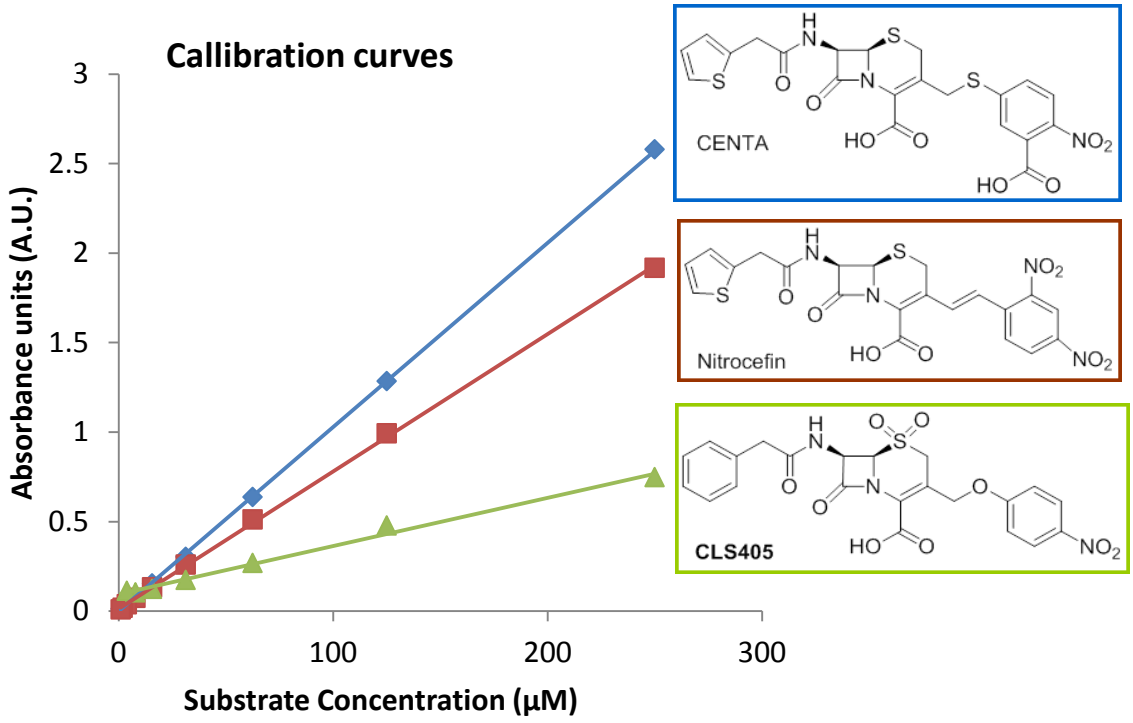


Figure 2-7: **Calibration curves of the hydrolysis products of CENTA, nitrocefin and CLS405 (ε = 10300, 7700 and 2600 M^{-1} cm^{-1} respectively).**

2.5.1.1 OVERALL CATALYTIC EFFICIENCY (k_{cat}/K_M)

CLS405-based assay was shown to be highly sensitive allowing the use of very low MBL concentration (in picomolar range). Among the tested MBLs, BcII concentration was highest at 400 pM, which was still less than half the enzyme concentration used for the other substrates (*Table 2-2*). The concentration of IMP-1 used in the **CLS405** assay was as low as 10 pM; while the NDM-1 concentration used was up to 20 times lower for **CLS405** compared to the other substrates. Notably, the overall catalytic efficiency (as defined by k_{cat}/K_M values) was highest with **CLS405** for all the tested MBLs, with NDM-1 manifesting a 70-fold higher k_{cat}/K_M value with **CLS405** compared to the other substrates. This is largely attributed to higher turnover rates as discussed below. The highest k_{cat}/K_M value recorded for **CLS405** was with IMP-1 (> 700 μM^{-1} s^{-1}) while the lowest activity was with BcII (3 μM^{-1} s^{-1}), which also reported relatively low k_{cat}/K_M values for the other substrates. It is notable that nitrocefin substrate/product inhibition was observed with SPM-1 (*Figure 2-8 E*).

2.5.1.2 BINDING AFFINITY (K_M)

There were no substantial difference in the K_M values reported for the substrates and no clear trend was observed when comparing the K_M values of **CLS405**, CENTA and nitrocefin for the different MBLs. It is however, notable that K_M values for **CLS405** were between 10-80 µM for the different MBLs tested, enabling subsequent inhibitor screens to be carried out at < 100 µM substrate concentration. The variation in binding affinities as defined by K_M values could reflect, in part, the relatively low sequence similarity between the different MBLs and the subsequent effects on substrate recognition.

Table 2-2: **Kinetic parameters for the 3 chromogenic substrates tested on 6 MBLs.**

	[E] (pM)			K_M (µM)[a]			k_{cat} (s^{-1})[b]			k_{cat}/K_M (μM^{-1} s^{-1})		
	CENTA	NIT	**CLS405**	CENTA	NIT	**CLS405**	CENTA	NIT	**CLS405**	CENTA	NIT	**CLS405**
NDM-1	1000	1000	50	35 ± 7	9 ± 1	10 ± 1	90	25	2120	3	3	210
IMP-1	100	50	10	17 ± 2	56 ± 5	74 ± 6	430	2800	55 x 10^3	25	50	740
VIM-1	1000	500	250	98 ± 11	150 ± 1	30 ± 3	134	130	435	1	1	15
VIM-2	1000	100	40	26 ± 3	7 ± 1	22 ± 2	48	225	1255	2	32	57
SPM-1	1x10^4	5x10^4	250	25 ± 6	16 ± 4	11 ± 1	6	1	410	0.2	0.1	41
BcII	1000	1000	400	136 ± 16	8 ± 1	65 ± 5	9	15	210	0.1	2	3

[a] K_M values are provided as means of triplicate experiments ± standard deviation;
[b] Standard deviation for k_{cat} values did not exceed 10%

2.5.1.3 TURNOVER RATES (k_{cat})

The k_{cat} values were significantly higher with **CLS405** in comparison with the other tested substrates. IMP-1 reported the highest turnover rate (55 x 10^3 s^{-1}) and both NDM-1 and VIM-2 reported k_{cat} values >1000 s^{-1}. Note that the elevate k_{cat} values for IMP-1 are associated with the significantly low enzyme concentration required and dilution errors at such low concentrations cannot be entirely ruled out. These relatively higher k_{cat} values could be a

reflection of the favourable positioning of the sulfone moiety of **CLS405** in the enzyme's active site, facilitating efficient substrate hydrolysis and subsequent product release.

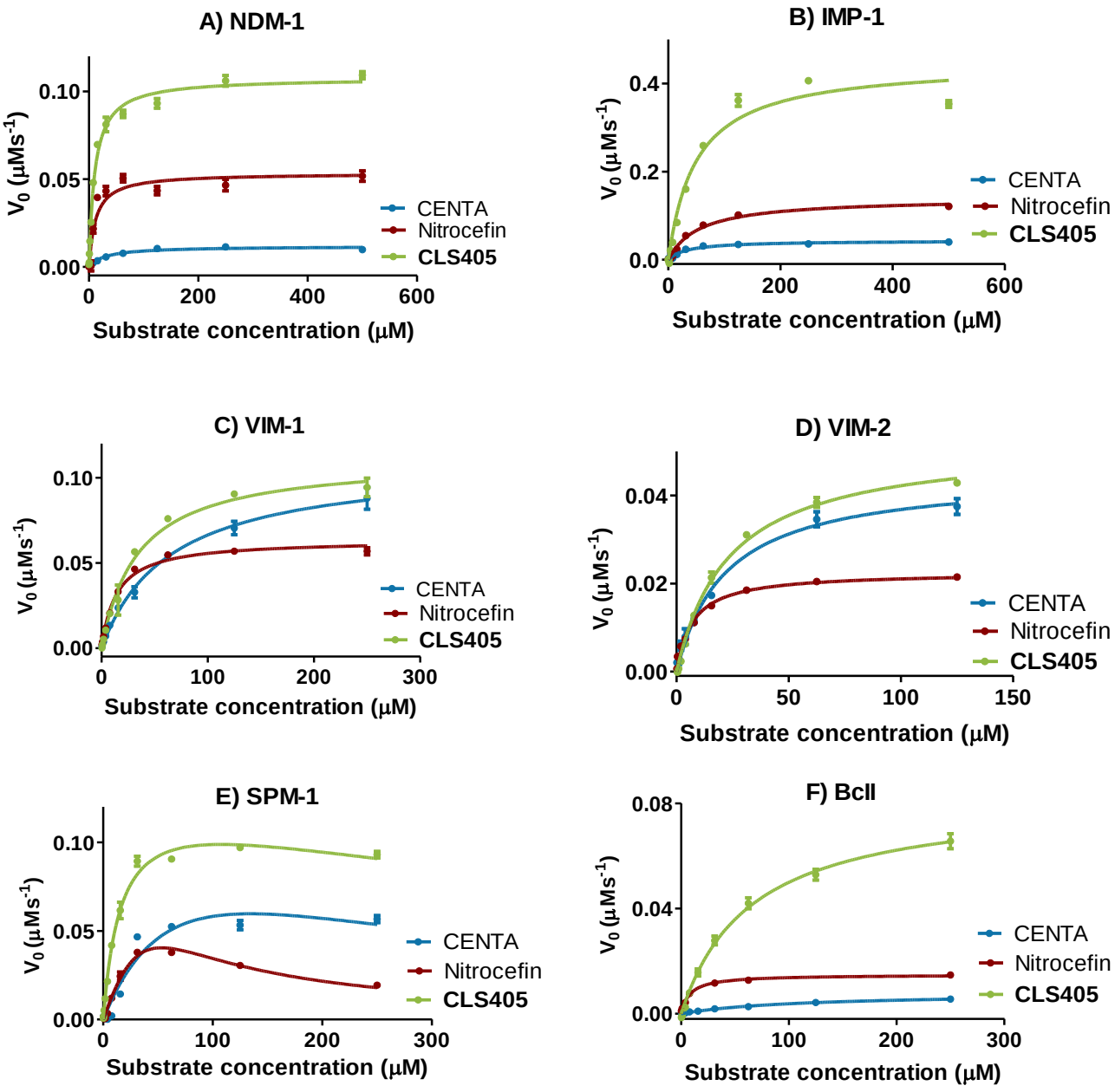


Figure 2-8: **Kinetic curves comparing the kinetics of different substrate - enzyme combinations.**

Altogether, these interesting kinetic results indicate that **CLS405** is indeed a superior substrate in comparison to the other substrates for evaluating activity of the tested class B1 MBL. Taking this into consideration, the **CLS405**-based assay was tested for utility with respect to MBL inhibitor screening.

2.6 ASSAY VALIDATION

To validate the utility of the **CLS405** based assay in inhibitor discovery, the substrate was used in an exemplary inhibitor screening assay using an in-house compound library comprising of known metallo-enzyme inhibitors.

2.6.1 RESIDUAL ACTIVITY DETERMINATION

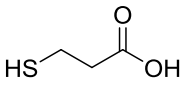
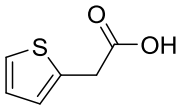
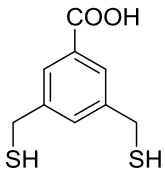
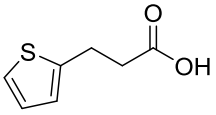
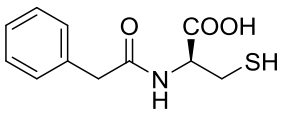
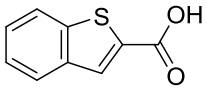
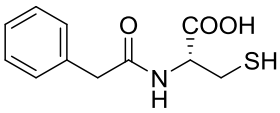
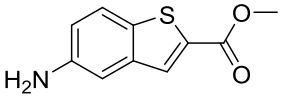
Inhibitors including thiols, hydroxamic acids, succinic acid analogues, triazoles and N-hydroxythiazoles were screened for inhibition of NDM-1 using **CLS405** as reporter substrate. These compounds were selected due to their reported inhibitory activities against β-lactamases and related enzymes, as is discussed below. Initially, the remaining activity (RA) of the enzyme in the presence of the inhibitor was determined at a single inhibitor concentration (100 µM). The enzyme (NDM-1) concentration was fixed at 50 pM and the substrate concentration used was close to the K_M value (10 µM). The enzyme was pre-incubated with the inhibitors for 10 minutes at room temperature, prior to the addition of the substrate as has been done in previous MBL inhibition studies [10,23]. The rate of hydrolysis of **CLS405** was determined by monitoring changes in absorbance at 405 nm (product formation) in the presence of the different inhibitors. A representative set of compounds with a residual activity <5 % were considered for further investigation.

2.6.1.1 THIOLS AND THIOPHENES

Due to their dependence on zinc ions for catalysis, MBLs are typically inhibited by thiols and chelating agents that bind to the metal centre and/or disrupt the interactions between the zinc ions and the hydrolytic water. Compounds containing zinc-binding sulfur atoms have formed one of the most common strategies for MBL inhibitor design. Previous structural studies of IMP-1 and VIM-2 complexed with thiol-based inhibitors revealed that the thiol groups intercalate the zinc ions, displacing the bridging water/hydroxide ions required for hydrolysis[34-36].

Of the thiol derivatives tested using the **CLS405**-based assay, only the mercaptopropionic acid (**1a**) and the dithiol (**1b)** were potent inhibitors of NDM-1 (*Table 2-3-1*). This was consistent with previous studies in which a series of mercaptoacetic acid thiol esters were shown to be potent inhibitors of BcII[37]. The dithiol **1b** had also been previously shown to have inhibitory activity against all three classes of MBLs, and particularly the monozinc CphA (K_i = 90 nM)[36]. Although cysteinyl derivatives have previously been reported as potent inhibitors of BcII and L1[38,39], similar compounds **1c** and **1d** manifested residual activities >30% with NDM-1 in this study. Therefore, for this set of compounds only the dithiol **1b** was used in the subsequent analyses.

***Table 2-3-1*: Set of thiol derivatives and the respective residual activities.**

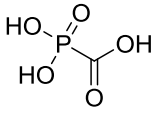
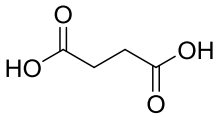
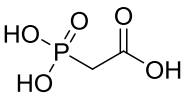
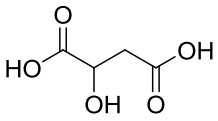
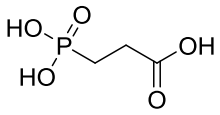
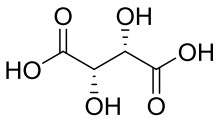
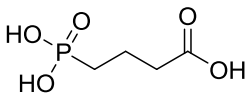
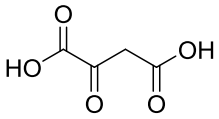
Entry	Thiols	RA (%)	Entry	Thiophenes	RA (%)
1a		< 1	1e		100
1b		< 1	1f		84
1c		32	1g		99
1d		66	1h		91

2.6.1.2 PHOSPHONATES AND SUCCINATES

Another set of metal chelators including phosphonic and succinic acid derivatives was also pre-screened for potential inhibition of NDM-1. Although the clinical potential of phosphonates is likely limited by their poor stability in aqueous solution and susceptibility to phosphodiesterases, phosphonate derivatives have been reported as effective β-lactamase inhibitors via acylation of the active site serines of class A, C and D β-lactamases[40-42].

Several succinic acid derivatives have also been identified as inhibitors of dizinc MBLs including IMP-1 and L1[43,44]. In this study, all the compounds from these classes exhibited residual activities >20% and therefore were not considered for IC_{50} determination (*Table 2-3-2*).

***Table 2-3-2*: Set of phosphonate and succinate derivatives and respective residual activities.**

Entry	Phosphonates	RA (%)	Entry	Succinic acid derivatives	RA (%)
2a		95	2e		80
2b		84	2f		51
2c		38	2g		52
2d		100	2h		100

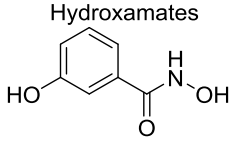
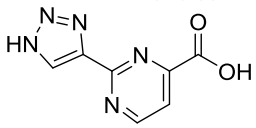
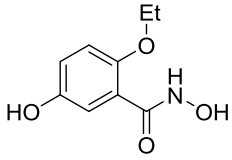
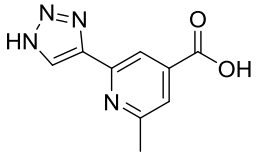
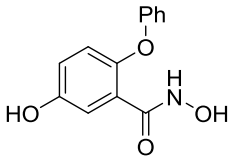
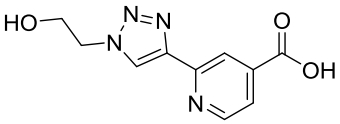
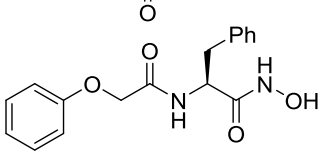
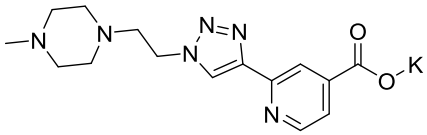
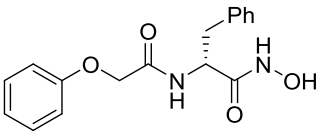
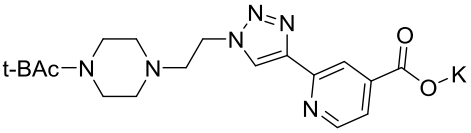
2.6.1.3 TRIAZOLES AND HYDROXAMATES

Hydroxamates were tested due to their structural similarity to α-amino trifluoromethyl ketones which have been shown previously to inhibit metallo-β-lactamases. Amino acid-derived hydroxamates have also been shown to inhibit MBLs from *A. hydrophila* but are inactive against MBLs from *B. cereus*[45]. More recent studies have also identified benzohydroxamic acids as potent inhibitors of class B3 FEZ-1 enzymes[46].

Inhibition of metallo-enzymes by triazole based compounds is also well documented. For MBLs in particular, a panel of compounds screened for potential inhibition of VIM-2 revealed two novel sulphonyl triazoles as potent VIM-2 inhibitors with Ki values in the sub-micromolar range[47,48] . Later studies have also identified mercaptotriazoles as potential IMP-1 inhibitors[49].

With the exception of the *S*-phenoxyacetamide derivative **3c**, the tested hydroxamates displayed relatively high RA values with NDM-1 and were therefore not used for subsequent IC_{50} determination. Equally, the triazoles used in this study were poor inhibitors of NDM-1 with RA values > 90% (*Table 2-3-3*).

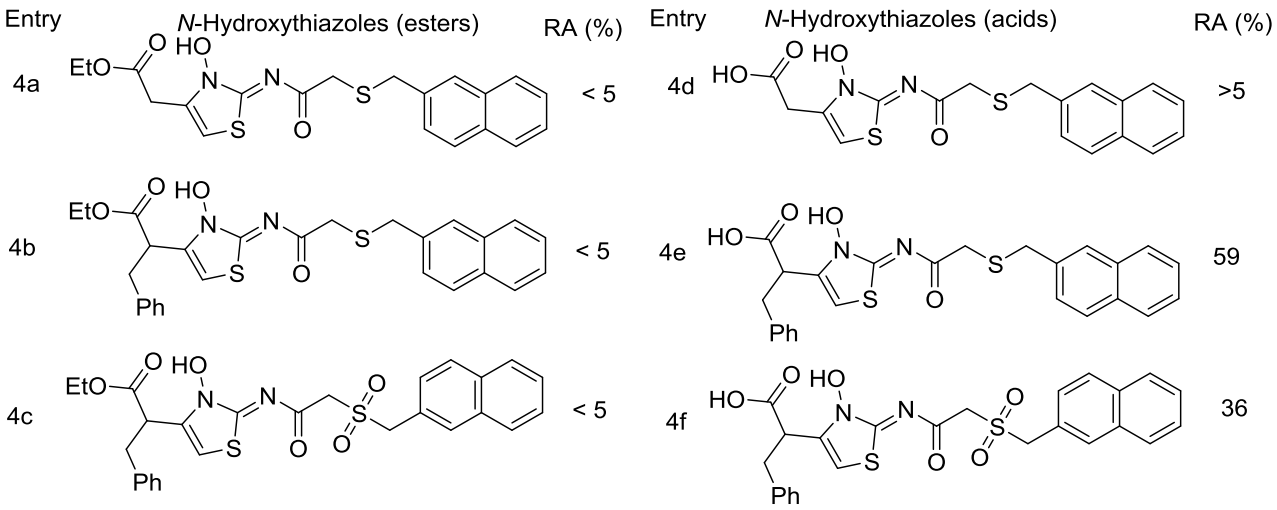
Table 2-3-3: **Triazole and hydroxamic acid derivatives used in this study.**

Entry	Hydroxamates	RA (%)	Entry	Triazoles	RA (%)
3a		83	3f		100
3b		78	3g		100
3c		22	3h		95
3d		75	3i		100
3e		71	3j		100

2.6.1.4 *N*-HYDOXYTHIAZOLES

Hydroxythiazoles have been reported as potential inhibitors of iron-containing enzymes including 2-oxogluterate dependent enzymes and lipooxygenases[50-52]. To test the potential for the cross-reactivity of these compounds, a panel of *N*-hydroxythiazole ester and carboxylic acid derivatives were screened. Interestingly, the ethyl ester derivatives of this class were shown to sufficiently inhibit NDM-1 with RA values being < 5 % and thus IC_{50} determinations were carried out. Their corresponding carboxylic acids were less potent, with the exception of compound **4d** (*Table 2-3-4*).

Table 2-4-4: **Set of the tested hydroxythiazole esters and corresponding acids.**



2.6.2 DETERMINATION OF IC_{50} VALUES

To further investigate the degree of inhibition of the tested inhibitors, IC_{50} values were determined for the compounds with a residual activity of < 5 %, including the hydroxythiazole ethyl esters (**4a, 4b** and **4c**), their corresponding acids (**4d** and **4f**) and the dithiol **1b** as a control. To obtain apparent IC_{50} values, the residual activities of a panel of 6 MBLs were determined (as previously described) at increasing inhibitor concentrations (0.8 – 400 µM). The enzyme concentrations used were the same as those used for kinetic analyses, and the concentration of the reporter substrate **CLS405** was maintained at or near the previously determined K_M values (*Table 2-2*). The % RA values were plotted against inhibitor concentrations and the data were analyzed with GraphPad Prism 5.01 software to obtain apparent IC_{50} values (*Table 2-4*).

The dithiol **1b** was found to be the most potent inhibitor, with IC_{50} values being < 5 µM for the tested MBLS. These results are in close agreement with previous studies on the inhibition of MBLs by this compound and warrant further investigation of derivatives of **1b** as potential broad-spectrum MBL inhibitors.

2.6.2.1 INHIBITION OF MBLS BY *N*-HYDOXYTHIAZOLES

An interesting result to emerge from this work was the differential inhibition of tested MBLs by *N*-hydroxythiazole derivatives (*Table 2-4*). In addition to identifying *N*-hydroxythiazoles as novel scaffolds for MBL inhibition, the results also indicated interesting structure-activity relationships with the small set of hydroxythiazoles tested.

Table 2-4: **IC_{50} values for the tested compounds with six MBLs.**

	IC_{50} (µM)					
Enzyme	**1b**	**4a (EtO)**	**4b (EtO)**	**4c (EtO)**	**4d (OH)**	**4f (OH)**
NDM-1	2 ± 1	9 ± 1	6 ± 1	13 ± 1	3 ± 1	27 ± 9
IMP-1	1 ± 0.3	>500	19 ± 8	>500	4 ± 1	155 ± 46
VIM-1	ND*	62 ± 21	16 ± 3	32 ± 6	6 ± 1	19 ± 9
VIM-2	3 ± 1	28 ± 7	11 ± 3	40 ± 17	162 ± 20	82 ± 19
SPM-1	1 ± 0.3	>500	3 ± 1	74 ± 20	2 ± 1	5 ± 1
BcII	2 ± 1	21 ± 13	8 ± 2	21 ± 8	81 ± 8	61 ± 20

*Not determined; EtO- ethyl ester derivatives; OH- carboxylic acid derivatives

The three tested ethyl esters (**4a, 4b** and **4c**) reported relatively low IC_{50} values with NDM-1 in agreement with the residual activity previously determined. Compound **4a** showed no significant inhibition of SPM-1 and IMP-1 (*Figure 2-9*) but displayed good inhibitory activity against NDM-1 (IC_{50} = 9 ± 1 µM) and modest inhibition of VIM-2 and BcII (IC_{50} < 30 µM). The ethyl ester **4b** was a potent inhibitor of SPM-1 (IC_{50} = 3 ± 1 µM) and exhibited a broad spectrum of activity, reporting < 20 µM IC_{50} values for all the tested MBLs. Whilst compound **4c** did not effectively inhibit IMP-1, it displayed relatively low IC_{50} values with NDM-1.

On the other hand, the corresponding carboxylic acid of **4a** (compound **4d**) showed poor inhibition of VIM-2 and BcII while having relatively good activity against the other tested MBLs (IC_{50} values < 10 µM). In contrast to the ethyl ester **4b**, its corresponding carboxylic acid **4e** reported residual activities above the cut-off values (5%) and as such was not considered for IC_{50} analysis. Interestingly, the carboxylic acid **4f** selectively inhibited SPM-1 and showed only modest inhibition of NDM-1 and VIM-2. It is worth noting that the enzymatic or non-enzymatic partial ester hydrolysis of the ethyl ester derivatives cannot be completely ruled out in the standard assay conditions.

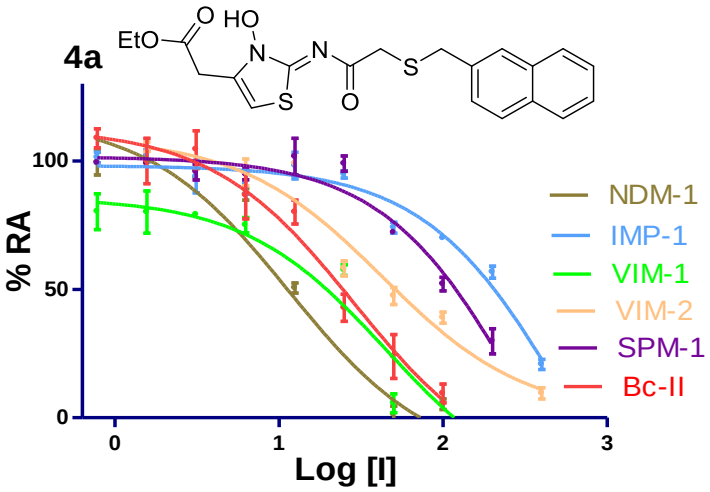
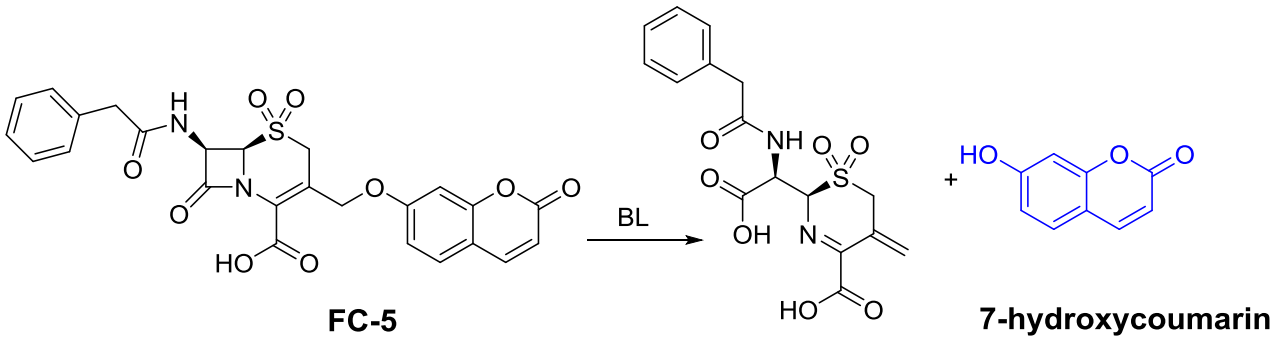


Figure 2-9: **IC_{50} curves for compound 4a with the 6 tested MBLs. CLS405 substrate was used as the reporter substrate at a concentration near Km values. Experiments were carried out at room temperature using the reported MBL assay conditions.**

The structural diversity of MBLs, which largely impedes effective inhibitor design, is further highlighted by the differences in inhibition profiles of the compounds used in this study. In addition, the indiscriminate inhibition of MBLs and oxygenases by the tested hydroxythiazoles emphasises the need to counter-screen potential MBL inhibitors for untoward interactions with mammalian metallo-enzymes of similar active site architecture.

2.7 FLUOROGENIC SUBSTRATE FOR CELL-BASED ASSAYS

Whilst my study was ongoing, novel cephalosporin-based fluorescent substrates for MBL assays were reported by van Berkel *et al* [23]. Upon the hydrolysis of the β-lactam ring, the fluorogenic substrate **FC-5** liberates 7-hydroxycoumarin resulting in an increased fluorescence signal (*Scheme 2-4*). Derivatives of 7-hydroxycoumarines have been widely used in screening platforms for various hydrolases and dealkylases[53-55], it was therefore of interest to investigate the potential of application of such substrates in screening MBL activity and inhibition *in vivo*.



Scheme 2-4: **Proposed mechanism of hydrolysis of FC-5 by β-lactamases and the fluorescent hydrolysis product.**

To investigate the potential use of an **FC-5** based assay for identification MBL producing organisms, BL21 (DE3) pLysS *E. coli* cells were transformed with pET-26b plasmids (with a periplasmic expression leader sequence) encoding VIM-2 and IMP-1 MBLs. The cells were cultured at 37 °C till an $OD_{600\ nm}$ of 0.7 was reached, and production of the MBLs induced by addition of 0.5 mM Isopropyl β-D-1-thiogalactopyranoside (IPTG). After incubation for a further 2 hours, the cell cultures were diluted in MBL assay for the fluorescence assay. Changes in fluorescence intensity upon the addition of the substrate was monitored in MBL assay buffer at the corresponding optimal wavelengths (λ_{ex} = 380 nm and λ_{em} = 460 nm). MBL inhibitor ML302F and SBL inhibitor avibactam were used for identification of the β-lactamase. Cells producing FIH (an asparagine hydroxylase involved in hypoxic response) were used as a negative control.

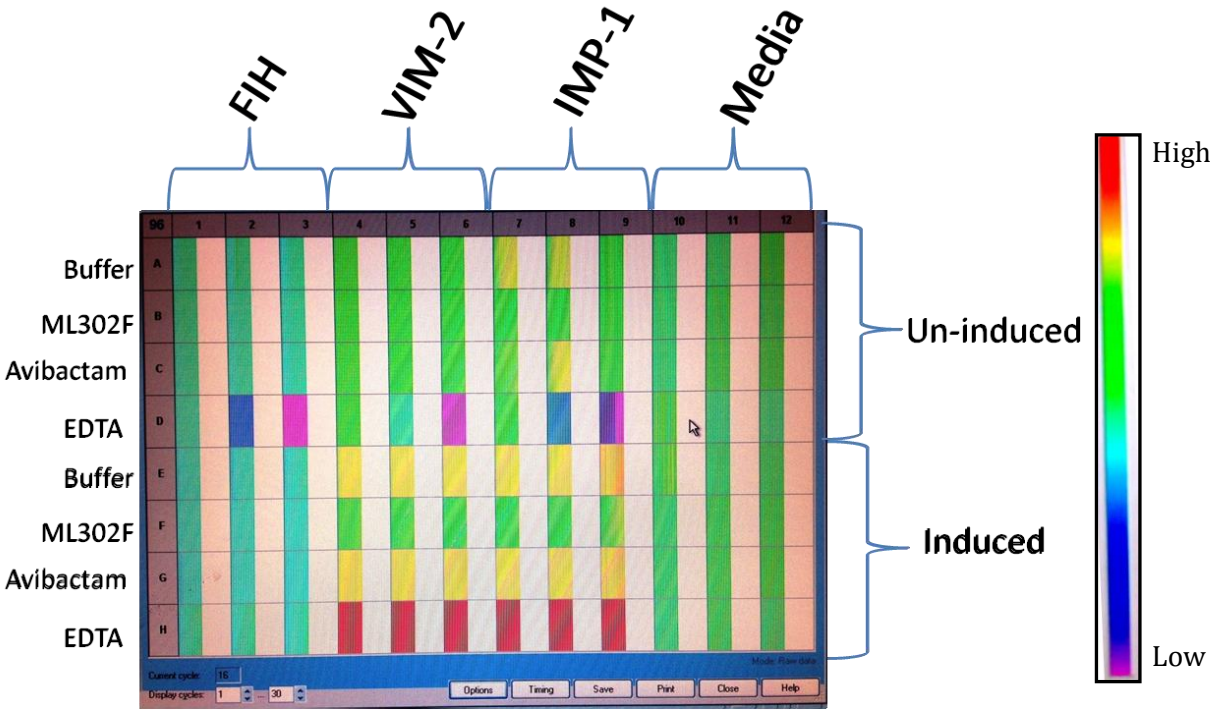


Figure 2-10: **Fluorescence scanning of wells containing cell cultures incubated with FC-5 indicating the relative fluorescent intensity. Inset: Colour gradient from high to low fluorescent intensity.**

According to the preliminary results (*Figure 2-10*), the highest fluorescence signal was recorded for the induced cells producing VIM-2 and IMP-1 (yellow). As expected, the presence of the MBL inhibitor ML302F led to a marked decrease in fluorescence, whereas the fluorescence intensity remained high in the presence of avibactam which does not inhibit MBLs. Fluorescence signal was significantly lower in the negative controls i.e. cells producing FIH and the media used as blank (green). There was some background expression especially in IMP-1 hence the elevated fluorescence signal in some of the un-induced cells. Surprisingly, EDTA interfered with the assay leading to high fluorescence intensity in the cells producing IMP-1 and VIM-2, the implications of which will require further investigation.

2.8 SUMMARY

A reliable MBL assay platform has been developed based on a stable and affordable chromogenic reporter substrate **CLS405**. The substrate was efficiently synthesized following a simple 3-step protocol. Comparison of the hydrolysis rates of 3 chromogenic substrate (CENTA, nitrocefin and **CLS405**) by six representative MBLs (NDM-1, IMP-1, VIM-1, VIM-2, SPM-1, and BcII) revealed substantial differences in the kinetic parameters of the different substrate-enzyme combinations. Besides being highly sensitive, the **CLS405** based assay was shown to be very efficient, recording the highest k_{cat}/K_M for all the tested MBLs compared to the other tested chromogenic substrates. The successful application of the substrate in an exemplary MBL inhibitor screening platform led to the identification of *N*-hydroxythiazoles as novel MBL inhibitor scaffolds with a wide-ranging potency against the tested MBLs. While the ethyl ester derivative **4b** displayed a modest but broad-spectrum inhibition of the MBLs, the carboxylic acid **4f** preferentially inhibited SPM-1 over the other tested MBLs. The results highlight the cross-reactivity of *N*-hydroxythiazoles as inhibitors of iron (II)-dependent oxygenases as well zinc (II)-dependent hydrolases, and specifically MBLs.

In an attempt to develop cell-based assays for detection of MBLs, a previously reported fluorogenic substrate **FC-5** was investigated for potential use in such assays. The substrate, based on the same cephalosporin background as **CLS405**, is coupled to a fluorescent leaving group at C-3 position. The assay was shown to efficiently identify MBL producing cells and was amenable to direct use in cell culture as well as in lysed cells. Although a good starting point, further optimisation will be required including using a more comprehensive panel of MBLs and inhibitors. Other efficient fluorophores should also be investigated and the potential for application for detection and identification of β-lactamases in clinical isolates explored.

2.9 REFERENCES

1. Drawz SM, Bonomo RA.Three decades of β-lactamase inhibitors. *Clin Microbiol Rev*. 2010;23:160-201.

2. Fast W, Sutton LD. Metallo-β-lactamase: Inhibitors and reporter substrates. *Biochim Biophys Acta*. 2013;1834(8):1648-1659.

3. Faridoon, Ul Islam N. An update on the status of potent inhibitors of metallo-β-lactamases. *Sci Pharm*. 2013;81(2):309-327.

4. Perret CJ. Iodometric assay of penicillinase. *Nature*. 1954;174(4439):1012-1013.

5. Hou JP, Poole JW. Measurement of β-lactamase activity and rate of inactivation of penicillins by a pH-stat alkalimetric titration method. *J Pharm Sci*. 1972;61(10):1594-1598.

6. Saz AK, Lowery DL, Jackson LJ. Staphylococcal penicillinase. I. inhibition and stimulation of activity. *J Bacteriol*. 1961;82:298-304.

7. Henry RJ, Housewright RD, Herring AS, Clemens H, Hartley JC. Studies on penicillinase. II. manometric methods of assaying penicillinase and penicillin, kinetics of the penicillin-penicillinase reaction, and the effects of inhibitors on penicillinase. *J Biol Chem*. 1947;167:559-571.

8. Lucas TJ. An evaluation of 12 methods for the demonstration of penicillinase. *J Clin Pathol*. 1979;32(10):1061-1065.

9. Oelschlaeger P, Aitha M, Yang H, et al. Meropenem and chromacef intermediates observed in IMP-25 metallo-β-lactamase-catalyzed hydrolysis. *Antimicrob Agents Chemother*. 2015;59(7):4326-4330.

10. Viswanatha T, Marrone L, Goodfellow V, Dmitrienko GI. Assays for β-lactamase activity and inhibition. *Methods Mol Med*. 2008;142:239-260.

11. Hamilton-Miller JM, Smith JT, Knox R. Interaction of cephaloridine with penicillinase-producing gram-negative bacteria. *Nature*. 1965;208(5007):235-237.

12. Ross GW, Chanter KV, Harris AM, Kirby SM, Marshall MJ, O'Callaghan CH. Comparison of assay techniques for β-lactamase activity. *Anal Biochem*. 1973;54(1):9-16.

13. O'Callaghan CH, Muggleton PW, Ross GW. Effects of β-lactamase from gram-negative organisms on cephalosporins and penicillins. *Antimicrob Agents Chemother (Bethesda)*. 1968;8:57-63.

14. Ross GW, O'Callaghan CH. β-lactamase assays. *Methods Enzymol*. 1975;43:69-85.

15. O'Callaghan CH, Morris A, Kirby SM, Shingler AH. Novel method for detection of β-lactamases by using a chromogenic cephalosporin substrate. *Antimicrob Agents Chemother*. 1972;1(4):283-288.

16. Samuni A. A direct spectrophotometric assay and determination of Michaeli's constants for the β-lactamase reaction. *Anal Biochem*. 1975;63(1):17-26.

17. Durkin JP, Dmitrienko GI, Viswanatha T. N-(2-furyl) acryloyl penicillin: A novel compound for the spectrophotometric assay of β-lactamase I. *J Antibiot (Tokyo)*. 1977;30(10):883-885.

18. Jones RN, Wilson HW, Novick WJ,Jr. *In vitro* evaluation of pyridine-2-azo-p-dimethylaniline cephalosporin, a new diagnostic chromogenic reagent, and comparison with

nitrocefin, cephacetrile, and other β-lactam compounds. *J Clin Microbiol*. 1982;15(4):677-683.

19. Bebrone C, Moali C, Mahy F, et al. CENTA as a chromogenic substrate for studying β-lactamases. *Antimicrob Agents Chemother*. 2001;45(6):1868-1871.

20. Yu S, Vosbeek A, Corbella K, Severson J, Schesser J, Sutton LD. A chromogenic cephalosporin for β-lactamase inhibitor screening assays. *Anal Biochem*. 2012;428(2):96-98.

21. Ghavami A, Labbe G, Brem J, et al. Assay for drug discovery: Synthesis and testing of nitrocefin analogues for use as β-lactamase substrates. *Anal Biochem*. 2015;486:75-77.

22. Zhang YL, Xiao JM, Feng JL, et al. A novel fluorogenic substrate for dinuclear zn(II)-containing metallo-β-lactamases. *Bioorg Med Chem Lett*. 2013;23(6):1676-1679.

23. van Berkel SS, Brem J, Rydzik AM, et al. Assay platform for clinically relevant metallo-β-lactamases. *J Med Chem*. 2013;56(17):6945-6953.

24. Li L, Li Z, Shi W, Li X, Ma H. Sensitive and selective near-infrared fluorescent off-on probe and its application to imaging different levels of β-lactamase in staphylococcus aureus. *Anal Chem*. 2014;86(12):6115-6120.

25. Makena A, van Berkel SS, Lejeune C, et al. Chromophore-linked substrate (CLS405): Probing metallo-β-lactamase activity and inhibition. *ChemMedChem*. 2013; 8(12):1923–1929.

26. de Seny D, Prosperi-Meys C, Bebrone C, et al. Mutational analysis of the two zinc-binding sites of the *Bacillus cereus* 569/H/9 metallo-β-lactamase. *Biochem J*. 2002;363(Pt 3):687-696.

27. Griffin DH, Richmond TK, Sanchez C, et al. Structural and kinetic studies on metallo-β-lactamase IMP-1. *Biochemistry*. 2011;50(42):9125-9134.

28. Berrow NS, Alderton D, Sainsbury S, et al. A versatile ligation-independent cloning method suitable for high-throughput expression screening applications. *Nucleic Acids Res*. 2007;35(6):e45.

29. Green VL, Verma A, Owens RJ, Phillips SE, Carr SB. Structure of New Delhi Metallo-β-lactamase 1 (NDM-1). *Acta Crystallogr Sect F Struct Biol Cryst Commun*. 2011;67(Pt 10):1160-1164.

30. Moore JC, Arnold FH. Directed evolution of a para-nitrobenzyl esterase for aqueous-organic solvents. *Nat Biotechnol*. 1996;14(4):458-467.

31. Hriscu, M., Chiş, L., Toşa, M. and Irimie, F. D. pH-profiling of thermoactive lipases and esterases: Caveats and further notes. *Eur J Lipid Sci Technol*. 2013;115:571-575.

32. Adam M, Damblon C, Plaitin B, Christiaens L, Frere JM. Chromogenic depsipeptide substrates for β-lactamases and penicillin-sensitive DD-peptidases. *Biochem J*. 1990;270(2):525-529.

33. Levine MN, Lavis LD, Raines RT. Trimethyl lock: A stable chromogenic substrate for esterases. *Molecules*. 2008;13(2):204-211.

34. Siemann S, Clarke AJ, Viswanatha T, Dmitrienko GI. Thiols as classical and slow-binding inhibitors of IMP-1 and other binuclear metallo-β-lactamases. *Biochemistry*. 2003;42(6):1673-1683.

35. Kurosaki H, Yamaguchi Y, Yasuzawa H, Jin W, Yamagata Y, Arakawa Y. Probing, inhibition, and crystallographic characterization of metallo-β-lactamase (IMP-1) with fluorescent agents containing dansyl and thiol groups. *ChemMedChem*. 2006;1(9):969-972.

36. Lienard BM, Garau G, Horsfall L, et al. Structural basis for the broad-spectrum inhibition of metallo-β-lactamases by thiols. *Org Biomol Chem*. 2008;6(13):2282-2294.

37. Payne DJ, Bateson JH, Gasson BC, et al. Inhibition of metallo-β-lactamases by a series of mercaptoacetic acid thiol ester derivatives. *Antimicrob Agents Chemother*. 1997;41:135-140.

38. Bounaga S, Galleni M, Laws AP, Page MI. Cysteinyl peptide inhibitors of *Bacillus cereus* zinc β-lactamase. *Bioorg Med Chem*. 2001;9(2):503-510.

39. Sun Q, Law A, Crowder MW, Geysen HM. Homo-cysteinyl peptide inhibitors of the L1 metallo-β-lactamase, and SAR as determined by combinatorial library synthesis. *Bioorg Med Chem Lett*. 2006;16(19):5169-5175.

40. Pratt RF. Inhibition of a class C β-lactamase by a specific phosphonate monoester. *Science*. 1989;246(4932):917-919.

41. Rahil J, Pratt RF. Phosphonate monoester inhibitors of class A β-lactamases. *Biochem J*. 1991;275 (Pt 3)(Pt 3):793-795.

42. Adediran SA, Nukaga M, Baurin S, Frere JM, Pratt RF. Inhibition of class D β-lactamases by acyl phosphates and phosphonates. *Antimicrob Agents Chemother*. 2005;49(10):4410-4412.

43. Toney JH, Hammond GG, Fitzgerald PM, et al. Succinic acids as potent inhibitors of plasmid-borne IMP-1 metallo-β-lactamase. *J Biol Chem*. 2001;276(34):31913-31918.

44. Olsen L, Jost S, Adolph HW, Pettersson I, Hemmingsen L, Jorgensen FS. New leads of metallo-β-lactamase inhibitors from structure-based pharmacophore design. *Bioorg Med Chem*. 2006;14(8):2627-2635.

45. Walter MW, Valladares MH, Adlington RM, Amicosante G, Baldwin JE, Frère J-M, Galleni M, Rossolini GR, Schofield CJ. Hydroxamate inhibitors of *Aeromonas hydrophila* AE036 metallo-β-lactamase. *Bioorg Chem*. 1999;27:35-40.

46. Lienard BM, Horsfall LE, Galleni M, Frère J-M, Schofield CJ. Inhibitors of the FEZ-1 metallo-β-lactamase. *Bioorg Med Chem Lett*. 2007;17(4):964-968.

47. Minond D, Saldanha SA, Subramaniam P, et al. Inhibitors of VIM-2 by screening pharmacologically active and click-chemistry compound libraries. *Bioorg Med Chem*. 2009;17(14):5027-5037.

48. Weide T, Saldanha SA, Minond D, et al. NH-1,2,3-triazole-based inhibitors of the VIM-2 metallo-β-lactamase: Synthesis and structure-activity studies. *ACS Med Chem Lett*. 2010;1(4):150-154.

49. Faridoon, Hussein WM, Vella P, et al. 3-mercapto-1,2,4-triazoles and N-acylated thiosemicarbazides as metallo-β-lactamase inhibitors. *Bioorg Med Chem Lett*. 2012;22(1):380-386.

50. Tegley CM, Viswanadhan VN, Biswas K, et al. Discovery of novel hydroxy-thiazoles as HIF-alpha prolyl hydroxylase inhibitors: SAR, synthesis, and modeling evaluation. *Bioorg Med Chem Lett*. 2008;18(14):3925-3928.

51. Kerdesky FA, Brooks CD, Hulkower KI, Bouska JB, Bell RL. Conversion of cyclooxygenase inhibitors into hydroxythiazole 5-lipoxygenase inhibitors. *Bioorg Med Chem*. 1997;5(2):393-396.

52. Kerdesky FA, Holms JH, Moore JL, et al. 4-hydroxythiazole inhibitors of 5-lipoxygenase. *J Med Chem*. 1991;34(7):2158-2165.

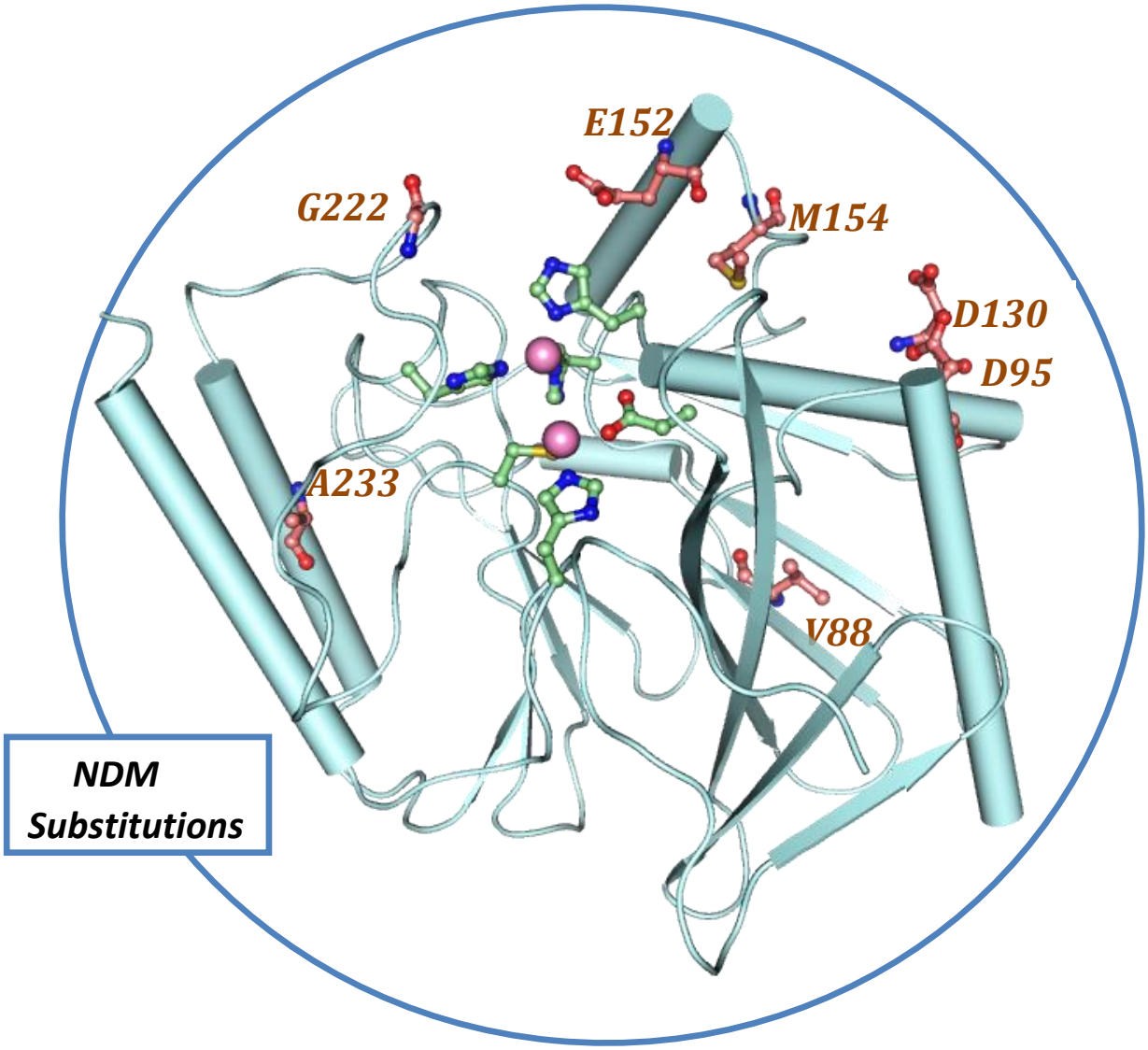
53. Babiak P, Reymond JL. A high-throughput, low-volume enzyme assay on solid support. *Anal Chem*. 2005;77(2):373-377.

54. Gee KR, Sun WC, Bhalgat MK, et al. Fluorogenic substrates based on fluorinated umbelliferones for continuous assays of phosphatases and β-galactosidases. *Anal Biochem*. 1999;273(1):41-48.

55. Yamazaki H, Inoue K, Mimura M, Oda Y, Guengerich FP, Shimada T. 7-ethoxycoumarin O-deethylation catalyzed by cytochromes P450 1A2 and 2E1 in human liver microsomes. *Biochem Pharmacol*. 1996;51(3):313-319.

CHAPTER 3: BIOCHEMICAL CHARACTERISATION OF NEW DELHI METALLO-β-LACTAMASE (NDM) VARIANTS

The rapid evolution of MBL variants poses a formidable challenge to the development of effective MBL inhibitors. The emergence of NDM variants over recent years is therefore a worrisome occurrence that merits critical examination. The work described in this chapter details a comparison of the biochemical and biophysical properties of seven of the first clinically reported NDM variants and identifies some interesting potential drivers of NDM evolution.



CONTENTS

CHAPTER 3: BIOCHEMICAL CHARACTERISATION OF NEW DELHI METALLO-β-LACTAMASE (NDM) VARIANTS 97

3.1 INTRODUCTION 99

3.1.1 Evolution of NDM variants 99

3.1.2 Biochemical Studies of NDMs 101

3.1.3 Chapter Objectives 101

3.2 β-LACTAM SUSCEPTIBILITY ANALYSES 102

3.2.1 Determination of MIC values 102

3.3 PRODUCTION AND PURIFICATION OF RECOMBINANT NDMS 104

3.3.1 Cloning and site directed mutagenesis 104

3.3.2 Protein production and purification 105

3.4 COMPARISON OF HYDROLYTIC ACTIVITIES OF NDM VARIANTS 106

3.4.1 Steady-state kinetic analyses 106

3.4.2 Investigation of inhibition by nitrocefin 112

3.5 BIOPHYSICAL CHARACTERISATION OF NDM VARIANTS 114

3.5.1 Secondary structure analyses by Circular Dichroism (CD) 114

3.5.2 Investigation of thermal stability of NDM variants 116

3.6 SUMMARY 119

3.7 REFERENCES 120

3.1 INTRODUCTION

In 2008, a new metallo-β-lactamase, New Delhi Metallo-β-lactamase-1 (NDM-1), was identified in a carbapenem resistant *Klebsiella pneumoniae* isolate. The plasmid encoding for the NDM-1 gene (bla_{NDM-1}) was also found to co-harbour another β-lactamase gene, bla_{CMY-4}, as well as a complex class 1 integron carrying genes conferring resistance to several antibiotics including macrolides and aminoglycosides[1]. Since then, bla_{NDM-1} genes have been identified in various pathogenic and environmental bacteria strains, including *E. coli*, *A. baumannii* and *P. aeruginosa*[2-4]. Although different biochemical characterisation studies have reported varying results on the substrate profile of NDM-1, the enzyme generally catalyses the hydrolysis of nearly all β-lactam antibiotics with the exception of the monobactam aztreonam, much like other B1 metallo-β-lactamases (MBLs)[5]. This broad spectrum activity coupled with the rapid dissemination of NDM-1-bearing plasmids to unrelated bacteria species is hence of great public health concern[6-8].

3.1.1 EVOLUTION OF NDM VARIANTS

The rapid adaptation of MBLs to antibiotic pressure has forged renewed interest in efforts to find sequence and structural determinants that induce substrate preferences[9]. Several studies have looked into the structural and functional differences of the clinically emergent and lab-generated Imipenemase (IMP) and Verona integron-encoded metallo-β-lactamase (VIM) variants[10-12]. At the onset of this work (less than five years after the discovery of NDM-1), eight different NDM variants had been reported in various parts of the world; this number has since doubled to 16 variants[13]. In comparison to the VIM and IMP enzymes, the clinically reported NDM variants are presently less diverse. With the exception of the more divergent NDM-10, the variants differ by 1 or 2 amino acid substitutions mostly located in positions that are remote from the active site metal center.

Of particular interest is the recurrent M154L substitution present in about half of the reported NDM variants (*Table 3-1*).

***Table 3-1*: Substitutions present in the reported NDM variants[13].**

NDM type	Residue substitution	Bacteria species	Geographic location identified [#]
NDM-2	P28A	*A. baumannii*	Egypt, Israel, United Arab Emirates[14,15]
NDM-3	D95N	*E. coli*	Australia, Japan[16,17]
NDM-4	M154L	*E. coli*, *E. cloacae*	France (Cameroun), Denmark (Vietnam), Czech Republic (Sri Lanka)[18-20]
NDM-5	V88L, M154L	*E. coli*	UK (India)[21]
NDM-6	A233V	*E. coli*	New Zealand (India) and USA[22,23]
NDM-7	D130N, M154L	*E. coli*	Germany (India) France (Burma)[24,25]
NDM-8	D130G, M154L	*E. coli*	Nepal[26]
NDM-9	E152K	*K. pneumoniae*	China[27]
NDM-10	R32S, G36D G69S, A74T, G200R	*K. pneumoniae*	India*
NDM-11	M154V	*E. coli*	India *
NDM-12	M154L, G222D	*E. coli*	Nepal[28]
NDM-13	D95N, M154L	*E. coli*	Nepal [29]
NDM-14	D130G	*A. lwoffii*	China [30]
NDM-15	M154L, A233V	*E. coli*	India*
NDM-16	T262H	*K. pneumoniae*	U.S.A*

[#] Locations of previous travel or hospitalisation are in parenthesis.

* NDM-10, NDM-11, NDM-15 and NDM-16 sequences have been directly submitted to Genbank under accession numbers KF361506, KP265939, KP735848 and KP862821, respectively.

3.1.2 BIOCHEMICAL STUDIES OF NDMS

Previous reports have shown that apparently subtle amino acid changes in MBLs can induce differences in the stability and hydrolytic activity and in some cases, can confer selective advantage during evolution of these drug resistance determinants[11,31,32]. In previous studies, NDM-4[18] was reported to have increased hydrolytic activity towards carbapenems and some cephalosporins, whilst NDM-3[17] and NDM-8[26] were reported to have similar activities as NDM-1 with various β-lactams. While these and other studies have characterised the individual NDM variants, the results are difficult to compare since the work was carried out using different experimental conditions. The correlation of antibiotic susceptibility profiles and biochemical properties of NDM variants was also not clearly defined.

3.1.3 CHAPTER OBJECTIVES

The primary goal of this work was to investigate whether there are significant differences in the substrate selectivity, secondary structure and thermal stabilities of seven of the clinically reported NDM variants. To address the challenge of comparing data from different studies, the analyses of the different NDMs were carried out under similar experimental conditions. The work described in this chapter evaluates the physiological effects of the NDM substitutions on the antibiotic susceptibility profiles of *E. coli* cells producing the different NDM variants. Furthermore, the studies in this chapter investigate the roles of the amino acid substitutions on the activity and stability of the enzymes by extensive biochemical and biophysical analyses on the recombinant enzymes. An in-depth comparison of NDM variants is thus described, with the aim of providing insights into the catalytic properties of the variants and shedding light on the possible drivers of the rapid NDM evolution.

This work was performed in collaboration with Dr. David Wareham at the Blizzard Institute, Queen Mary University London, who carried out the antimicrobial susceptibility tests. Most of the work described in this chapter has been reported in the academic literature[33].

3.2 β-LACTAM SUSCEPTIBILITY ANALYSES

Previous clinical and epidemiological studies have reported a wide range of minimum inhibitory concentration (MIC) values of NDM producing bacteria with various β-lactam antibiotics[14,18,21]. To ensure a fair comparison, the same expression system was used to assess the differences in the effects of the reported NDM variants on the antibiotic susceptibility of *E. coli* cells to a range of β-lactams antibiotics.

3.2.1 DETERMINATION OF MIC VALUES

Full-coding sequences of the NDM variant genes (NDM-1, 2, 4, 5, 6 and 7) with either the native IS*Ab125* promoter[22] or a T7 promoter were amplified using DNA templates prepared from NDM producing clinical isolates or *E. coli* transconjugants[22-24]. The NDM encoding genes were cloned into the pCR-Blunt II TOPO vectors (Invitrogen, Paisley, UK) to generate the ***pCR2.1 NDM*** vectors which employ a T7 promoter and the ***pCR2.1 NDM P+*** vectors, which employ the native promoter. The vectors were then transformed *E. coli* TOP10 cells. The E-test method (Biomeriuex, Basingstoke, UK) was used to determine the susceptibility of the transformants (on Mueller-Hinton agar) to ampicillin, cephalothin, cefoxitin, ceftazidime, ertapenem, imipenem, meropenem and doripenem.

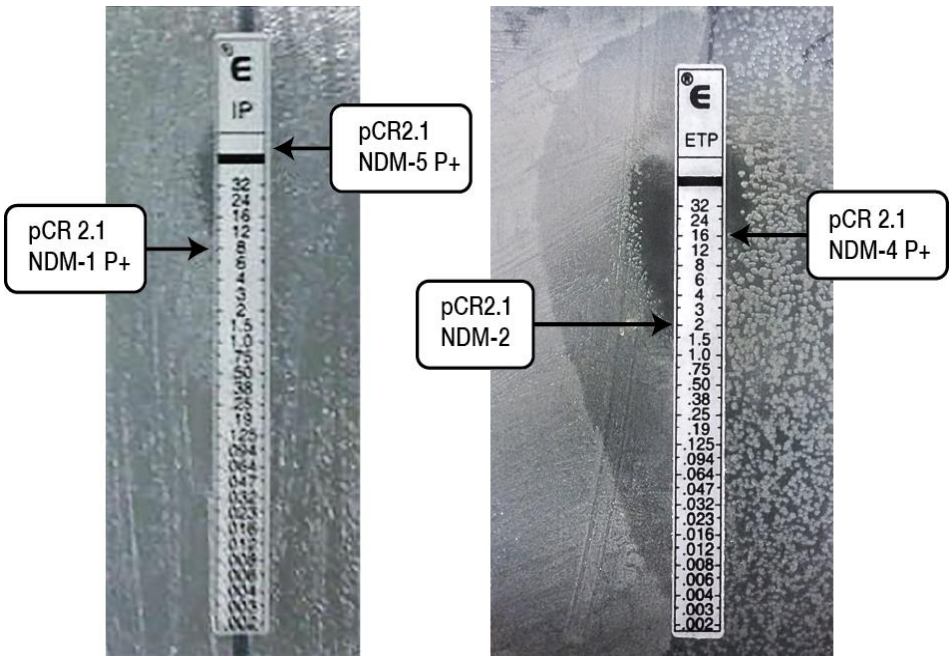


Figure 3-1: **Comparison of susceptibility of *E. coli* TOP10 transformants to imipenem (IP) and ertapenem (ETP), showing the elevated MIC values when native promoters are used (*pCR2.1 NDM P+*).**

In agreement with previous results[21,24], almost all of the tested NDM variant transformants, with either the native or the T7 promoter, were resistant to ampicillin, cephalothin, cefoxitin and ceftazidime (MIC >256 mg/L) (*Table 3-2*). Interestingly, clear differences in the susceptibility of the variants to carbapenems were observed only when the genes were expressed under the native promoter (*Figure 3-1*). Notably, the ***pCR2.1 NDM P+*** transformants producing NDM-4, NDM-5 and NDM-7 manifested > 4 fold higher MIC values for imipenem compared to the other tested variants.

***Table 3-2:* Susceptibility of *E. coli* transformed with plasmids containing NDM variants; showing differences in MIC values of carbapenems for *pCR2.1 NDM P+* transformants.**

Plasmid[1]	MIC (mg/L)							
	[2]AMP	CEP	FOX	CAZ	ERT	IMP	DOR	MEM
pCR2.1	4	0.008	0.008	0.125	0.008	0.25	0.032	0.047
pCR2.1 NDM-1	>256	>256	24	>256	0.38	0.38	0.25	0.38
pCR2.1 NDM-1 P+	>256	>256	>256	>256	8	8	8	4
pCR2.1 NDM-2	>256	>256	>256	>256	2	0.38	0.38	0.38
pCR2.1 NDM-2 P+	>256	>256	>256	>256	16	8	8	4
[3]pHSG398/NDM-3	256	N/A	32	256	N/A	0.25	0.125	0.25
pCR2.1 NDM-4	>256	>256	>256	>256	2	0.25	0.032	0.38
pCR2.1 NDM-4 P+	>256	>256	>256	>256	16	>32	12	8
pCR2.1 NDM-5	>256	>256	>256	>256	2	0.25	0.5	0.38
pCR2.1 NDM-5 P+	>256	>256	>256	>256	>32	>32	12	>32
pCR2.1 NDM-6	>256	>256	>256	>256	1	0.38	0.125	0.38
pCR2.1 NDM-6 P+	>256	>256	>256	>256	>32	8	1.5	>32
pCR2.1 NDM-7	>256	>256	>256	32	2	2	0.5	1
pCR2.1 NDM-7 P+	>256	>256	>256	>256	>32	>32	8	>32
[3]pHSG398/NDM-8	256	N/A	64	256	N/A	0.5	N/A	0.25

[1] P+ indicates plasmids containing the native *ISAba125* promoter.
[2]AMP: Ampicillin, CEP: Cephalothin, FOX: Cefoxitin, CAZ: Ceftazidime, ERT: Ertapenem, IMP: Imipenem, DOR: Doripenem, MEM: Meropenem.
[3]Data from Tada *et al.*[17,26]; MICs determined by broth microtitre dilution using *E. coli* DH5α cells.

3.3 PRODUCTION AND PURIFICATION OF RECOMBINANT NDMS

To investigate whether the observed differences in MIC values reflected changes in biochemical activities of the enzymes, further analyses were carried out using the recombinant enzymes.

3.3.1 CLONING AND SITE DIRECTED MUTAGENESIS

To generate the target NDM variants, site directed mutagenesis was carried out employing an optimised Stratagene QuikChange protocol. DNA encoding a ΔN42-NDM-1 construct (amino acids G42-R270) with a cleavable *N*-terminal His_6-tag, were inserted into the previously reported pTriEx-based pOPIN-F plasmid[34] (Chapter 7.2). This plasmid was used as a template for site-directed mutagenesis to generate the target NDM variants using the primers listed (*Table 3-3*). Initially, a plasmid encoding for the NDM-4 variant (with the M154L substitution) was generated, and then used as a template for the production of the doubly substituted NDM-5, 7 and 8 variants. The optimised mutagenesis protocol ensured the successful incorporation of the desired substitutions as confirmed by gene sequencing (SourceBioscience), allowing the subsequent production of the recombinant proteins.

Table 3-3: **Primers used for generation of NDM variants by site-directed mutagenesis.**

NDM	Residue	Forward primer (5'-3')	Reverse primer (5'-3')
NDM-3	D54N	GATACCGCATGGACCAATGATCAGACCGCAC	GTGCGGTCTGATCATTGGTCCATGCGGTATC
NDM-4	M113L	ATGGTGGTCGTGTTCTGCTGGTTGATACCGCATGGAC	GCTGCAACCAGACCTTCTTGCGGAGCCAGC
NDM-5	V47L	ATGGTGGTCGTGTTCTGCTGGTTGATACCGCATGGAC	GTCCATGCGGTATCAACCAGCAGAACACGACCACCAT
NDM-6	V192A	ACATTATGCAGCAAGCGTACGTGCATTTGGTGCAG	CTGCACCAAATGCACGTACGCTTGCTGCATAATGT
NDM-7	D89N	ACAAAATGGGTGGTATGAATGCACTGCATGCAGCA	TGCTGCATGCAGTGCATTCATACCACCCATTTTGT
NDM-8	D89G	CAAAATGGGTGGTATGGGTGCACTGCATGCAGCAG	CTGCTGCATGCAGTGCACCCATACCACCCATTTTG

3.3.2 PROTEIN PRODUCTION AND PURIFICATION

Following extensive expression trials, favourable conditions were determined for the production of the recombinant NDM variants. The respective plasmids were transformed into *E. coli* BL21 (DE3) pLysS cells and the cells were cultured in modified auto-induction media as described in Chapter 7[35,36]. All the NDM variants were produced at similar levels under the employed growth conditions.

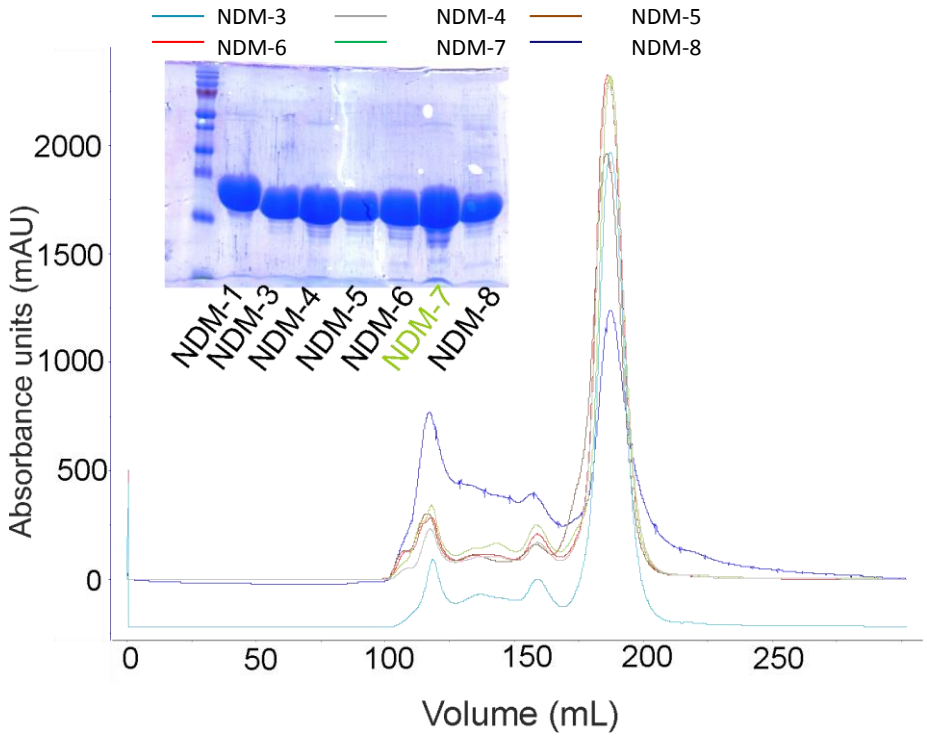
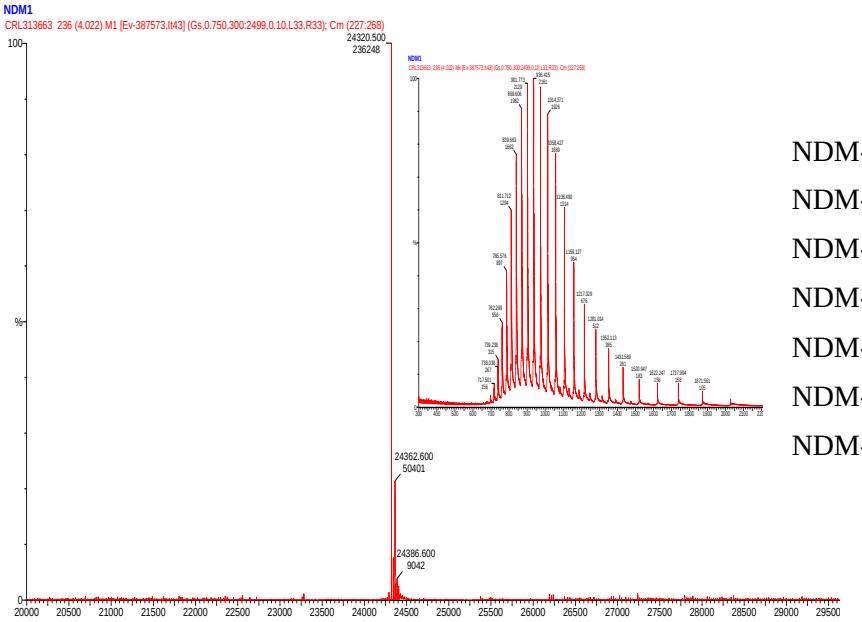


Figure 3-2: **Overlay of gel filtration chromatograms of NDM variants. Inset: SDS PAGE gel analysis.**

The recombinant proteins were then purified using the previously optimised 3-step purification protocol for NDM-1 (Chapter 2) yielding protein concentrations of ~5 mg/L of culture. The purity of the resulting proteins was verified to be >90% by SDS PAGE analyses (*Figure 3-2*); the activity of the enzymes was confirmed by monitoring nitrocefin hydrolysis. To verify the identities of the purified proteins, electrospray ionisation mass spectrometric (ESI-MS) analyses were carried out using denaturing conditions for the ΔN42-NDM variants after cleavage of the *N*-terminal His_6-tag (Chapter 7.5). The obtained masses were in close agreement with theoretical values obtained using the ExPasy ProtParam tool (*Figure 3.3*)[37].



	Predicted	Observed	Shift
NDM-1	24318	24320	2
NDM-3	24317	24319	2
NDM-4	24300	24302	2
NDM-5	24314	24316	2
NDM-6	24346	24347	1
NDM-7	24299	24300	1
NDM-8	24242	24244	2

Figure 3-3: **Deconvoluted mass spectra and combined ion series (inset) for ΔN42 NDM-1 and a comparison of predicted and observed masses (in Daltons) for NDM variants.**

3.4 COMPARISON OF HYDROLYTIC ACTIVITIES OF NDM VARIANTS

To examine the roles of the clinically observed substitutions in NDM catalysis, the hydrolytic activities of the purified recombinant proteins were investigated. Steady-state kinetic parameters for the hydrolysis of a representative set of β-lactam antibiotics (including carbapenems, penicillin and cephalosporins) by the NDM variants were determined.

3.4.1 STEADY-STATE KINETIC ANALYSES

The enzyme-mediated hydrolysis of a panel of β-lactam substrates was monitored using the MBL assay buffer as previously described[38]. To counter the high background hydrolysis of ampicillin in HEPES buffer, MOPS buffer was used instead[39]. The relative molar extinction coefficients of the β-lactams were determined by plotting the absorbance units against increasing concentrations of the substrates or product (Chapter 7.6).

To generate Michaelis-Menten and substrate inhibition curves, the dependence of the initial reaction rates on the substrate concentration was fitted. Data were analysed using GraphPad Prism software to obtain the kinetic constants (K_M and k_{cat}).

3.4.1.1 CARBAPENEM SUBSTRATES

As is characteristic of MBLs, the NDM variants all efficiently hydrolysed the tested carbapenems, with k_{cat}/K_M values being > 2 $s^{-1}\mu M^{-1}$ (*Table 3-4*). In contrast to some previous assertions[17], no substantial differences were observed in catalytic efficiencies of the different NDM variants with carbapenems as reflected in k_{cat}/K_M values (*Figure 3-4*). The largest differences observed in k_{cat}/K_M values were in the hydrolysis of doripenem, with NDM-6 having ~4 times higher compared to NDM-1 and NDM-8. This was attributed to the higher k_{cat} values for NDM-6 with doripenem, which was ~5 times higher than for NDM-1. Relatively larger differences were also observed in the k_{cat} values for imipenem; with NDM-1 having ~ 10-fold higher k_{cat} compared to NDM-8.

Overall, only minor differences (3 to 5 fold) were observed in the k_{cat}/K_M values for NDM variants with the tested carbapenem substrates, which may be within experimental error. Interestingly, the more recently identified NDM-12, NDM-13 and NDM-14 variants also display minimal differences in the k_{cat}/K_M values for carbapenems in comparison to NDM-1[28-30]. It is therefore plausible that the NDM variants have not necessarily evolved to increase catalytic efficiency with respect to carbapenems.

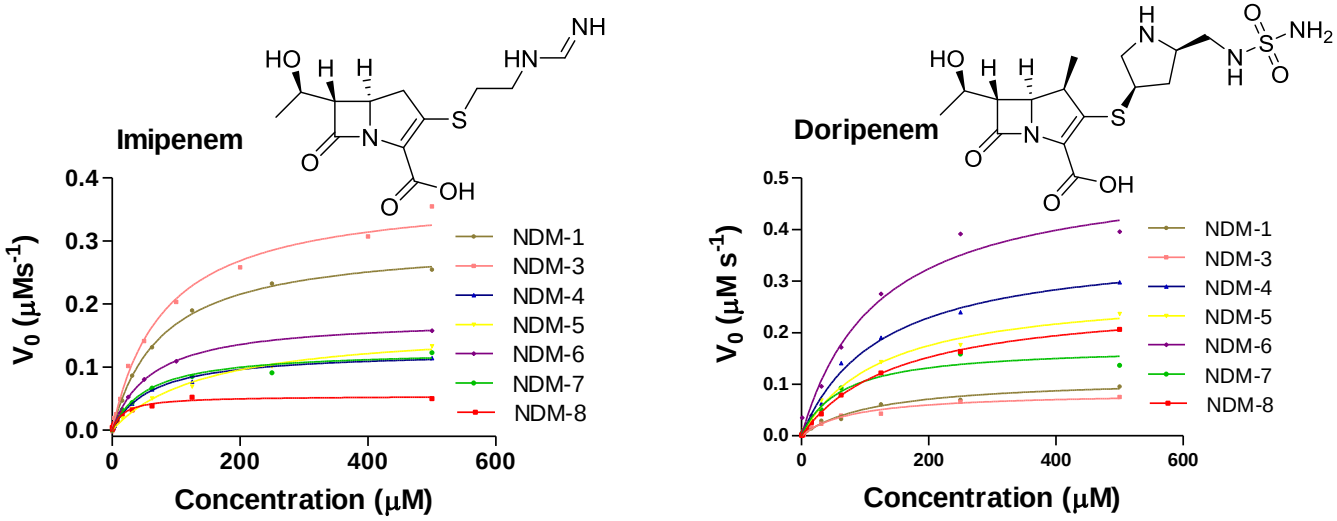


Figure 3-4: **Comparison of the hydrolysis of carbapenems by the tested NDM variants.**

3.4.1.2 PENICILLIN

Similar to carbapenems hydrolysis, all the tested NDM variants efficiently hydrolysed ampicillin, albeit with relatively high apparent K_M values, particularly for NDM-4 and NDM-6. With the exception of NDM-8, the apparently elevated K_M values were, in part, compensated for by increased k_{cat} values, resulting in similar k_{cat}/K_M values for all the variants (*Figure 3-5*).

Despite the relatively low differences in their catalytic efficiencies (2-3 fold differences), all the NDM variants reported lower k_{cat}/K_M values than for NDM-1, with NDM-8 reporting the lowest activity.

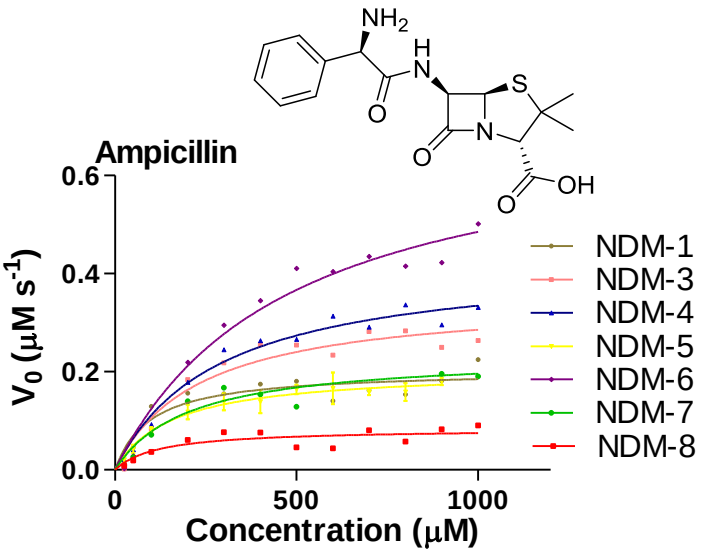


Figure 3-5: **Kinetic curves comparing the hydrolysis of ampicillin by the tested NDM variants. Steady-state kinetics experiments were carried out at room temperature in MBL assay buffer supplemented with 1µM $ZnSO_4$.**

Table 3-4: **Kinetic parameters of seven NDM variants with representative β-lactam antibiotics.** ***Measurements were carried out in triplicate (n ≥ 3) using a single batch of enzyme; K_M values are the means of three independent measurements ± standard deviation. Standard deviation values for k_{cat} and k_{cat}/K_M values did not exceed 10 %.***

Antibiotic	NDM-1	NDM-3	NDM-4	NDM-5	NDM-6	NDM-7	NDM-8
Imipenem							
K_M (μM)	78 ± 4	82 ± 12	62 ± 8	148 ± 16	62 ± 6	56 ± 6	20 ± 3
k_{cat} (s^{-1})	600	757	252	332	355	127	54
k_{cat}/K_M ($s^{-1}\mu M^{-1}$)	8	9	4	2	6	2	3
Meropenem							
K_M (μM)	57 ± 9	58 ± 11	119 ± 9	99 ± 4	49 ± 4	45 ± 5	54 ± 5
k_{cat} (s^{-1})	301	238	583	413	362	194	142
k_{cat}/K_M ($s^{-1}\mu M^{-1}$)	5	4	5	4	7	4	3
Doripenem							
K_M (μM)	119 ± 17	83 ± 15	125 ± 10	126 ± 11	119 ± 18	64 ± 11	151 ± 9
k_{cat} (s^{-1})	226	170	743	570	1032	348	267
k_{cat}/K_M ($s^{-1}\mu M^{-1}$)	2	2	6	5	9	5	2
Ampicillin							
K_M (μM)	110 ± 23	258 ± 54	305 ± 48	156 ± 20	455 ± 69	207 ± 55	229 ± 45
k_{cat} (s^{-1})	447	724	900	408	1375	477	273
k_{cat}/K_M ($s^{-1}\mu M^{-1}$)	4	3	3	3	3	2	1
Cephalothin							
K_M (μM)	29 ± 6	13 ± 3	11 ± 2	15 ± 3	10 ± 2	11 ± 3	5 ± 1
k_{cat} (s^{-1})	75	53	45	25	63	18	9
k_{cat}/K_M ($s^{-1}\mu M^{-1}$)	3	5	4	2	6	2	2
Cefoxitin							
K_M (μM)	43 ± 6	50 ± 6	63 ± 7	27 ± 5	107 ± 9	23 ± 3	16 ± 3
k_{cat} (s^{-1})	10	6	14	4	18	4	3
k_{cat}/K_M ($s^{-1}\mu M^{-1}$)	0.2	0.1	0.2	0.1	0.2	0.2	0.2
Ceftazidime							
K_M (μM)	100 ± 19	115 ± 15	133 ± 18	86 ± 11	144 ± 25	79 ± 10	19 ± 5
k_{cat} (s^{-1})	24	23	28	15	29	16	5
k_{cat}/K_M ($s^{-1}\mu M^{-1}$)	0.2	0.2	0.2	0.2	0.2	0.2	0.3
Nitrocefin							
K_M (μM)	11 ± 2	4 ± 1	4 ± 1	6 ± 1	8 ± 2	5 ± 1	4 ±1
K_i (μM)	NR	NR	102 ± 32	139 ± 28	NR*	79 ± 18	146 ± 47
k_{cat} (s^{-1})	65	30	38	33	49	15	44
k_{cat}/K_M ($s^{-1}\mu M^{-1}$)	6	8	6	6	6	3	11

*NR: Not reported.

3.4.1.3 CEPHALOSPORIN SUBSTRATES

The most evident differences in the kinetic parameters of the NDM variants were observed with the tested cephalosporins. Substantial differences were observed in the separate k_{cat} and K_M values for the NDM variants, which in some cases, contributed to differences in the overall catalytic efficiency (*Figure 3-6*).

The doubly substituted variants, i.e. those with the M154L substitution and an additional amino acid change, showed consistently lower k_{cat} values for the tested cephalosporins, with the exception of nitrocefin. NDM-8 (D130G, M154L) manifested an 8 and 7-fold lower k_{cat} value for cephalothin than NDM-1 or NDM-6, respectively. NDM-5 (V88L, M154L) and NDM-7 (D130N, M154L) also manifested relatively lower k_{cat} values for the tested cephalosporins (*Table 3-4*). Additionally, NDM-8 showed a considerably lower K_M for ceftazidime (7 fold lower than NDM-4 and NDM-6).

Overall, the differences in k_{cat}/K_M values for the cephalosporins were at most 3-4 fold for the NDM variants. Consistent with previously reported results on NDM-1 and NDM-14[1,30], this study revealed relatively poor hydrolysis of cefoxitin and ceftazidime by the tested NDM variants with k_{cat}/K_M values being <1 $s^{-1}\mu M^{-1}$. These results are also in agreement with recent *in vivo* studies showing minimal interaction of ceftazidime and cefotaxime with NDM-1-producing *E. coli* cells[40].

Observations from this and other studies thus indicate that the recent generation of cephalosporins may be less optimal substrates for NDMs and could be considered as possible therapeutic agents for infections caused by NDM-carrying bacteria.

It is notable that there are some variations between the results of this study and literature values and also between different literature studies[17,18,26]. For instance, the previously reported k_{cat}/K_M value for NDM-1 with imipenem was > 30 times lower than the value obtained in this study (*Table 3-5*). This may reflect differences in the purity, protein folding and metal content of the recombinant enzymes, influenced by enzyme preparation procedures and/or assay conditions. The results described thus provide a reliable direct comparison of the enzymatic activities of NDM variants as the analyses were carried out under similar experimental conditions.

Table 3-5: **Comparison of kinetic parameters from this study with literature values for NDM-1, NDM-3, NDM-4 and NDM-8.** ***The shaded regions show data obtained from this study while the unshaded sections represent data obtained from previous studies.*** [1, 17, 18, 26]

Substrate	**NDM-1**[1]			**NDM-3**[17]			**NDM-4**[18]			**NDM-8**[26]		
	K_M (μM)	k_{cat} (s^{-1})	k_{cat}/K_M (s^{-1}/μM)	K_M (μM)	k_{cat} (s^{-1})	k_{cat}/K_M (s^{-1}/μM)	K_M (μM)	k_{cat} (s^{-1})	k_{cat}/K_M (s^{-1}/μM)	K_M (μM)	k_{cat} (s^{-1})	k_{cat}/K_M (s^{-1}/μM)
Imipenem	94	20	0.20	148 ± 13	25 ±1	0.17	86	40	0.46	167 ± 8	46 ± 2	0.28
This study	78 ± 4	600	8	82 ± 12	757	9	62 ± 8	252	4	20 ± 3	54	3
Meropenem	49	12	0.25	81 ± 4	32 ± 1	0.4	95	30	0.31	127 ±20	169 ± 12	1.3
This study	57 ± 9	301	5	58 ± 11	238	4	119 ± 9	583	5	54 ± 5	142	3
Ampicillin	22	15	0.66	228 ± 35	73 ± 7	0.32	ND	ND	ND	193 ± 6	158 ± 5	0.82
This study	110 ± 23	447	4	258 ± 54	724	3	305 ± 48	900	3	229 ± 45	273	1
Cephalothin	10	4	0.4	ND	ND	ND	46	24	0.5	ND	ND	ND
This study	29 ± 6	75	3	13 ± 3	53	5	15 ± 3	25	2	5 ± 1	9	2
Cefoxitin	49	1	0.02	17 ± 1	2 ± 0.2	0.1	NH	NH	NH	34 ± 1	3 ± 0.1	0.1
This study	43 ± 6	10	0.2	50 ± 6	6	0.1	63 ± 7	14	0.2	16 ± 3	3	0.2
Ceftazidime	181	5	0.03	64 ± 9	11 ± 9	0.17	72	4	0.06	63 ± 3	12 ± 0.2	0.2
This study	100 ± 19	24	0.2	115 ± 15	23	0.2	133 ± 18	28	0.2	19 ± 5	5	0.3

NH: Not hydrolysed; ND:Not determined

3.4.2 INVESTIGATION OF INHIBITION BY NITROCEFIN

One of the interesting findings from this study was the observation of apparent nitrocefin substrate inhibition with NDM-4, NDM-5, NDM-7 and NDM-8 (*K_i* values of 102 ± 32, 139 ± 28, 79 ± 18 and 146 ± 47 µM, respectively). The inhibition was only observed for the enzymes containing the M154L substitution (*Figure 3-6*), implying that this substitution could play a role in the interaction of the enzymes with nitrocefin. Although nitrocefin is only used for screening purposes and not in clinical practice, there have been other reports of nitrocefin substrate inhibition for IMP variants with S121G and F218Y substitutions, which like the M154L substitution are found relatively remote from the active site[31]. It is possible that these remote substitutions interfere with substrate-enzyme interactions and may potentially contribute to differences in kinetic properties of the clinically reported NDM variants with related β-lactams.

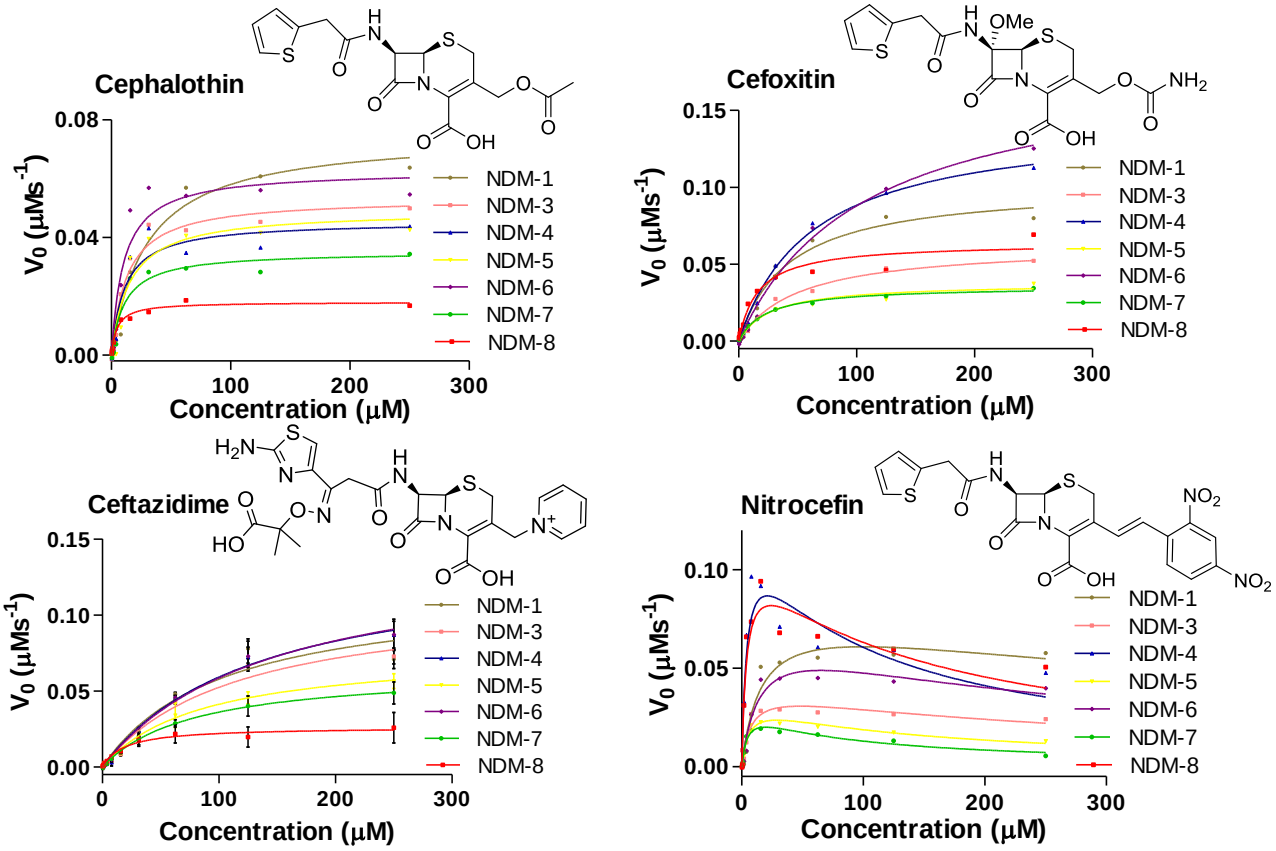


Figure 3-6: **Comparison of the hydrolysis of different cephalosporin substrates with the tested NDM variants, indicating the inhibition of NDM-4, 5, 7 and 8 by nitrocefin.**

To further investigate the differences in nitrocefin inhibition, structural features of NDM-1 were explored. A crystal structure of NDM-1 complexed with hydrolysed oxacillin (PDB code 4EYB)[41] reveals apparently favourable aryl-sulfur interactions between M154 and aromatic side-chain of the antibiotic, which may contribute to the NDM catalytic activity (*Figure 3-7*). A probable hypothesis is that the M154 residue facilitates hydrolysis by interacting with the aromatic rings in the hydrolysed product. It seems likely that the M154L substitution may alter interactions between residue M154 and the nitrocefin dinitroaryl-substituent thus slowing catalysis.

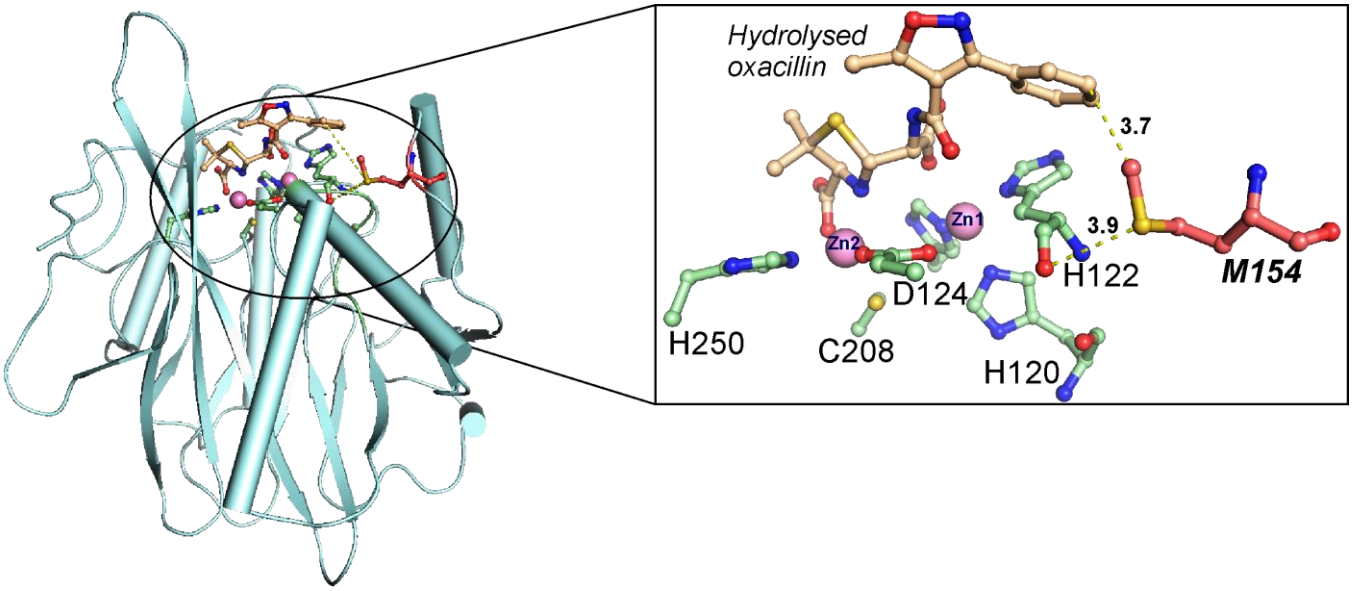


Figure 3-7: **View from a structure of NDM-1 complexed with hydrolysed oxacillin (PDB code 4EYB)[41] showing the proximity (in Å) of M154 side chain with the active site residues and the aromatic ring of the substrate.**

Notably, the proximity of the M154 side chain to the backbone of the loop containing three zinc-binding residues (H120, H122, and D124) suggests that the M154L substitution could have an impact on the metal site configuration (*Figure 3-8*)[9,41]. Although further structural and mechanistic investigation is necessary to elucidate the role of this substitution, these observations may be useful considerations in the development of NDM inhibitors and β-lactam antibiotics with reduced susceptibility to MBL catalysis.

3.5 BIOPHYSICAL CHARACTERISATION OF NDM VARIANTS

In spite of the minimal differences in the catalytic efficiencies of the isolated NDM variants, the positions of some of the substitutions in the MBL fold suggested that they may affect the biophysical properties of the variants. It was thus interesting to explore other factors that may influence the rapid evolution of the NDMs and possibly contribute to the observed differences in the β-lactam susceptibility of the variants. Secondary structure and thermal stability analyses were carried out to further investigate the effect of the substitutions on the structural features of the enzymes.

3.5.1 SECONDARY STRUCTURE ANALYSES BY CIRCULAR DICHROISM (CD)

To investigate the secondary structure profiles of the NDM variants, CD spectra were obtained using a Chirascan CD spectrometer (Applied Photophysics model) equipped with a peltier temperature-controlled cell holder. The proteins were dialysed and diluted to 0.2 mg/ mL in CD buffer (10 mM sodium phosphate, pH 8.0); the CD spectra were collected in triplicates at 23°C using a 0.1 cm pathlength cuvette. The CD spectra were recorded in millidegrees from 260 to 185 nm at 0.5 nm intervals with each data point being averaged for 1 second.

Spectra were base-line corrected and smoothed using the Savitzky-Golay filter[42] (window size 8). To account for minor differences in protein concentrations, data were normalised to the CD signal at 207 nm and the CD spectra curves of the normalised data generated using Graphpad prism[43]. To estimate the secondary structural content, the CD raw data (190-240 nm range) were analysed in DichroWeb[44] using the CDSSTR deconvolution method (reference set 4)[45].

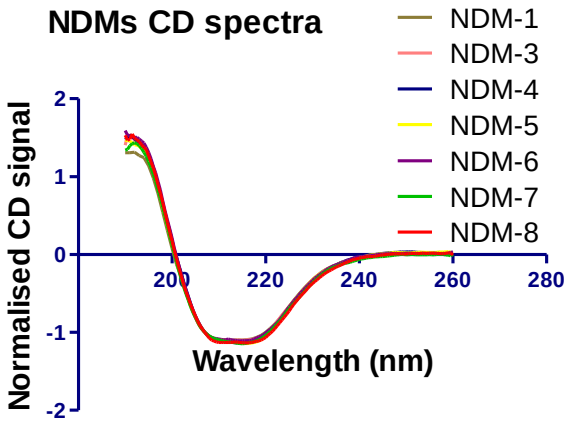


***Figure 3-8*: Overlay of the CD spectra of the different NDM variants showing the similarities of the secondary structures of the enzymes.**

All the tested NDM variants displayed CD spectra that are characteristic of well-folded, structured proteins [46] and the calculated β-sheet and α-helical content from the deconvolution was in close agreement with the structural features reported for NDM-1[34]. The CD spectra for NDM-1 and the other variants were almost completely aligned, other than the slight differences observed in the lower wavelengths due to the instrument's limits of detection (*Figure 3-8*). The predicted secondary structural content for all the variants was also very similar (*Table 3-4*), indicating that the substitutions present do not substantially affect the overall folds and structural composition of the NDM variants.

***Table 3-4:* Comparison of secondary structure content of NDM variants as predicted from CD spectra using the CDSSTR deconvolution method (reference set 4) in Dichroweb.**

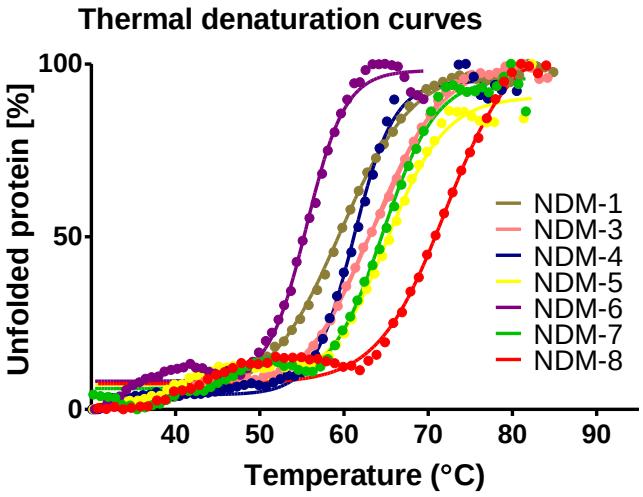
	Helix 1	Helix 2	Strand 1	Strand 2	Turns	Un-ordered	Total
NDM-1	0.05	0.07	0.21	0.12	0.23	0.31	0.99
NDM-3	0.05	0.07	0.23	0.13	0.21	0.31	1
NDM-4	0.05	0.07	0.21	0.12	0.22	0.32	0.99
NDM-5	0.05	0.07	0.23	0.13	0.21	0.31	1
NDM-6	0.05	0.06	0.21	0.12	0.23	0.32	0.99
NDM-7	0.05	0.06	0.23	0.13	0.22	0.31	1
NDM-8	0.05	0.06	0.23	0.12	0.23	0.31	1

3.5.2 INVESTIGATION OF THERMAL STABILITY OF NDM VARIANTS

The effects of the substitutions on the thermal stability of the NDM variants were further investigated using temperature-dependent CD and Differential Scanning Flourimetry (DSF).

3.5.2.1 Determination of melting temperatures by CD

The proteins were subjected to thermal denaturation and the temperature-induced changes in secondary structure were monitored by recording the CD signal at 222 nm, i.e. by following unfolding of proteins' α-helices[46]. The temperature was ramped at a rate of 1 °C/minute from 10 – 90 °C and the CD signal was recorded in triplicate every 1 °C. The data were baseline-corrected and smoothed as previously described. To obtain the apparent T_m values, normalised data were fitted to a Boltzmann sigmoidal curve in GraphPad Prism software.



NDM	T_m (°C)
NDM-1	60 ± 0.1
NDM-3	63 ± 0.1
NDM-4	61 ± 0.2
NDM-5	65 ± 0.3
NDM-6	55 ± 0.2
NDM-7	65 ± 0.2
NDM-8	72 ± 0.4

Figure 3-9: **Thermal stability melting curves and the respective melting temperatures of the NDM variants as determined by temperature dependent CD.**

Unlike the secondary structure, substantial differences were observed in T_m values (> 10 °C), revealing clear changes in the thermal stability of the NDM variants. NDM-6 (A233V) was the least stable of the tested variants with a T_m of 55 °C while the wild type NDM-1 reported a T_m value of 60 °C. The other single-substituted variants, NDM-3 (D95N) and NDM-4 (M154L), also recorded slightly higher T_m values of 63 °C and 61 °C, respectively.

In contrast, the doubly-substituted variants displayed elevated apparent T_m values with NDM-8 (D130G, M154L) being the most stable variant with a melting temperature of 72 °C. NDM-5 (V88L, M154L) and NDM-7 (D130N, M154L) also displayed T_m values 10 °C and 5 °C higher than NDM-6 and NDM-1 respectively.

To verify these interesting results, the NDM variants' melting temperatures were determined by DSF analyses.

3.5.2.2 Determination of melting temperatures by DSF

For DSF analyses, melting curves of NDM variants were compared in both HEPES and Tris buffers using a MiniOpticon™ Real-Time PCR (BioRad) and SYPRO® Orange Protein Gel Stain (Life Technologies Corporation) as the reporter fluorescent dye. The enzymes were diluted to a final concentration of 2 µM in 50 mM HEPES or Tris buffer (pH 7.5), supplemented with 200 mM NaCl. To investigate the stabilising effect of Zn^{2+} ions, a comparison was carried out in the absence or presence of 50 µM $ZnCl_2$. The temperature was ramped linearly in steps of 1 °C/ minute and fluorescence readings (λ_{ex} = 92 nm and λ_{em} = 610 nm) were taken in triplicate between 25 °C and 80 °C. Thermal denaturation profiles were generated by monitoring the increase in fluorescence (upon non-specific binding of the dye to hydrophobic residues) as a function of temperature. Data were analysed using GraphPad Prism software, and a Boltzmann curve was fitted to determine T_m values (*Figure 3-11*). To compare the thermal stability data from DSF and CD, Spearman's rank correlation analyses were carried out using StatsDirect (http://www.statsdirect.com/). Although the differences in T_m values were less dramatic in the DSF results, the results were still in close agreement with the CD results. A strong positive correlation between the DSF and CD data was obtained in the Spearman's rank correlation coefficient analysis ($\rho = 0.76$, $p < 0.05$).

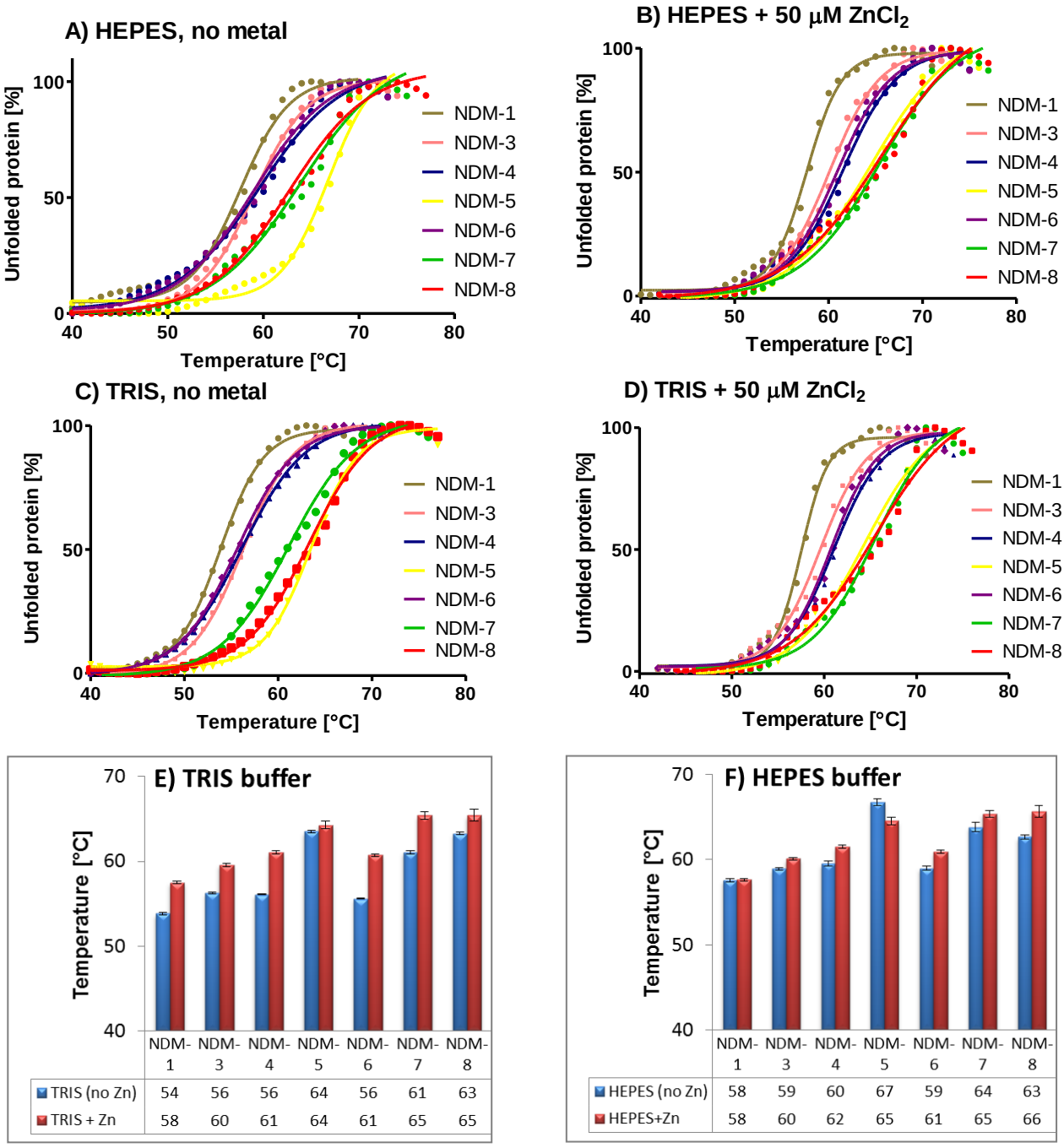


Figure 3-10: **Comparison of thermal stability melting curves of NDM variants in TRIS and HEPES buffers, showing stabilisation effect of Zn^{2+} ions.**

As was the case in CD analyses, the doubly substituted variants displayed higher T_m values, with NDM-5, NDM-7 and NDM-8 still being the more stable variants. Although some NDM variants exhibited higher melting temperatures in HEPES buffer, the addition of zinc ions stabilised the NDM variants in both buffers with the exception of NDM-5 (*Figure 3-10*). These results are consistent with previous reports on the effect of zinc ions on NDM-1[47].

3.6 SUMMARY

MBL variants with a wide range of activity towards different β-lactam antibiotics continue to be reported globally. Exposure to imipenem is reported to promote selection of strains producing IMP and VIM MBLs, which comprise the most diversified of the clinically relevant B1 MBLs, with > 40 variants reported[13]. Contrary to some previous proposals[18], the observations in this and other studies[17,28,29], report no substantial differences in the catalytic efficiencies of the studied NDM-variants towards carbapenem or penicillin substrates. There is therefore no compelling evidence that the studied variants have evolved to directly improve kinetic parameters for carbapenem hydrolysis. Notably, differences in the kinetics of cephalosporin hydrolysis were observed, in that the variants with the M154L substitution (NDM-4, NDM-5, NDM-7 and NDM-8) display substrate inhibition kinetics with nitrocefin. The second sphere interaction of M154 with the NDM's active site and its influence on the substrate profiles of the NDM variants is explored further using structural and kinetic analyses in the next chapter.

Although the amino acid substitutions present in NDM variants did not alter their overall secondary structural composition, the variants manifested substantial differences in their thermal stabilities, with >10 °C differences in T_m values being observed in some cases. Strikingly, the more stable variants, NDM-5 and NDM-7, also reported an increase in MIC values for selected carbapenems in comparison to the less stable variants. It is worth noting that truncated NDM constructs were used for this study, thermal stabilities of the more biologically relevant full-length NDM variants are compared in the subsequent chapter.

Although the biological relevance of the increased thermal stability, if any, is still unclear, it is possible that the relative differences in thermodynamic stabilities reflect environmental pressures and could contribute to increased cellular lifetimes of the enzymes, resulting in

elevated MIC values. Equally, the higher melting temperatures could allow the enzymes to acquire multiple destabilising substitutions without losing the ability to fold into a functional enzyme, suggesting that protein stability may be an important factor in MBL evolution.

3.7 REFERENCES

1. Yong D, Toleman MA, Giske CG, *et al*. Characterization of a new metallo-β -lactamase gene, *bla*$_{\text{NDM-1,}}$ and a novel erythromycin esterase gene carried on a unique genetic structure in *Klebsiella pneumoniae* sequence type 14 from India. *Antimicrob Agents Chemother*. 2009;53(12):5046-5054.

2. Walsh TR, Weeks J, Livermore DM, Toleman MA. Dissemination of NDM-1 positive bacteria in the New Delhi environment and its implications for human health: An environmental point prevalence study. *Lancet Infect Dis*. 2011;11:355-362.

3. Lascols C, Hackel M, Marshall SH, *et al*. Increasing prevalence and dissemination of NDM-1 metallo-β-lactamase in India: Data from the SMART study (2009). *J Antimicrob Chemother*. 2011;66(9):1992-1997.

4. Lachish T, Elimelech M, Arieli N, Adler A, Rolain JM, Assous MV. Emergence of new delhi metallo-β-lactamase in Jerusalem, Israel. *Int J Antimicrob Agents*. 2012;40:566-567.

5. Page MI, Badarau A. The mechanisms of catalysis by metallo β-lactamases. *Bioinorg Chem Appl*. 2008:576297.

6. Shahid M. Environmental dissemination of NDM-1: Time to act sensibly. *Lancet Infect Dis*. 2011;11:334-335.

7. Biedenbach D, Bouchillon S, Hackel M, *et al*. Dissemination of NDM metallo-β-lactamase genes among clinical isolates of *Enterobacteriaceae c*ollected during the SMART global surveillance study from 2008 to 2012. *Antimicrob Agents Chemother*. 2015;59(2):826-830.

8. Kumarasamy KK, Toleman MA, Walsh TR, *et al*. Emergence of a new antibiotic resistance mechanism in India, Pakistan, and the UK: A molecular, biological, and epidemiological study. *Lancet Infect Dis*. 2010;10:597-602.

9. Meini MR, Llarrull LI, Vila AJ. Evolution of metallo-β-lactamases: Trends revealed by natural diversity and evolution. *Antibiotics (Basel)*. 2014;3(3):285-316.

10. Widmann M, Pleiss J, Oelschlaeger P. Systematic analysis of metallo-β-lactamases using an automated database. *Antimicrob Agents Chemother*. 2012;56(7):3481-3491.

11. Borgianni L, Vandenameele J, Matagne A, *et al*. Mutational analysis of VIM-2 reveals an essential determinant for metallo-β-lactamase stability and folding. *Antimicrob Agents Chemother*. 2010;54(8):3197-3204.

12. Oelschlaeger P. Outsmarting metallo-β-lactamases by mimicking their natural evolution. *J Inorg Biochem*. 2008;102(12):2043-2051.

13. Bush K, Palzkill T, Jacoby G. β-Lactamase Classification Lahey Web site. http://www.lahey.org/studies/other.asp. Updated October, 2015. Accessed February, 2016.

14. Espinal P, Fugazza G, López Y, *et al*. Dissemination of an NDM-2-producing *Acinetobacter baumannii* clone in an Israeli rehabilitation center. *Antimicrob Agents Chemother*. 2011;55:5396-5398.

15. Espinal P, Poirel L, Carmeli Y, *et al*. Spread of NDM-2-producing *Acinetobacter baumannii* in the Middle East. *J Antimicrob Chemother*. 2013;68(8):1928-1930

16. Rogers BA, Sidjabat HE, Silvey A, *et al*. Treatment options for New Delhi metallo-β-lactamase-harboring *Enterobacteriaceae*. *Microb Drug Resist*. 2013;19:100-103.

17. Tada T, Miyoshi-Akiyama T, Shimada K, Kirikae T. Biochemical analysis of the metallo-β-lactamase NDM-3 from a multidrug-resistant *Escherichia coli* strain isolated in Japan. *Antimicrob Agents Chemother*. 2014;58(6):3538-3540.

18. Nordmann P, Boulanger AE, Poirel L. NDM-4 metallo-β-lactamase with increased carbapenemase activity from *Escherichia coli*. *Antimicrob Agents Chemother*. 2012;56(4):2184-2186.

19. Jakobsen L, Hammerum AM, Hansen F, Fuglsang-Damgaard D. An ST405 NDM-4-producing *Escherichia coli* isolated from a Danish patient previously hospitalized in Vietnam. *J Antimicrob Chemother*. 2013;69(2):559-560

20. Papagiannitsis CC, Studentova V, Chudackova E, *et al*. Identification of a New Delhi metallo-β-lactamase-4 (NDM-4)-producing *Enterobacter cloacae* from a Czech patient previously hospitalized in Sri Lanka. *Folia Microbiol (Praha)*. 2013;58(6):547-549

21. Hornsey M, Phee L, Wareham DW. A novel variant, NDM-5, of the New Delhi metallo-β-lactamase in a multidrug-resistant *Escherichia coli* ST648 isolate recovered from a patient in the United Kingdom. *Antimicrob Agents Chemother*. 2011;55(12):5952-5954.

22. Rasheed JK, Kitchel B, Zhu W, *et al*. New Delhi metallo-β-lactamase-producing *Enterobacteriaceae*, United States. *Emerg Infect Dis*. 2013;19(6):870-878.

23. Williamson DA, Sidjabat HE, Freeman JT, *et al*. Identification and molecular characterisation of New Delhi metallo-β-lactamase-1 (NDM-1)- and NDM-6-producing *Enterobacteriaceae* from New Zealand hospitals. *Int J Antimicrob Agents*. 2012;39:529-533.

24. Göttig S, Hamprecht AG, Christ S, Kempf VA, Wichelhaus TA. Detection of NDM-7 in Germany, a new variant of the New Delhi metallo-β-lactamase with increased carbapenemase activity. *J Antimicrob Chemother*. 2013; 68(8):1737-1740.

25. Cuzon G, Bonnin RA, Nordmann P. First identification of novel NDM carbapenemase, NDM-7, in *Escherichia coli* in France. *PLoS One*. 2013;8(4):e61322.

26. Tada T, Miyoshi-Akiyama T, Dahal RK, *et al*. NDM-8 metallo-β-lactamase in a multidrug-resistant *Escherichia coli* strain isolated in Nepal. *Antimicrob Agents Chemother*. 2013;57(5):2394-2396.

27. Wang X, Li H, Zhao C, *et al*. Novel NDM-9 metallo-β-lactamase identified from a ST107 *Klebsiella pneumoniae* strain isolated in China. *Int J Antimicrob Agents*. 2014;44(1):90-91.

28. Tada T, Shrestha B, Miyoshi-Akiyama T, *et al*. A novel NDM variant, NDM-12, from a carbapenem-resistant *Escherichia coli* clinical isolate in Nepal. *Antimicrob Agents Chemother*. 2014; 58(10):6302-6305.

29. Shrestha B, Tada T, Miyoshi-Akiyama T, *et al*. Identification of a novel NDM variant, NDM-13, from a multidrug-resistant *Escherichia coli* clinical isolate in Nepal. *Antimicrob Agents Chemother*. 2015;59(9):5847-5850.

30. Zou D, Huang Y, Zhao X, *et al*. A novel New Delhi metallo-β-lactamase variant, NDM-14, isolated in a Chinese hospital possesses increased enzymatic activity against carbapenems. *Antimicrob Agents Chemother*. 2015;59(4):2450-2453.

31. Oelschlaeger P, Mayo SL, Pleiss J. Impact of remote mutations on metallo-β-lactamase substrate specificity: Implications for the evolution of antibiotic resistance. *Protein Sci*. 2005;14(3):765-774.

32. Tomatis PE, Rasia RM, Segovia L, Vila AJ. Mimicking natural evolution in metallo-β-lactamases through second-shell ligand mutations. *Proc Natl Acad Sci U S A*. 2005;102(39):13761-13766.

33. Makena A, Brem J, Pfeffer I, *et al*. Biochemical characterization of New Delhi metallo-β-lactamase variants reveals differences in protein stability. *J Antimicrob Chemother*. 2015;70(2):463-469.

34. Green VL, Verma A, Owens RJ, Phillips SE, Carr SB. Structure of New Delhi metallo-β-lactamase 1 (NDM-1). *Acta Crystallogr Sect F Struct Biol Cryst Commun*. 2011;67:1160-1164.

35. Studier FW. Protein production by auto-induction in high density shaking cultures. *Protein Expr Purif*. 2005;41(1):207-234.

36. Rydzik AM, Brem J, van Berkel SS, *et al*. Monitoring conformational changes in the NDM-1 metallo-β-lactamase by ^{19}F NMR spectroscopy. *Angew Chem Int Ed Engl*. 2014;53(12):3129-3133.

37. Wilkins MR, Gasteiger E, Bairoch A, *et al*. Protein identification and analysis tools in the ExPASy server. *Methods Mol Biol*. 1999;112:531-552.

38. Makena A, van Berkel SS, Lejeune C, *et al*. Chromophore-linked substrate (CLS405): Probing metallo-β-lactamase activity and inhibition. *ChemMedChem*. 2013; 8(12):1923-1929.

39. Horton LB, Shanker S, Mikulski R, *et al*. Mutagenesis of zinc ligand residue Cys221 reveals plasticity in the IMP-1 metallo-β-lactamase active site. *Antimicrob Agents Chemother*. 2012;56(11):5667-5677.

40. Ma J, McLeod S, Maccormack K, *et al*. Real-time monitoring of New Delhi metallo-β-lactamase activity in living bacterial cells by ^{1}H NMR spectroscopy. *Angew Chem Int Ed Engl*. 2014; 53(8):2130-2133.

41. King DT, Worrall LJ, Gruninger R, Strynadka NC. New Delhi metallo-β-lactamase: Structural insights into β-lactam recognition and inhibition. *J Am Chem Soc*. 2012;134:11362-11365.

42. Savitzky A GM. Smoothing and differentiation of data by simplified least-squares procedures. *Anal Chem*. 1964;36(8):1627-1639.

43. Raussens V, Ruysschaert JM, Goormaghtigh E. Protein concentration is not an absolute prerequisite for the determination of secondary structure from circular dichroism spectra: A new scaling method. *Anal Biochem*. 2003;319(1):114-121.

44. Whitmore L, Wallace BA. Protein secondary structure analyses from circular dichroism spectroscopy: Methods and reference databases. *Biopolymers*. 2008;89(5):392-400.

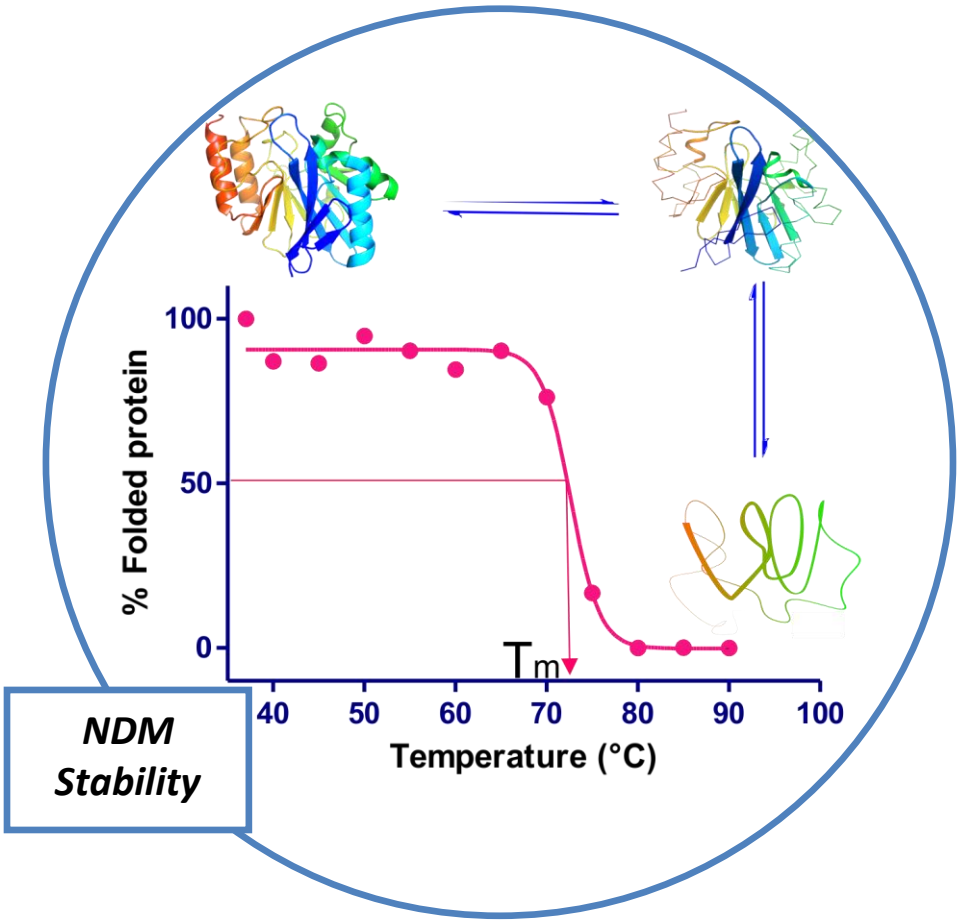
45. Sreerama N, Woody RW. Estimation of protein secondary structure from circular dichroism spectra: Comparison of CONTIN, SELCON, and CDSSTR methods with an expanded reference set. *Anal Biochem*. 2000;287(2):252-260.

46. Greenfield NJ. Using circular dichroism spectra to estimate protein secondary structure. *Nat Protoc*. 2006;1(6):2876-2890.

47. Li T, Wang Q, Chen F, *et al*. Biochemical characteristics of New Delhi metallo-β-lactamase-1 show unexpected difference to other MBLs. *PLoS One*. 2013;8:e61914.

CHAPTER 4: ROLE OF M154L SUBSTITUTION IN THE ACTIVITY AND STABILITY OF NDM VARIANTS

As described in Chapter 3, biochemical analyses of NDM variants revealed increased thermal stabilities of variants containing the M154L substitution, including NDM-5, NDM-7 and NDM-8. These variants also displayed some degree of inhibition by the cephalosporin substrate nitrocefin. This chapter thus seeks to characterise the differences in activity and stability of NDM variants in relation to the M154L substitution. The results provide insights into the evolution of NDM variants and have important ramifications for future MBL inhibitor development programs.



CONTENTS

CHAPTER 4: ROLE OF M154L SUBSTITUTION IN THE ACTIVITY AND STABILITY OF NDM VARIANTS 127

4.1 INTRODUCTION 129

4.1.1 NDM substitutions 130

4.1.2 Chapter Objectives 131

4.2 PROTEIN PRODUCTION 132

4.2.1 Cloning and Mutagenesis 132

4.2.2 Purification of Recombinant NDM Variants 133

4.2.3 Size Exclusion Chromatography-Multi-Angle Light Scattering (SEC-MALS) Analyses 134

4.3 HYDROLYSIS OF CEPHALOSPORINS BY NDM VARIANTS 135

4.3.1 Steady-State Kinetic Analyses 135

4.4 CRYSTALLOGRAPHIC ANALYSES OF NDM VARIANTS 139

4.4.1 Overall Structural Properties of NDM Variants 139

4.5 M154L SUBSTITUTION INFLUENCE ON STABILITY OF NDM VARIANTS 144

4.5.1 Circular Dichroism Analyses (CD) 144

4.5.2 Dynamic Scanning Calorimetric Analyses 146

4.5.3 Cellular Thermal Shift Assays (CETSA) 148

4.6 SUMMARY 151

4.7 REFERENCES 152

4.1 INTRODUCTION

Amino acid substitutions either occurring naturally or produced by protein engineering have been shown to confer different catalytic and biophysical profiles to the resultant enzymes[1-3]. For metallo-β-lactamases (MBLs) in particular, variants with varying activity towards different classes of β-lactam antibiotics continue to be reported worldwide[4,5]. In light of the apparent adaptation of bacteria to counter β-lactam antibiotic exposure, it is critical to develop a better understanding of the complex interplay between the sequence, structure, stability and function of MBLs. Since the first identification of New Delhi Metallo-β-lactamase-1 (NDM-1), 16 different NDM variants have been reported, which manifest largely similar hydrolytic profiles (Chapter 3)[6]. The currently reported NDM variants differ by one or two amino acid substitutions relative to NDM-1, with the notable exception of NDM-10 (*Table 4-1*).

***Table 4-1*: Reported substitutions in the NDM variants relative to NDM-1, showing the frequency of substitutions at residue 154 (in red).**

NDM type	Residue substitution	NDM type	Residue substitution
NDM-2	P28A[7]	NDM-5	V88L, M154L[8]
NDM-3	D95N[9]	NDM-7	D130N, M154L[10]
NDM-4	M154L[11]	NDM-8	D130G, M154L[12]
NDM-6	A233V[13]	NDM-10	R32S, G36D, G69S, A74T,G200R
NDM-9	E152K[14]	NDM-12	M154L, G222D[15]
NDM-11	M154V	NDM-13	D95N, M154L[16]
NDM-14	D130G[17]	NDM-15	M154L, A233V
NDM-16	T262H		

4.1.1 NDM SUBSTITUTIONS

While most of the substitutions on NDM variants are relatively remote from the zinc-binding site, related B1 MBLs such as SPM-1 have been shown to maintain a conserved active site while accumulating mutations in second sphere residues, which influence the activity and stability of the enzymes (the term second sphere residues generally refers to residues located relatively far from the metal center, but involved in a network of interactions with the zinc-binding residues)[18-20]. M154 is a mutation hot spot, being the most frequently substituted residue in the NDM variants (*Table 4-1)*. This second sphere residue (M154) is substituted to a valine in NDM-11 and a leucine in NDM-4. In the six doubly-substituted NDM variants, the M154L substitution occurs in association with V88L (NDM-5), D130N (NDM-7), D130G (NDM-8), G222D (NDM-12), D95N (NDM-13) and A233V (NDM-15).

Although some previous studies indicate that the M154L substitution confers increased hydrolytic activity towards carbapenems and several cephalosporins[11], the results reported in Chapter 3 do not manifest significant changes in catalytic efficiencies of the enzymes containing the M154L substitution. Despite this observation, the frequency of substitutions at position 154 and the variability of the residues associated with the M154L substitution are of great interest in understanding the evolution of NDM variants.

4.1.2 CHAPTER OBJECTIVES

The primary aim of the work described in this chapter was to investigate whether the recurrent substitution at position 154 in NDM variants influences the biochemical and biophysical properties of the NDM variants. Comparative analyses of the activity and thermal stability of NDM-1 and four clinically reported variants containing the M154L substitution (NDM-4, NDM-5, NDM-7 and NDM-12) were performed. The work also describes the characterisation of NDM-1 single-mutants V88L, D130N and G222D.

The work described in this chapter details extensive analyses on the thermal stabilities of the NDM variants using Circular Dichroism (CD), Differential Scanning Calorimetry (DSC), and a cell-based thermal shift assay (CETSA). Following from the previous report of inhibition of some, but not all NDM variants by nitrocefin (Chapter 3)[6], comparison of catalytic efficiencies of the NDM variants towards a set of cephalosporin substrates was also carried out. Furthermore, five novel crystal structures of previously described NDM variants (Chapter 3) are reported, providing insights to the function and stability of NDM variants.

The work described in this chapter was carried out in collaboration with Dr. David Staunton (Department of Biochemistry, University of Oxford) and Dr. Bhaskar Bhushan who provided training and technical support for DSC and CETSA analyses. Mr. James Ferguson, Dr. Michael McDonough and Dr. Jurgen Brem facilitated the crystallisation and carried out the refinement of the NDM structures.

4.2 PROTEIN PRODUCTION

The target NDM variants were produced and purified using previously optimized protocols (Chapter 3) [6], to yield proteins sufficient for subsequent analyses.

4.2.1 CLONING AND MUTAGENESIS

The previously described pOPINF vectors (Chapter 3) were constructed to include the NDM-1 full coding sequence (M27-R270) and a cleavable *N*-terminal His_6 tag, lacking the *N*-terminal leader sequence. Using NDM-1-bearing vectors as templates, site directed mutagenesis was carried out to generate NDM-4 (M154L) as well as the single-mutants V88L, D130G and G222D. Plasmids encoding for NDM-4 were used as templates to generate the doubly substituted NDM-5, NDM-7 and NDM-12 variants. Standard mutagenesis protocols (Chapter 7.2) using relevant primers (*Table 4-2*) were employed for the efficient introduction of the desired mutations.

***Table 4-2*: Mutagenic primers used for generation of target NDM variants.**

NDM-4	Forward	5' CTGTGCTGCAACCAGACCTTCTTGCGGAG 3'
A440C	Reverse	5' CTCCGCAAGAAGGTCTGGTTGCAGCACAG 3'
NDM-5	Forward	5' CCATGCGGTATCAACCAGCAGAACACGACCACC 3'
GT242CG	Reverse	5' GGTGGTCGTGTTCTGCTGGTTGATACCGCATGG 3'
NDM-7	Forward	5' CTGCATGCAGTGCATTCATACCACCCATTTTG 3'
G368A	Reverse	5' CAAAATGGGTGGTATGAATGCACTGCATGCAG 3'
NDM-12	Forward	5' CGGTATCTGCATCATCCAGATTGCCCAGGC 3'
G645A	Reverse	5' GCCTGGGCAATCTGGATGATGCAGATACCG 3'

4.2.2 PURIFICATION OF RECOMBINANT NDM VARIANTS

Plasmids encoding for the *N*-His_6 tagged NDM mutants were transformed into *E. coli* BL21 (DE3) pLysS cells and cultured in auto-induction media for the production of recombinant proteins as previously described[6] (Chapter 3). Protein purification was carried out using nickel affinity and size exclusion chromatography, yielding homogeneous recombinant proteins with >90% purity as ascertained by SDS PAGE analysis (*Figure 4-1*).

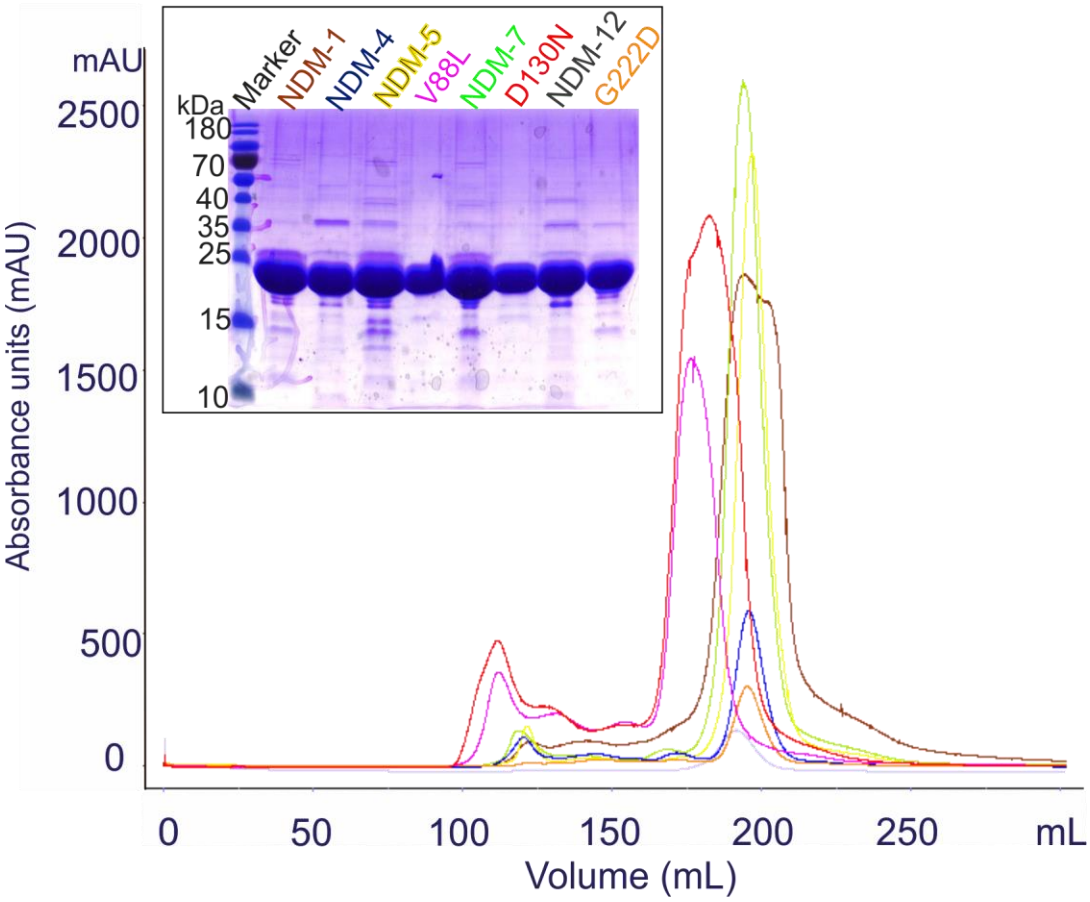


***Figure 4-1*: Overlay of size exclusion chromatograms of the purified NDM variants. Inset: SDS PAGE analyses showing the purity of the recombinant NDM variants.**

4.2.3 SIZE EXCLUSION CHROMATOGRAPHY-MULTI-ANGLE LIGHT SCATTERING (SEC-MALS) ANALYSES

To verify the homogeneity and oligomeric state of the purified proteins SEC-MALS analyses were carried out. Analysis of the purified NDM variants was performed using an Agilent 1260 HPLC column coupled to a DAWN HELEOS II scattering detector and an Optilab differential refractive index detector. The MALS detector was equilibrated overnight to ensure minimal background light scattering. Roughly 50 µg of protein was loaded onto the column and data was collected for 45 minutes. Samples were run at a flow rate of 75 µL per minute using 50 mM Tris buffer (pH 7.5) supplemented with 500 mM NaCl. Data acquisition and analysis was performed using Astra 6.1 software (Wyatt Technologies).

The NDM variants displayed very similar SEC-MALS profiles, with the obtained molar masses being in close agreement to the predicted values (*Figure 4-2*). The single peak also indicated that the NDM variants were monomeric and homogenous, with no detectable evidence for aggregation.

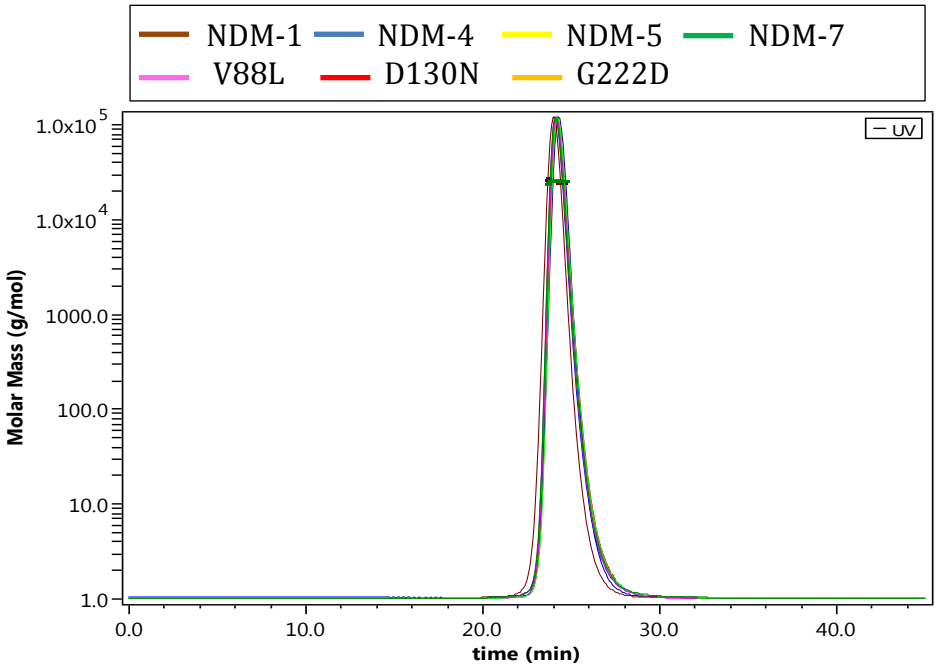


***Figure 4-2*: SEC-MALS chromatograms for the NDM variants showing similarities in their masses and monomeric states.**

4.3 HYDROLYSIS OF CEPHALOSPORINS BY NDM VARIANTS

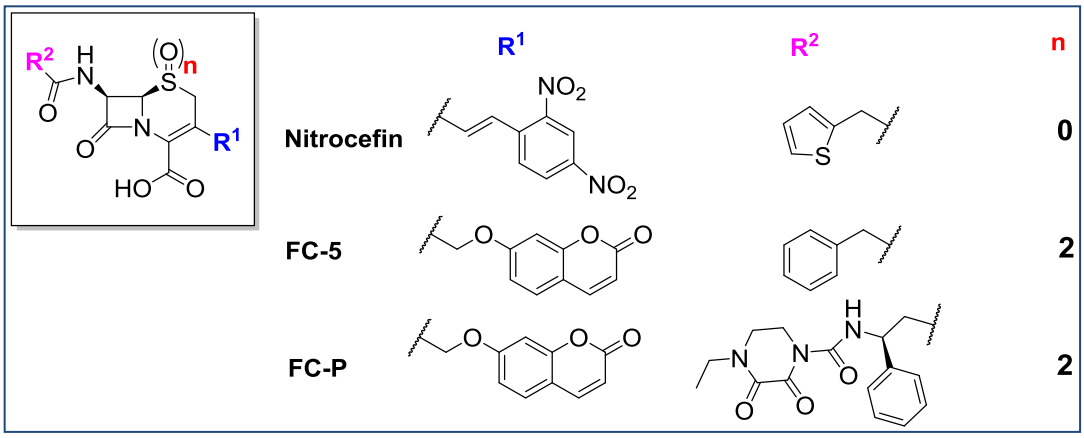
In the previously reported work, nitrocefin substrate/product inhibition was observed with NDM variants containing the M154L substitution (Chapter 3)[6]. Recently, nitrocefin analogues have also been shown to exhibit substrate/product inhibition of SPM-1 and, to a lesser extent, NDM-1[21]. Inhibition by nitrocefin has also been noted in S121G and F218Y mutants of IMP-1 but not in the wild type IMP-1[22]. Steady-state kinetic analyses were thus carried out to investigate the implications of the M154L substitution on the activity and inhibition of the NDM variants.

4.3.1 STEADY-STATE KINETIC ANALYSES

Kinetic parameters were determined for the hydrolysis of three cephalosporin substrates by the NDM variants as previously described (Chapters 2 and 3)[6,23]. The tested substrates included nitrocefin, and two coumarin-linked cephalosporin fluorogenic substrates, **FC-5** and **FC-P** (*Table 4-3*).

The kinetic parameters obtained in this study were in close agreement with the previously described results (Chapter 3)[6], particularly the k_{cat}/K_M values for NDM-5 and NDM-7 (*Table 4-3*). The K_M values for the hydrolysis of nitrocefin reported in this study were between 2 and 5 fold lower than the previously reported values. This difference is likely due to the differences in the enzyme constructs used and is probably within experimental error margins.

Table 4-3: **Kinetic parameters for the hydrolysis of tested cephalosporin substrates by full-length NDM variants.** ***The shaded row indicates variants inhibited by nitrocefin and respective K_i values. Measurements were carried out in triplicate; K_M values are given as the mean of three independent measurements ± standard deviation. Standard deviation values for k_{cat} and k_{cat}/K_M did not exceed 10 %.***



		NDM-1	NDM-4	NDM-5	V88L	NDM-7	D130N	NDM-12	G222D
Nitrocefin	K_M (µM)	2 ± 0.4	1 ± 0.1	2 ± 0.5	5 ± 0.9	2 ± 0.4	5 ± 1.2	1 ± 0.2	5 ± 0.9
	K_i (µM)	[a]ND	490 ± 200	350 ± 150	ND	370 ± 140	ND	ND	ND
	k_{cat} (s^{-1})	38	15	9	24	8	27	7	23
	k_{cat}/K_M ($s^{-1}µM^{-1}$)	19	15	5	5	4	5	7	4
Nitrocefin *	K_M (µM)	11 ± 2	4 ± 1	6 ± 1	[b]NR	5 ± 1	NR	NR	NR
	K_i (µM)	ND	102 ± 32	139 ± 28		79 ± 18			
	k_{cat} (s^{-1})	65	38	33		15			
	k_{cat}/K_M ($s^{-1}µM^{-1}$)	6	6	6		3			
FC-5	K_M (µM)	6 ± 0.7	18 ± 1.8	8 ± 0.9	1 ± 0.3	18 ± 1.4	6 ± 0.8	7 ± 0.5	6 ± 0.8
	k_{cat} (s^{-1})	570	1800	740	80	1320	410	460	390
	k_{cat}/K_M ($s^{-1}µM^{-1}$)	95	100	92	80	73	68	66	65
FC-P	K_M (µM)	10 ± 1.1	20 ± 0.9	11 ± 1.8	2 ± 0.3	18 ± 1.2	12 ± 1.1	34 ± 2.7	23 ± 2.3
	k_{cat} (s^{-1})	870	1650	320	110	1180	760	500	660
	k_{cat}/K_M ($s^{-1}µM^{-1}$)	87	83	29	55	66	63	15	29

[a]ND: Inhibition not detected; [b]NR: Data not reported in the previous study.

*Previously described values for nitrocefin hydrolysis by truncated (△42) NDM variants (Chapter 3)[6]

Consistent with previously described results (Chapter 3), NDM-4, NDM-5 and NDM-7 exhibited apparent inhibition by nitrocefin at a relatively high substrate concentration (Ki values >300 μM) (*Table 4-3*). Inhibition by nitrocefin was not observed for the single-mutants V88L, D130N and G222D. NDM-1 and NDM-4 manifested relatively higher k_{cat}/K_M values for nitrocefin hydrolysis compared to the other tested variants, an effect largely attributed to the elevated k_{cat} values. Despite the observed substrate/product inhibition for some of the variants, the tested NDM variants exhibited similar catalytic efficiencies for the hydrolysis of nitrocefin, with less than five-fold differences reported in k_{cat}/K_M values (*Table 4-3*).

In agreements with the results described by van Berkel *et al*[24], the two fluorogenic substrates were hydrolysed with high efficiencies by all the tested NDM variants, as judged by k_{cat}/K_M values (*Figure 4-3 A* and B). Interestingly, the single mutant V88L displayed a relatively low k_{cat} value for **FC-5**, (22 and 9 fold lower than for NDM-4 (M154L) and NDM-5 (V88L, M154L), respectively). This effect was balanced by a lower K_M value for the V88L variant, resulting in similar k_{cat}/K_M values for all the variants. The observed k_{cat}/K_M values for **FC-5** and **FC-P** remained similar across the tested NDM variants suggesting that altering the substituents on the cephalosporins' C7/amide side chain did not significantly affect the rate of hydrolysis (*Figure 4-3*).

Overall, the previously observed inhibition by nitrocefin of some, but not all, NDM variants has been validated by the kinetic analyses. However, the results do not reveal substantial differences in the hydrolysis of the tested cephalosporin substrates by the NDM variants.

Further investigations were thus carried out to explore the possible roles of the M154L substitution on the biophysical properties of the NDM variants.

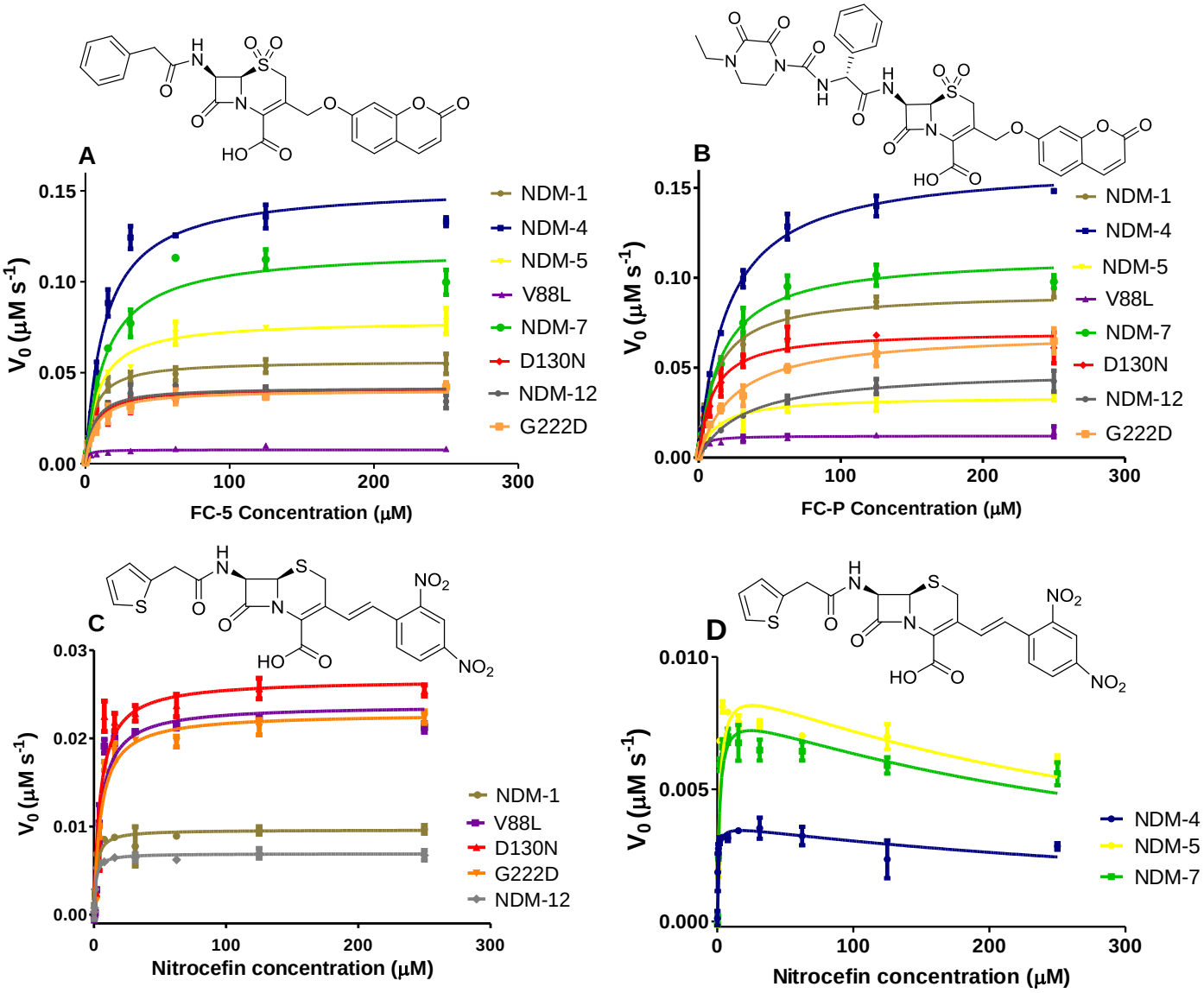


Figure 4-3: **Kinetic plots illustrating the hydrolysis of FC-5 (A), FC-P (B) and nitrocefin (C) and substrate/product inhibition of NDM variants by nitrocefin (D).**

4.4 CRYSTALLOGRAPHIC ANALYSES OF NDM VARIANTS

To further explore the roles of the NDM substitutions on the structural features of the enzymes, crystallographic analyses were carried out. Crystallisation broad screens employing an array of conditions were set up with the truncated constructs of the NDM variants (△42 NDMs, Chapter 3). Diffracting protein crystals were obtained for the different NDM variants, providing a series of structures for comparative analyses.

4.4.1 OVERALL STRUCTURAL PROPERTIES OF NDM VARIANTS

High resolution crystal structures (1.1 -2.1 Å) in different space groups were obtained for the NDM variants including NDM-3, NDM-4, NDM-5, NDM-6, and NDM-8 (PDB accession code: 4TZ9, 4TYF, 4TZE, 4TZB, 4TZF respectively). The crystallisation conditions and refinement data are outlined in *Table 4-4*.

Superimposition of the crystal structures of the NDM variants revealed similar overall folds (RMSD values over Cα atoms between 0.25 and 0.35 Å, relative to NDM-1) with the classical MBL αβ/βα sandwich fold being virtually identical to that of the previously reported structures of NDM-1 and other MBLs[25-27] (*Figure 4-8 A*). With the exception of NDM-3 and NDM-6, the NDM structures revealed two zinc (II) ions bound in the active site at a metal-metal distance of 3.5 Å, with the bridging water/hydroxide ion being 2.0 ± 0.1 Å and 2.1 ± 0.1 Å from Zn1 and Zn2 respectively (*Figure 4-8 B*). It has been proposed that the distance between the two zinc (II) ions in NDM structures is pH-dependent, with shorter distances being observed at higher pH[28]. In contrast to this proposal, the Zn1-Zn2 distance (3.5 Å) remained similar for NDM-5 and NDM-8 structures, which were crystallised at a pH of 7.5 and 5.5 respectively.

Table 4-4: **Crystallography data collection and refinement statistics of NDM variants.**

Data set	**NDM-3 (4TZ9)**	**NDM-4 (4TYF)**	**NDM-5 (4TZE)**	**NDM-6 (4TZB)**	**NDM-8 (4TZF)**
Crystallisation condition	Metal mix[#], 0.1M HEPES pH 7.5, 14% PEG 3350	10% PEG 1000, 10% PEG 8000	25% PEG 10000, 0.1 M HEPES pH 7.5	Metal mix[#], 0.1M HEPES, pH 7.5, 14% PEG 3350	0.1M Bis-Tris pH 5.5, 25% PEG 3350
Data collection					
Beamline	DLS I02	DLS I03	DLS I03	DLS I02	DLS I02
Resolution range (Å)	46.37-2.10 (2.10-2.18) *	41.33-1.10 (1.10-1.13) *	35-1.57 (1.57-1.63) *	50.00-2.05 (2.05-2.10) *	42.47-1.22 (1.22-1.25) *
Space group	*I*422	$P2_1$	$P2_1$	I422	$P2_12_12_1$
Unit cell dimensions					
a,b,c (Å)	121,121,90	42,59,42	54,59,63	120,120,89	41,58, 85
α,β,γ (°)	90,90,90	90,98,90	90,92,90	90,90,90	90,90,90
No. of molecules/ASU	1	1	2	1	1
No. of unique reflections	18919	80791	51507	21307	61432
Completeness (%)	91.6 (88.3)*	98.8 (96.4)*	99.5 (99.6)*	100 (100)*	99.7 (99.6)*
Redundancy	6.5 (5.8)*	4.3 (3.9)*	10.5 (8.1)*	10.6 (10.5)*	6.2 (6.1)*
R_{merge}	0.217	0.676	0.087	0.162	0.065
Mean I/σ(I)	6.12 (1.5)*	13.8 (1.8)*	9.48 (2.5)*	10.0 (3.1)*	13.4 (2.4)*
Wilson B value ($Å^2$)	36.74	13.85	16.10	34.17	9.128
Refinement					
R_{factor}	0.2286	0.1503	0.1949	0.1771	0.1517
R_{free}	0.2485	0.1735	0.2343	0.2063	0.1778
RMSD					
Bond length (Å)	0.007	0.017	0.015	0.016	0.015
Bond angle (°)	0.74	1.674	1.566	1.286	1.594
No. of atoms	1859	2007	3815	1916	2076
Protein	1695	1736	3362	1696	1688
Solvent	120	271	269	164	287
$<B_{factor}>$ ($Å^2$)					
Protein	36.8	18.3	22.2	37.1	18.4
Solvent	37.5	31.0	26.8	45.6	32.8

[#] 0.008 M $CdCl_2$, $NiCl_2$, $MgCl_2$, $CoCl_2$; *Numbers in parentheses refer to the highest resolution shell. R_{merge} is the unweighted R-value on I between merged reflections.

The NDM-3 and NDM-6 structures appeared to contain a cadmium (II) ion in the second metal site (3.6 Å from Zn1). The presence of cadmium in the second site was likely due to presence of different metal ions in the crystallization conditions (*Table 4-4*) and has been previously reported for NDM-1 crystal structures obtained using similar conditions (PDB code 3ZR9)[29].

Despite the differences in the bound metal ions, the active site metal coordination remained consistent for all of the NDM variants with the H120, H122, H189 triad and D124, C208 and H250 coordinating the first and the second metal centers respectively (*Figure 4-8 B*). The flexible active site loops, loop 3 and loop 10, proposed to be involved in substrate interactions[28,29], were similarly oriented in the NDM structures, apart from a slight shift of loop 3 away from the active site observed in the NDM-3 and NDM-6 structures (*Figure 4-8 A*). This effect may be caused by differences in crystal packing.

As previously stated, the substitutions on the NDM variants are all located away from the active site and, as expected, they did not cause major perturbations in the overall structures of the variants (*Figure 4-8 C*). Notably, a shift in the position of the loop containing A149-H159 (Loop 8) was observed in the structures of NDM-3 and NDM-6 relative to the NDM-4, NDM-5 and NDM-8 structures (*Figure 4-8 D*). In the case of NDM-3 and NDM-6, the presence of cadmium (II) ion in the active site and the differences in crystal packing could, in part, account for the observed differences. However, since this shift is also observed in the di-zinc NDM-1 structures (4EYL)[30], it seems more likely that the M154L substitution is responsible for the observed movement of loop 8. The shift of loop 8 towards the active site in the NDM-3 and NDM-6 structures results in a shorter interaction distance between the carboxyl oxygen of E152 and the Nε2 of the imidazole moiety of the metal-binding residue H122, (from 5.2 Å in NDM-5 to 3.9 Å and 3.8 Å in NDM-3 and NDM-6, respectively). Although there is, as yet, no evidence for other residues in loop 8 affecting the substrate profiles of NDMs (except M154), the interaction between E152 and H122 merits further investigation.

In agreement with proposals from other studies[5] and the hypothesis made in Chapter 3, the Sδ of the M154 is positioned in close proximity to the carboxyl oxygen of the zinc binding residue H122 (4.6 Å), suggesting that it may have an impact the metal binding site structure by influencing the flexibility of H122 (*Figure 4-8 D*). Previous studies on SPM-1 and Bc-II MBLs have indicated that substitutions second sphere residues (residues that share hydrogen bonding network spanning below the active site) can influence the plasticity of the metal center[18,19,31].

Interestingly, the M154 residue is replaced by similarly hydrophobic but significantly smaller residues, including valine in NDM-11 and leucine in close to half of the reported NDM variants (*Table 4-1*). It was previously postulated (Chapter 3) that the proximity of M154 to hydrophobic substituents of β-lactam substrates may play a role in substrate recognition and/or the expulsion of hydrolysed products from the active site. The M154L substitution is therefore likely to interfere with this interaction, possibly contributing to the observed inhibition by nitrocefin.

The crystallographic analyses of the NDM variants thus reveal similar overall structural properties of the enzymes but also point to interesting interactions of the residues in loop 8 (A149-H159) with the zinc binding residue H122. It would therefore be desirable to further investigate differences in metal binding affinities of the NDM variants and the subsequent effects on the substrate profile of NDM variants, with respect to substitutions on loop 8 residues.

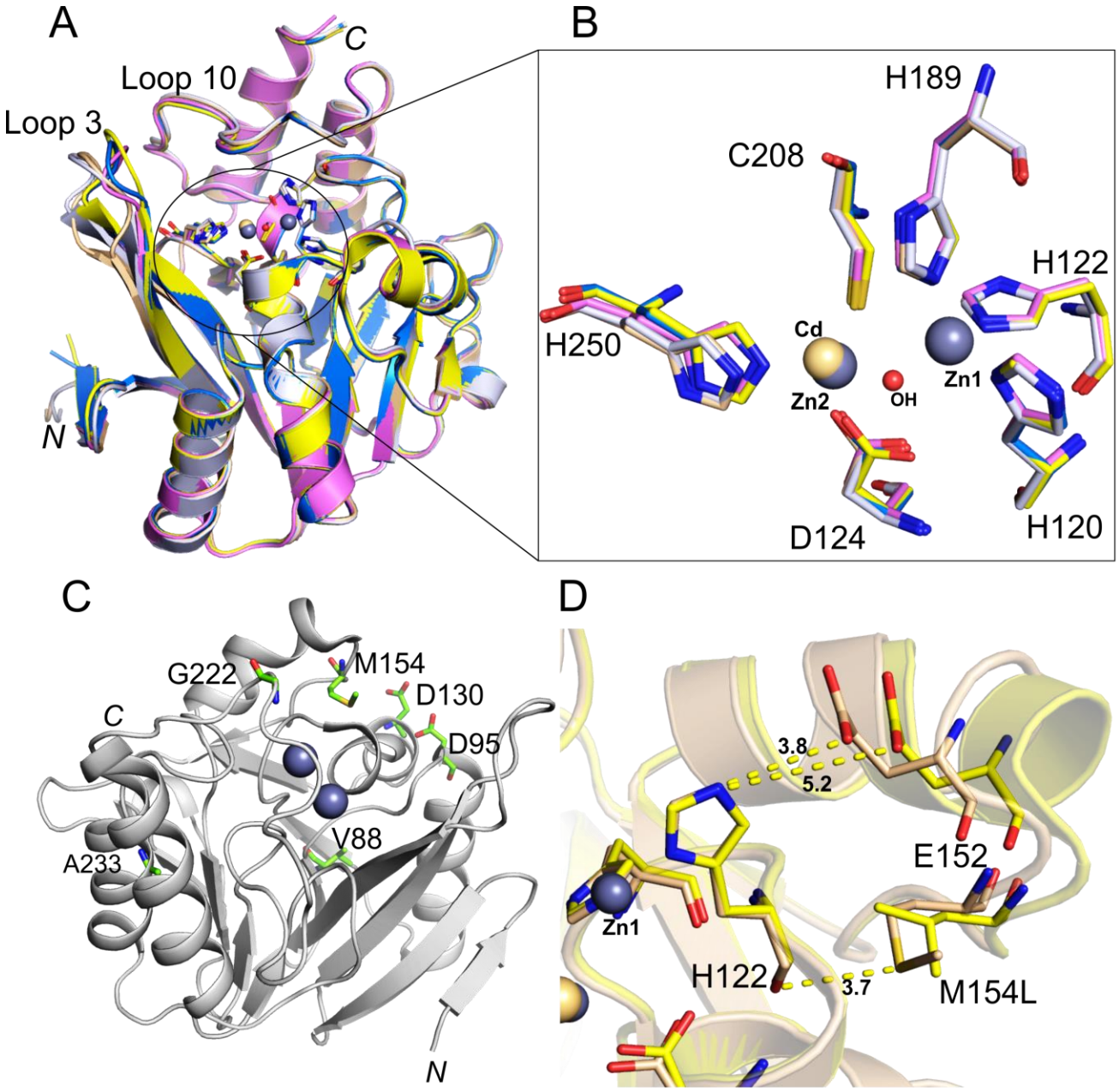


Figure 4-8: **A) Overlay of ribbon representations of NDM-3 (light blue), NDM-4 (dark blue), NDM-5 (yellow), NDM-6 (wheat) and NDM-8 (magenta) showing the similar overall folds of the enzymes. B) Close-up view of the active site co-ordination in the NDM structures with Cd(II) ion bound in the second site for NDM-3 and NDM-6. C) View of NDM-1 structure[30] indicating the positions of the observed substitutions. D) Close-up view of the interactions of E152 and M154 with the metal binding residue H122 in NDM-5 and NDM-6.**

4.5 M154L SUBSTITUTION INFLUENCE ON STABILITY OF NDM VARIANTS

Having observed increased thermal stability of the doubly substituted NDM variants (NDM-5, NDM-7 and NDM-8) previously (Chapter 3)[6], studies were undertaken to investigate whether the stability of the enzymes was influenced by the residue at position 154. It was particularly desirable to compare the stability profiles of the full-length NDM variants, since the previous analyses were performed with truncated NDM constructs (△42 NDMs), which are optimised for protein stability and solubility[32].

The stability of purified NDM variants to thermal denaturation was assessed using Circular Dichroism (CD) and Differential Scanning Calorimetry (DSC). Preliminary investigations were also carried out using a newly developed cell-based thermal shift assay (CETSA).

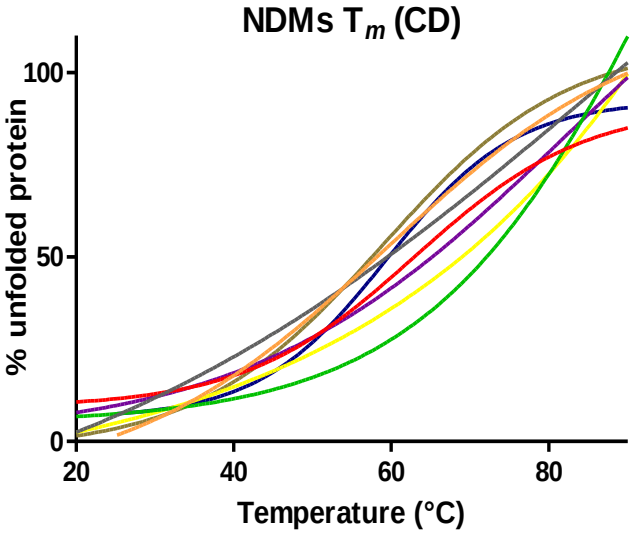
4.5.1 CIRCULAR DICHROISM ANALYSES (CD)

To validate the previous results and compare the stabilities of the singly and doubly substituted NDM variants, CD analyses were carried out as previously described in Chapter 3. The temperature dependence of protein secondary structures was assessed by monitoring the CD signal at 222 nm at increasing temperatures (20 - 90 °C). The baseline-corrected and normalised CD data was then fitted to a Boltzmann sigmoidal curve using GraphPad Prism software to obtain the melting temperature (T_m) values (*Figure 4-4*).

In agreement with the earlier study (Chapter 3), the full-length NDM-1 and NDM-4 (M154L) variants exhibited considerably low T_m values (59 °C). The single-mutants G222D and D130N manifested similar T_m values as NDM-1 and NDM-4 (M154L).

Surprisingly, the T_m value of the V88L variant was > 20 °C higher than that of NDM-1 (*Figure 4-4*). The doubly substituted variants NDM-5 (V88L, M154L), NDM-7 (D130N, M154L) and NDM-12 (M154L, G222D) were the most stable variants, with apparent T_m values around 90 °C. It should be noted that apparent T_m values were reported for NDM-5 and NDM-7, since the thermal denaturation plots did not plateau at the highest temperature recorded (90 °C).

Overall, the CD analyses revealed substantial differences in the melting temperatures of the NDM variants (> 20 °C), while maintaining a similar trend as previously described (Chapter 3)[6]. To verify the CD results and counter the limitations of the CD temperature ranges, further analyses were carried out using Dynamic Scanning Calorimetry.



Variant	T_m (°C)	*T_m (°C)
NDM-1	59 ± 0.7	60 ± 0.1
NDM-4	59 ± 1.0	61 ± 0.2
NDM-5	> 90	65 ± 0.3
V88L	82 ± 11	-
NDM-7	>90	65 ± 0.2
D130N	63 ± 2.7	-
NDM-12	89 ± 11	-
G222D	59 ± 1.2	-

Figure 4-4: **Thermal denaturation profiles and corresponding T_m values of the full length NDM variants as determined by CD analyses, showing the differences in thermal stabilities of the variants.* T_m values of the truncated △42 NDM variants as described in Chapter 3.**

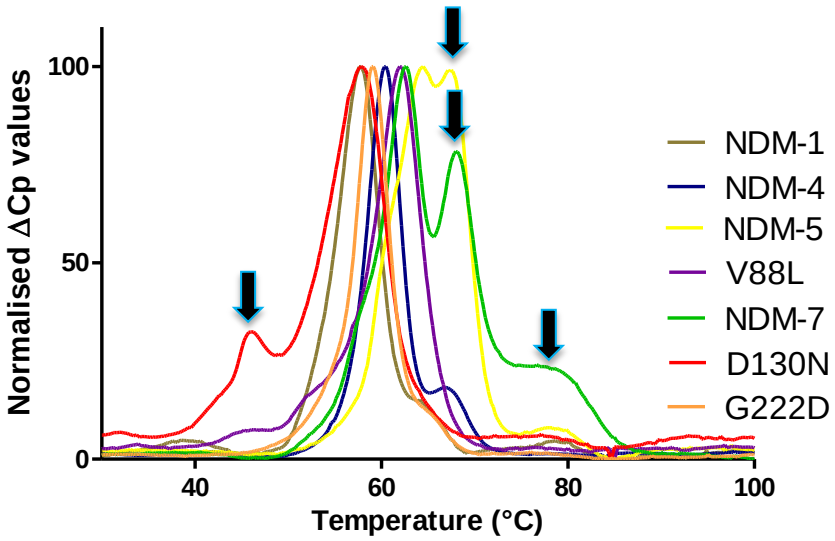
4.5.2 DYNAMIC SCANNING CALORIMETRIC ANALYSES

Unlike CD and DSF techniques, DSC is advantageous in that the analyses do not rely on changes in spectroscopic signals. In addition to the ability to collect data at higher temperatures (up to 130 °C), the DSC technique provides a direct measure of the heat absorption associated with the unfolding process and is therefore more capable of resolving multiple unfolding transitions[33].

The unfolding of NDM variants was thus monitored using a Malvern VP Capillary DSC system equipped with a 96 well plate auto-sampler. The temperature-induced changes in the heat capacity of the proteins (ΔCp) was recorded in the 15 - 105 °C temperature range at a scan rate of 1 °C per minute, with 50 mM Tris (pH 7.5), 200 mM NaCl buffer as the reference. Changes in protein heat capacity (ΔCp) was obtained by subtracting a scan of a buffer blank (buffer/buffer runs) from the scan of the sample (protein/buffer runs) before analysis. The data was analysed in GraphPad Prism software with the transition midpoint indicating the apparent protein melting temperatures (T_m).

The DSC results were in close agreement with the data obtained from CD analyses, although the differences in T_m values were not as dramatic (*Figure 4-5*). NDM-1 and the singly substituted variants NDM-4, G22D and D130N displayed similarly low T_m values (58 - 59 °C) while the V88L variant had a slightly higher T_m value of 62 °C. NDM-5 and NDM-7 were the more stable enzymes with the apparent T_m values of 65 °C and 63 °C respectively, obtained from the main peaks of the thermograms.

The increased thermal stability of the doubly substituted variants (NDM-5 and NDM-7) is consistent with the CD results. With the exception of V88L, all the single substitutions including M154L (as in NDM-4) do not seem to affect the stability of the enzymes relative to NDM-1. It is therefore likely that the elevated stability is induced by a synergy arising from two or more substitutions.



Variant	T_m (°C)
NDM-1	58
NDM-4	61
NDM-5	65, 67
V88L	62
NDM-7	63, 67, 78
D130N	47, 58
G222D	59

Figure 4-5: **Normalised and baseline-subtracted thermograms of the NDM variants and the respective T_m values from the midpoints of the transitions. The black arrows point to the 'shoulder peaks' of the thermograms and the corresponding T_m values shown in red.**

Interestingly, the thermograms of D130N, NDM-5 and NDM-7 variants manifested more than one endothermic heat absorption peak, corresponding to different melting temperature values (*Figure 5-7*). This observation suggests that the thermal unfolding of these variants may proceed via a relatively stable intermediate, although heat-induced protein aggregation and/or oligomerization cannot be ruled out[34,35]. The 'shoulder peaks' observed with NDM-5 and NDM-7 corresponded to T_m values of 67 °C and 78 °C respectively, suggesting that the thermal unfolding of these full-length NDM variants may proceed via several overlapping stages over a range of temperatures[34,36].

4.5.3 CELLULAR THERMAL SHIFT ASSAYS (CETSA)

To investigate whether the observed thermal stability differences are biologically relevant, a cell-based assay was developed to assess the susceptibility of NDM variants to thermal denaturation in cells. The western blot-based thermal stability assay was adapted from a previously reported protocol using mammalian cells[37,38]. The technique relies on the principle that heat-induced unfolding should lead to protein precipitation; hence the amount of soluble protein should correlate with the amount of residual folded protein. The amount of soluble protein at each temperature is quantified and the CETSA melting curves obtained by plotting the amount of soluble protein against the temperature[39,40].

E. coli BL21 DE3 (pLysS) cells expressing NDM-1, NDM-7 and NDM-12 were cultured in 2TY media at 37 °C for 3 hours before induction with 0.5 mM IPTG (the rhodanine inhibitor ML302[41] was added at induction time as a control). The cells were grown for a further 4 hours and harvested by centrifugation. The cell pellets were re-suspended in the media and divided into 12 aliquots, which were heated at different temperatures for 3 minutes (37 - 90 °C). The cells were lysed; the cell-debris and precipitated proteins were separated by ultracentrifugation. Standard western blotting was then carried out (Chapter 7.4) using anti-NDM-1 as the primary antibody. The protein bands were visualised using the LI-COR Odyssey CLx imaging system and the band intensity quantified using Image Studio Version 3:1 software. The temperature-induced aggregation curves were fitted in GraphPad Prism to obtain apparent T_m (or more accurately T_{agg}) values (*Figure 4-6*).

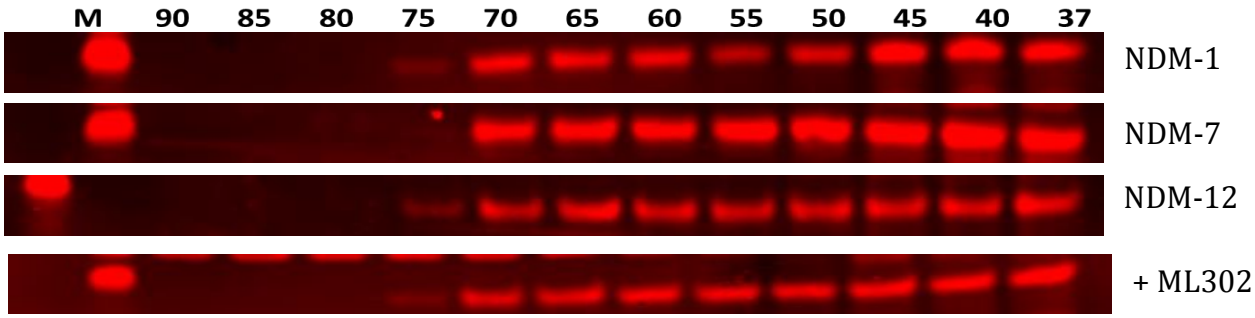
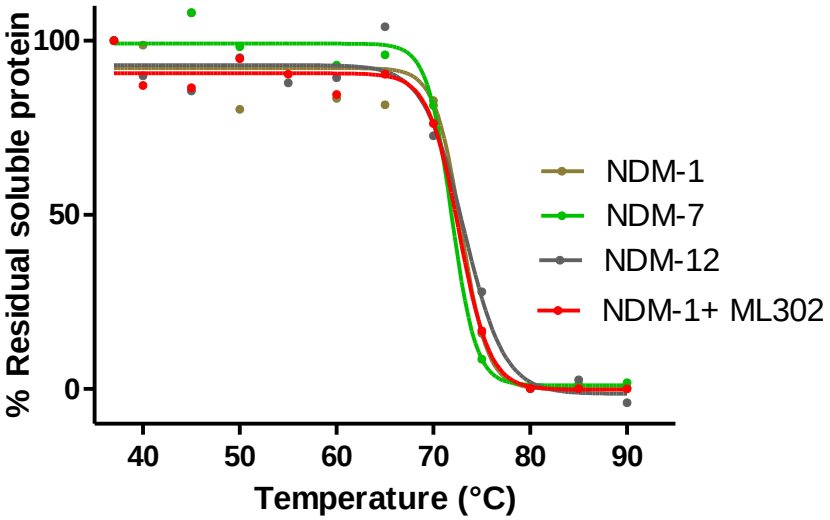


Figure 4-6: **Comparison of band intensities of NDM variants at different temperatures.**

The doubly substituted variants, NDM-7 and NDM-12, which exhibited considerably higher in T_m values in comparison to NDM-1 were selected for comparative analyses of the cellular thermal stabilities. The preliminary results from CETSA analyses revealed a similar thermal stability profile for the tested NDM variants with apparent T_m values ranging between 71-73 °C (*Figure 4-7*). The presence of the rhodanine inhibitor ML302 did not induce a substantial stabilisation of NDM-1; similar T_m values were obtained for the inhibitor control (73 °C). The lack of observed stabilization may be the consequence of off-target binding of the inhibitor due to the promiscuity of rhodanine inhibitors[41,42]. It is also possible that the incubation time was not sufficient for significant protein-inhibitor interaction.

Due to the complexity of the cellular environment, the protein unfolding and precipitation are not completely independent of other processes such as molecular crowding and interactions with several chaperone systems[43,44]. Therefore, although the differences observed with the purified proteins do not seem to cause major perturbations in a cellular context, further optimization of the assay will be necessary in order to obtain more conclusive results.



Variant	T_m (°C)
NDM-1	72 ± 0.9
NDM-7	71 ± 0.5
NDM-12	73 ± 0.7
NDM-1 + ML302	73 ± 0.5

Figure 4-7: **CETSA melting curves obtained from band intensities (normalized to the intensity at 37 °C) and the corresponding apparent T_m values, showing similar cellular thermal stabilities of the NDM variants.**

Table 4-5: **Comparison of melting temperatures (T_m) of NDM variants obtained using different techniques showing a similar trend in thermal stability of the variants**

Variant	CD	DSC	CETSA
NDM-1	59 ± 0.7	58	72 ± 0.9
NDM-4	59 ± 1.0	61	*NR
NDM-5	> 90	65, 67	NR
V88L	82 ± 11	62	NR
NDM-7	>90	63, 67, 78	71 ± 0.5
D130N	63 ± 2.7	47, 58	NR
NDM-12	89 ± 11	NR	73 ± 0.7
G222D	59 ± 1.2	59	NR

*NR: Not reported; The DSC T_m values from the shoulder peaks are indicated in red

4.6 SUMMARY

In agreement with the results for the comparison of the hydrolytic activities of NDM variants obtained in Chapter 3, the kinetic analyses in the study do not demonstrate significant differences in the catalytic efficiency of the NDM variants with the tested cephalosporin substrates (nitrocefin, FC-5 and FC-P; *Table 4-3*). Although inhibition by nitrocefin is observed, the reported K_i values are higher than the previously reported values (Chapter 3)[6]. This could be a reflection of differences in the NDM constructs used in the analyses. Despite the similarities in kinetic parameters, further analyses with different classes of β-lactam antibiotics would be necessary before ruling out the involvement of the M154L substitution in altering substrate selectivity of NDM variants.

Crystallographic analyses revealed the relatively close positioning of M154 with respect to the active site metal center. Due to the stringent control of metal content in the periplasmic space, it has been suggested that higher zinc affinity confers a selective advantage during the evolution of MBLs[1,45]. The influence of the residue the position 154 on the zinc binding H122, and its possible implication on the metal binding affinities of NDM variants thus presents an interesting possible future line of investigation.

The thermal stabilities profiles obtained with purified NDM variants indicates an improved protein stability for the doubly substituted variants NDM-5, NDM-7 and NDM-12, as previously described in Chapter 3. Interestingly, the frequently observed M154L substitution in isolation did not significantly affect the susceptibility of the NDM variants to thermal denaturation as indicated by the nearly identical thermal stabilities of NDM-1 and NDM-4 (*Table 4-5*).

The singly substituted variants D130N and G222D manifested T_m values closer to the wild-type NDM-1 suggesting the elevated stability was not dependent on a single substitution but rather induced by the interaction of two or more substitutions. In light of the persistence of the M154L substitution in the recently identified NDM variants, NDM-13 (D95N, M154L) and NDM-15 (M154L, A233V), it would be of interest to further investigate the relevance of the M154L substitution in a physiologically relevant context.

Although the thermal stability analyses in cells did not yield conclusive results, the work described in this and the preceding chapter supports the proposal that protein stability may, in part, influence the evolution of MBLs and particularly NDM variants.β

4.7 REFERENCES

1. Tomatis PE, Fabiane SM, Simona F, Carloni P, Sutton BJ, Vila AJ. Adaptive protein evolution grants organismal fitness by improving catalysis and flexibility. *Proc Natl Acad Sci U S A*. 2008;105(52):20605-20610..

2. Pal A, Tripathi A. An *in silico* approach for understanding the molecular evolution of clinically important metallo-β-lactamases. *Infect Genet Evol*. 2013;20C:39-47.

3. Sun S, Zhang W, Mannervik B, Andersson DI. Evolution of broad spectrum β-lactam resistance in an engineered metallo-beta-lactamase. *J Biol Chem*. 2013;288(4):2314-2324.

4. Widmann M, Pleiss J, Oelschlaeger P. Systematic analysis of metallo-β-lactamases using an automated database. *Antimicrob Agents Chemother*. 2012;56(7):3481-3491.

5. Meini MR, Llarrull LI, Vila AJ. Evolution of metallo-β-lactamases: Trends revealed by natural diversity and evolution. *Antibiotics (Basel)*. 2014;3(3):285-316.

6. Makena A, Brem J, Pfeffer I, et al. Biochemical characterization of New Delhi metallo-β-lactamase variants reveals differences in protein stability. *J Antimicrob Chemother*. 2015;70(2):463-469.

7. Kaase M, Nordmann P, Wichelhaus TA, Gatermann SG, Bonnin RA, Poirel L. NDM-2 carbapenemase in *Acinetobacter baumannii* from Egypt. *J Antimicrob Chemother*. 2011;66(6):1260-1262.

8. Hornsey M, Phee L, Wareham DW. A novel variant, NDM-5, of the New Delhi metallo-β-lactamase in a multidrug-resistant *Escherichia coli* ST648 isolate recovered from a patient in the United Kingdom. *Antimicrob Agents Chemother*. 2011;55(12):5952-5954.

9. Rogers BA, Sidjabat HE, Silvey A, et al. Treatment options for New Delhi metallo-β-lactamase-harboring *Enterobacteriaceae*. *Microb Drug Resist*. 2013;19:100-103.

10. Göttig S, Hamprecht AG, Christ S, Kempf VA, Wichelhaus TA. Detection of NDM-7 in Germany, a new variant of the New Delhi metallo-β-lactamase with increased carbapenemase activity. *J Antimicrob Chemother*. 2013;68(8):1737-1740.

11. Nordmann P, Boulanger AE, Poirel L. NDM-4 metallo-β-lactamase with increased carbapenemase activity from *Escherichia coli*. *Antimicrob Agents Chemother*. 2012;56(4):2184-2186.

12. Tada T, Miyoshi-Akiyama T, Dahal RK, et al. NDM-8 metallo-β-lactamase in a multidrug-resistant *Escherichia coli* strain isolated in Nepal. *Antimicrob Agents Chemother*. 2013;57(5):2394-2396.

13. Williamson DA, Sidjabat HE, Freeman JT, et al. Identification and molecular characterisation of New Delhi metallo-β-lactamase-1 (NDM-1)- and NDM-6-producing *Enterobacteriaceae* from New Zealand hospitals. *Int J Antimicrob Agents*. 2012;39(6):529-533.

14. Wang X, Li H, Zhao C, et al. Novel NDM-9 metallo-β-lactamase identified from a ST107 *Klebsiella pneumoniae* strain isolated in China. *Int J Antimicrob Agents*. 2014;44(1):90-91.

15. Tada T, Shrestha B, Miyoshi-Akiyama T, et al. NDM-12, a novel New Delhi metallo-β-lactamase variant from a carbapenem-resistant *Escherichia coli* clinical isolate in Nepal. *Antimicrob Agents Chemother*. 2014;58(10):6302-6305.

16. Shrestha B, Tada T, Miyoshi-Akiyama T, et al. Identification of a novel NDM variant, NDM-13, from a multidrug-resistant *Escherichia coli* clinical isolate in Nepal. *Antimicrob Agents Chemother*. 2015;59(9):5847-5850.

17. Zou D, Huang Y, Zhao X, et al. A novel New Delhi metallo-β-lactamase variant, NDM-14, isolated in a Chinese hospital possesses increased enzymatic activity against carbapenems. *Antimicrob Agents Chemother*. 2015;59(4):2450-2453.

18. Tomatis PE, Rasia RM, Segovia L, Vila AJ. Mimicking natural evolution in metallo-β-lactamases through second-shell ligand mutations. *Proc Natl Acad Sci U S A*. 2005;102(39):13761-13766.

19. Gonzalez LJ, Moreno DM, Bonomo RA, Vila AJ. Host-specific enzyme-substrate interactions in SPM-1 metallo-β-lactamase are modulated by second sphere residues. *PLoS Pathog*. 2014;10(1):e1003817.

20. Skagseth S, Carlsen TJ, Bjerga GE, Spencer J, Samuelsen O, Leiros HK. Role of residues W228 and Y233 in the structure and activity of metallo-β-lactamase GIM-1. *Antimicrob Agents Chemother*. 2015;60(2):990-1002.

21. Ghavami A, Labbe G, Brem J, et al. Assay for drug discovery: Synthesis and testing of nitrocefin analogues for use as β-lactamase substrates. *Anal Biochem*. 2015;486:75-77.

22. Oelschlaeger P, Mayo SL, Pleiss J. Impact of remote mutations on metallo-β-lactamase substrate specificity: Implications for the evolution of antibiotic resistance. *Protein Sci*. 2005;14(3):765-774.

23. Viswanatha T, Marrone L, Goodfellow V, Dmitrienko GI. Assays for β-lactamase activity and inhibition. *Methods Mol Med*. 2008;142:239-260.

24. van Berkel SS, Brem J, Rydzik AM, et al. Assay platform for clinically relevant metallo-β-lactamases. *J Med Chem*. 2013;56(17):6945-6953.

25. Zhang H, Hao Q. Crystal structure of NDM-1 reveals a common β-lactam hydrolysis mechanism. *FASEB J*. 2011;25:2574-2582.

26. King D, Strynadka N. Crystal structure of New Delhi metallo-β-lactamase reveals molecular basis for antibiotic resistance. *Protein Sci*. 2011;20:1484-1491.

27. Palzkill T. Metallo-β-lactamase structure and function. *Ann N Y Acad Sci*. 2013;1277:91-104.

28. Kim Y, Cunningham MA, Mire J, Tesar C, Sacchettini J, Joachimiak A. NDM-1, the ultimate promiscuous enzyme: Substrate recognition and catalytic mechanism. *FASEB J*. 2013;27(5):1917-1927.

29. Green VL, Verma A, Owens RJ, Phillips SE, Carr SB. Structure of New Delhi metallo-β-lactamase 1 (NDM-1). *Acta Crystallogr Sect F Struct Biol Cryst Commun*. 2011;67:1160-1164.

30. King DT, Worrall LJ, Gruninger R, Strynadka NC. New Delhi metallo-β-lactamase: Structural insights into β-lactam recognition and inhibition. *J Am Chem Soc*. 2012;134:11362-11365.

31. Murphy TA, Catto LE, Halford SE, et al. Crystal structure of *Pseudomonas aeruginosa* SPM-1 provides insights into variable zinc affinity of metallo-β-lactamases. *J Mol Biol*. 2006;357(3):890-903.

32. Kim Y, Tesar C, Mire J, et al. Structure of apo- and monometalated forms of NDM-1--a highly potent carbapenem-hydrolyzing metallo-β-lactamase. *PLoS One*. 2011;6:e24621.

33. Freire E. Differential scanning calorimetry. *Methods Mol Biol*. 1995;40:191-218.

34. Fan DJ, Ding YW, Pan XM, Zhou JM. Thermal unfolding of *Escherichia coli* trigger factor studied by ultra-sensitive differential scanning calorimetry. *Biochim Biophys Acta*. 2008;1784(11):1728-1734.

35. Johnson CM. Differential scanning calorimetry as a tool for protein folding and stability. *Arch Biochem Biophys*. 2013;531(1-2):100-109.

36. Ibarra-Molero B, Naganathan AN, Sanchez-Ruiz JM, Munoz V. Modern analysis of protein folding by differential scanning calorimetry. *Methods Enzymol*. 2016;567:281-318.

37. Martinez Molina D, Jafari R, Ignatushchenko M, et al. Monitoring drug target engagement in cells and tissues using the cellular thermal shift assay. *Science*. 2013;341(6141):84-87.

38. Jafari R, Almqvist H, Axelsson H, et al. The cellular thermal shift assay for evaluating drug target interactions in cells. *Nat Protoc*. 2014;9(9):2100-2122.

39. Jensen AJ, Martinez Molina D, Lundback T. CETSA: A target engagement assay with potential to transform drug discovery. *Future Med Chem*. 2015;7(8):975-978.

40. Martinez Molina D, Nordlund P. The cellular thermal shift assay: A novel biophysical assay for in situ drug target engagement and mechanistic biomarker studies. *Annu Rev Pharmacol Toxicol*. 2016;56:141-161.

41. Brem J, van Berkel SS, Aik W, et al. Rhodanine hydrolysis leads to potent thioenolate mediated metallo-β-lactamase inhibition. *Nat Chem*. 2014;6(12):1084-1090.

42. Mendgen T, Steuer C, Klein CD. Privileged scaffolds or promiscuous binders: A comparative study on rhodanines and related heterocycles in medicinal chemistry. *J Med Chem*. 2012;55(2):743-753.

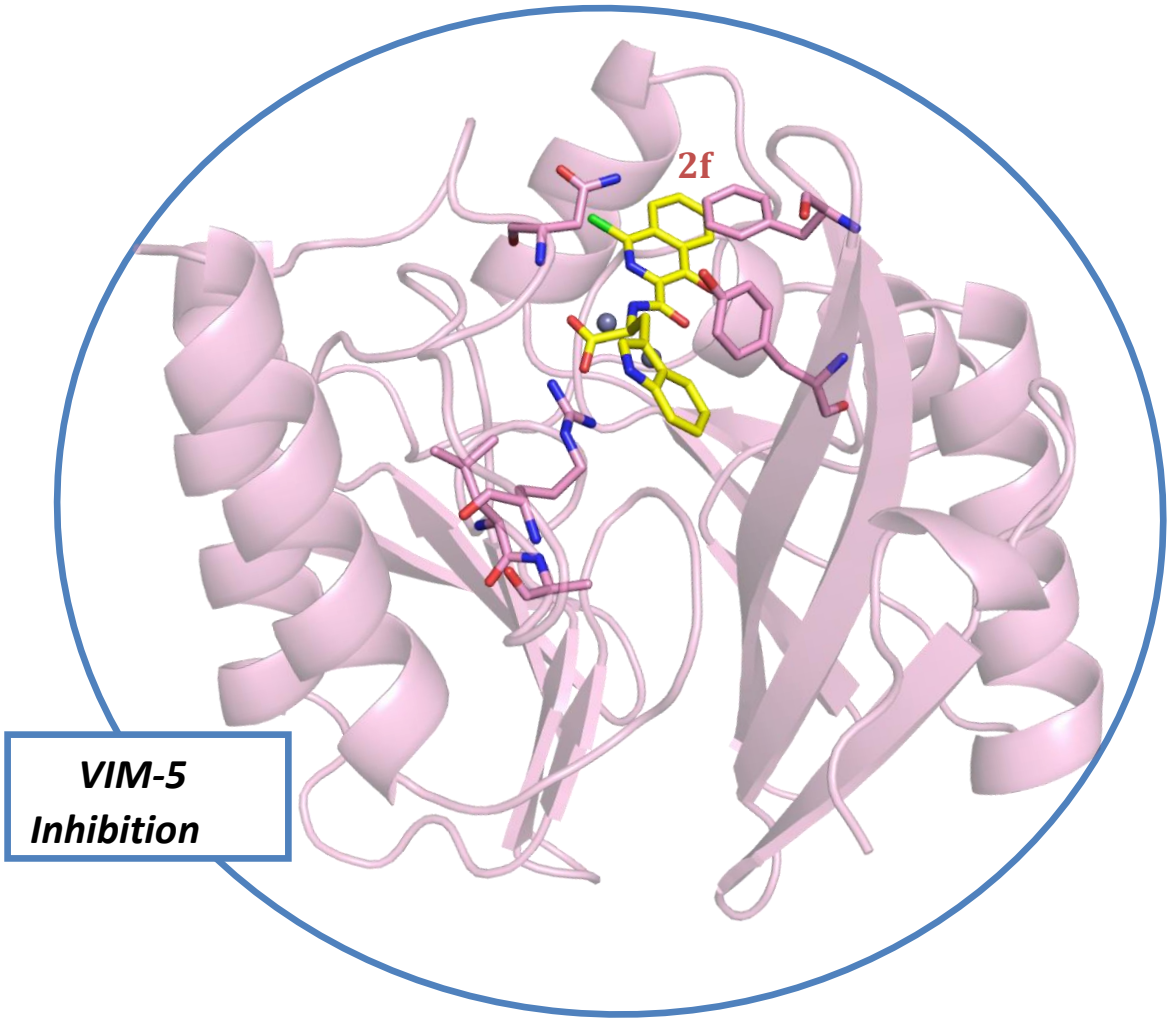
43. Mourao MA, Hakim JB, Schnell S. Connecting the dots: The effects of macromolecular crowding on cell physiology. *Biophys J*. 2014;107(12):2761-2766.

44. Muga A, Moro F. Thermal adaptation of heat shock proteins. *Curr Protein Pept Sci*. 2008;9(6):552-566.

45. Gonzalez JM, Meini MR, Tomatis PE, Medrano Martin FJ, Cricco JA, Vila AJ. Metallo-β-lactamases withstand low zn(II) conditions by tuning metal-ligand interactions. *Nat Chem Biol*. 2012;8(8):698-700.

CHAPTER 5: COMPARISON OF STABILITY AND INHIBITION PROFILES OF VERONA INTEGRON-BORNE METALLO-β-LACTAMASE (VIM) VARIANTS

The Verona integron-borne metallo-β-lactamases (VIM) enzymes are among the most widely distributed MBLs and constitute one of the largest groups of B1 MBLs, with > 40 reported variants. Limited information is available on the structural and biochemical properties of VIM enzymes, even with increasing clinical reports of VIM variants. In addition, the implications of the rapid evolution of MBLs on inhibitor development have not been addressed. The work described in this chapter thus compares the hydrolytic activities, thermal stability and inhibition profiles of five clinically relevant VIM variants. Structural analyses of VIM-5 are also reported, which provide insights into the observed differences in inhibition.



CONTENTS

CHAPTER 5: COMPARISON OF STABILITY AND INHIBITION PROFILES OF VERONA INTEGRON-BORNE METALLO-β-LACTAMASE (VIM) VARIANTS 160

5.1 INTRODUCTION 162

5.1.1 Evolution and Biochemistry of VIM variants 162

5.1.2 Chapter Objectives 165

5.2 PRODUCTION AND PURIFICATION OF RECOMBINANT VIM VARIANTS 166

5.2.1 Cloning and Mutagenesis 166

5.2.2 Protein production and purification 167

5.2.3 Mass spectrometric analyses 167

5.3 FUNCTIONAL ANALYSES OF VIM VARIANTS 169

5.3.1 Steady-state kinetic analyses 169

5.4 INHIBITION PROFILES OF VIM VARIANTS 174

5.4.1 Determination of residual activities 174

5.4.2 Differential inhibition of VIM variants 176

5.5 BIOPHYSICAL CHARACTERISATION 178

5.5.1 Structural properties of VIM-5 178

5.5.2 Investigation of thermal stability 179

5.5.3 Crystallographic Analyses of VIM-5 181

5.6 SUMMARY 186

5.7 REFERENCES 187

5.1 INTRODUCTION

The first enzyme of the Verona integron-borne metallo-β-lactamase (VIM-1) was isolated from a carbapenem resistant *Pseudomonas aeruginosa* clinical isolate from an Italian patient in 1997[1]. The gene encoding VIM-1 (bla_{VIM-1}) was carried on a mobile gene cassette inserted into a class 1 integron; the expression of bla_{VIM-1} in *E. coli* cells resulted in a significant decrease in the *in vitro* susceptibility of the cells to a broad array of β-lactam antibiotics[1]. Subsequent biochemical studies revealed the broad substrate profile of VIM-1[2,3], including for penicillins, cephalosporins, carbapenems and mechanism-based serine-β-lactamase inactivators. The second VIM variant to be reported, VIM-2, was in fact, isolated earlier than VIM-1 in France (1996) [4] and later in Italy[5], from a *Pseudomonas aeruginosa* clinical isolate in both cases. VIM-2 is currently the most dominant of the VIM variants in terms of clinical prevalence, with cases being reported in five continents[6,7]. Presently, the VIM enzymes constitute the second largest group of the B1 MBLs with 46 variants reported worldwide (http://www.lahey.org/Studies/other.asp). The VIM variants exhibit wide variation in reported hydrolytic activity conferring varied antibiotic susceptibility profiles to VIM-bearing bacteria.

5.1.1 EVOLUTION AND BIOCHEMISTRY OF VIM VARIANTS

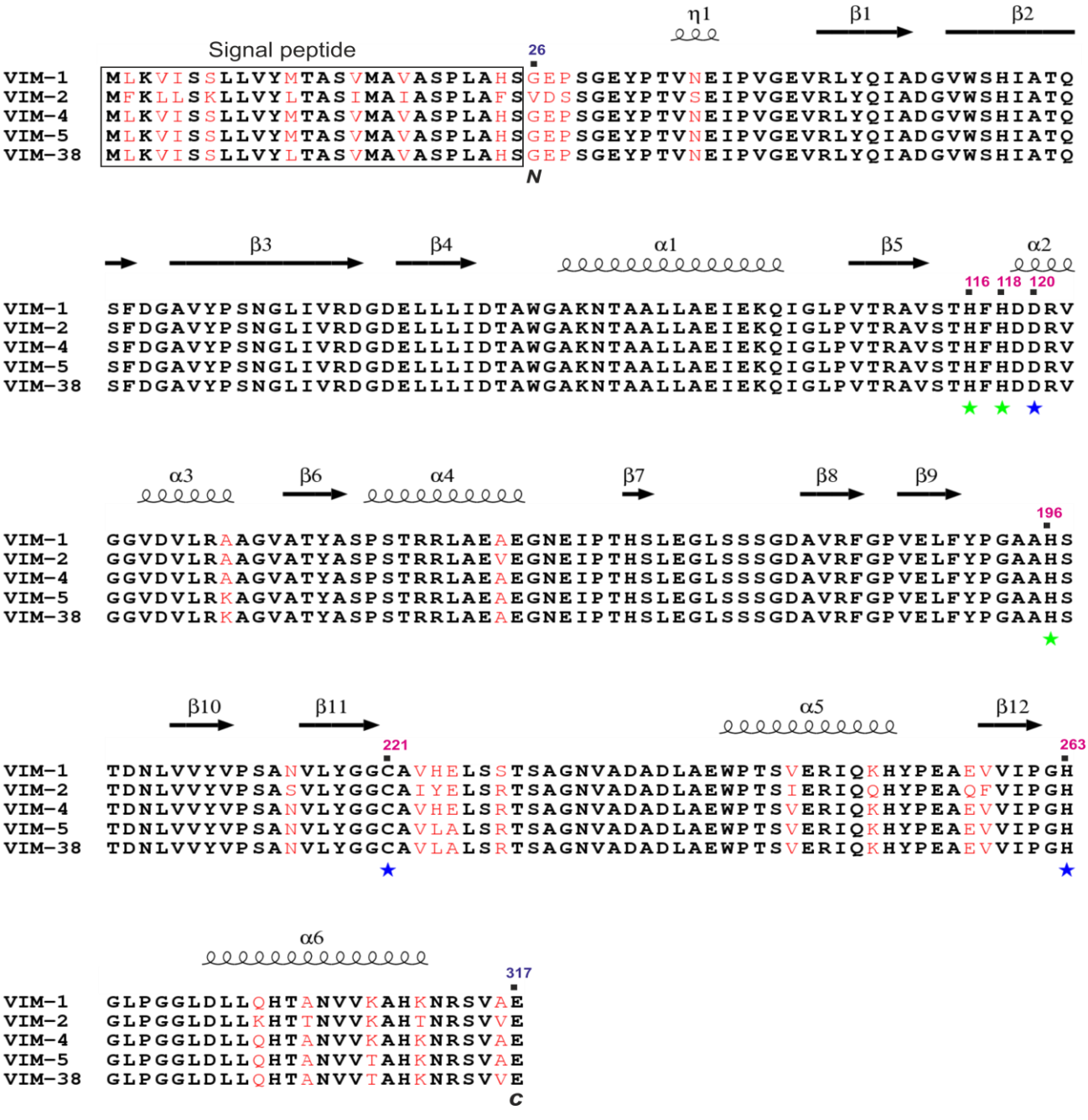
VIM variants manifest a highly directional and monophyletic mode of evolution with the formation of VIM-1 and VIM-2 major clusters[8]. There are however, apparent intermediate variants in between VIM-1 and VIM-2 clusters, including VIM-5[9], VIM-12[10] and VIM-13[11]. Previous biochemical analyses indicate an overall increase in hydrolytic activity of VIM-2 compared to VIM-1 particularly for imipenem and meropenem[3]. VIM-5 has been reported to exhibit a similar level of carbapenemase activity as VIM-2, but with greater efficiency towards imipenem than meropenem[12].

The differences in substrate specificity of VIM variants have been attributed changes in residues at positions 223, 224 and 228 (BBL numbering[13]), located on the active site L10 loop (residues 223-242) [3,14-16].

For effective comparison of the substrate profiles and biophysical properties of the VIM variants, representative enzymes of the two clusters as well as the intermediate variants were selected. The tested variants comprised of VIM-1, VIM-2, VIM-4, VIM-5 and VIM-38. VIM-4 belongs to the VIM-1 cluster and differs from VIM-1 by one substitution (S228R) [17], which has been proposed to have a major impact on the VIM-4 catalytic efficiency (*Figure 5-1*).

The intermediate variants VIM-5 and VIM-38 differ by one residue, A316V[18], a conservative *C*-terminal substitution present in about half of the reported VIM variants. Although VIM-5 and VIM-38 are closely related to VIM-1 (97% amino acid identity), the two variants contain H224L, E225A and S228R substitutions relative to VIM-1 (*Figure 5-1*). These residues are positioned on the L10 loop and are proposed to influence the substrate specificity of VIM variants [3,15,19,20].

Whilst kinetic parameters have been reported for the individual variants (except VIM-38), it is desirable to compare the activities of MBL variants under the same experimental conditions to allow for reliable comparison of results[21]



.

Figure 5-1: **Sequence alignment of the VIM-1, VIM-2, VIM-5 and VIM-38 MBLs, indicating the differences in the amino acid sequences of the tested variants. Amino acid sequence alignment was generated using ESPript 3.0 software with the secondary structure assignments based on the VIM-5 structure (PDB code 5A87). The green and blue stars indicate the active site residues (labelled in magenta) interacting with the Zn1 and Zn2 ions respectively.**

5.1.2 CHAPTER OBJECTIVES

Despite several clinical reports of VIM variants, biochemical characterisation has been carried out for fewer than 10 VIM variants and structural information is available for only five of these variants (VIM-2, VIM-4, VIM-7, VIM-26 and VIM-31) [16,20,22-25]. Additionally, the important question of whether all the clinically relevant MBL variants are similarly inhibited has not been addressed.

The work described in this chapter thus aims to compare the biochemical and biophysical properties five VIM variants including VIM-1, VIM-4, VIM-2 and the intermediate variants VIM-5 and VIM-38. The analyses described were carried out under the same experimental conditions to ensure a reliable comparison.The study also investigates the differences in the interactions of the VIM variants with inhibitors of varying chemotypes by comparing the degree of inhibition of the VIM variants by a library of known metallo-enzyme inhibitors. The structural features of VIM-5 are also explored by crystallographic analyses to expound on the observed inhibitor-enzyme interactions.

The work described in this chapter was performed in collaboration with Dr. Azer Özad Düzgün who obtained the VIM-5 and VIM-38 constructs and helped with the cloning. Dr. Jürgen Brem, Dr. Li Guobo and Dr. Michael A. McDonough facilitated the crystallographic analyses of VIM-5. Most of the work described in this chapter has been reported in academic literature[26].

5.2 PRODUCTION AND PURIFICATION OF RECOMBINANT VIM VARIANTS

Efficient protein production and purification protocols were employed to generate high yields of purified and functional recombinant VIM-1, VIM-2, VIM-4, VIM-5 and VIM-38 enzymes.

5.2.1 CLONING AND MUTAGENESIS

A VIM-38 construct was obtained from collaborators at the Department of Genetics and Bioengineering, Gümüşhane University, Turkey. The construct containing DNA encoding for full-length VIM-38 (S21-E317, lacking its *N*-terminal periplasmic signalling sequence) was cloned into the pET-28a vector (Novagen) for the production of recombinant protein with an *N*-terminal His_6-tag (pET28a-bla_{VIM-38}). To generate the VIM-5 construct, site-directed mutagenesis (V316A substitution) was performed using standard protocols (Chapter 7.2) using the pET28a-bla_{VIM-38} as a template. Further modification of the plasmids was carried out to incorporate a cleavage site for human rhinovirus 3C (HRV3C) protease at the 5′ end of the VIM-5 and VIM-38 sequences. Primers used for site-directed and insertion mutagenesis are listed in *Table 5-1*.

Table 5-1: **Primers used for cloning of VIM variants.**

Primers	Forward (5′- 3′)	Reverse (5′- 3′)
V316A substitution	CACAAAAATCGCTCAGTCGCCGAG	CTCGGCGACTGAGCGATTTTTGTG
HRV3C protease cleavage site insertion	GGCTAGCATGACTGAATTCCTGGA AGTGCTGTTTCAGGGCCCGAGTC CGTTAGCCCATTC	GAATGGGCTAACGGACTCGGGCCCT GAAACAGCACTTCCAGGAATTC AGTCATGCTAGCC

E. coli codon-optimized full-length VIM-1 coding sequences were successfully inserted into pNIC28-Bsa4 using standard ligation-independent cloning procedures[27], allowing for production of *N*-terminal His_6-tagged VIM-1. Previously reported constructs were employed for the production of VIM-2, VIM-4 and *C*-terminal His_6-tagged VIM-1[24,28,29].

5.2.2 PROTEIN PRODUCTION AND PURIFICATION

The vectors containing the VIM variants were transformed into *E. coli* BL21 (DE3) cells and the proteins produced using optimised protocols (Chapter 7.3). Nickel ion affinity chromatography and size exclusion chromatography were employed for protein purification; *N*-terminal His_6-tags were cleaved by incubation with His-tagged HRV3C protease or tobacco etch virus (TEV) protease as appropriate (Chapter 7.4). The employed protocols yielded relatively high quantities of purified recombinant VIM variants (~ 5 mg/L of culture) as ascertained by SDS-PAGE analyses (*Figure 5-2*).

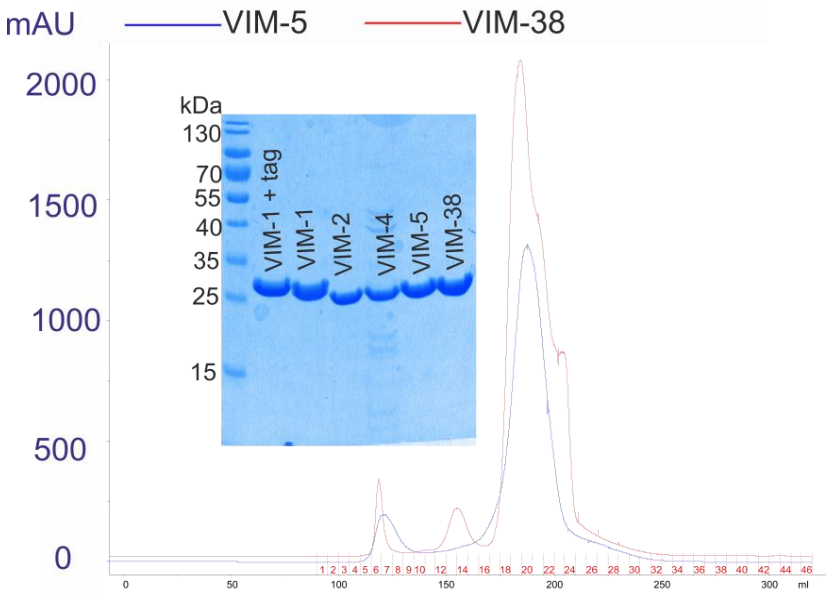
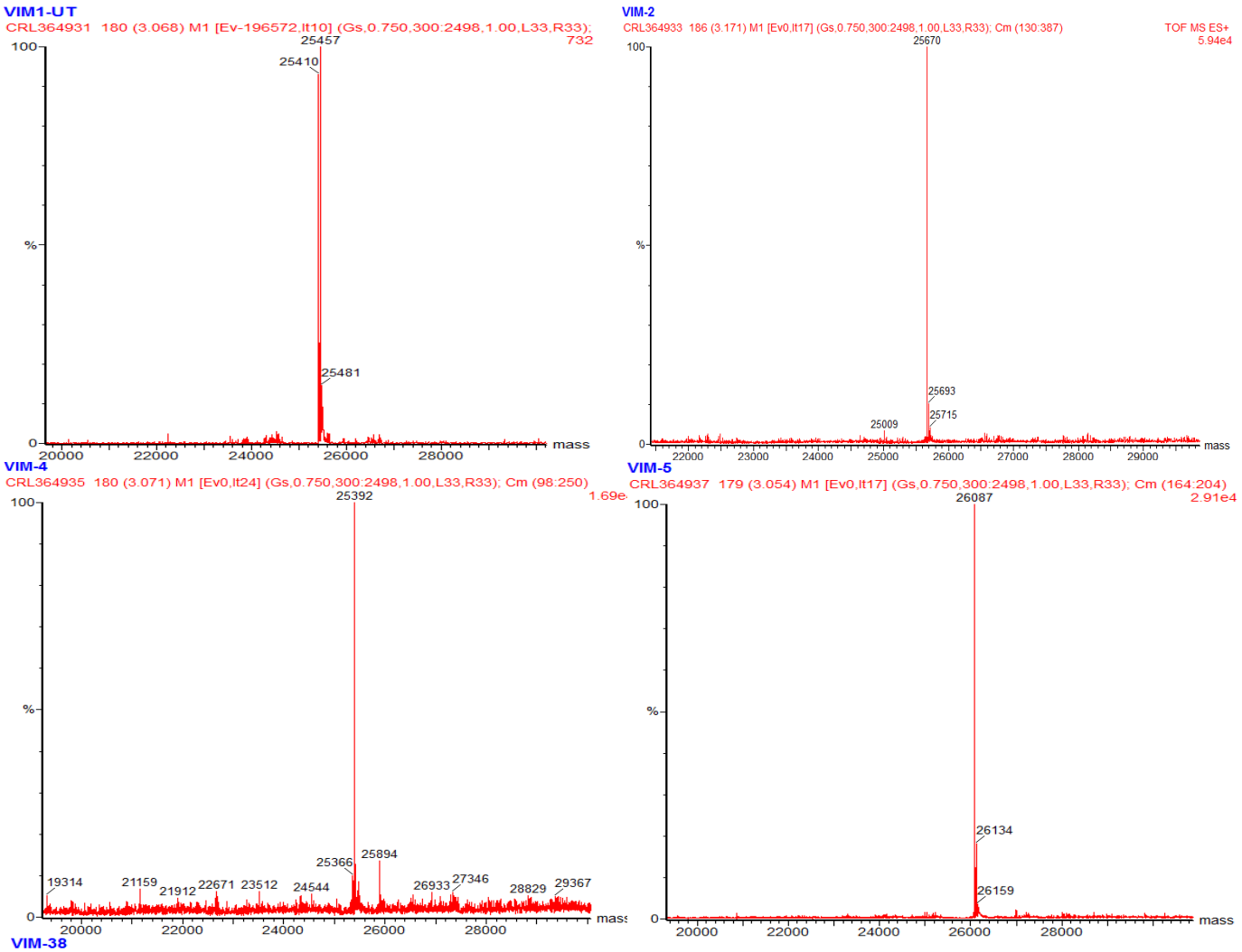


Figure 5-2: **Size exclusion chromatograms for VIM-5 and VIM-38 Inset: SDS-PAGE analysis of the VIM variants after the cleavage of the N-terminal His_6-tag, showing single protein bands with >95% purity.**

5.2.3 MASS SPECTROMETRIC ANALYSES

To verify the mass and metal content of purified enzymes, denaturing and non-denaturing mass spectrometric analysis were carried out. Non-denaturing electrospray ionization mass spectrometric analyses validated the identities of the VIM-5 and VIM-38 variants with the difference between the obtained and predicted mass (shift) corresponding to the presence of two zinc ions (130 ± 14 Da) for each of the purified proteins (*Figure 5-3*). Additionally, the molecular masses obtained by LC-MS analyses in denaturing conditions were in close agreement with the theoretical values predicted using the Expasy protparam tool (http://web.expasy.org/protparam/).



Enzyme	Obtained	Predicted	Shift
VIM-1 (*C*-His$_6$-tagged)	26273	26275	-2
VIM-1 (untagged)	25410	25409	+1
VIM-2	25670	25669	+1
VIM-4	25392	25391	+1
VIM-5	26087	26086	+1
VIM-38	26115	26114	+1

Figure 5-3: **LC-MS analyses under denaturing conditions showing deconvoluted spectra and a comparison of the masses (in Daltons) of the recombinant proteins with theoretical values determined using the Expasy protparam tool. The mass spectra data were extracted using the MaxEnt feature of MassLynx v4.0.**

5.3 FUNCTIONAL ANALYSES OF VIM VARIANTS

Previous biochemical studies have reported variations in the substrate specificity of the VIM variants[30]. To investigate the possible differences in the catalytic activity of the VIM variants, the hydrolytic activities of the VIM variants against a representative set of β-lactam substrates were compared under similar assay conditions.

5.3.1 STEADY-STATE KINETIC ANALYSES

Steady-state kinetic assays were carried out as previously described[21]. The enzyme-mediated hydrolysis of the β-lactam substrates was monitored by recording the changes in absorbance of the substrates or product at varying substrate concentrations. The initial velocity data was fitted to the Michaelis-Menten equation using the Graph Prism 5.01 software, to obtain the steady-state kinetic parameters, K_M and k_{cat}. The untagged proteins were used for the kinetic analyses, with the exception of VIM-1 where the *C*-terminal His_6-tagged VIM-1 construct was used. The tag did not have a significant effect on the activity of the enzyme, as confirmed by comparable kinetic parameters for nitrocefin hydrolysis.

5.3.1.1 CARBAPENEM SUBSTRATES

The VIM variants effciiently hydrolysed the tested carbapenem substrates, as is typical of B1 MBLs. In particular cases, the differences observed in the individual kinetic parameters, contributed to changes (albeit relatively small ones) in k_{cat}/K_M values (*Table 5-2*). VIM-2 manifested > 5 fold higher k_{cat}/K_M value with imipenem compared to VIM-1 and VIM-38. This effect is largely attributed to the lower K_M value reported for imipenem with VIM-2, which was 5 fold lower compared to VIM-38. This improved imipenem activity for VIM-2 is consistent with previous reports, although to a lesser degree[3]. Although the K_M value for meropenem was > 6 fold higher for VIM-1 than VIM-2, this difference was apparently counterbalanced by the high k_{cat} values for VIM-1 (> 7 fold higher than for VIM-2) resulting in similar k_{cat}/K_M values (*Table 5-2*).

Overall, only minor differences were observed in the hydrolytic efficiency (as defined by k_{cat}/K_M values) for the VIM variants with the tested carbapenem substrates (*Figure 5-4*).

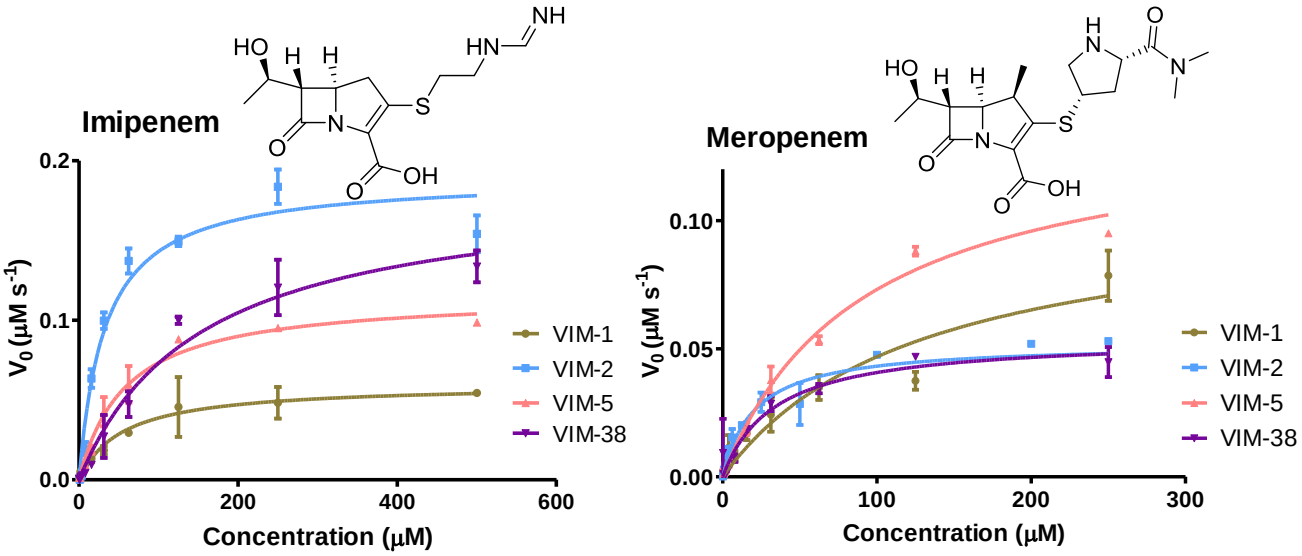


Figure 5-4: **Kinetic curves showing the hydrolysis of imipenem and meropenem by the tested VIM variants.**

5.3.1.2 AMPICILLIN

The VIM variants efficiently hydrolysed ampicillin with VIM-1 recording the lowest k_{cat}/K_M value compared to the other variants. Relatively high apparent K_M values (> 300 µM) were recorded for all VIM variants with ampicillin indicating a low affinity for this penicillin , consistent with the literature values for VIM-1 and VIM-4[2,24](*Figure 5-5*).

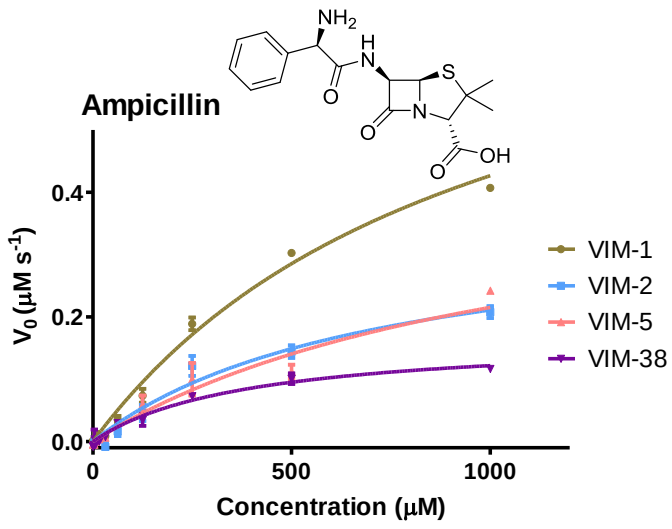


Figure 5-5: **Comparison of the hydrolysis of ampicillin by the tested VIM variants. Fitting traces indicate that the enzymes are not fully saturated hence the reporting of apparent kinetic parameters.**

Table 5-2: **Kinetic parameters for VIM variants with a representative panel of β-lactams.** ***K_M values are reported as the means of three independent measurements ± standard deviation. Standard deviation values for k_{cat} and k_{cat}/K_M did not exceed 10 %. Apparent kinetic parameters were reported for ampicillin and ceftazidime hydrolysis.***

Antibiotic	*VIM-1	VIM-2	#VIM-4	VIM-5	VIM-38
Imipenem					
K_M (μM)	60 ± 10	30 ± 4	3	60 ± 6	150 ± 20
k_{cat} (s^{-1})	30	100	70	60	90
k_{cat}/K_M ($s^{-1}\mu M^{-1}$)	0.5	3.3	23	1.0	0.6
Meropenem					
K_M (μM)	130 ± 20	20 ± 4	8	70 ± 10	30 ± 4
k_{cat} (s^{-1})	50	7	7	20	10
k_{cat}/K_M ($s^{-1}\mu M^{-1}$)	0.4	0.3	0.9	0.3	0.3
Ampicillin					
K_M (μM)	>1000	>500	>3000	>1000	380 ± 80
k_{cat} (s^{-1})	120	180	>210	230	170
k_{cat}/K_M ($s^{-1}\mu M^{-1}$)	0.1	0.4	0.07	0.2	0.4
Cephalothin					
K_M (μM)	140 ± 10	50 ± 6	55	100 ± 8	60 ± 8
k_{cat} (s^{-1})	450	210	500	200	120
k_{cat}/K_M ($s^{-1}\mu M^{-1}$)	3.2	4.2	36	2.0	2.0
Cefoxitin					
K_M (μM)	170 ± 50	40 ± 10	NR	320 ± 60	230 ± 60
k_{cat} (s^{-1})	30	50	NR	460	340
k_{cat}/K_M ($s^{-1}\mu M^{-1}$)	0.2	1.3	NR	1.4	1.5
Ceftazidime					
K_M (μM)	180 ± 60	120 ±20	NR	340 ± 80	430 ± 140
k_{cat} (s^{-1})	3	2	NR	4	4
k_{cat}/K_M ($s^{-1}\mu M^{-1}$)	0.02	0.02	NR	0.01	0.01
Nitrocefin					
K_M (μM)	15 ± 1	50 ± 5	22	50 ± 5	70 ± 10
k_{cat} (s^{-1})	130	510	690	420	720
k_{cat}/K_M ($s^{-1}\mu M^{-1}$)	8.7	10.2	31	8.4	10.3

*C-terminal His_6-tagged VIM-1 was used for kinetic analyses.
#VIM-4 data was obtained from literature values[24]. NR: Not reported.

5.3.1.3 CEPHALOSPORIN SUBSTRATES

Some notable differences were observed in the individual kinetic parameters for the hydrolysis of the tested cephalosporins. Cephalothin and nitrocefin were the preferential substrates for all the VIM variants, manifesting the highest k_{cat}/K_M values compared to the other β-lactam subtrates (*Figure 5-6*). On the other hand, ceftazidime was poorly hydrolysed by the tested VIM variants, with k_{cat}/K_M values of < 0.1 s^{-1} μM^{-1}. Interestingly, VIM-2, VIM-5 and VIM-38 manifested a > 6 fold increase in k_{cat}/K_M values for cefoxitin compared to VIM-1. For VIM-2, the increased cefoxitin hydrolysis was attributed to the lower K_M values while for VIM-5 and VIM-38, the elevated k_{cat} values (> 10 fold higher than VIM-1) contributed to the higher k_{cat}/K_M values.

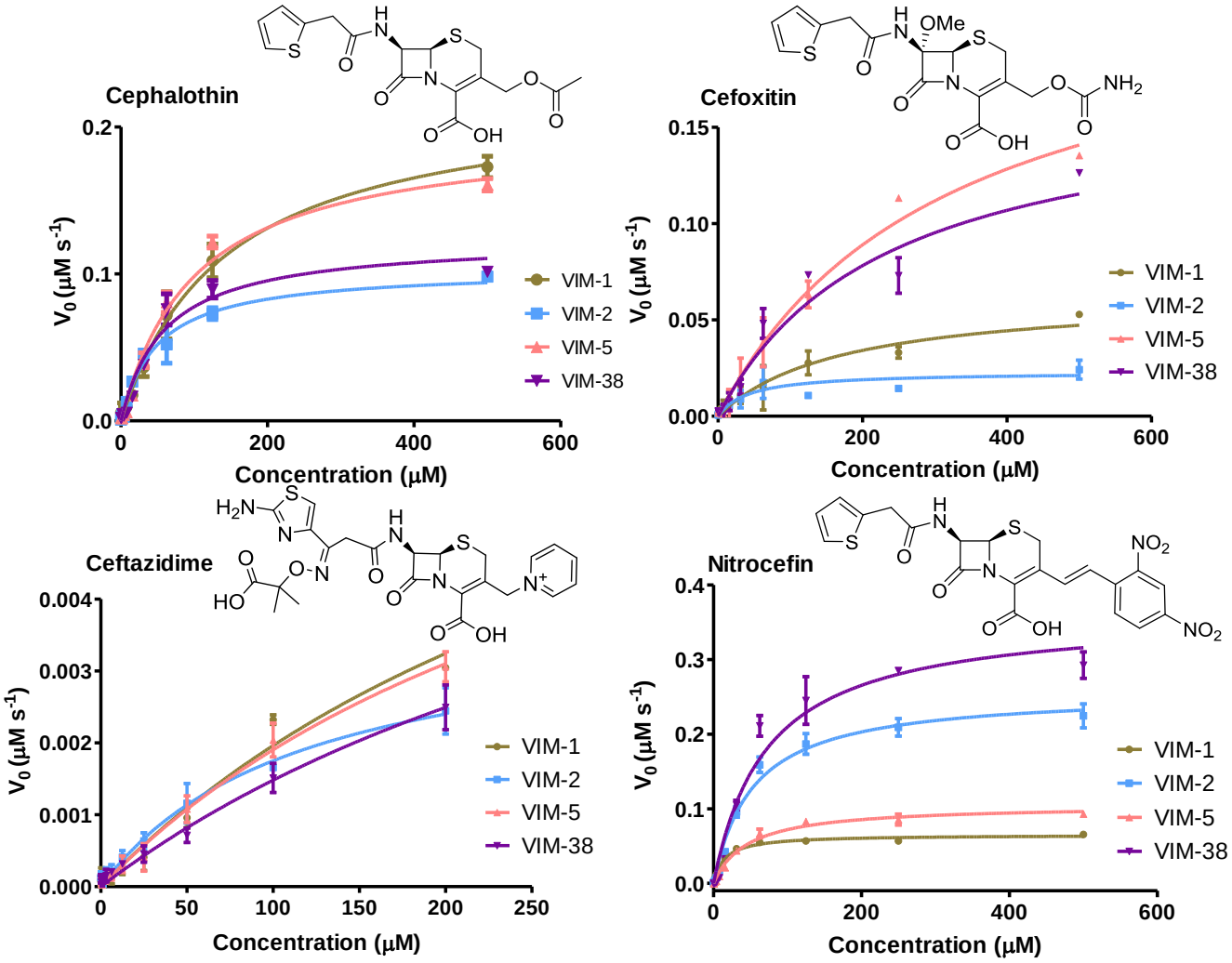


Figure 5-6: **Kinetic curves comparing the hydrolysis of cephalosporin substrates by the tested VIM variants.**

It should be noted that apparent kinetic parameters were reported for ceftazidime and ampicillin hydrolysis (*Table 5-2*), because the initial velocity remained proportional to the substrate concentration up to 300 µM. This observation has been previously reported in kinetic studies on VIM-2 and VIM-4[3,24].

Though results from this study were consistent with previous results for some substrates (meropenem and imipenem), some discrepancies were observed with regards to other substrates (ceftazidime). Whilst the reported k_{cat}/K_M values for meropenem with VIM-1 and VIM-2 are close to the previously reported values[2,4], VIM-5 hydrolyses ceftazidime with a 10 fold higher efficiency in this study than that previously reported[12] (*Table 5-3*).

Table 5-3: **Kinetic parameters from this study (shaded rows) with data from previous studies (non-shaded rows) for some of the tested antibiotics. The previously reported kinetic data for VIM-1, VIM-2 and VIM-5 are from Franceschini *et al.*[2], Poirel *et al.* [4] and Garcar *et al.* [12], respectively.**

Substrate	K_m (µM)			k_{cat} (s^{-1})			k_{cat}/K_m (s^{-1} μM^{-1})		
	*VIM-1	VIM-2	VIM-5	VIM-1	VIM-2	VIM-5	VIM-1	VIM-2	VIM-5
Meropenem	48	5	49	13	1.4	2.4	0.27	0.28	0.05
	130 ± 20	20 ± 4	70 ± 10	50	7	16	0.35	0.31	0.22
Imipenem	1.5	10	12	2	9.9	3.5	1.3	0.99	0.29
	6 ± 11	33 ± 4	58 ± 6	30	95	58	0.55	2.87	1
Ampicillin	917	[#]ND	125	37	ND	14	0.04	ND	0.11
	>1000	>500	>1000	122	180	230	0.1	0.25	0.2
Ceftazidime	794	98	149	60	89	0.2	0.076	0.9	0.001
	180 ± 60	120 ±20	340 ± 75	3	2	4	0.02	0.02	0.01

[#]ND, not determined

These inconsistencies may reflect differences in enzyme preparation and assay conditions, stressing the need to carry out comparative kinetic studies under identical experimental conditions to ensure consistent and reliable data comparison.

5.4 INHIBITION PROFILES OF VIM VARIANTS

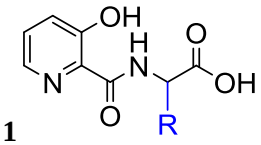
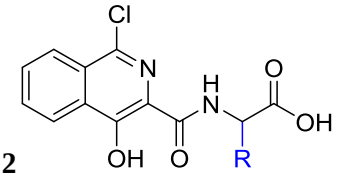
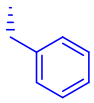
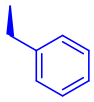
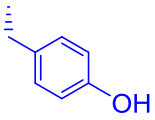
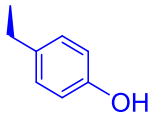
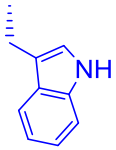
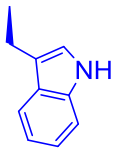
Further investigation was then carried out to compare the inhibitory effects of a set of compounds containing different potential metal chelating motifs[28,31] on the VIM variants. Analogues of pyridine carboxylates are known inhibitors of monometallic enzymes including hypoxia-inducible factor (HIF) prolyl hydroxylases, γ-butyrobetaine (BBOX) hydroxylases and CphA, a mono-zinc B2 MBL[31-33]. To explore the potential utility of these compounds for inhibition of VIM variants, a set of compounds comprising of pyridine-2 carboxylate and 4-hydroxyisoquinoline analogues were screened for potential inhibition of the VIM variants. To investigate whether the VIM variants displayed different degrees of inhibition, IC_{50} values were determined for a representative set of inhibitors.

5.4.1 DETERMINATION OF RESIDUAL ACTIVITIES

The stock solutions of the inhibitors were prepared in DMSO and the inhibition assays were carried out as previously described[28,29,34] (see Chapter 2), with nitrocefin being used as the reporter substrate. To obtain the residual activity values, enzyme-mediated hydrolysis of nitrocefin was monitored by determining the changes in absorbance at 495 nm in the presence of a fixed concentration of the inhibitors (100 μM). The residual activities were obtained at increasing inhibitor concentrations (0.2-2000 μM), with the nitrocefin concentration maintained at near K_M values (*Table 5-2*); data were fitted to dose-response inhibition curve using the GraphPad Prism 5.01 software to obtain the IC_{50} values.

Most of the compounds in this series manifested residual activities > 40%, with the exception of the tryptophan-substituted compounds **2f, 1g and 2g** (*Table 5-4*).

Table 5-4: **Comparison of the residual activities (%) of the VIM variants with the tested inhibitors.**

		 **1**				 **2**			
Entry	(R)	VIM-1	VIM-2	VIM-5	VIM-38	VIM-1	VIM-2	VIM-5	VIM-38
a	-H Gly	100	95	94	100	100	92	87	90
b	 S-Phe	48	64	97	100	65	78	88	93
c	 R-Phe	59	45	90	93	59	84	79	80
d	 S-Tyr	55	86	88	83	100	82	100	81
e	 R-Tyr	61	57	78	81	100	80	100	73
f	 S-Trp	100	50	82	48	**42**	**64**	**38**	**40**
g	 R-Trp	**35**	**52**	**43**	**40**	**79**	**39**	**<0.5**	**1**

Strikingly, VIM-5 and VIM-38 exhibited very low residual activities with the isoquinoline **2g** compared to the other variants. The extent of inhibition of the VIM variants by the highlighted compounds was further characterised by determination of IC_{50} values. The kinetic results were validated by ^{1}H CPMG NMR binding assays (done by Martine Abboud). Apparent K_D values were obtained by determining the displacement of the reporter ligand (50 μM thiomandelic acid) at increasing inhibitor concentrations (0-300 μM) [35].

5.4.2 DIFFERENTIAL INHIBITION OF VIM VARIANTS

One of the most interesting results to emerge from this work was the differential inhibition of the VIM variants by some of the tested inhibitors. In particular, the isoquinoline derivative **2g** exhibited substantially lower IC_{50} values with VIM-5 and VIM-38 (2 μM) in comparison with the other variants. VIM-2 and VIM-4 manifested > 40 fold higher IC_{50} value (IC_{50} = 90 μM and 200 μM respectively) with the inhibitor **2g** compared to VIM-5, while VIM-1 was not effectively inhibited by the compound (IC_{50} > 1 mM).

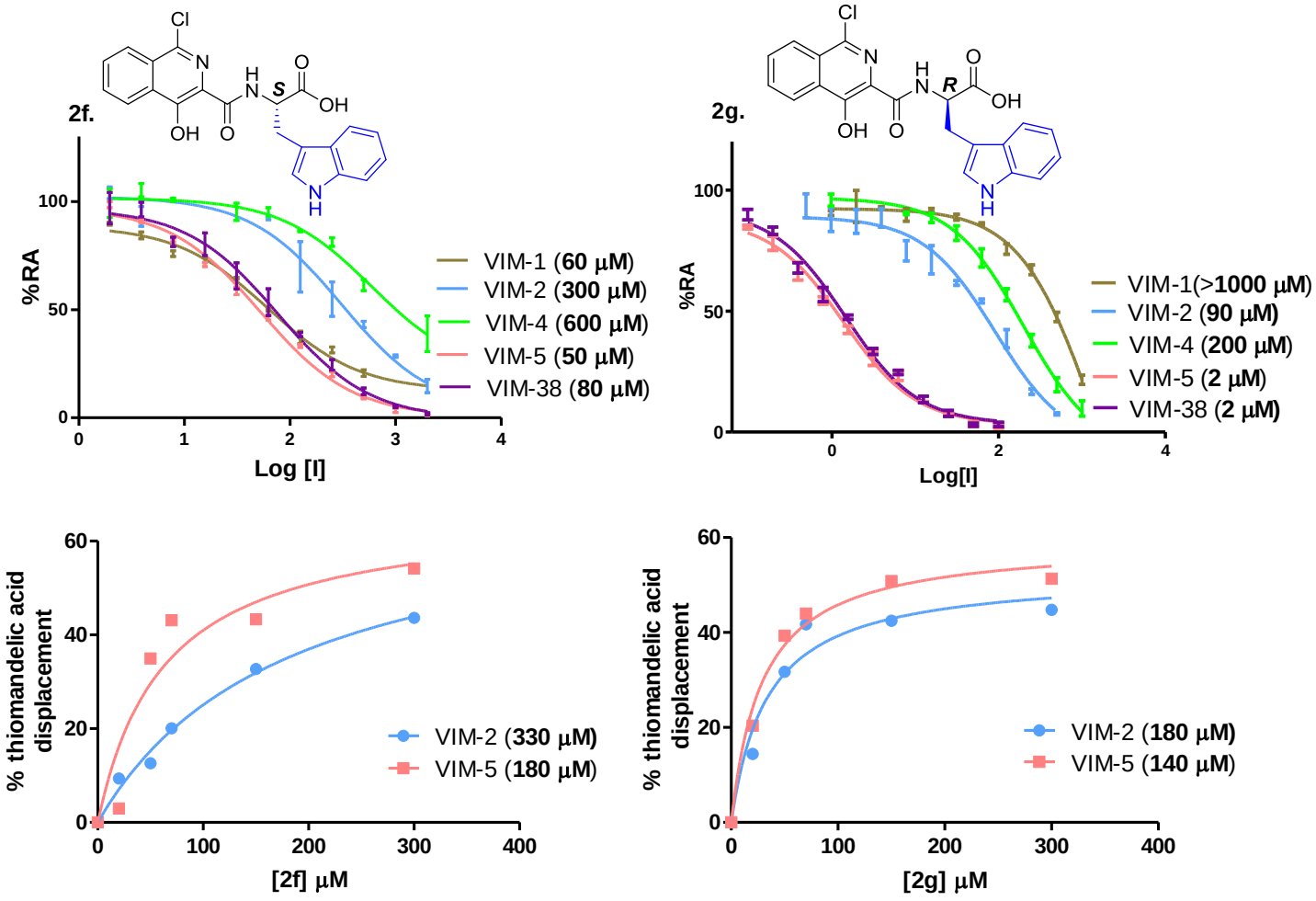


Figure 5-7: **Differences in the potency of inhibition of VIM variants by the tested isoquinoline derivatives indicating the influence of the configuration of inhibitors' side chain stereocentre; apparent IC_{50} and K_D values are in parenthesis.**

In contrast, the (*S*)-enantiomer **2f** manifested >10 fold lower IC_{50} values with VIM-1 and VIM-5 (IC_{50} = 60 μM and 50 μM respectively) compared to VIM-4 (600 μM). With the exception of VIM-1, the (*R*)-enantiomer **2g** was shown to be a more potent inhibitor than the (*S*)-enantiomer **2f** for all the variants, highlighting the effect of the configuration of the stereocentre of the inhibitor side chain on the degree of inhibition (*Figure 5-7*). The observed differences were corroborated by binding assays employing ^{1}H CPMG NMR, with the (*R*)-enantiomer **2g** being shown to be a stronger binder to VIM-2 (K_D = 180 μM) compared to the (*S*)-enantiomer **2f** (K_D= 330 μM). NMR results also indicated that both isoquinoline inhibitors **2f** and **2g** bound more strongly to VIM-5 compared to VIM-2, supporting the kinetic analyses.

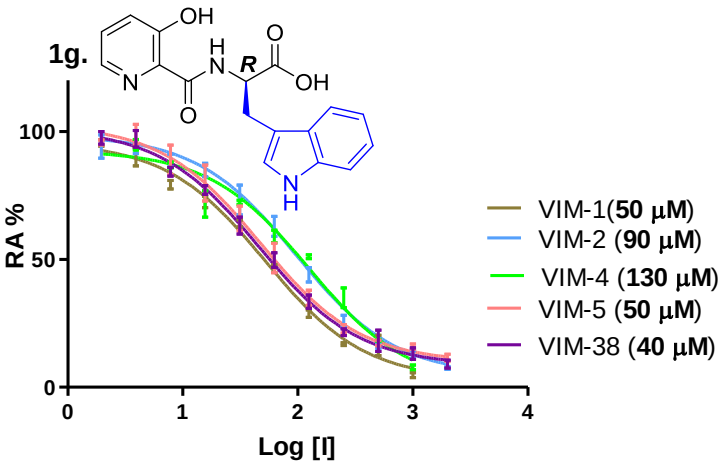


Figure 5-8: **Inhibition curves illustrating the modest inhibition of VIM variants by the pyridine-2 carboxylate derivative 1g.**

Interestingly, the pyridine-2 carboxylate derivative **1g,** with an analogous (*R*)-tryptophan side chain to that of **2g,** displayed a similar inhibition profile for all the tested VIM variants (IC_{50} values ranging 40-130 μM). Inhibitors **1f** and **1g** manifested only modest, if any, inhibition of the VIM variants, illustrating the importance of isoquinoline ring system with regard to the potency of inhibition (*Figure 5-8*).

Overall, notable differences were observed in the degree of inhibition of the VIM variants, particularly by the isoquinoline inhibitors. Additionally, VIM-4 exhibits IC_{50} values similar to VIM-2 for the tested compounds (around 2 fold differences), despite being more closely related to VIM-1 than VIM-2.

5.5 BIOPHYSICAL CHARACTERISATION

Further structural analyses were then carried out to explore the enzyme-inhibitor interactions contributing to the observed differences in inhibition potency. Circular Dichroism (CD) was employed for secondary structural analyses and the determination of thermal denaturation profiles of the VIM variants. Additionally, a crystal structure of VIM-5 was solved, both in the apo-form and in complex with inhibitor **2f,** revealing important enzyme-inhibitor interactions.

5.5.1 STRUCTURAL PROPERTIES OF VIM-5

Far-UV CD spectra were obtained for the recombinant untagged VIM variants in the 185-260 nm ranges as previously described (Chapter 3) [21]. The spectra were baseline-corrected, smoothed and normalized at 207 nm to account for difference in protein concentrations[36]. The secondary structural content was estimated in DichroWeb[37] using the CONTIN Analysis Programme (reference set 6) [38].

As was observed with the NDM variants, the five tested VIM variants displayed very similar CD spectra (*Figure 5-9*), indicating that the differences in amino acid sequences did not have significant effects on the secondary structures of the enzymes. Similarly, the estimated secondary structural content of the VIM variants were very similar, reiterating the minimal differences in overall folds of the enzymes.

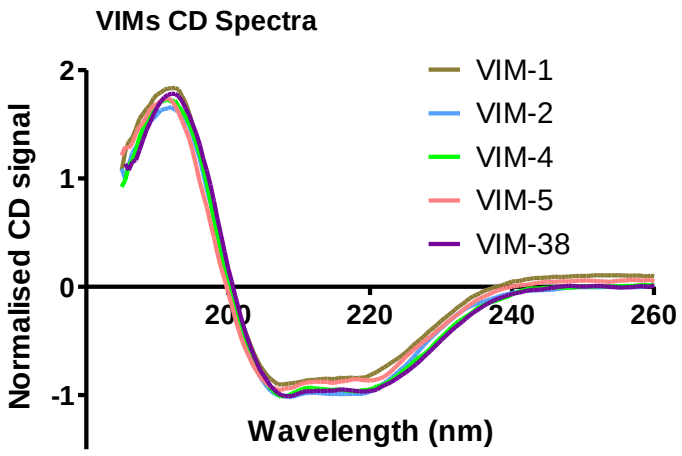


Figure 5-9: **CD spectra analyses of the tested VIM variants illustrating the similarity of the overall folds of the variants.**

5.5.2 INVESTIGATION OF THERMAL STABILITY

Protein stability has been proposed to be a potential constraint on antibiotic resistant evolution, with some studies proposing that increased stability may confer a selective advantage during the evolution of drug resistance[39,40]. For MBLs, including NDM and VIM groups, particular residue substitutions have been linked to changes in the stabilities of the resultant enzymes[21,25,41,42]. To investigate possible differences in the relative thermal stabilities of the tested VIM variants, the melting temperatures of the enzymes were determined using temperature-dependent CD.

Temperature-induced changes in the CD signal at 222 nm were monitored between 25-92 °C with a ramp rate of 1 °C per minute. To ensure reversibility of the thermal denaturation, the samples were cooled from 92-25 °C at the same rate and the CD spectra and hydrolytic activity of the refolded proteins verified. With the exception of VIM-1 and VIM-4, the refolded VIM variants maintained their secondary structural features as exhibited by the CD spectra of the cooled samples. Similarly, the efficiency of nitrocefin hydrolysis of the variants was substantially restored upon refolding, with < 2 fold differences being observed in k_{cat}/K_m values. Since the variants were shown to regain their native structure upon refolding, the apparent melting temperatures (T_m) values were obtained by fitting the thermal denaturation data to a Boltzmann's sigmoidal curve using Graphpad prism 5.0 Software.

Substantial differences were observed in the T_m values of the five VIM variants (*Figure 5-10*). VIM-1 and VIM-4 displayed the lowest apparent T_m values of 60 °C and 64 °C respectively. These results are consistent with previous studies that have reported equally low melting temperatures for VIM-4[24]. VIM-2 exhibited a > 14 °C increase in T_m value (78 °C) whilst VIM-5 and VIM-38 were the most stable variants with an apparent T_m > 83 °C, which is > 20 °C higher than that determined for VIM-1.

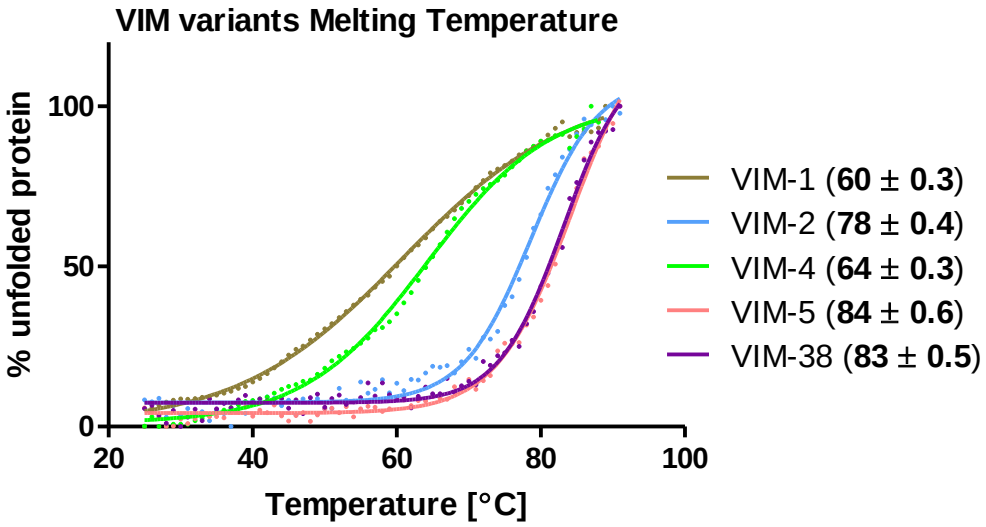


Figure 5-10: **Comparison of T_m values of the tested VIM variants, as determined by temperature-dependent circular dichroism, indicating substantial differences in thermal stabilities.**

Without excluding the possibility of an 'evolutionary drift', this trend of increased thermal stability of, at least some, VIM variants is a fascinating observation, and is similar to previously reported observations with NDM variants[21]. Although the biological relevance of increased thermal stabilities of MBL variants is not quite clear yet, improved protein stability has been shown to promote evolvability by allowing a protein to maintain its native structure while accepting a wider range of functionally beneficial mutations[43-45].

The increased thermal stability could also reflect reduced propensity for proteolysis or aggregation which may result in increased cellular lifetimes of the resultant proteins thus ameliorating the fitness cost of antibiotic resistance[21].

5.5.3 CRYSTALLOGRAPHIC ANALYSES OF VIM-5

Following the interesting observations made with regards to stability and inhibition susceptiblity of VIM variants, crystallographic studies were carried out in an attempt to explain these differences. Purified recombinant VIM-5 was crystallised using the sitting drop vapour diffusion method with crystal being formed in well conditions containing 0.1 M Tris buffer (pH 8.5), 25% PEG 3350 and 0.2 M NaCl. Diffraction data was collected from a single crystal and processed at the Diamond Light Source synchrotron beamline by Dr. Jurgen Brem and Dr. Michael McDonough. The structure of VIM-4 (PDB code: 2WRS) [46] was used as a search model for initial phasing by molecular replacement; the crystallographic structure refinement was performed using Coot [47] and PHENIX[48] (*Table 5-5*).

Table 5-5: **Crystallography data collection and refinement statistics of VIM-5 (PDB code:5A87)**

Data set	VIM-5
Data collection	
Resolution range (Å) (outer shell)	39.90-1.50 (1.54-1.50)
Space group	$P\ 1\ 2_1\ 1$
Unit cell dimensions	
a,b,c (Å)	41.27, 78.96, 64.03
α,β,γ (°)	90, 104.82, 90
No. of molecules/ASU	4
No. of unique reflections	61764
Completeness (%)	97.4 (96.6)
Redundancy	7.0 (7.1)
R_{merge}	0.132 (1.499)
Mean I/σ(I)	9.7 (1.2)
Wilson B value ($Å^2$)	14.86
Refinement	
R_{factor}	0.1552 (0.2655)
R_{free}	0.1915 (0.2949)
RMSD	
Bond length (Å)	0.008
Bond angle (°)	1.166
No. of atoms	7266
Protein	3487
Ligand	24
Ion	5
Water	408
$<B_{factor}>$ ($Å^2$)	
Protein	19.03
Ligand	44.44
Ion	16.5
Water	33.77

5.5.3.1 OVERALL STRUCTURAL FEATURES OF VIM-5

Coordinates and structure factors for the VIM-5 structure have been deposited in the Protein Data Bank under the accession code 5A87. The obtained VIM-5 crystal structure, solved to 1.5 Å resolution, depicted an overall fold of VIM-5 almost identical to that reported for a VIM 2[49] (PDB code: 4BZ3) with a Cα root mean square deviation (RMSD) of 0.206 Å. The VIM-5 structure revealed the canonical MBL αβ/βα sandwich structure and two zinc (II) ions (3.5 Å apart) bound in the active site (*Figure 5-11*). The active site co-ordination of the zinc (II) ions is similar that observed in other VIM variants[23,24], with the nucleophilic hydroxide/water molecule bridging the two zinc (II) ions, 1.9 Å and 2.0 Å from Zn1 and Zn2, respectively (*Figure 5-11 B*).

The flexible active site L3 loop appears closer to the active site in the VIM-5 structure compared to VIM-2 despite the two variants having identical sequences at this region (*Figure 5-11 C*). This flexibility has been previously observed in VIM-4 and VIM-31[20,24], highlighting the role of the active site loops in substrate interactions. Another interesting feature of the VIM-5 structure is the 'flipping' of the main-chain carbonyl of A231 (located in the L10 loop), as depicted by a 4.8 Å shift in the carbonyl oxygen position of A231 in comparison to the VIM-2 structure (*Figure 5-11 D*). The A231 main chain shift is seemingly influenced by the residue at position 224, with other enzymes possessing L224, such as VIM-26[16], showing a similar A231 main chain 'flipping', in comparison with variants with bulky histidine or tyrosine residues at this position (*Figure 5-11 D*). Interactions between Y224 and A231 in H224Y VIM-7 mutants have been proposed to influence the stability and activity profile of the enzymes[25]. It is therefore possible that A231 shift alters the entrance to the active site thus influencing substrate and inhibitor binding.

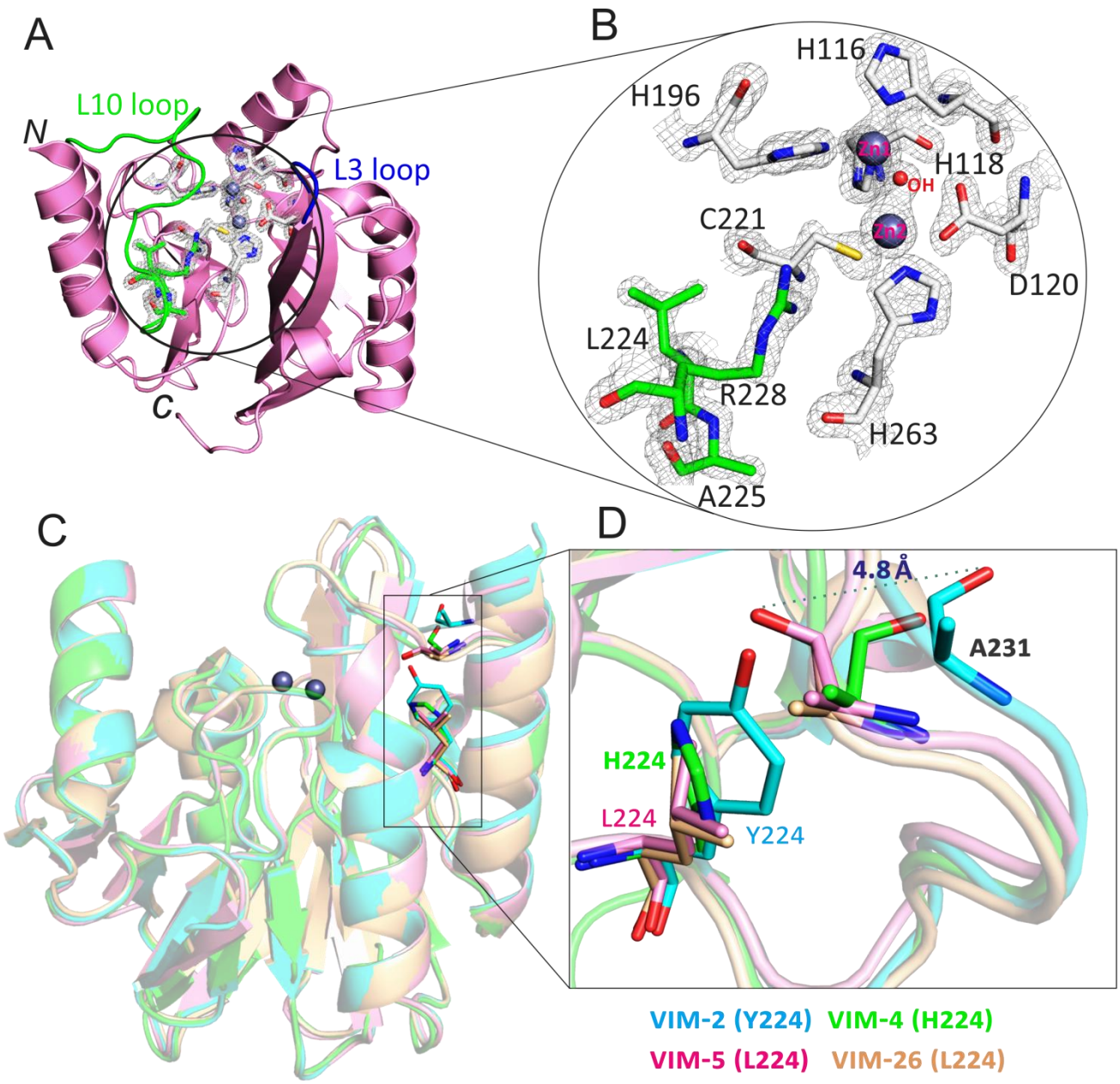


Figure 5-11: **A) Ribbon representation of VIM-5 crystal structure indicating the overall folds and active site loop, L3 and L10; B) Close-up view of the VIM-5 active site co-ordination with representative electron density ($2F_o$-F_c contoured to 2σ) shown as grey mesh; C) View from a structural overlay of VIM-2, VIM-5, VIM-4 and VIM-26 (PDB codes: 4BZ3, 5A87, 2WRS, 4UWO) [16,46,49] showing similarities of the overall folds; D) Close-up view showing a shift in carbonyl oxygen position of A231 in VIM-5 and VIM-26 compared to VIM-2 and VIM-4.**

5.5.3.2 STRUCTURAL BASIS OF DIFFERENCES IN INHIBITION POTENCY

To shed light on the structural features contributing to the observed differences on the inhibition of VIM variants, a VIM-5 crystal structure was solved complexed with the isoquinoline inhibitor **2f.** The cysteine at the second zinc site (C221) was oxidised in this structure, resulting in binding of one zinc ion at the active site. This is a common phenomenon in crystallisation of MBLs, resulting from protein purification procedures, crystallisation conditions and/or X-ray radiation damage[16,22,46,49]. Despite metal occupancy, the binding mode of the inhibitor **2f** provided some interesting insights into the inhibitor-enzyme interactions (*Figure 5-12*).

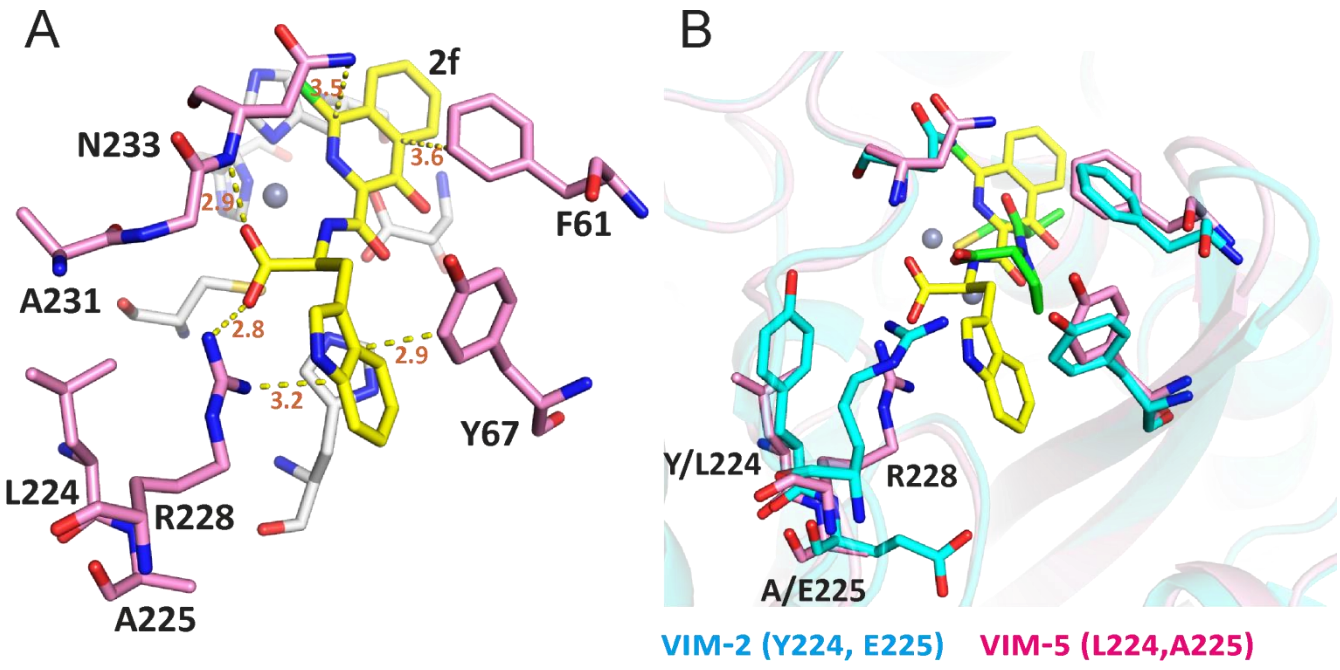


Figure 5-12: **A) View of VIM-5:2g complex revealing the binding mode and the interaction of the isoquinoline inhibitor 2f with the VIM-5 residues. B) Overlay of VIM-5:2f (pink) and VIM-2: D-captopril (blue) showing the residues contributing to the observed differences in inhibition potency; Inhibitor 2f is represented in yellow and D-captopril in green[49]. Dotted lines and accompanying numbers indicate distances in Å.**

Consistent with previous assertions, the residues at positions 224 and 228, located on the L10 loop play critical roles in the interactions of the enzyme with the inhibitor and likely contribute to the differential inhibition profiles observed. For instance, the tryptophan indole rings of the inhibitor **2f** form cation-π interactions with the guanidino group of R228 in VIM-5, facilitating better binding of the inhibitor (*Figure 5-12 A*). The close proximity of the R228 in VIM-2 to the inhibitor introduces a steric clash which could account for the reduced binding affinity of the inhibitor to VIM-2 (*Figure 5-12 B).* Previous structural studies on VIM-2 have proposed that E225 rigidifies and partially neutralizes the side chain of R228 *via* electrostatic interactions, influencing the binding of β-lactam substrates[22,24]. In the case of VIM-5 and VIM-38, this residue (E225) is substituted with A225, a substitution that may allow for a greater degree of flexibility of the R228 side chain.

The substitution of Y224 in VIM-2 with L224 in VIM-5 and VIM-38 is also likely to provide a more spacious active site that may better accommodate bulky tryptophan groups of the tested inhibitors, as reflected by the increased inhibition of VIM-5 and VIM-38 by inhibitors **2f** and **2g** compared to VIM-2. Additionally, the structure of VIM-5 reveals that the tryptophan-derived carboxylate moiety is positioned to favourably interact with the conserved asparagine (N233) as has been previously observed in VIM-2: captopril structures[49].

The VIM-5 structure also reveal hydrophobic interactions between the indole groups of inhibitor **2f** with residue Y67, located on the L3 loop (residues 60 to 67) [22]. These observations are agreement with the reported interactions of the hydrophobic substituents of cephalosporin and penicillin MBL substrates with the L3 loop[50]. The bicyclic isoquinoline ring system of inhibitor **2f** is positioned to interact with another residue in the L3 loop, F60, as well as the side chain of the conserved N233, consistent with the observation of increased inhibition potency of inhibitors **2f** and **2g** in comparison to the pyridine-2 carboxylate analogues **1f** and **1g** for the VIM variants (*Figure 5-12 A*).

5.6 SUMMARY

Overall, the kinetic analyses revealed relatively small differences in the catalytic efficiencies of the five VIM variants towards the tested β-lactam substrates (*Table 5-1*). VIM-5 and VIM-38, in particular, manifest very similar kinetic parameters for the tested substrates. This is as expected, given that the two variants differ by one substitution (A316V) at the *C*-terminus of the enzymes. These observations suggest that changes in substrate selectivity may not be the sole driving force for the evolution of MBLs, as has been proposed for NDM variants (Chapter 3)[21].

The tested VIM variants also display very similar CD spectra, implying similar secondary structure, in spite of the differences in the amino acid sequences (*Figure 5-9*). This is also as predicted, since the greatest variability in amino acid sequence across the five VIM variants is found in the *N*-terminal leader sequence, which is cleaved in the mature protein. This observation is also corroborated by crystallographic analyses, in which the tested VIM variants manifest very similar overall folds. Interestingly, considerable differences in thermal stability were observed for the VIM variants as observed for NDM variants[21]. While the biological relevance of the increased thermal stability among MBL variants merits further investigation, these and previous results suggest that protein stability may reflect a selection pressure for these enzymes.

In contrast to the minimal differences observed in the kinetic parameters, very clear differences were manifested in the inhibition profiles of the different VIM variants, as exemplified by the relatively low IC_{50} values reported for VIM-5 and VIM-38 with isoquinoline compound **2g** compared to VIM-1, VIM-2 and VIM-4 (*Figure 5-7*). Crystallographic analyses of VIM-5 complexed with the inhibitor **2f** reveal important residues on the L3 and L10 loops that mediate the enzyme-inhibitor interactions. The

differences in residues at positions 224, 225 and 228 on the L10 loop seemingly contribute to the differences in susceptibility of the VIM variants to the tested inhibitors.

This first report of variation in inhibition profiles within a group of MBLs is an important observation that should be taken into account at an early stage in future MBL inhibitor development programs.

5.7 REFERENCES

1. Lauretti L, Riccio ML, Mazzariol A, et al. Cloning and characterization of *bla*$_{VIM}$, a new integron-borne metallo-β-lactamase gene from a *Pseudomonas aeruginosa* clinical isolate. *Antimicrob Agents Chemother*. 1999;43(7):1584-1590.

2. Franceschini N, Caravelli B, Docquier JD, et al. Purification and biochemical characterization of the VIM-1 metallo-β-lactamase. *Antimicrob Agents Chemother*. 2000;44(11):3003-3007.

3. Docquier JD, Lamotte-Brasseur J, Galleni M, Amicosante G, Frere JM, Rossolini GM. On functional and structural heterogeneity of VIM-type metallo-β-lactamases. *J Antimicrob Chemother*. 2003;51(2):257-266.

4. Poirel L, Naas T, Nicolas D, et al. Characterization of VIM-2, a carbapenem-hydrolyzing metallo-β-lactamase and its plasmid- and integron-borne gene from a *Pseudomonas aeruginosa* clinical isolate in France. *Antimicrob Agents Chemother*. 2000;44(4):891-897.

5. Pallecchi L, Riccio ML, Docquier JD, Fontana R, Rossolini GM. Molecular heterogeneity of *bla*$_{VIM-2}$-containing integrons from *Pseudomonas aeruginosa* plasmids encoding the VIM-2 metallo-β-lactamase. *FEMS Microbiol Lett*. 2001;195(2):145-150.

6. Walsh TR. Emerging carbapenemases: A global perspective. *Int J Antimicrob Agents*. 2010;36 Suppl 3:S8-14.

7. Walsh TR, Toleman MA, Poirel L, Nordmann P. Metallo-β-lactamases: The quiet before the storm? *Clin Microbiol Rev*. 2005;18(2):306-325.

8. Pal A, Tripathi A. An i*n silico* approach for understanding the molecular evolution of clinically important metallo-β-lactamases. *Infect Genet Evol*. 2013;20C:39-47.

9. Midilli K, Aygün G, Kuskucu M,. A new variant of metallo-β-lactamase detected in a*Klebsiella pneumoniae* strain: VIM-5.*Abstr KLIMIK Congr*, Istanbul, Turkey . abstr S-21: 275

10. Kontou M, Pournaras S, Kristo I, Ikonomidis A, Maniatis AN, Stathopoulos C. Molecular cloning and biochemical characterization of VIM-12, a novel hybrid VIM-1/VIM-2 metallo-β-lactamase from a *Klebsiella pneumoniae* clinical isolate, reveal atypical substrate specificity. *Biochemistry*. 2007;46(45):13170-13178.

11. Juan C, Beceiro A, Gutierrez O, et al. Characterization of the new metallo-β-lactamase VIM-13 and its integron-borne gene from a *Pseudomonas aeruginosa* clinical isolate in Spain. *Antimicrob Agents Chemother*. 2008;52(10):3589-3596.

12. Gacar GG, Midilli K, Kolayli F, et al. Genetic and enzymatic properties of metallo-β-lactamase VIM-5 from a clinical isolate of *Enterobacter cloacae*. *Antimicrob Agents Chemother*. 2005;49(10):4400-4403.

13. Garau G, Garcia-Saez I, Bebrone C, et al. Update of the standard numbering scheme for class B β -lactamases. *Antimicrob Agents Chemother*. 2004;48(7):2347-2349.

14. Merino M, Perez-Llarena FJ, Kerff F, et al. Role of changes in the L3 loop of the active site in the evolution of enzymatic activity of VIM-type metallo- β -lactamases. *J Antimicrob Chemother*. 2010;65(9):1950-1954.

15. Mojica MF, Mahler SG, Bethel CR, et al. Exploring the role of residue 228 in substrate and inhibitor recognition by VIM metallo-β-lactamases. *Biochemistry*. 2015;54(20):3183-3196.

16. Leiros HK, Edvardsen KS, Bjerga GE, Samuelsen O. Structural and biochemical characterization of VIM-26 shows that Leu224 has implications for the substrate specificity of VIM metallo-β-lactamases. *FEBS J*. 2015;282(6):1031-1042.

17. Pournaras S, Tsakris A, Maniati M, Tzouvelekis LS, Maniatis AN. Novel variant *bla*$_{\text{VIM-4}}$ of the metallo-β-lactamase gene *bla*$_{\text{VIM-1}}$ in a clinical strain of *Pseudomonas aeruginosa*. *Antimicrob Agents Chemother*. 2002;46(12):4026-4028.

18. Iraz M, Duzgun AO, Cicek AC, et al. Characterization of novel VIM carbapenemase, VIM-38, and first detection of GES-5 carbapenem-hydrolyzing β-lactamases in *Pseudomonas aeruginosa* in Turkey. *Diagn Microbiol Infect Dis*. 2014;78(3):292-294.

19. Merino M, Perez-Llarena FJ, Kerff F, et al. Role of changes in the L3 loop of the active site in the evolution of enzymatic activity of VIM-type metallo-β-lactamases. *J Antimicrob Chemother*. 2010;65(9):1950-1954.

20. Kupper MB, Herzog K, Bennink S, et al. The three-dimensional structure of VIM-31, a metallo-β-lactamase from *Enterobacter cloacae* in its native and oxidized form. *FEBS J*. 2015; 282(12):2352-2360.

21. Makena A, Brem J, Pfeffer I, et al. Biochemical characterization of New Delhi metallo-β-lactamase variants reveals differences in protein stability. *J Antimicrob Chemother*. 2015;70(2):463-469.

22. Garcia-Saez I, Docquier JD, Rossolini GM, Dideberg O. The three-dimensional structure of VIM-2, a zn-β-lactamase from *Pseudomonas aeruginosa* in its reduced and oxidised form. *J Mol Biol*. 2008;375(3):604-611.

23. Aitha M, Marts AR, Bergstrom A, et al. Biochemical, mechanistic, and spectroscopic characterization of metallo-β-lactamase VIM-2. *Biochemistry*. 2014;53(46):7321-7331.

24. Lassaux P, Traore DA, Loisel E, et al. Biochemical and structural characterization of the subclass B1 metallo-β-lactamase VIM-4. *Antimicrob Agents Chemother*. 2011;55(3):1248-1255.

25. Leiros HK, Skagseth S, Edvardsen KS, et al. His224 alters the R2 drug binding site and Phe218 influences the catalytic efficiency of the metallo-β-lactamase VIM-7. *Antimicrob Agents Chemother*. 2014;58(8):4826-4836.

26. Makena A, Duzgun AO, Brem J, et al. Comparison of Verona integron-borne metallo-β-lactamase variants reveals differences in stability and inhibition profiles. *Antimicrob Agents Chemother*. 2015;60(3):1377-1384

27. Savitsky P, Bray J, Cooper CD, et al. High-throughput production of human proteins for crystallization: The SGC experience. *J Struct Biol*. 2010;172(1):3-13.

28. van Berkel SS, Brem J, Rydzik AM, et al. Assay platform for clinically relevant metallo-β-lactamases. *J Med Chem*. 2013;56(17):6945-6953.

29. Makena A, van Berkel SS, Lejeune C, et al. Chromophore-linked substrate (CLS405): Probing metallo-β-lactamase activity and inhibition. *ChemMedChem*. 2013; 8(12):1923-1929.

30. Meini MR, Llarrull LI, Vila AJ. Evolution of metallo-β-lactamases: Trends revealed by natural diversity and evolution. *Antibiotics (Basel)*. 2014;3(3):285-316.

31. Rydzik AM, Chowdhury R, Kochan GT, et al. Modulating carnitine levels by targeting its biosynthesis – selective inhibition of *g*butyrobetaine hydroxylase. *Chemical Science*. 2014;5:1765–1771.

32. Ivan M, Haberberger T, Gervasi DC, et al. Biochemical purification and pharmacological inhibition of a mammalian prolyl hydroxylase acting on hypoxia-inducible factor. *Proc Natl Acad Sci U S A*. 2002;99(21):13459-13464.

33. Horsfall LE, Garau G, Liénard BM, et al. Competitive inhibitors of the CphA metallo-β-lactamase from *Aeromonas hydrophila*. *Antimicrob Agents Chemother*. 2007;51:2136-2142.

34. Viswanatha T, Marrone L, Goodfellow V, Dmitrienko GI. Assays for β-lactamase activity and inhibition. *Methods Mol Med*. 2008;142:239-260.

35. Leung IK, Demetriades M, Hardy AP, et al. Reporter ligand NMR screening method for 2-oxoglutarate oxygenase inhibitors. *J Med Chem*. 2013;56(2):547-555.

36. Raussens V, Ruysschaert JM, Goormaghtigh E. Protein concentration is not an absolute prerequisite for the determination of secondary structure from circular dichroism spectra: A new scaling method. *Anal Biochem*. 2003;319(1):114-121.

37. Whitmore L, Wallace BA. Protein secondary structure analyses from circular dichroism spectroscopy: Methods and reference databases. *Biopolymers*. 2008;89(5):392-400.

38. Sreerama N, Woody RW. Estimation of protein secondary structure from circular dichroism spectra: Comparison of CONTIN, SELCON, and CDSSTR methods with an expanded reference set. *Anal Biochem*. 2000;287(2):252-260.

39. Brown NG, Pennington JM, Huang W, Ayvaz T, Palzkill T. Multiple global suppressors of protein stability defects facilitate the evolution of extended-spectrum TEM β-lactamases. *J Mol Biol*. 2010;404(5):832-846.

40. Thomas VL, McReynolds AC, Shoichet BK. Structural bases for stability-function tradeoffs in antibiotic resistance. *J Mol Biol*. 2010;396(1):47-59.

41. Tomatis PE, Rasia RM, Segovia L, Vila AJ. Mimicking natural evolution in metallo-β-lactamases through second-shell ligand mutations. *Proc Natl Acad Sci U S A*. 2005;102(39):13761-13766.

42. Oelschlaeger P, Mayo SL, Pleiss J. Impact of remote mutations on metallo-β-lactamase substrate specificity: Implications for the evolution of antibiotic resistance. *Protein Sci*. 2005;14(3):765-774.

43. Bloom JD, Labthavikul ST, Otey CR, Arnold FH. Protein stability promotes evolvability. *Proc Natl Acad Sci U S A*. 2006;103(15):5869-5874.

44. Beadle BM, Shoichet BK. Structural bases of stability-function tradeoffs in enzymes. *J Mol Biol*. 2002;321(2):285-296.

45. Bjorkman J, Nagaev I, Berg OG, Hughes D, Andersson DI. Effects of environment on compensatory mutations to ameliorate costs of antibiotic resistance. *Science*. 2000;287(5457):1479-1482.

46. Lassaux P, Hamel M, Gulea M, et al. Mercaptophosphonate compounds as broad-spectrum inhibitors of the metallo-β-lactamases. *J Med Chem*. 2010;53(13):4862-4876.

47. Emsley P, Lohkamp B, Scott WG, Cowtan K. Features and development of coot. *Acta Crystallogr D Biol Crystallogr*. 2010;66(Pt 4):486-501.

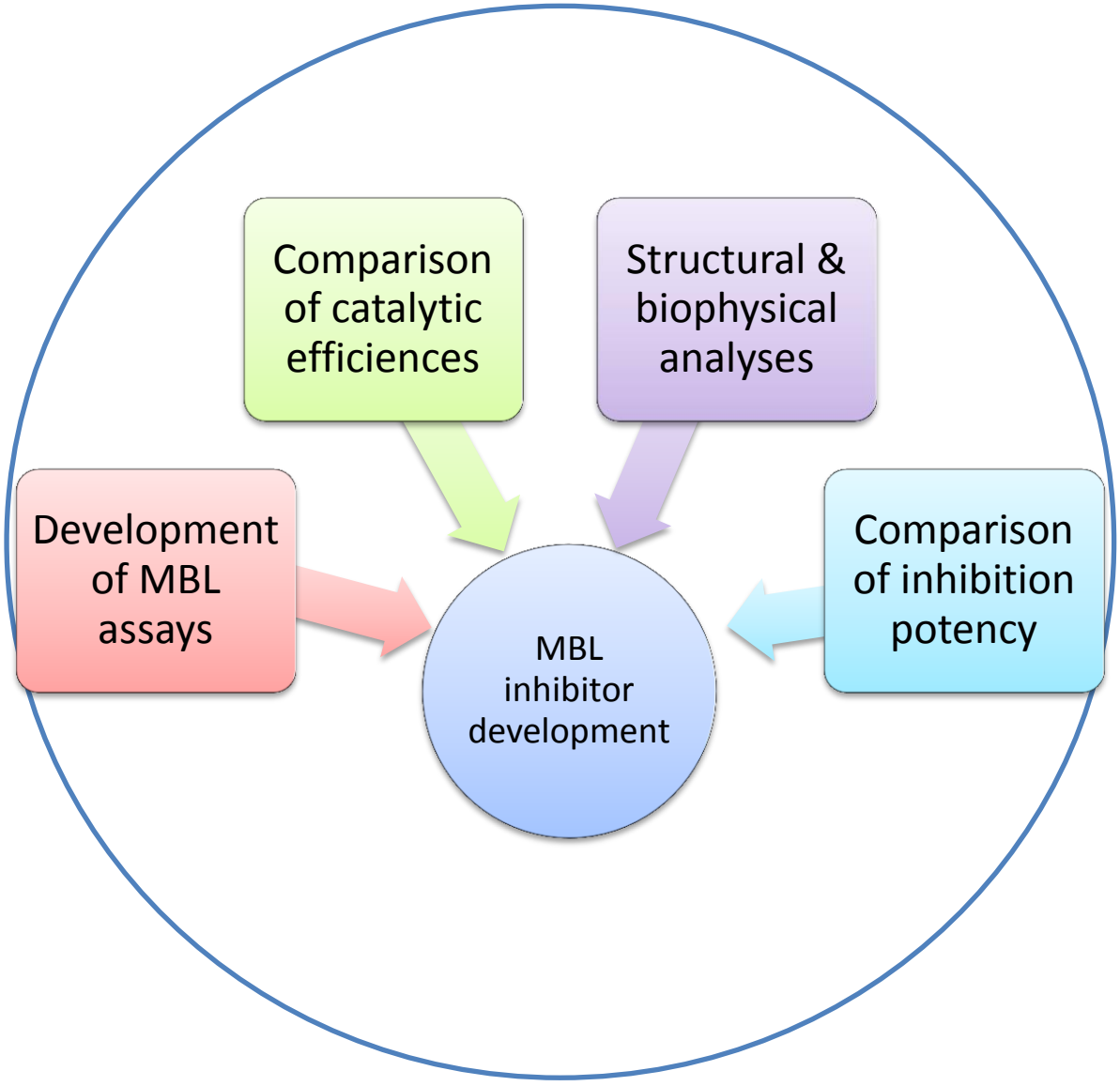
48. Adams PD, Afonine PV, Bunkoczi G, et al. PHENIX: A comprehensive python-based system for macromolecular structure solution. *Acta Crystallogr D Biol Crystallogr*. 2010;66(Pt 2):213-221.

49. Brem J, van Berkel SS, Zollman D, et al. Structural basis of metallo-β-lactamase inhibition by captopril stereoisomers. *Antimicrob Agents Chemother*. 2015;60(1):142-150.

50. Zhang H, Hao Q. Crystal structure of NDM-1 reveals a common β-lactam hydrolysis mechanism. *FASEB J*. 2011;25:2574-2582.

CHAPTER 6: CONCLUSIONS AND FUTURE WORK

The overall aims of my thesis work as outlined in Chapter 1, were to provide relevant insights for future MBL inhibitor development programs by performing extensive biochemical and biophysical analyses of MBL variants. This chapter summarises the work done thus far including on work MBL assay development and comparison of the activity, stability and inhibition of MBL variants as well as the structural analyses of NDM and VIM variants. Potential avenues for future studies are also suggested.



CONTENTS

CHAPTER 6: CONCLUSIONS AND FUTURE WORK 194

6.1 **CLS405**: AN EFFICIENT SUBSTRATE FOR SCREENING MBL ACTIVITY AND INHIBITION 196

6.2 **FC-5**: A POTENTIAL SUBSTRATE FOR CELL-BASED ASSAYS 197

6.3 MBL VARIANTS DISPLAY SIMILAR HYDROLYTIC EFFICIENCIES 198

6.4 PROTEIN STABILITY: A POTENTIAL DRIVER THE EVOLUTION OF MBLS 198

6.5 EVOLUTION OF MBLS AFFECTS INHIBITOR DEVELOPMENT 200

6.6 STRUCTURAL ANALYSES REVEAL SUBTLE BUT CRUCIAL INTERACTIONS 201

6.7 GENERAL CONCLUSIONS 202

6.8 REFERENCES 203

6.1 CLS405: AN EFFICIENT SUBSTRATE FOR SCREENING MBL ACTIVITY AND INHIBITION

The quest to develop an efficient MBL assay platform for high throughput screening of inhibitors led to the identification of a novel cephalosporin-based chromogenic substrate **CLS405** (Chapter 2)[1]. In addition to having optimal spectral properties ($\Delta\lambda_{max}$ of 100 nm), **CLS405** was shown to be stable over a wide pH range and importantly in the typical MBL assay conditions. In a comparative MBL activity assay, **CLS405** was efficiently hydrolysed by six representative B1 MBLs (*Figure 6-1*), recording higher k_{cat}/K_M values for all the enzymes in comparison to the currently available substrates (nitrocefin and CENTA)[1].

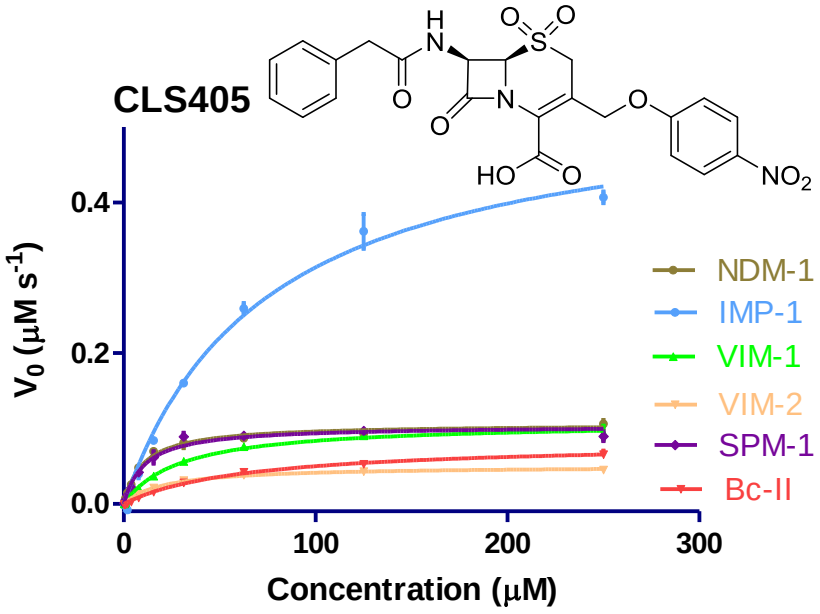


***Figure 6-1*: Kinetic plots showing the efficient hydrolysis of CLS405 by MBLs**

The utility of the **CLS405**-based assay for inhibitor development was validated in an exemplary MBL inhibitor screen, involving a series of known metallo-enzymes inhibitors. The inhibitor screening platform identified *N*-hydroxythiazoles as novel MBL inhibitor scaffolds with a wide-ranging potency against the tested MBLs. The indiscriminate inhibition of bacterial MBLs and iron (II) dependent oxygenases by the tested *N*-hydroxythiazoles underlines the importance of cross-screening MBL inhibitors for potential inhibition of related human metallo-enzymes.

6.2 FC-5: A POTENTIAL SUBSTRATE FOR CELL-BASED ASSAYS

Building on an earlier study that identified cephalosporin-based fluorescent substrates for MBL assays[2], a study was set up to investigate the possible application of the fluorogenic substrates for cell-based MBL assays. The preliminary results from this ongoing study reveal the potential for the application of the fluorogenic substrate (**FC-5)** in identifying bacterial cells producing IMP-1 and VIM-2 MBLs (Chapter 2). There is a scope for the development of a functional assay using the fluorogenic substrate **FC-5**. To this effect, a second compound with an additional piperazine group at the amino-side chain relative to **FC-5**, **FC-P** has been identified (*Figure 6-2*)

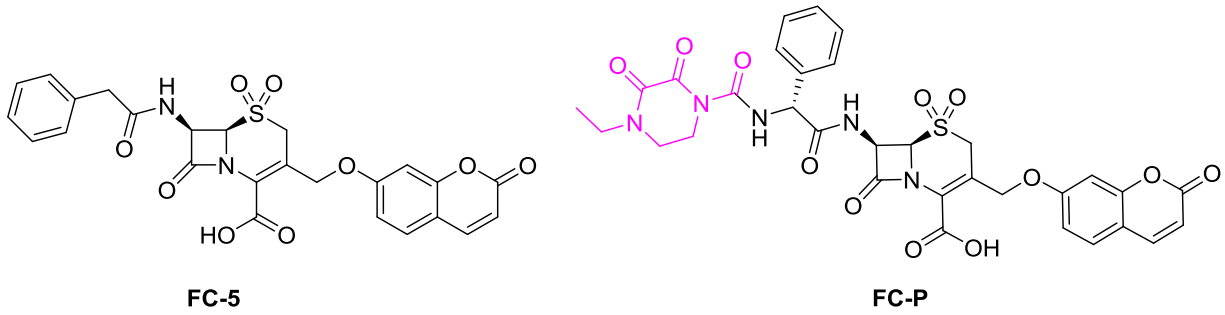


***Figure 6-2*: Fluorogenic substrates FC-5 and FC-P identified in this study.**

The fluorogenic substrate **FC-P** is expected to have increased cell permeability and to discriminate against serine β-lactamases for improved specificity towards MBLs. The substrate **FC-P** is readily hydrolysed by NDM variants *in vitro*; further studies to assess the hydrolytic susceptibility of the substrate in cells will be necessary. Another potential modification would be to replace the coumarin groups of **FC-P** with red-shifted fluorophores. This would facilitate improved cell penetration, reduce phototoxicity and also improve the sensitivity of the assay by allowing for better spectral separation from cellular auto-fluorescence[3]. With further development, the assay has potential applications in live cell imaging using MBL as reporters or, possibly, in the identification of MBL producing bacteria in clinical samples.

6.3 MBL VARIANTS DISPLAY SIMILAR HYDROLYTIC EFFICIENCIES

In order to shed light on potential drivers of MBL evolution, comparative analyses were carried out on the catalytic efficiencies of the NDM and VIM variants towards a representative panel of β-lactam substrates. The activity assays were carried out under similar experimental conditions to ensure a reliable comparison of the results. There were no substantial differences observed in the hydrolytic activities of the NDM and VIM variants, towards the tested β-lactam antibiotics. However, inhibition of NDM variants with the M154L substitution (NDM-4, NDM-5, NDM-7 and NDM-8) by nitrocefin was reported in two separate studies, suggesting a possible interference of the M154L substitution with the hydrolysis of some cephalosporin substrates (Chapters 3 and 4)[4]. The tested VIM variants from different clusters (VIM-1/VIM-4, VIM-2 and VIM-5/VIM-38) also displayed similar kinetic profiles for the β-lactam antibiotics.

In contrast with some previous proposals[5], there is as yet no compelling evidence that the studied NDM and VIM variants have evolved to directly improve kinetic parameters for β-lactam hydrolysis. The results emphasise the critical need to establish a standardised protocol for screening the activity of the existing and new MBL variants to ensure the data obtained from different studies is comparable.

6.4 PROTEIN STABILITY: A POTENTIAL DRIVER THE EVOLUTION OF MBLS

An interesting finding from the studies described in this thesis is the improved thermal stability of some MBL variants. Thermal stability analyses of NDM variants using different techniques yielded reproducible results, indicating elevated T_m values for the doubly substituted variants NDM-5 (V88L, M154L), NDM-7 (D130N, M154L), NDM-8 (D130G, M154L) and NDM-12 (G222D,M154L)[4]. With the exception of the V88L mutant, the singly substituted NDM variants M154L (NDM-4), D130N and G222D had similar T_m values as the wild type NDM-1, suggesting that the elevated thermal stability was a result of more than one substitution (Chapter 4).

As with the NDM variants, the tested VIM variants displayed a significant differences in their thermal stabilities, with VIM-5 and VIM-38 being the most stable variants[6] (Chapter 5). The VIM variants exhibit more differences in the amino acid sequences than the NDM variants; hence the differences in thermal stability could not be attributed to any single substitution (*Figure 6-3*).

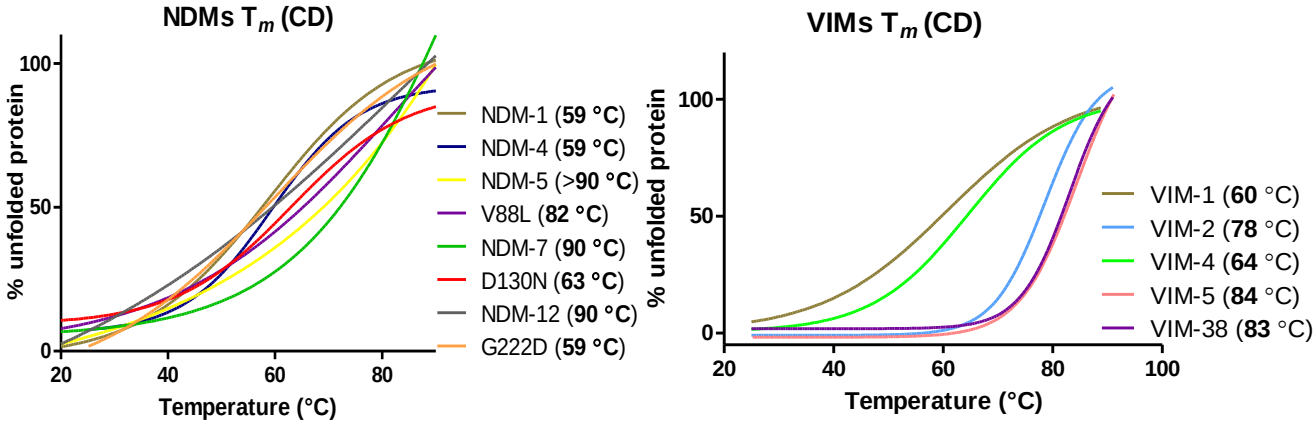


***Figure 6-3*: CD analyses showing the differences in thermal stabilities of NDM and VIM variants.**

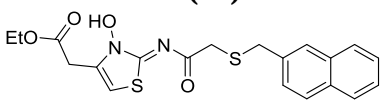
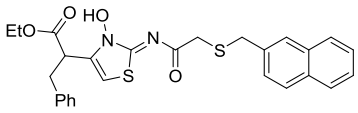
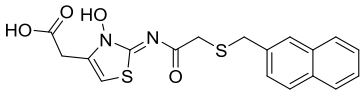
In an attempt to elucidate the possible biological relevance of the improved thermal stability, a cell-based thermal shift assay (CETSA) was set up. The results from the analyses showed a similar stability for the enzymes *in vivo*, with NDM-1, NDM-7 and NDM-12 having an apparent T_m of 73 ± 1 °C (Chapter 4). However, to obtain more conclusive results, the assay will need to be optimised by identifying reference proteins with a high and constitutive expression in *E. coli* BL21 (DE3) pLysS cells. It would also be desirable to assess the thermal stability of the MBLs in the periplasm to simulate a physiologically relevant environment.

Although further investigation will be necessary to clarify the biological relevance, if any, of the increased thermal stabilities of the MBL variants, it is likely that the improved thermal stability reflects a reduced propensity to aggregate or a decreased susceptibility to proteolytic degradation. The results thus far therefore suggest that protein stability may be an important factor in the evolution of MBLs.

6.5 EVOLUTION OF MBLS AFFECTS INHIBITOR DEVELOPMENT

The work described in this thesis addressed the important question of whether the different MBL variants interact similarly with potential MBL inhibitors. Initially, the differences in inhibition of different B1 MBLs were exemplified in Chapter 2, with the *N*-hydroxythiazole inhibitors **4a** and **4c** being potent inhibitors for NDM-1 but having no inhibitory effect on IMP-1. Interestingly, in the same chapter, the compound **4d** was shown to display a significantly lower IC_{50} value with VIM-1 compared to VIM-2 (*Table 6-1)*.

Table 6-1: **IC_{50} values for the selected N-hydroxythiazole inhibitors with six MBLs.**

	IC_{50} (μM)		
Enzyme	**4a (Et)** 	**4c (Et)** 	**4d (OH)** 
NDM-1	9 ± 1	13 ± 1	3 ± 1
IMP-1	>500	>500	4 ± 1
VIM-1	62 ± 21	32 ± 6	6 ± 1
VIM-2	28 ± 7	40 ± 17	162 ± 20
SPM-1	>500	74 ± 20	2 ± 1
Bc-II	21 ± 13	21 ± 8	81 ± 8

Subsequently, the inhibition of five different VIM variants (VIM-1, VIM-2, VIM-4, VIM-5 and VIM-38) by different metallo-enzymes inhibitors was investigated (Chapter 5). The isoquinoline inhibitor **2g** was shown to preferentially inhibit VIM-5 and VIM-38 over VIM-1, VIM-2 and VIM-4, validating the earlier observations (*Figure 6-4*). The configuration of the stereocenter of the inhibitor's side chain was also shown to influence the inhibition potency of the inhibitors towards the VIM variants.

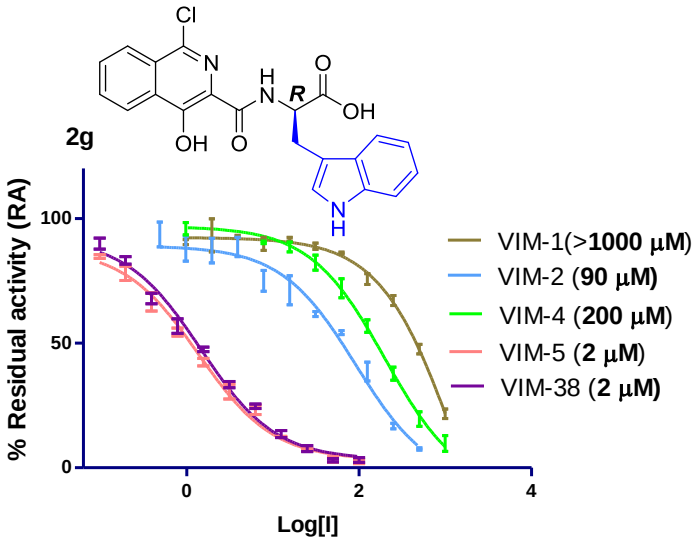


***Figure 6-4*: Inhibition plots and respective IC_{50} values, illustrating the differences in the inhibition of VIM variants.**

It is well established that amino acid substitutions in class A serine β-lactamases TEM and SHV, can confer resistance to the mechanism based β-lactamase inhibitors such as clavulanic acid[7-9]. The variation in inhibition potency of potential MBL inhibitors towards MBL variants thus likely poses a formidable challenge in the development of novel MBL inhibitors with a sufficient breadth of selectivity for clinical use. This observation highlights the need to counter-screen inhibitors both across and within MBL groups in future MBL inhibitor development programs.

6.6 STRUCTURAL ANALYSES REVEAL SUBTLE BUT CRUCIAL INTERACTIONS

Circular dichroism analyses of NDM variants indicated that the variants had similar secondary structural features, suggesting that the present substitutions did not have a significant impact on the overall folds of the NDM variants (Chapter 3). Likewise, the tested VIM variants displayed similar CD spectra, despite the differences in amino acid sequences (Chapter 5). Crystallographic analyses corroborated the CD results, with both the NDM and VIM variants manifesting very similar overall folds.

Interestingly, a comparison of different NDM structures revealed close interactions of M154 with the zinc-binding residue H122. The interaction of M154 with H122, likely influences the positions of other residues on loop 8, particularly E152, and may have an impact on the zinc binding affinity of the NDM variants. Although it would be desirable to obtain di-zinc NDM-3 and NDM-6 structures for a more reliable comparison, the effects of the M154L substitution on the metal binding affinities of NDMs merit further investigation.

Additionally, a crystal structure of VIM-5 complexed with the isoquinoline inhibitor **2f** provided important insights into the effects of residues at positions 224, 225 and 228 (on the L10 loop) on interactions of the isoquinoline inhibitors with different VIM variants. While L224 seemingly provided a more spacious active site for inhibitor binding in VIM-5 and VIM-38, the presence of a tyrosine at the same position in VIM-2 (Y224) likely introduces a steric clash with the bulky indole rings of the isoquinioline inhibitors, resulting in the observed decreased inhibition potency.

6.7 GENERAL CONCLUSIONS

The work described in this thesis details the development of an efficient MBL screening platform based on a reliable and stable chromogenic substrate **CLS405**. The utility of a cell-based assay is hinted at, with the aim to optimise the fluorogenic substrates for the *in vivo* detection of MBLs. The comprehensive analyses of VIM and NDM variants reveals an interesting mode of protein evolution, with the variants showing significant differences thermal stability with little or no changes in their catalytic efficiency. The results described highlight the potential of MBLs to employ substitutions on second spheres residues in fine-tuning zinc-binding affinities and possibly influencing substrate and inhibitor interactions. Of particular interest is the reported difference in the degree of inhibition of the MBL variants, an observation that has critical implications for future MBL inhibitor development programs.

6.8 REFERENCES

1. Makena A, van Berkel SS, Lejeune C, et al. Chromophore-linked substrate (CLS405): Probing metallo-β-lactamase activity and inhibition. *ChemMedChem*. 2013;8(12):1923-1929.

2. van Berkel SS, Brem J, Rydzik AM, et al. Assay platform for clinically relevant metallo-β-lactamases. *J Med Chem*. 2013;56(17):6945-6953.

3. Roth A, Li H, Anorma C, Chan J. A reaction-based fluorescent probe for imaging of formaldehyde in living cells. *J Am Chem Soc*. 2015;137(34):10890-10893.

4. Makena A, Brem J, Pfeffer I, et al. Biochemical characterization of New Delhi metallo-β-lactamase variants reveals differences in protein stability. *J Antimicrob Chemother*. 2015;70(2):463-469.

5. Nordmann P, Boulanger AE, Poirel L. NDM-4 metallo-β-lactamase with increased carbapenemase activity from *Escherichia coli*. *Antimicrob Agents Chemother*. 2012;56(4):2184-2186.

6. Makena A, Duzgun AO, Brem J, et al. Comparison of Verona Integron-borne metallo-β-lactamase variants reveals differences in stability and inhibition profiles. *Antimicrob Agents Chemother*. 2015;60(3):1377-1384

7. Dubois V, Poirel L, Arpin C, et al. SHV-49, a novel inhibitor-resistant β-lactamase in a clinical isolate of *Klebsiella pneumoniae*. *Antimicrob Agents Chemother*. 2004;48(11):4466-4469.

8. Vedel G, Belaaouaj A, Gilly L, et al. Clinical isolates of *Escherichia coli* producing TRI beta-lactamases: Novel TEM-enzymes conferring resistance toβ-lactamase inhibitors. *J Antimicrob Chemother*. 1992;30(4):449-462.

9. Drawz SM, Bonomo RA.Three decades of β-lactamase inhibitors. *Clin Microbiol Rev*. 2010;23:160-201.

CHAPTER 7: APPENDICES

This experimental section details the general methods applied in the thesis. The materials and protocols employed for cloning, protein production, and enzyme kinetic analyses are sufficiently explained.

CONTENTS

CHAPTER 7: APPENDICES 204

7.1 REAGENTS AND GENERAL PRACTICE 206

7.2 MOLECULAR BIOLOGY 206

7.2.1 Site-Directed Mutagenesis 206

7.2.2 Transformation 207

7.2.3 Preparation of competent cells 208

7.3 PROTEIN PRODUCTION 208

7.3.1 Bacterial Growth Media 208

7.3.2 Protein expression trials 210

7.3.3 Large scale protein production 210

7.4 PROTEIN PURIFICATION 212

7.4.1 Protein purification buffers 213

7.4.2 Cell lysis 213

7.4.3 Purification protocol 213

7.4.4 Determination of protein concentrations 214

7.4.5 SDS PAGE analyses 214

7.4.6 Western blot analysis 215

7.5 MASS SPECTROMETRIC ANALYSES 216

7.5.1 Non-denaturing mass spectrometry 216

7.5.2 Denaturing mass spectrometry 217

7.6 ENZYME ASSAYS 217

7.6.1 Steady-state kinetic assays 218

7.6.2 Enzyme Inhibition assay 218

7.1 REAGENTS AND GENERAL PRACTICE

Unless otherwise stated, all reagents were obtained in the highest quality available from Sigma-Aldrich, Stratagene, New England Biolabs (NEB), Invitrogen, Bio-Rad or Roche. Water used for the experiments was purified using a Millipore Elix® Reverse Osmosis system and then passed through a 0.22 μm filter by a Millipore Milli-Q system. Microbiology equipment and media were sterilised by autoclaving for 20 minutes at 121 °C, while the heat sensitive solutions (antibiotics, IPTG, etc) were sterilised using Minisart® 0.22 μm filters. Standard sterile procedures were followed throughout.

7.2 MOLECULAR BIOLOGY

Oligonucleotides (primer sequences) were designed using the QuikChange® Primer Design tool (Agilent Genomics). Oligonucleotides were obtained from Sigma-Aldrich as lyophillised pellets and resuspended using sterile Milli-Q water to 100 μM.

7.2.1 SITE-DIRECTED MUTAGENESIS

Modified Stratagene QuikChange® and the NEB Q5® site directed mutagenesis protocils were employed depending on the polymerase used. The reaction mixture comprised of the following;

Stratagene QuikChange® protocol		**NEB Q5® site protocol**	
Buffer (10X)	5	Buffer (5 X)	10
Milli-Q water	38	Milli-Q water	23
Forward primer (10 μM)	2	Q5 High GC enhancer (10X)	10
Reverse primer (10 μM)	2	Forward primer (10 μM)	2.5
dsDNA template (20 ng/μL)	1	Reverse primer (10 μM)	2.5
dNTPs (10 mM)	1	dsDNA template (20 ng/μL)	2
Pfu Turbo DNA polymerase	1	dNTPs (10 mM)	1
		Q5 polymerase	0.5
Total	50 μL	*Total*	50 μL

A typical mutagenesis PCR protocol was set up with the cycling parameters as follows;

Step		Temperature (°C)	Time (minutes)
Initial denaturation		94	2
For 19 cycles	Denaturation	94	1
	Annealing	55	1
	Extension	68	12
Final Extension		68	20

The annealing temperature was varied (55-60 °C) depending on the melting temperatures of the primers. The template DNA was digested by incubation of the PCR product with 1µL Dpn1 restriction enzymes at 37 °C for 3 hours. Dpn1 enzyme digests methlylated or hemimethlyted DNA; hence it could efficiently digest the DNA template which was isolated from a Dam+ E. coli strain.

7.2.2 TRANSFORMATION

A 50 µL aliquot of XL-10 gold ultracompetent cells was incubated with 2 µL of the Dpn1 treated PCR product for 30 minutes on ice. The cells were subjected to a 'heat shock' (42 °C for 42 seconds and back on ice for 2 minutes) to facilitate DNA uptake. The cells were then incubated for an hour at 37 °C in 300 µL SOC media (2TY media supplemented with 20 mM glucose) for recovery from the heat shock. To select the transformed cells, the cell culture was plated onto agar plates supplemented with ampicillin and incubated at 37 °C overnight. Asingle colony of the transformed cells was inoculated into 5 mL of 2TY media and cultured overnight at 37 °C, to amplify the plasmid DNA. This was followed by plasmid extraction using the GenJet Miniprep kit (Thermo Fisher Scientific Inc., UK). Subsequent sequencing using the vector primers (T7 reverse and forward primers) confirmed the presence of the desired mutations in the plasmids (Source BioScience, Oxford).

7.2.3 PREPARATION OF COMPETENT CELLS

E. coli XL-10 Gold ultracompetent cells were used for production of DNA and *E. coli* BL21 (DE3) pLysS cells for bacterial expression of proteins. The competent cells were prepared from commercial stocks obtained from Stratagene. The cells were first streaked onto antibiotic-free agar plates and grown overnight at 37 °C. 100 mL sterile antibiotic-free 2TY media was inoculated with a single colony from the freshly-prepared plates and the cells grown overnight at 37 °C, in a shaking incubator (220 rpm), to produce the starter culture. 400 mL 2TY media was inoculated with 800 µLof the starter culture and further grown (37 °C, 220 rpm) to an OD600 of 0.6. Pre-chilled centrifuge tubes were used to pellet cells (750 × g, 5 min, 4 °C). The cells were then gently resuspended in 200 mL ice-cold 100 mL CaCl2, 20 % (v/v) glycerol and incubated on ice for 20 min. Cells were again pelleted (750 × g, 5 min, 4 °C) and resuspended in 8 mL of the same solution. The cell suspension was aliquoted (50 µL) in sterile Eppendorf vials, flash frozen in liquid nitrogen and immediately stored at -80 °C for future use.

7.3 PROTEIN PRODUCTION

7.3.1 BACTERIAL GROWTH MEDIA

2TY Media: 2TY media (prepared by Mr. Herminio Manso Jubier) comprised of tryptone (16g), yeast extract (10g) and NaCl (5g) dissolved in 1L of Milli-Q water.

Terrific Broth (TB) Media: TB media used for expression trials was prepared as follows; tryptone (12 g), yeast extract (24 g) and glycerol (4 mL) were added to 800 mL of water and sterilised by autoclaving. The buffer mixture comprising of 0.17 M KH_2PO_4 and 0.72 M K_2HPO_4 was prepared in distilled water and filter sterilised. 100 mL of the salt mixture was added to the media and the solution made up to 1 L with distilled water.

Autoinduction media: For preparation of autoinduction media, modified 2TY media was constituted by dissolving tryptone (10 g) and yeast extract (5 g) in distilled water to make 1 L. 50X salt mix was prepared comprising of 1.25 M Na_2HPO_4, 1.25 M KH_2PO_4, 2.5 M NH_4Cl and 0.25 M Na_2SO_4, dissolved in milli-Q water. 50 X sugars solution comprising 25% (v/v) glycerol, 2.5% (w/v) glucose, 10% (w/v) α-lactose was prepared in distilled water. The auto-induction media was then made up as follows;

Reagents	To make 1 L
2TY Media	958 mL
50X salt mix	20 mL
50X sugar solution	20 mL
1 M $MgSO_4$	2 mL
1 M $ZnSO_4$	0.2 mL

The media was autoclaved and cooled to 25 °C before the addition of filter sterilized $MgSO_4$ and $ZnSO_4$ solutions.

7.3.1.1 ANTIBIOTICS

Chloramphenicol and ampicilin stock solutions (50 mg/ mL) were prepared in ethanol and milli-Q water respectively. The antibiotics were filter sterilised using 0.2 µm filters and stored in -20 °C. The final concentration of the antibiotics used in culture media was 50 µg/mL.

7.3.1.2 CLYCEROL STOCKS

Plasmid vectors encoding the proteins of interest (as verified by gene sequencing) were used to transform cells for protein production (E. coli BL21 (DE3) and BL21 (DE3) pLysS cells) as previously described. 100mL of 2TY media supplemented with the appropriate antibiotic was inoculated with a single bacteria colony and grown overnight (37 °C, 220 rpm) to produce the starter culture. Glycerol stocks were prepared by gently mixing 750 µL of culture with 250 µL sterile glycerol and flash freezing in liquid nitrogen before storage at -80 °C.

7.3.2 PROTEIN EXPRESSION TRIALS

Expression trials were carried out for NDM-1 to determine the best conditions for protein production. 100 mL of media (2TY, TB and auto-induction media), supplemented with 50 µg/ mL ampicillin and chloramphenicol, was inoculated with 1 mL starter culture. Different growth conditions were tested including temperature (37, 30 and 18 °C), induction (different IPTG concentrations, autoinduction), time of growth after induction (4 and 18 hours) as well as the inclusion of enzyme cofactors (addition of 100 µM $ZnSO_4$). Afterwards, the cells were harvested by centrifugation (4,500 rpm, 30 minutes, 4°C). Cell pellets were resuspended in 2.5 mL Bugbuster protein extraction reagent supplemented with 10 µL of lysonase enzyme and vortexed. 1 mL of the crude cell lysate was centrifuged (10,000 rpm, 5minutes) to remove cell debris and the protein-containing supernatant was mixed with Ni^{2+}-charged Profinity IMAC resins. To allow efficient binding of the target proteins, protein solution was incubated with for 90 minutes at 4°C. The samples were then centrifuged and the supernatant discarded. The protein bound resins were washed with 20mM Tris buffer (pH7.5) containing 200mM NaCl and 20mM imizadole. The bound proteins were eluted by addition of 500 µL elution buffer (20mM Tris buffer (pH7.5), NaCl, 500mM Imidazole). The expression levels were qualitatively determined by performing SDS PAGE analyses on the eluted proteins.

7.3.3 LARGE SCALE PROTEIN PRODUCTION

7.3.3.1 PLASMID VECTORS USED IN THE STUDY

For NDM-1 and the NDM variants, DNA encoding the full coding sequences (△27) or the truncated protein (△42), including a cleavable *N*-terminal His_6-tag, were inserted into pTriEx-based pOPINF vectors (designed by the Oxford Protein Production facility,OPPF). The same pOPINF vectors were used for VIM-1 (with either a *C*-terminal) and VIM-2 (with a cleavable *N*-terminal His_6-tag). The untagged VIM-1 was generated by subcloning using the ligation independent cloning technique (LIC) from the pOPINF vector to the pNIC28-

Bsa4 encoding a cleavable *N*-terminal His_6-tag[1] (conducted by Dr. Sarah Wilkins). For VIM-38, DNA encoding for full-length protein, lacking its *N*-terminal periplasmic signaling sequence, was cloned into the pET-28a vector (Novagen) by collaborators at the Department of Medical Microbiology, Recep Tayyip Erdoğan University, Turkey. VIM-5 was then generated form the VIM-38 template by site directed mutagenesis (V316A). IMP-1, BC-II and SPM-1 were obtained by Dr. Jürgen Brem from the OPPF.

Enzyme	Construct	Vector	Tag / cleavage site Selection antibiotic	Selection antibiotics
NDM variants (Chapter 3)	G42-R273	pOPINF	*N*-His_6 / HRV3C	Ampicillin/ chloramphenicol
NDM variants (Chapter 4)	M27-R273	pOPINF	*N*-His_6 / HRV3C	Ampicillin/ chloramphenicol
VIM-1 (*C*-his)	M1-E317	pOPINF	*C*-His_6	Ampicillin/ chloramphenicol
VIM-1 (untagged)	S26-E317	pNIC28-Bsa4	*N*-His_6/ TEV	Kanamycin
VIM-2	V27-E317	pOPINF	*N*-His_6/ HRV3C	Ampicillin/ chloramphenicol
VIM-5	S21-E317	pET-28a	*N*-His_6/ HRV3C	Kanamycin
VIM-38	S21-E317	pET-28a	*N*-His_6/ HRV3C	kanamycin

The plasmid vectors encoding the different MBLs were transformed into *E. coli* BL21 (DE3) PlysS or *E. coli* BL21 (DE3) cells for protein production, using the previously described protocol.

7.3.3.2 GENERAL PROTEIN PRODUCTION PROCEDURE

For Δ42 NDM-1 (chapter 2), 12 × 2 L flasks containing 600 mL 2TY media, supplemented with the appropriate antibiotics were each inoculated with 6 mL starter culture. The cells were cultured at 37 °C until an OD_{600} of 0.6-0.8 was reached, prior to induction with 0.5 mM isopropyl β-D-1-thiogalactopyranoside (IPTG) and further grown for 17 hours at 20 °C.

For the Δ42 and Δ27 NDM variants (chapter 3 and chapter 4, respectively), cells cultured in auto-induction media. 12 flasks containing 1L auto-induction media, supplemented with the

ampicillin and chloramphenicol (50µg/mL) were inoculated with 5 mL starter culture each. The cells were grown for 5h at 37 °C, after which the temperature was lowered to 18 °C for a further 17 hours.

For the VIM variants, the cells were culture in 2TY media supplemented with the appropriate antibiotic as described above. Protein expression was induced by addition of IPTG at appropriate concentrations and the cells cultured for a further 4 hours or overnight, as appropriate (see below).

After the appropriate incubation times, the cells were then pelleted by centrifugation (7,000 x g, 10 minutes, 4 °C) and stored in resealable plastic bags at –80 °C.

Enzyme	Growth media	IPTG (mM)	Post-induction Temperature (°C)	Induction time
NDM-1 △42 (chapter 2)	2TY	0.5	20	Overnight
NDM variants (Chapter 3)	Autoinduction	none	18	Overnight
NDM variants (Chapter 4)	Autoinduction	none	18	Overnight
VIM-1 (*C*-his)	2TY	0.5	37	4 hours
VIM-1 (untagged)	2TY	0.2	20	Overnight
VIM-2	2TY	0.5	30	4 hours
VIM-5	2TY	0.1	18	Overnight
VIM-38	2TY	0.1	18	Overnight

7.4 PROTEIN PURIFICATION

Enzymes were purified at 4 °C using an AKTA Fast Protein Liquid Chromatography (FPLC) system (Amersham Pharmacia Biotech), controlled by the UNICORN v.4 software. All the buffers used were prepared using milli-Q water, filtered using 0.2 µM millipore filter and pH corrected to pH 7.5 using 1M NaOH and/or HCl.

7.4.1 PROTEIN PURIFICATION BUFFERS

Nickle affinity chromatography (HisTrap) buffers were prepared as follows:

Buffer	HEPES/Tris (mM)	NaCl (mM)	Imidazole (mM)	EDTA (mM)
Binding	50	500	5	-
Wash	50	500	20	-
Elution	50	500	500	-
Stripping	50	500	-	100

The elution buffer used for size exclusion chromatography (SEC) contained 20mM Tris, 200mM NaCl and 100µM $ZnCl_2$ was added in some cases.

7.4.2 CELL LYSIS

Cell pellets were re-suspended in the HisTrap binding buffer (supplemented with DNase 1 (0.02 mg/ML), lysozyme, and EDTA-free protease inhibitor tablet (Roche). The cells were further lysed by sonication using a SONICs VibraCell sonicator, for 7 minutes (10 second pulse and rest intervals) with the microtip at 60% amplitude. To remove the cell debris, the cell lysates were clarified by centrifugation at 20,000 rpm for 20 min at 4 °C and filtered using a 0.4 µm filter before application to a purification column.

7.4.3 PURIFICATION PROTOCOL

A 3- step protocol involving nickel affinity and size exclusion chromatography was employed for the purification of the recombinant MBLs. The cell lysates were first loaded onto a 5 mL HisTrap HP column (GE Healthcare) pre-equilibrated with the binding buffer. After a thorough wash (10 column volumes) with the wash buffer, the bound proteins were eluted with a 20-500 mM imidazole gradient. SDS PAGE analysis was then carried out to determine the protein- containing fractions from the chromatogram peaks.To cleave the *N*-terminal His_6 tag, the enzymes were incubated with His_6-tagged recombinant Human Rhinovirus 3C protease (1:100 w/w) and His_6-tagged TEV for VIM-1 (1:20 w/w) overnight at 4 °C . The

untagged proteins were purified using a 5 mL HisTrap HP column and eluted with wash buffer (containing 20 mM imidazole). The cleaved protein were collected in the flow-through and concentrated for further purification.

The proteins were then loaded onto Superdex S75-300 mL column (GE Healthcare) eqillibrated with 1 column volume of the SEC elution buffer. The proteins were eluted using 1 column volume the elution buffer flowing at a rate of 2 mL/ minute. 5 mL fractions were collected and fractions analysed by SDS-PAGE on the basis of the peaks of the chromatograms' UV traces. The purified proteins were then concentrated, aliquoted and frozen at -80 °C for future use.

7.4.4 DETERMINATION OF PROTEIN CONCENTRATIONS

The concentrations of the purified proteins were determined by measuring the absorbance at 280 nm, using 2 µL protein solution on a NanoDrop ND-1000 UV/Vis spectrophotometer. The extinction coefficient (ε) was calculated using the ProtParam tool on the ExPASY Proteomics Server (www.expasy.org) and concentration calculated using the equation, $A = \varepsilon.c.l$.

7.4.5 SDS PAGE ANALYSES

SDS PAGE gels were prepared using the following recipe (to make 4 gels);

	16 ml of 12% Separating Gel	10 ml of 6% Stacking Gel:
Tris.HCL (1.5M,pH 8.8)	4	2.5 mL (0.5 M Tris.HCL pH 6.8)
milliQ water	5.3 mL	5.3 mL
30% Acrylamide	6.4 mL	2 mL
10% SDS	160 µl	100 µl
10% APS	160 µl	100 µl
TEMED	16 µl	10 µl

The composition of the buffers used for SDS PAGE analyses are outlined below;

10X SDS PAGE running buffer (To make I L)	
250mM Tris base	30g
1.92M glycine	144g
1%w/v SDS	10g

2X SDS Sample loading buffer (To make 100 mL)	
Tris HCL (0.5M, pH 6.8)	10ml
Bromophenol blue	0.2%
10% w/v SDS	20mL
Glycerol	12mL
β-Mercaptoethanol	5mL

	Staining solution	Destain solution
Glacial Acetic acid	10% v/v	10% v/v
Methanol	50% v/v	25%v/v
MilliQ water	39.75%	65%
Coomassie Brilliant blue	0.25% w/v	-

The protein samples (~20 µg) were mixed with the loading buffer and heated at 105 °C for 5 minutes and loaded onto the gels. Molecular weight markers were obtained from Invitrogen. Electrophoresis was typically conducted using the SDS loading buffer, at constant voltage (180 V) for ~1 hour.

The gels were stained for 5 minutes in Coomasie blue staining solution and destained until clear. The gels were visualized using a UV-light box (Jencons Scientiffic)

7.4.6 WESTERN BLOT ANALYSIS

Western blotting was employed to quantify residual proteins after heat-induced aggregation during the cell-based thermal Shift assay (CETSA). After cell lysis and centrifugation to remove cell debris, 15 µL of the supernatant was added to 5 µL of protein loading dye and incubate at 88 °C for 7 minutes. SDS PAGE analysis was carried out using 4-12% NuPAGE

BisTris precast gels (Bio-rad). The samples were run for 40 minutes at 200V, in MES-SDS buffer. Protein bands were transferred to the nitrocellulose membrane using the iBlot® Dry Blotting System (program P3) for 7 minutes. The membranes were blocked for 1 hour using 30 mg/mL BSA in PBS-0.1%T buffer, pH 7.5 and washed for 5 minutes (3X) in PBS-0.1%T buffer. The membranes were then incubated overnight at room temperature with anti-NDM-1 primary antibody (Novus Biologicals), prepared in the blocking buffer (1:1000). After three washes in PBS-0.1%T buffer, the membranes were incubated for 1 hour in the anti-rabbit secondary antibody prepared in blocking buffer (1:10, 000). After another three washes, the membranes were visualised using the LI-COR Odyssey CLx imaging system and the intensity of the bands quantified using the Image Studio Version 3:1.

7.5 MASS SPECTROMETRIC ANALYSES

7.5.1 NON-DENATURING MASS SPECTROMETRY

Native mass spectrometric analyses were carried out for the NDM variants and VIM-5 and VIM-38 to ascertain the masses and metal content of the enzymes. The proteins were first desalted using a Bio-Spin 6 Column (Bio-Rad, Hemel Hempstead, UK) into 15 mM ammonium acetate (pH 7.5) and diluted in the same buffer to a final concentration of 100 µM. Data were acquired on a Q-TOF mass spectrometer (Q-TOF micro, Micromass, Waters, Altrincham, UK) equipped with a Nanomate (Advion Biosciences, Ithaca, NY, USA) interface. The experiments were carried out at a chip voltage of 1.70 kV and a delivery pressure 0.25 psi (1 psi = 6.81 kPa). The sample cone voltage was typically 60 V with a source temperature of 40 ºC and with an acquisition/scan time of 10s/1s. Calibration and sample acquisition were performed in the positive ion mode in the range of 500-5,000 *m/z*. The pressure at the interface between the atmospheric source and the high vacuum region was fixed at 6.60 mbar.

7.5.2 DENATURING MASS SPECTROMETRY

To verify the masses of the purified proteins, denaturing mass spectrometric analyses were carried. An LCT Premier mass spectrometer (Waters) was coupled to an Agilent 1100 Series HPLC using a Chromolith® FastGradient RP-18 endcapped column equipped with a 50-2 HPLC column, made of monolithic silica (C_{18}, 2 x 50 mm, macropores with 1.6 µm diameter, *Merck*). The instrument was connected to a CTC-autosampler inlet system. A multi-step gradient over 10 min was run (solvent A 94.9% H_2O/5% CH_3CN/0.1% formic acid, solvent B 99.9% CH_3CN/0.1% formic acid; 0-1 min 5% B for equilibration, followed by a linear gradient to 100% B over 4 min, then 100% B for an additional 3 min, followed by a linear gradient over 2 min back to 5% B to re-equilibrate the column) to separate the protein samples at flow rates of 0.4 ml/min for the first 5 min and then 1.0 ml/min for the remaining time. The electrospray ionisation source used a capillary voltage of 3.2 kV and cone voltage of 25 V. Nitrogen was used as the nebulizer and desolvation gas at a flow rate of 600 l/h. Protein typically eluted as a peak between 3 and 5 min under these conditions. Calculated masses were obtained using the ExPasy ProtParam tool (http://web.expasy.org/protparam/).

7.6 ENZYME ASSAYS

The optimized MBL assay buffer was used for all enzyme activity and inhibition assays. The antibiotics and substrates used were dissolved in milli-Q water or the appropriate solvents. All the experiments were performed at 25 °C, and the absorbance values were read using the BMG Labtech Pheraster spectrophotometer.

MBL assay buffer (To make 1 L)	
50 mM Hepes	10 mL
10 mg/mL BSA	100 µL
100 mM $ZnSO_4$	10 µL
10% Triton X 100	1 mL

7.6.1 STEADY-STATE KINETIC ASSAYS

Antibiotics used for steady-state kinetic analyses are as listed below. Standard curves for the antibiotics and the substrates were generated by plotting the absorbance units of the substrates/product at increasing concentrations. The extinction coefficients were determined as the gradient of the standard curve. The optimum enzyme concentration for steady state kinetics was measured by determining the rate of substrate degradation or product formation at varying enzyme concentrations. The enzyme concentration at which the steady state was maintained for approximately 10 minutes was selected for use in the subsequent experiments.

Antibiotic	Source	Coefficient ($\mu M.AU^{-1}$)	Wavelength λmax (nm)
Imipenem	Molekula Limited, UK	0.0019	300
Meropenem	Molekula Limited, UK	0.0098	300
Doripenem	Sigma-Aldrich, UK	0.0079	300
Ampicillin	Apollo scientific,UK	0.0024	230
Cephalothin	Sigma-Aldrich, UK	0.0058	265
Cefoxitin	Sigma-Aldrich, UK	0.0060	265
Ceftazidime	Sigma-Aldrich, UK	0.0113	265
Nitrocefin	Merck Millipore, Germany	0.0077	495

Initial rates were obtained from the changes in absorbance at varying substrate concentrations. Steady state kinetic parameters (K_M and k_{cat}) were determined by fitting the initial velocity data to the Michaelis-Menten equation using the Graph Prism 5.01 software.

7.6.2 ENZYME INHIBITION ASSAY

Inhibitors were dissolved in DMSO to make 100mM stock solutions and further diluted in the assay buffer. The final concentration of DMSO in all the experiments was <5% which was shown to not have an inhibitory effect on the enzymes.

For residual activity determination, the rate of enzyme-hydrolysis of the reporter substrate (at a concentration close to the K_M value) was determined in presence of 100 µM solutions of the inhibitors. The residual activity was calculated as follows;

*Rate of hydrolysis in presence of the inhibitor / rate of hydrolysis without the inhibitor*100*

For determination of IC_{50} values, on the residual activities were obtained at increasing inhibitor concentrations, and data analysed using GraphPad Prism software. The data was transformed to logarithmic scale (X=Log(X)) and then fitted to an inhibition dose response curve (log [inhibitor] vs. residual activity). The IC_{50} value was taken as the concentration of the inhibitor that provokes a response half way between the maximal (Top) response and the maximally inhibited (Bottom) response.